2014 / Volume 52 / Number 2
ISSN 1641-4640

Folia NEUROPATHOLOGICA

www.folianeuro.termedia.pl

Official Journal of Mossakowski Medical Research Centre Polish Academy of Sciences
and
Polish Association of Neuropathologists

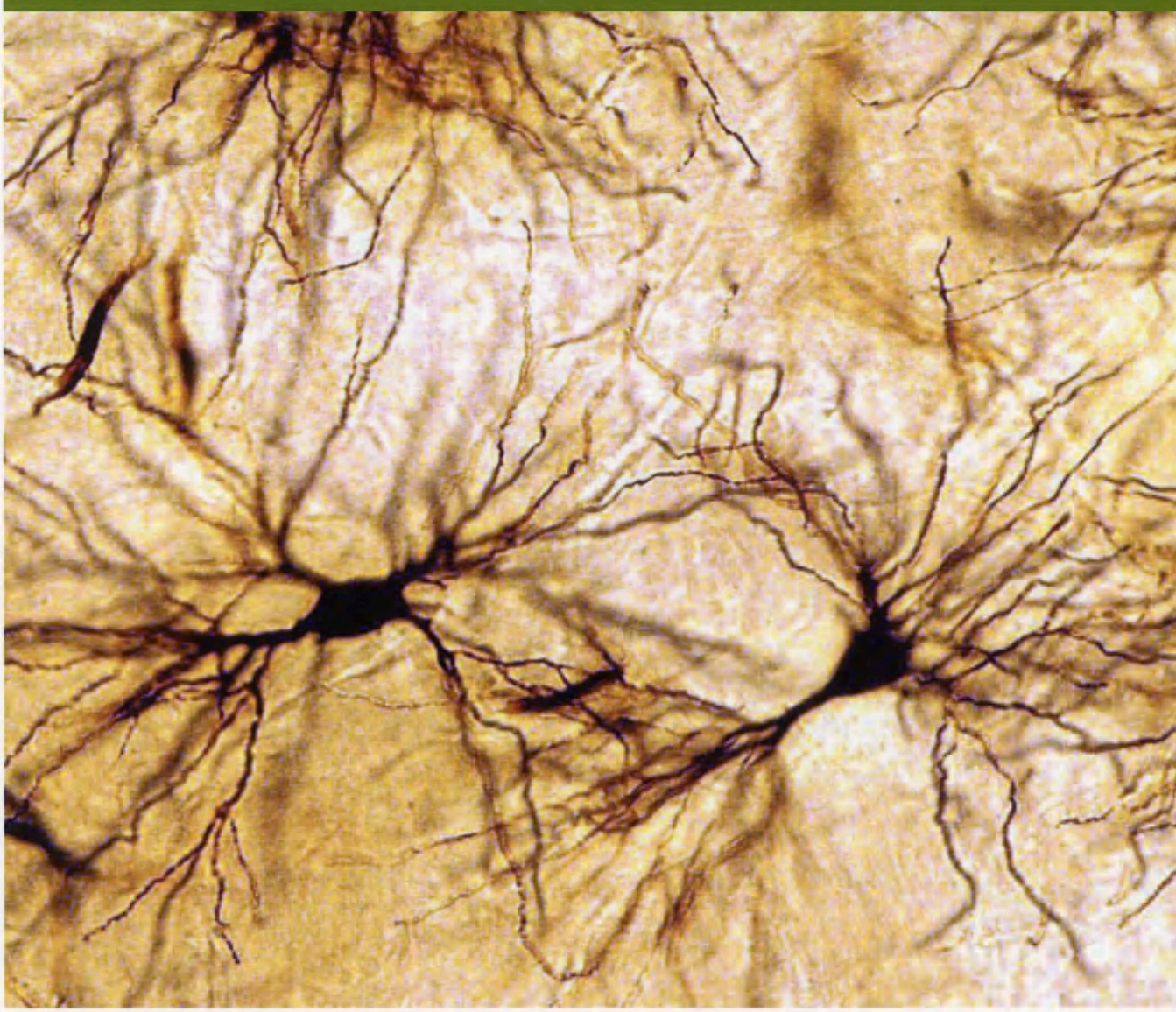

ISSN 1641-4640

Folia Neuropathologica

TERMEDIA Publishing House

Folia
Neuropathologica
former *Neuropatologia Polska*

Official Journal of Mossakowski Medical Research Centre Polish Academy of Sciences and Polish Association of Neuropathologists

The journal is partly financially supported
by the Ministry of Science and Higher Education

termedia

Termedia Publishing House
Kleeberga 2, 61-615 Poznan, Poland
phone/fax: +48 61 822 77 81
e-mail: termedia@termedia.pl
www.termedia.pl
www.folianeuro.termedia.pl

Warsaw office
phone/fax: +48 22 827 75 14
e-mail: biuro.warszawa@termedia.pl

president of the management board
editor-in-chief of the Publishing House, director
Janusz Michalak
e-mail: j.michalak@termedia.pl

director of the Publishing House
Andrzej Kordas
e-mail: a.kordas@termedia.pl

Marketing and Advertising Department
Renata Dolata
phone: +48 61 822 77 81 ext. 508
e-mail: r.dolata@termedia.pl

Distribution Subscription Department
Jolanta Jankowiak
phone: +48 61 656 22 00
e-mail: prenumerata@termedia.pl

Impact Factor for Folia Neuropathologica equals 1.547
MNiSW score for Folia Neuropathologica equals 15.00
Index Copernicus score (2011) for Folia Neuropathologica equals 18.13
Position in Index Copernicus ranking systems available at http://www.indexcopernicus.pl

Abstracted and indexed in Index Medicus/MEDLINE, Neuroscience Citation Index, SciSearch, Research Alert, Chemical Abstracts, EMBASE/Excerpta Medica, Polish Medical Bibiography, Index Copernicus

The journal is financially supported by the Ministry of Sciences and Higher Education.

Print run: 450 copies

Folia
Neuropathologica
2014; 52/2: 111-210

Contents

Original article

Folia Neuropathologica

Poly(ADP-ribose) polymerase-1 (PARP1) and p53 labelling index correlates with tumour grade in meningiomas

Tamás Csonka[1], Balázs Murnyák[1], Rita Szepesi[2], Andrea Kurucz[1], Álmos Klekner[3], Tibor Hortobágyi[1]

[1]Division of Neuropathology, Institute of Pathology, [2]Department of Neurology, [3]Department of Neurosurgery, Faculty of Medicine, University of Debrecen, Debrecen, Hungary

Folia Neuropathol 2014; 52 (2): 111-120 DOI: 10.5114/fn.2014.43782

Abstract

Meningiomas are one of the most frequent intracranial tumours, with 13 histological types and three grades according to the 2007 WHO Classification of Tumours of the Central Nervous System. p53, as one of the most potent tumour suppressor proteins, plays a role in nearly 50% of human tumours. Poly(ADP-ribose) polymerase (PARP) is a DNA repair enzyme with high ATP demand. It plays a role in apoptosis by activating an apoptosis inducing factor, and in necrosis by consuming NAD+ and ATP. Only PARP1 has been investigated in detail in tumours out of the 17 members of the PARP superfamily; however, its role has not been studied in meningiomas yet. The aim of this study was to determine the role of p53 and PARP1 in meningiomas of different grade and to establish whether there is any correlation between the p53 and PARP1 expression. Both PARP1 and p53 have been expressed in all examined meningiomas. PARP1 labelled grade II tumours with a higher intensity as compared to grade I and III neoplasms, respectively. An increased p53 expression was noted in grade III meningiomas. There was no statistical correlation between p53 and PARP1 expression. Our data indicate that both PARP1 and p53 activation is a feature in meningiomas of higher grade, PARP1 overexpression being an early, whereas p53 overexpression, a late event in tumour progression.

Key words: *meningioma, poly(ADP-ribose) polymerase (PARP), p53.*

Introduction

Meningiomas are frequent primary brain tumours representing approximately 30% of all primary intracranial tumours. The incidence is increasing with age and has a slight female predominance [32,59]. The aetiology is not entirely understood, but the increased risk after whole brain radiation therapy is well known [38]. There are several subtypes, like meningothelial, fibrous, transitional, psammomatous, angiomatous, microcystic, secretory, lymphoplasmacyte-rich, sometimes with crystalline inclusions [5], metaplastic, choroid, clear cell, rhabdoid, papillary and other rare or miscellaneous types [34]. According to the ultrastructural findings, some of the intranuclear vacuoles are produced during autophagy [18]. The heterogeneous glycosylation pattern has also been demonstrated in different subtypes of meningiomas, and it indicates the usefulness of lectins in the evaluation of pluripotential differentiation

Communicating author:
Tibor Hortobágyi, MD, PhD, FRCPath, Division of Neuropathology, Institute of Pathology, University of Debrecen, 98. Nagyerdei krt. Debrecen, H-4032, Hungary, fax: +3652255248, e-mail: hortobagyi@med.unideb.hu

of meningioma cells [56]. The current prediction of clinical behaviour is based on the morphological findings, brain invasion, mitosis index and Mib1 immunostaining [1,47,48]. Meningiomas show positive immunoreactivity for epithelial membrane antigen, oestrogen and progesterone receptors [45]; however these immunohistochemical markers do not help with the determination of the grade. CD31 immunostaining is good for revealing the blood vessel number that is higher in atypical meningiomas than WHO grade I tumours [31], but this marker is not used in routine diagnostic work-up. Despite these findings, there is a need for more "malignant" markers for meningiomas that can be used in routine diagnostic work and a group of them could be the DNA repair genes like p53 or poly(ADP-ribose) polymerase (PARP) in the future.

PARP protein superfamily has 17 members. All of them have four domains: catalytic, auto-modification, caspase-cleaved and DNA-binding domain. Some of them have PARP activity, as PARP1 or PARP2 and some of them do not, as PARP3 or PARP6.

PARP1 is a 113 kDa protein, located in the nucleus. The gene of PARP1 is located on the long arm of chromosome 1 (1q42.12). The cDNA was isolated and sequenced first by Kurosaki *et al.* [26]. One of the main functions of PARP1 is its role in the repair of single-stranded DNA breaks (SSB). After detecting the SSB damage by chemical, radiation or metabolic induction, the enzyme is activated and binds to the DNA, undergoes a structural transformation before it produces poly(ADP-ribose) (PAR) chain by a nicotinamide adenine dinucleotide (NAD+), consuming the process. PAR is a signal for other repair genes during base excision repair (BER) [9,29,35]. Activated PARP1 can poly(ADP-ribosyl)ate (PARylate) nuclear enzymes thereby increasing the negative charge and preventing the interaction with other anionic molecules including the DNA. Among the DNA repair functions, activated PARP1 has a vital role in apoptosis by translocation of the apoptosis inducing factor (AIF) from the mitochondria to the nucleus [60,61]. However, if there is a high level of DNA damage, necrotic cell death is triggered by activating a large number of PARP1, consuming NAD+ and the ensuing ATP depletion [3]. The role of PARP1 activation cascade has also been demonstrated in neuronal stem cell transplantation after brain injury in rats [27], as well as PARP1 is also activated in the ischemia-reperfusion injury [55], and the early activation of PARP1 after cold lesion that is – at least in part – related to neuronal NO synthetase (nNOS) induction [16]. The role of PARP1 has been revealed in the regulation of glycogen synthase kinase-3 (GSK3) that is responsible for the hyperphosphorylation of tau [54], and the amyloid peptide affected signal transduction to PARP1 in Alzheimer's disease [2].

It has been demonstrated that PARP1 has a role in the BRCA1/BRCA2 mutated breast carcinomas because PARP1 inhibitors can trigger the effectiveness of the chemotherapeutic agents by inhibiting the SSB-repair, when the double-stranded DNA repair is also diminished by the BRCA mutation [11]. The role of PARP1 has been described in other tumours such as breast [51], ovarian [6], pancreatic carcinomas [24], gastric carcinomas [62], prostate carcinomas [53], melanomas [13,40] and glioblastomas [12,21] but has not been investigated in meningiomas yet.

p53 is one of the most significant tumour suppressor proteins, encoded by the *TP53* gene on the short arm of chromosome 17 (17p13.1) [17,33]. The physiological functions of p53 are cell cycle regulation and conservation of the stability of the genome by preventing mutations. The 393 amino acid long, 43.7 kDa weight protein has 7 domains, such as two activation domains (AD1 and AD2), a proline-rich domain, a DNA-binding core domain (DBD), a signalling domain, a homo-oligomerisation domain (OD) and a C-terminal downregulation domain. p53 can be activated by DNA damage, oxidative stress, osmotic shock, ribonucleotide depletion or oncogene expression. The activation is marked by an increase in the half-life of p53 and a change of its conformation [22]. Mdm2 is responsible for the low level of p53 in an unstressed cell, by binding to p53 and preventing its action, and it also transports p53 to the cytosol, and attaches ubiquitin to it covalently.

The anticancer activity of p53 works through several mechanisms: it activates DNA repair proteins, induces growth arrest at the G1/S regulation point through p21 [10] or initiates apoptosis if the DNA damage is irreversible. Mutagens can damage *TP53* causing unregulated cell proliferation; more than 50 percent of human tumours contain a deletion or mutation of the TP53 gene [15]. p53 was voted the molecule of the year in 1993 by the *Science* magazine [25], due to its key roles.

The role of p53 has already been examined in the meningiomas: some of the examinations ended with negative or equivocal findings [43,48-50], but some

of them showed a significant correlation between the p53 status and the grade or recurrence of the tumour [4,7,8,19,20,28,37,41,44,46,57]. It is also described that p53 immunopositive cells are more frequent in the perinecrotic areas of post-embolised cases than in preserved parts of the tumour [39].

Several theses have been written about the interaction between the PARP1 and the p53. Wieler *et al.* showed that the inhibition of endogenous PARP1 functions suppresses the transactivation function of p53 in response to ionizing radiation; hence PARP1 is a key regulator of the p53 response to DNA damage [58]. Malanga *et al.* showed that ADP-ribose polymers play a role in regulating the DNA binding properties of p53 by preventing and reversing p53 binding to the palindromic p53 consensus sequence [36]. Lee *et al.* has recently discovered a novel role for PARylation of p53 in the gene-specific regulation of the transcriptional mode of p53 on the promoter of MTA1 [30]. Godoy *et al.* revealed overexpression of PARP1 and p53 in high-grade and advanced stage tumours in epithelial ovarian cancer, and it indicated that these 2 markers might serve as a marker of aggressive disease behaviour [14]. Sabisz *et al.* showed the crucial part of PARP1 activity in the maintenance of the G2 arrest induced by DNA damaging drugs; thus, inhibitors of PARP1 may be used as non-genotoxic agents to activate p53 in cancer cells with non-functional p53 pathways [52]. PARylation of transcription factors such as p53, NFkB, and Sp1 prevents their binding to DNA and formation of transcription complexes [42].

The aim of this study is to find any correlation between the PARP1 and p53 immunostaining and the WHO grade of the tumours, and between the PARP1 and p53 immunopositivity.

Material and methods

The histological slides of 31 meningioma patients have been studied. Patients have been divided into three groups according to the WHO Classification of Tumours of the Central Nervous System [34]. After the surgical removal, sections were created and stained for haematoxylin-eosin (H&E) from formalin-fixed and paraffin-embedded (FFPE) blocks for a routine diagnostic procedure in the Institute of Pathology. All of the cases have been revised by a consultant neuropathologist (TH).

Immunohistochemistry (IHC) has been performed according to standardized methods as described in detail, in earlier publications [16,17]. In brief, 4 μm thick sections from FFPE blocks have been stained for PARP1 rabbit polyclonal antibody (ab6079) (Abcam Plc., Cambridge, England) and p53 DO-7 mouse monoclonal antibody (M7001) (DAKO, Denmark) according to the manufacturer's protocol. Using a 1 : 500 and 1 : 700 dilution for PARP1 and p53, respectively, with Novocastra Bond™ Polymer Refine Detection kit on Leica Bond Max™ fully automated IHC stainer, with negative controls (Fig. 1).

100 cells in 10 fields of vision on 40x magnification have been examined; the staining intensity has been evaluated as none (0), weak (1+), moderate (2+) and strong (3+) from all of the slides for both PARP1 and p53 (Fig. 2). We have created two parameters in all cases regarding to the staining intensity (Si) ratio of the 1+, 2+ and 3+ cells Si1-3, and ratio of the 2+ and 3+ cells Si2-3, similarly as HER2 immunohistochemistry evaluation in breast carcinomas (Table I).

The results have been analysed by SPSS 19.0 for Windows statistical software. After comparing with Kruskal-Wallis H test the Si1-3 and Si2-3, performing Mann-Whitney *U* test on all of the grade pairs for both PARP1 and p53. Next, we have created two groups – low grade (WHO grade I) and high grade (WHO grade II and WHO grade III) [23] and have compared them by Mann-Whitney *U* test. We also have performed Spearman's rank order correlation analysis to determine whether there is any correlation between the PARP1 and p53 immunopositivity.

Ethical approval has been sought from the Institutional Research Ethics Committee.

Results

Both PARP1 and p53 have been expressed in all of the 41 cases.

There was a significant correlation between tumour grade and presence of PARP1 expression (staining intensity (Si)1-3) ($p = 0.001$) and presence of explicit positivity (Si2-3) for p53 ($p = 0.012$), respectively, with Kruskal-Wallis H test. In contrast, there was no statistically significant association between grade and Si2-3 for PARP1, Si1-3 for p53, $p = 0.523$ and $p = 0.141$, respectively.

As next, we have compared different grades and performed Mann-Whitney *U* test. The Si1-3 for PARP1 between grade I and grade II, as well as grade II and

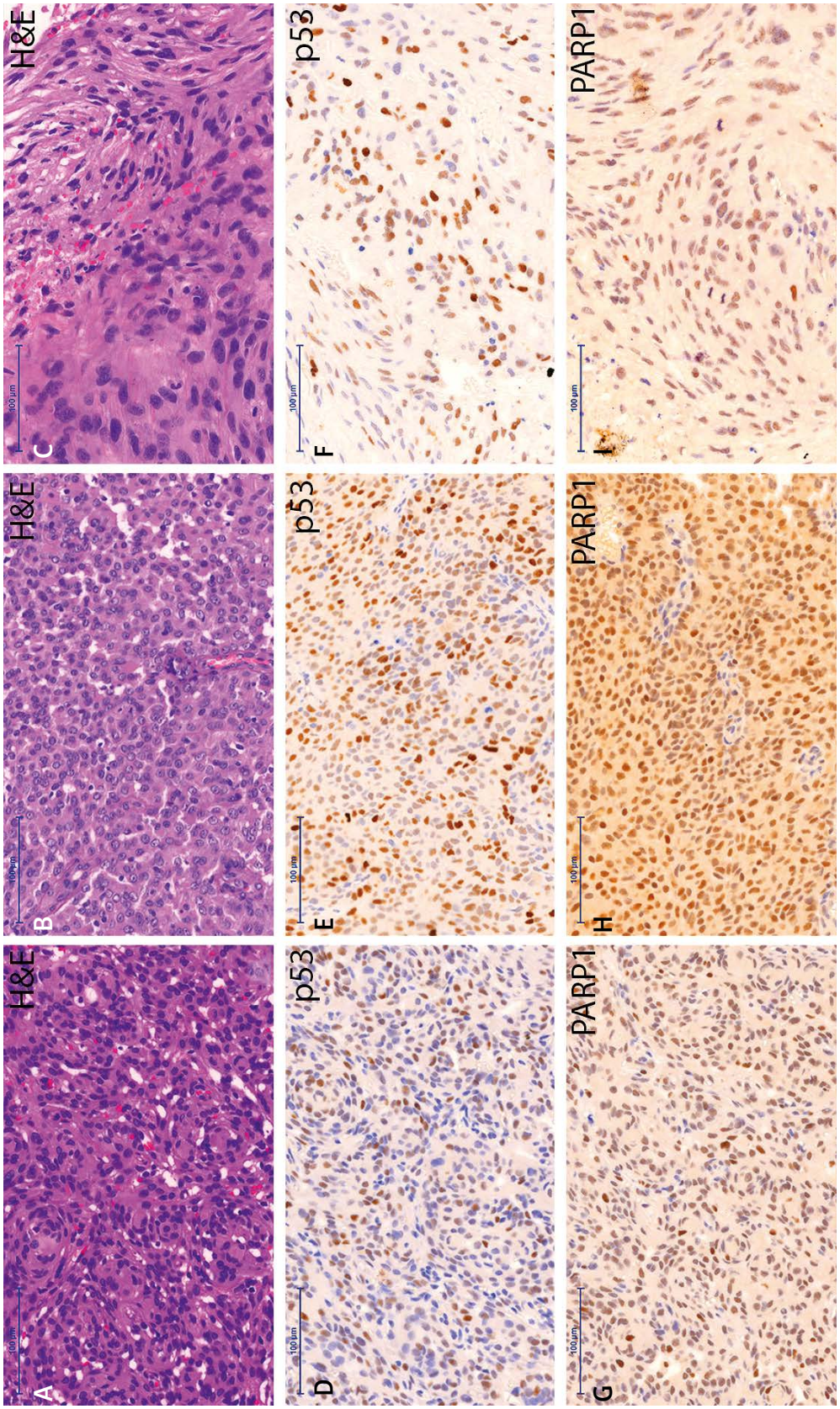

Fig. 1. p53 and PARP1 immunostaining in meningiomas of different WHO grades. Haematoxylin-eosin **(A, B, C)** and immunohistochemical staining for p53 **(D, E, F)** and PARP1 **(G, H, I)** of grade I **(A, D, G)**, grade II **(B, E, H)** and grade III **(C, F, I)** tumours. (PARP1 – poly(ADP-ribose) polymerase 1) (scale bar 100 µm).

grade III (Fig. 3A); and the Si2-3 for p53 between grade I and grade III (Fig. 3B) significantly correlated with the WHO grades (p = 0.001 and p = 0.005, p = 0.002, respectively). Grade II tumours showed the highest mean index of the PARP1 staining (Fig. 3A), while grade III tumours had the highest staining index for p53 (Fig. 3B).

The Mann-Whitney *U* test, performed on the low-grade and high-grade groups, showed a significant correlation between Si1-3 for PARP1 (Fig. 3C) and Si2-3 for p53 (Fig. 3D), p = 0.028 and p = 0.018, respectively.

Among grade I tumours there were 11 meningothelial, 8 transitional, 1 secretory, 1 fibrous and 1 microcystic; among grade II tumours – 8 atypical and 3 clear cell; all the grade III tumours were anaplastic (i.e. not papillary and rhabdoid). There was no significant difference between the staining intensity of PARP and p53 between subtypes of any grades; however, the case numbers were rather low to make statistically valid comparisons.

There was no significant correlation between PARP1 and p53 with Spearman's rank order correlation analysis (Fig. 4).

Discussion

Meningiomas are one of the most frequent intracranial tumours with diverse morphological variants. The current WHO classification [34] distinguishes 13 histological types. Nine of them belong to grade I; 2 and 2 belong to grade II and grade III, respectively. There are morphological criteria that define atypical (WHO grade II) and anaplastic (WHO grade III) meningiomas; however, the distinction is often difficult. Until now there has been no highly trusted immunohistochemical marker that can separate the different WHO grades reliably.

PARP1 protein role has been demonstrated in the repair of the damaged DNA, however this protein also has an important role in the caspase independent apoptotic pathway and in necrotic cell death. p53 is one of the most important tumour suppressor proteins, it has a role in almost half of the human tumours. Several studies have been performed about the p53 marker, but those ended with equivocal results. PARP1 protein expression in meningiomas has not been examined yet.

In this study, all of the 41 cases showed immunopositivity for both PARP1 and p53. The proportion

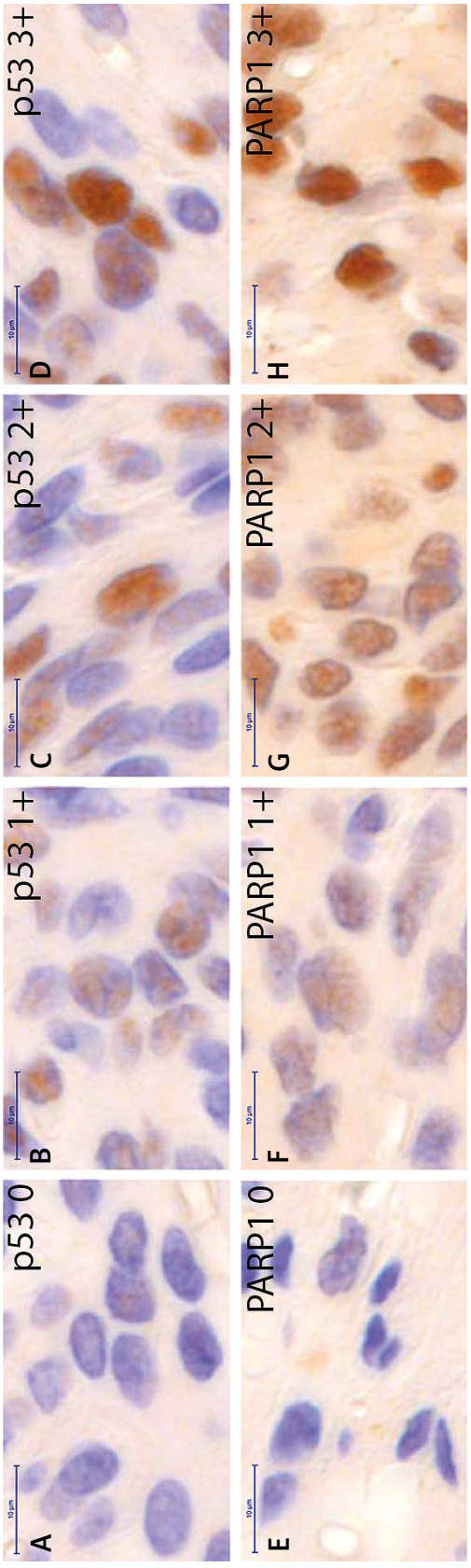

Fig. 2. Representative images of the different staining intensities. Immunostaining is performed for p53 **(A, B, C, D)** and PARP1 **(E, F, G, H)**. There are negative **(A, E)**, weak – 1+ **(B, F)**, moderate – 2+ **(C, G)** and strong – 3+ **(D, H)** positive cells. (PARP1 – poly(ADP-ribose) polymerase 1) (scale bar 10 µm).

Table I. Data sheet on cell counts showing staining intensities and their respective proportion to all counted cells. Staining index (Si)1-3 is the ratio of the immunopositive (1+, 2+, 3+) cells; and the Si2-3 is the ratio of the intense positive (2+, 3+) cells. (PARP1 – poly(ADP-ribose) polymerase 1)

Patient No.	Slide No.	WHO Grade	Subtype	PARP1						p53					
				0	1+	2+	3+	Si1-3	Si2-3	0	1+	2+	3+	Si1-3	Si2-3
1	1	I	Meningothelial	5	85	9	1	0.95	0.1	49	34	14	3	0.51	0.17
2	2	I	Meningothelial	16	39	37	8	0.84	0.45	49	43	8	0	0.51	0.08
3	3	I	Meningothelial	22	74	4	0	0.78	0.04	70	27	3	0	0.3	0.03
4	4	I	Transitional	10	65	25	0	0.9	0.25	46	50	4	0	0.54	0.04
5	5	I	Meningothelial	26	50	13	11	0.74	0.24	57	39	4	0	0.43	0.04
6	6	I	Meningothelial	8	83	9	0	0.92	0.09	76	24	0	0	0.24	0
7	7	I	Transitional	32	66	2	0	0.68	0.02	75	24	1	0	0.25	0.01
8	8	I	Meningothelial	15	83	2	0	0.85	0.02	52	34	14	0	0.48	0.14
9	9	I	Secretory	22	75	3	0	0.78	0.03	75	17	7	1	0.25	0.08
10	10	I	Meningothelial	23	37	38	2	0.77	0.4	71	23	6	0	0.29	0.06
11	11	I	Fibrous	21	30	24	25	0.79	0.49	47	50	3	0	0.53	0.03
12	12	I	Transitional	15	66	19	0	0.85	0.19	53	38	9	0	0.47	0.09
13	13	I	Meningothelial	7	93	0	0	0.93	0	86	12	2	0	0.14	0.02
14	14	I	Meningothelial	11	68	20	1	0.89	0.21	76	23	1	0	0.24	0.01
15	15	I	Microcystic	5	36	59	0	0.95	0.59	83	17	0	0	0.17	0
16	16	I	Transitional	10	85	4	1	0.9	0.05	52	43	5	0	0.48	0.05
17	17	I	Transitional	6	89	5	0	0.94	0.05	73	21	6	0	0.27	0.06
18	18	I	Transitional	16	33	48	3	0.84	0.51	79	18	3	0	0.21	0.03
19	19	II	Atypical	10	77	11	2	0.9	0.13	60	30	10	0	0.4	0.1
20	20	II	Atypical	8	64	26	2	0.92	0.28	76	24	0	0	0.24	0
21	21	II	Atypical	1	67	32	0	0.99	0.32	85	13	2	0	0.15	0.02
22	22	II	Clear cell	2	80	18	0	0.98	0.18	68	29	3	0	0.32	0.03
23	23	II	Atypical	14	71	10	5	0.86	0.15	78	18	4	0	0.22	0.04
23	24	I	Transitional	9	72	16	3	0.91	0.19	69	31	0	0	0.31	0
24	25	II	Atypical	6	71	21	2	0.94	0.23	80	18	2	0	0.2	0.02
25	26	II	Atypical	1	84	15	0	0.99	0.15	72	23	5	0	0.28	0.05
25	27	II	Clear cell	1	44	53	2	0.99	0.55	44	39	15	2	0.56	0.17
25	28	II	Clear cell	0	27	49	24	1	0.73	38	32	27	3	0.62	0.3
25	29	I	Meningothelial	10	81	9	0	0.9	0.09	67	29	4	0	0.33	0.04
25	30	I	Meningothelial	4	77	16	3	0.96	0.19	71	21	6	2	0.29	0.08
25	31	I	Transitional	9	82	9	0	0.91	0.09	67	27	6	0	0.33	0.06
26	32	II	Atypical	0	33	63	4	1	0.67	35	39	26	0	0.65	0.26
27	35	III	Anaplastic	10	81	9	0	0.9	0.09	59	29	10	2	0.41	0.12
27	34	III	Anaplastic	8	42	40	10	0.92	0.5	30	47	22	1	0.7	0.23
27	33	II	Atypical	4	83	10	3	0.96	0.13	71	21	7	1	0.29	0.08
28	36	III	Anaplastic	10	74	15	1	0.9	0.16	42	28	17	13	0.58	0.3
28	37	III	Anaplastic	20	66	14	0	0.8	0.14	49	20	17	14	0.51	0.31
28	38	III	Anaplastic	4	47	48	1	0.96	0.49	79	19	2	0	0.21	0.02
29	39	III	Anaplastic	14	71	14	1	0.86	0.15	68	22	7	3	0.32	0.1
30	40	III	Anaplastic	25	73	2	0	0.75	0.02	54	26	13	7	0.46	0.2
31	41	III	Anaplastic	28	62	10	0	0.72	0.1	76	15	9	0	0.24	0.09

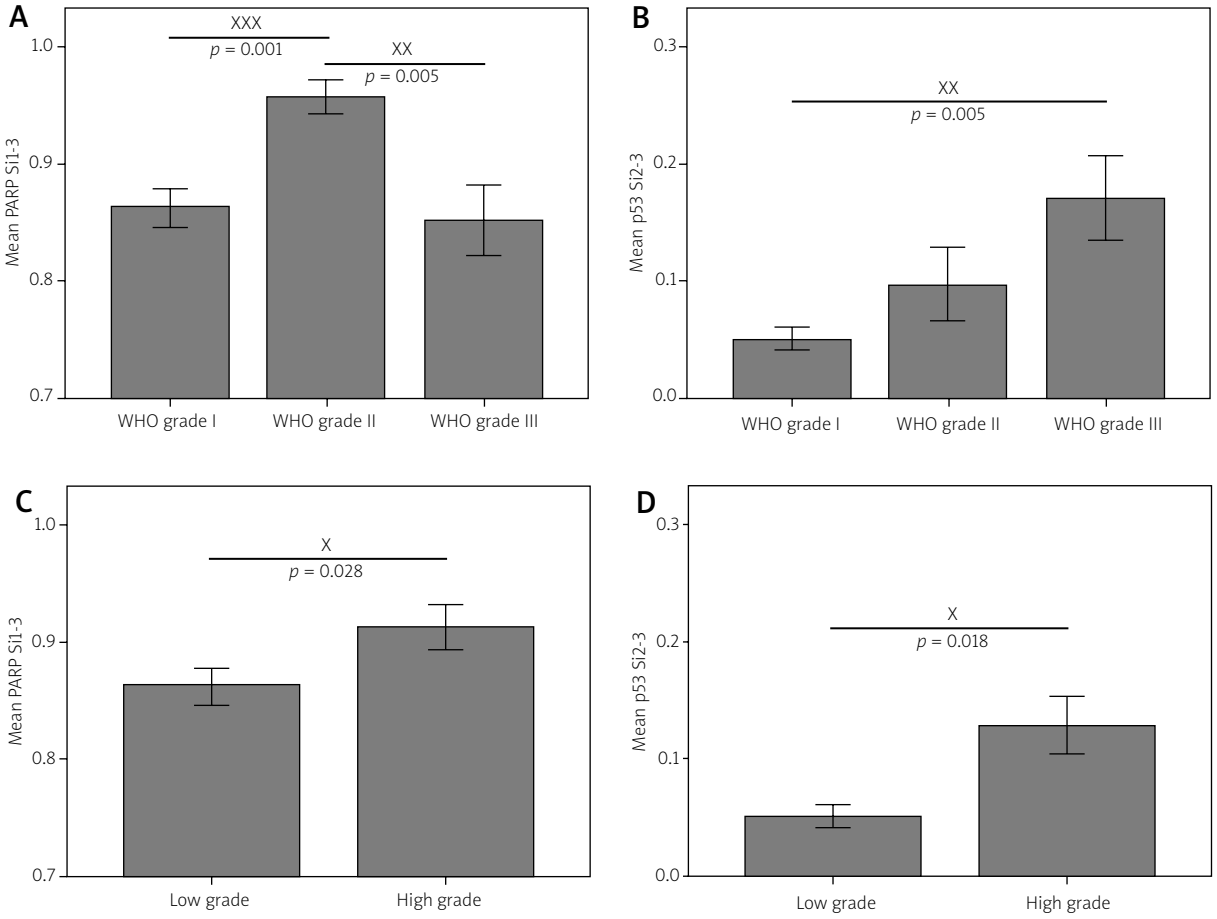

Fig. 3. p53 and PARP staining intensity varies according to the tumour grade. Mean values of the staining index (Si)1-3 for PARP1 **(A, C)** and Si2-3 for p53 **(B, D)** regarding to the WHO grades **(A, B)**, and low grade – WHO grade I and high grade – WHO grade II and WHO grade III **(C, D)**. Error bars ± standard error of mean (SEM). *p* values are calculated by Mann-Whitney *U* test. (PARP1 – poly(ADP-ribose) polymerase 1; staining index (Si)1-3 is the ratio of the immunopositive (1+, 2+, 3+) cells; and the Si2-3 is the ratio of the intense positive (2+, 3+) cells).

of positive cells (Si1-3) was higher in grade II tumours for PARP1, as compared to grade I and grade III meningiomas, respectively. Increased immunopositivity (Si2-3) was noted in grade III tumours for p53. Comparing the immunopositive cells in the low-grade meningiomas (grade I) and in the high-grade meningiomas (grade II and grade III) we found more immunopositive cells (Si1-3) for PARP1 and a higher staining intensity (Si2-3) for p53 in the high-grade tumours.

Performing a Spearman's rank order correlation and linear regression, there was no statistical correlation between either the presence of positivity or the intense immunoreactions for p53 and PARP1, thus the expression of these two proteins does not appear to be related to each other. We suggest that PARP1 activation increases in grade II tumours to cope with the DNA damage, whereas in grade III tumours PARP1 activity is decreased as a consequence of apoptotic-necrotic cell death and preceding overactivation and consecutive consumption of the protein and substrates.

Our data confirm that p53 protein plays a role in meningiomas, and indicate that the p53 activation might be a late event in the progression of meningothelial neoplasms.

Although further studies are necessary to elucidate the role of PARP1 and p53 in meningiomas,

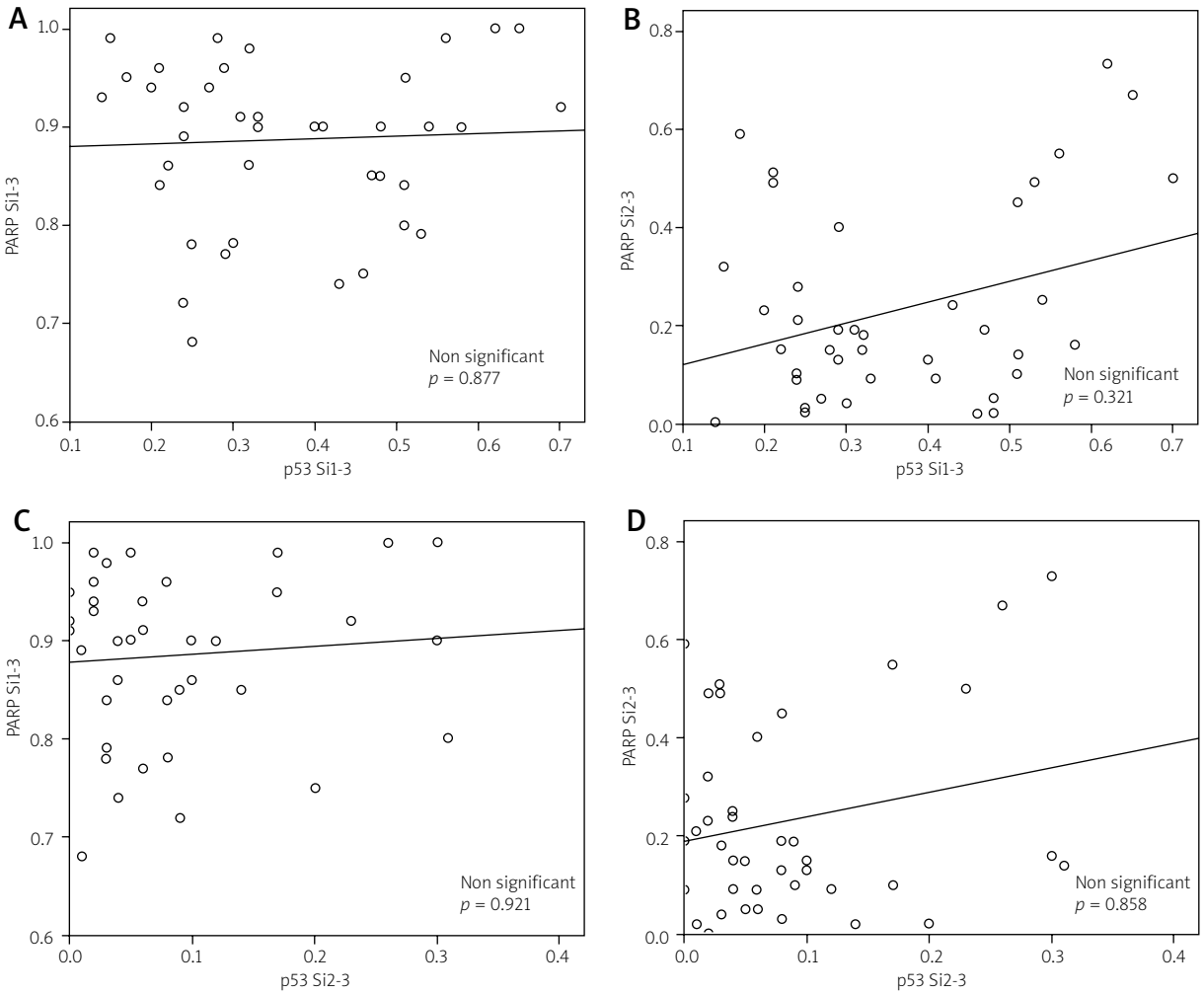

Fig. 4. Correlation between p53 and PAPR1 staining intensity. There is a dot plot and linear correlation of the results of staining indices. The *p* values are evaluated by Spearman's rank order correlation test. There are no significant correlations between the staining indices. (PARP1 – Poly(ADP-ribose) polymerase 1, staining index (Si)1-3 is the ratio of the immunopositive (1+, 2+, 3+) cells; and the Si2-3 is the ratio of the intense positive (2+, 3+) cells).

our data indicate that PARP1 and p53 immunohistochemistry represents useful and simple methods aiding the accurate diagnosis and grading of meningiomas.

Acknowledgements

The authors are thankful to Mrs Lívia Beke for technical assistance.

This study was supported by the Hungarian Brain Research Program – Grants No. KTIA_13_NAP-A-11/7 and V-3 (to T.H. and A.K.).

Disclosure

Authors report no conflict of interest.

References

1. Abramovich CM, Prayson RA. Histopathologic features and MIB-1 labeling indices in recurrent and nonrecurrent meningiomas. Arch Pathol Lab Med 1999; 123: 793-800.
2. Adamczyk A, Jesko H, Strosznajder RP. Alzheimer's disease related peptides affected cholinergic receptor mediated poly(ADP-ribose) polymerase activity in the hippocampus. Folia Neuropathol 2005; 43: 139-142.

3. Affar el B, Shah RG, Dallaire AK, Castonguay V, Shah GM. Role of poly(ADP-ribose) polymerase in rapid intracellular acidification induced by alkylating DNA damage. Proc Natl Acad Sci U S A 2002; 99: 245-250.
4. Amatya VJ, Takeshima Y, Sugiyama K, Kurisu K, Nishisaka T, Fukuhara T, Inai K. Immunohistochemical study of Ki-67 (MIB-1), p53 protein, p21WAF1, and p27KIP1 expression in benign, atypical, and anaplastic meningiomas. Hum Pathol 2001; 32: 970-975.
5. Bodi I, Hortobagyi T, Buk S. A 72-year-old woman with right frontal extra-axial mass. Brain Pathol 2008; 18: 279-282.
6. Brustmann H. Poly(adenosine diphosphate-ribose) polymerase expression in serous ovarian carcinoma: correlation with p53, MIB-1, and outcome. Int J Gynecol Pathol 2007; 26: 147-153.
7. Cho H, Ha SY, Park SH, Park K, Chae YS. Role of p53 gene mutation in tumor aggressiveness of intracranial meningiomas. J Korean Med Sci 1999; 14: 199-205.
8. Chozick BS, Benzil DL, Stopa EG, Pezzullo JC, Knuckey NW, Epstein MH, Finkelstein SD, Finch PW. Immunohistochemical evaluation of erbB-2 and p53 protein expression in benign and atypical human meningiomas. J Neurooncol 1996; 27: 117-126.
9. De Vos M, Schreiber V, Dantzer F. The diverse roles and clinical relevance of PARPs in DNA damage repair: Current state of the art. Biochem Pharmacol 2012; 84: 137-146.
10. el-Deiry WS, Tokino T, Velculescu VE, Levy DB, Parsons R, Trent JM, Lin D, Mercer WE, Kinzler KW, Vogelstein B. WAF1, a potential mediator of p53 tumor suppression. Cell 1993; 75: 817-825.
11. Farmer H, McCabe N, Lord CJ, Tutt AN, Johnson DA, Richardson TB, Santarosa M, Dillon KJ, Hickson I, Knights C, Martin NM, Jackson SP, Smith GC, Ashworth A. Targeting the DNA repair defect in BRCA mutant cells as a therapeutic strategy. Nature 2005; 434: 917-921.
12. Galia A, Calogero AE, Condorelli R, Fraggetta F, La Corte A, Ridolfo F, Bosco P, Castiglione R, Salemi M. PARP-1 protein expression in glioblastoma multiforme. Eur J Histochem 2012; 56: e9.
13. Gehl Z, Bai P, Bodnár E, Emri G, Remenyik É, Németh J, Gergely P, Virág L, Szabó É. Poly(ADP-ribose) in the skin and in melanomas. Histol Histopathol 2012; 27: 651-659.
14. Godoy H, Mhawech-Fauceglia P, Beck A, Miller A, Lele S, Odunsi K. Expression of poly (adenosine diphosphate-ribose) polymerase and p53 in epithelial ovarian cancer and their role in prognosis and disease outcome. Int J Gynecol Pathol 2011; 30: 139-144.
15. Hollstein M, Sidransky D, Vogelstein B, Harris CC. p53 mutations in human cancers. Science 1991; 253: 49-53.
16. Hortobagyi T, Görlach C, Benyó Z, Lacza Z, Hortobágyi S, Wahl M, Harkany T. Inhibition of neuronal nitric oxide synthase-mediated activation of poly(ADP-ribose) polymerase in traumatic brain injury: neuroprotection by 3-aminobenzamide. Neuroscience 2003; 121: 983-990.
17. Hortobagyi T, Troakes C, Nishimura AL, Vance C, van Swieten JC, Seelaar H, King A, Al-Sarraj S, Rogelj B, Shaw CE. Optineurin inclusions occur in a minority of TDP-43 positive ALS and FTLD-TDP cases and are rarely observed in other neurodegenerative disorders. Acta Neuropathol 2011; 121: 519-527.
18. Jaskolski D, Papierz T, Liberski PP, Sikorska B. Ultrastructure of meningiomas: autophagy is involved in the pathogenesis of "intranuclear vacuoles". Folia Neuropathol 2012; 50: 187-193.
19. Kamei Y, Watanabe M, Nakayama T, Kanamaru K, Waga S, Shiraishi T. Prognostic significance of p53 and p21WAF1/CIP1 immunoreactivity and tumor micronecrosis for recurrence of meningiomas. J Neurooncol 2000; 46: 205-213.
20. Karamitopoulou E, Perentes E, Tolnay M, Probst A. Prognostic significance of MIB-1, p53, and bcl-2 immunoreactivity in meningiomas. Hum Pathol 1998; 29: 140-145.
21. Kase M, Vardja M, Lipping A, Asser T, Jaal J. Impact of PARP-1 and DNA-PK expression on survival in patients with glioblastoma multiforme. Radiother Oncol 2011; 101: 127-131.
22. Kastan MB, Kuerbitz SJ. Control of G1 arrest after DNA damage. Environ Health Perspect 1993; 101 Suppl 5: 55-58.
23. Kato Y, Nishihara H, Mohri H, Kanno H, Kobayashi H, Kimura T, Tanino M, Terasaka S, Tanaka S. Clinicopathological evaluation of cyclooxygenase-2 expression in meningioma: immunohistochemical analysis of 76 cases of low and high-grade meningioma. Brain Tumor Pathol 2014; 31: 23-30.
24. Klauschen F, von Winterfeld M, Stenzinger A, Sinn BV, Budczies J, Kamphues C, Bahra M, Wittschieber D, Weichert W, Striefler J, Riess H, Dietel M, Denkert C. High nuclear poly-(ADP-ribose)-polymerase expression is prognostic of improved survival in pancreatic cancer. Histopathology 2012; 61: 409-416.
25. Koshland DE Jr. Molecule of the year. Science 1993; 262: 1953.
26. Kurosaki T, Ushiro H, Mitsuuchi Y, Suzuki S, Matsuda M, Matsuda Y, Katunuma N, Kangawa K, Matsuo H, Hirose T, Inayamall S, Shizuta Y. Primary structure of human poly(ADP-ribose) synthetase as deduced from cDNA sequence. J Biol Chem 1987; 262: 15990-15997.
27. Lacza Z, Horváth EM, Komjáti K, Hortobágyi T, Szabó C, Busija DW. PARP inhibition improves the effectiveness of neural stem cell transplantation in experimental brain trauma. Int J Mol Med 2003; 12: 153-159.
28. Lanzafame S, Torrisi A, Barbagallo G, Emmanuele C, Alberio N, Albanese V. Correlation between histological grade, MIB-1, p53, and recurrence in 69 completely resected primary intracranial meningiomas with a 6 year mean follow-up. Pathol Res Pract 2000; 196: 483-488.
29. Le Page F, Schreiber V, Dherin C, De Murcia G, Boiteux S. Poly(ADP-ribose) polymerase-1 (PARP-1) is required in murine cell lines for base excision repair of oxidative DNA damage in the absence of DNA polymerase beta. J Biol Chem 2003; 278: 18471-18477.
30. Lee MH, Na H, Kim EJ, Lee HW, Lee MO. Poly(ADP-ribosyl)ation of p53 induces gene-specific transcriptional repression of MTA1. Oncogene 2012; 31: 5099-5107.
31. Lewy-Trenda I, Omulecka A, Janczukowicz J, Papierz W. The morphological analysis of vasculature and angiogenic potential in meningiomas: immunoexpression of CD31 and VEGF antibodies. Folia Neuropathol 2003; 41: 149-153.
32. Longstreth WT Jr, Dennis LK, McGuire VM, Drangsholt MT, Koepsell TD. Epidemiology of intracranial meningioma. Cancer 1993; 72: 639-648.
33. Louis DN, Ohgaki H., Wiestler OD, Cavenee WK (eds.). WHO Classification of Tumours of the Central Nervous System. IARC, Lyon 2007.
34. Louis DN, Ohgaki H, Wiestler OD, Cavenee WK, Burger PC, Jouvet A, Scheithauer BW, Kleihues P. The 2007 WHO classifi-

cation of tumours of the central nervous system. Acta Neuropathol 2007; 114: 97-109.
35. Makogon NV, Aleksieieva IM. Poly(ADP-ribose) polymerase (PARP): physiological and pathological roles. Fiziol Zh 2012; 58: 95-112.
36. Malanga M, Pleschke JM, Kleczkowska HE, Althaus FR. Poly(ADP-ribose) binds to specific domains of p53 and alters its DNA binding functions. J Biol Chem 1998; 273: 11839-11843.
37. Matsuno A, Nagashima T, Matsuura R, Tanaka H, Hirakawa M, Murakami M, Tamura A, Kirino T. Correlation between MIB-1 staining index and the immunoreactivity of p53 protein in recurrent and non-recurrent meningiomas. Am J Clin Pathol 1996; 106: 776-781.
38. Matyja E, Kroh H, Bojarski P. Intracranial meningiomas following irradiation therapy for brain tumors. Folia Neuropathol 1994; 32: 253-254.
39. Matyja E, Taraszewska A, Marszalek P. Necrosis and apoptosis of tumor cells in embolized meningiomas: histopathology and P53, BCL-2, CD-68 immunohistochemistry. Folia Neuropathol 1999; 37: 93-98.
40. Molloy-Simard V, St-Laurent JF, Vigneault F, Gaudreault M, Dargis N, Guérin MC, Leclerc S, Morcos M, Black D, Molgat Y, Bergeron D, de Launoit Y, Boudreau F, Desnoyers S, Guérin S. Altered expression of the poly(ADP-ribosyl)ation enzymes in uveal melanoma and regulation of PARG gene expression by the transcription factor ERM. Invest Ophthalmol Vis Sci 2012; 53: 6219-6231.
41. Nagashima G, Aoyagi M, Yamamoto M, Yamamoto S, Wakimoto H, Ohno K, Yamamoto K, Hirakawa K. P53 overexpression and proliferative potential in malignant meningiomas. Acta Neurochir (Wien) 1999; 141: 53-61.
42. Oei SL, Keil C, Ziegler M. Poly(ADP-ribosylation) and genomic stability. Biochem Cell Biol 2005; 83: 263-269.
43. Ohgaki H, Eibl RH, Schwab M, Reichel MB, Mariani L, Gehring M, Petersen I, Höll T, Wiestler OD, Kleihues P. Mutations of the p53 tumor suppressor gene in neoplasms of the human nervous system. Mol Carcinog 1993; 8: 74-80.
44. Ohkoudo M, Sawa H, Hara M, Saruta K, Aiso T, Ohki R, Yamamoto H, Maemura E, Shiina Y, Fujii M, Saito I. Expression of p53, MDM2 protein and Ki-67 antigen in recurrent meningiomas. J Neurooncol 1998; 38: 41-49.
45. Omulecka A, Papierz W, Nawrocka-Kunecka A, Lewy-Trenda I. Immunohistochemical expression of progesterone and estrogen receptors in meningiomas. Folia Neuropathol 2006; 44: 111-115.
46. Ozen O, Demirhan B, Altinors N. Correlation between histological grade and MIB-1 and p53 immunoreactivity in meningiomas. Clin Neuropathol 2005; 24: 219-224.
47. Perry A, Scheithauer BW, Stafford SL, Lohse CM, Wollan PC. "Malignancy" in meningiomas: a clinicopathologic study of 116 patients, with grading implications. Cancer 1999; 85: 2046-2056.
48. Perry A, Stafford SL, Scheithauer BW, Suman VJ, Lohse CM. The prognostic significance of MIB-1, p53, and DNA flow cytometry in completely resected primary meningiomas. Cancer 1998; 82: 2262-2269.
49. Prayson RA. Malignant meningioma: a clinicopathologic study of 23 patients including MIB1 and p53 immunohistochemistry. Am J Clin Pathol 1996; 105: 719-726.
50. Pykett MJ, Landers J, George DL. Expression patterns of the p53 tumor suppressor gene and the mdm2 proto-oncogene in human meningiomas. J Neurooncol 1997; 32: 39-44.
51. Rojo F, García-Parra J, Zazo S, Tusquets I, Ferrer-Lozano J, Menendez S, Eroles P, Chamizo C, Servitja S, Ramírez-Merino N, Lobo F, Bellosillo B, Corominas JM, Yelamos J, Serrano S, Lluch A, Rovira A, Albanell J. Nuclear PARP-1 protein overexpression is associated with poor overall survival in early breast cancer. Ann Oncol 2012; 23: 1156-1164.
52. Sabisz M, Wesierska-Gadek J, Skladanowski A. Increased cytotoxicity of an unusual DNA topoisomerase II inhibitor compound C-1305 toward HeLa cells with downregulated PARP-1 activity results from re-activation of the p53 pathway and modulation of mitotic checkpoints. Biochem Pharmacol 2010; 79: 1387-1397.
53. Schiewer MJ, Goodwin JF, Han S, Brenner JC, Augello MA, Dean JL, Liu F, Planck JL, Ravindranathan P, Chinnaiyan AM, McCue P, Gomella LG, Raj GV, Dicker AP, Brody JR, Pascal JM, Centenera MM, Butler LM, Tilley WD, Feng FY, Knudsen KE. Dual roles of PARP-1 promote cancer growth and progression. Cancer Discov 2012; 2: 1134-1149
54. Songin M, Jeśko H, Czapski G, Adamczyk A, Strosznajder RP. GSK-3beta and oxidative stress in aged brain. Role of poly(ADP-ribose) polymerase-1. Folia Neuropathol 2007; 45: 220-229.
55. Strosznajder R, Gadamski R, Walski M. Inhibition of poly(ADP-ribose) polymerase activity protects hippocampal cells against morphological and ultrastructural alteration evoked by ischemia-reperfusion injury. Folia Neuropathol 2005; 43: 156-165.
56. Taraszewska A, Matyja E. Lectin binding pattern in meningiomas of various histological subtypes. Folia Neuropathol 2007; 45: 9-18.
57. Terzi A, Saglam EA, Barak A, Soylemezoglu F. The significance of immunohistochemical expression of Ki-67, p53, p21, and p16 in meningiomas tissue arrays. Pathol Res Pract 2008; 204: 305-314.
58. Wieler S, Gagné JP, Vaziri H, Poirier GG, Benchimol S. Poly(ADP-ribose) polymerase-1 is a positive regulator of the p53-mediated G1 arrest response following ionizing radiation. J Biol Chem 2003; 278: 18914-18921.
59. Wiemels J, Wrensch M, Claus EB. Epidemiology and etiology of meningioma. J Neurooncol 2010; 99: 307-314.
60. Yu SW, Andrabi SA, Wang H, Kim NS, Poirier GG, Dawson TM, Dawson VL. Apoptosis-inducing factor mediates poly(ADP-ribose) (PAR) polymer-induced cell death. Proc Natl Acad Sci USA 2006; 103: 18314-18319.
61. Yu SW, Wang H, Poitras MF, Coombs C, Bowers WJ, Federoff HJ, Poirier GG, Dawson TM, Dawson VL. Mediation of poly(ADP-ribose) polymerase-1-dependent cell death by apoptosis-inducing factor. Science 2002; 297: 259-263.
62. Zhang Q, Li Y, Li X, Zhou W, Shi B, Chen H, Yuan W. PARP-1 Val762Ala polymorphism, CagA+ H. pylori infection and risk for gastric cancer in Han Chinese population. Mol Biol Rep 2009; 36: 1461-1467.

Original article

Folia Neuropathologica

Neuroprotective properties of ciliary neurotrophic factor on retinoic acid (RA)-predifferentiated SH-SY5Y neuroblastoma cells

Ke Wang[1], Fanfan Zhou[2], Xue Zhu[1], Kai Zhang[1], Biao Huang[1], Lan Zhu[1], Ling Zhu[3]

[1]Key Laboratory of Nuclear Medicine, Ministry of Health, Jiangsu Key Laboratory of Molecular Nuclear Medicine, Jiangsu Institute of Nuclear Medicine, Wuxi, Jiangsu Province, China, [2]The Faculty of Pharmacy, University of Sydney, New South Wales, Australia, [3]Save Sight Institute, University of Sydney, New South Wales, Australia

Folia Neuropathol 2014; 52 (2): 121-127 DOI: 10.5114/fn.2014.43783

Abstract

Ciliary neurotrophic factor (CNTF) is a neurocytokine, which could promote survival and/or differentiation in many cell types. In this study, the biological effects of CNTF on retinoic acid (RA)-predifferentiated SH-SY5Y neuroblastoma cells and the underlying molecular mechanism of this effect were investigated for the first time. The results showed that RA was able to increase cells susceptibility to CNTF via regulating the expression levels of CNTF receptors. A further study revealed that CNTF could induce phosphorylation of STAT3, Akt and ERK1/2 in RA-predifferentiated SH-SY5Y neuroblastoma cells, while the promoting activity of CNTF on survival and neurite growth of cells was attenuated by co-treatment with JAK2 inhibitor AG490 (25 μM), STAT3 inhibitor Curcumin (50 μM), PI3K inhibitor LY-294002 (50 μM), but not by co-treatment with MEK inhibitor PD98059 (50 μM). These findings suggested that JAK2/STAT3, as well as PI3K/Akt, play important roles in mediating the survival and neurite growth response of RA-predifferentiated cells to CNTF. Our study may be useful to further understand the functional role of CNTF and offer a convenient model to explore the therapeutic potential of CNTF in neurodegenerative diseases.

Key words: *CNTF, SH-SY5Y neuroblastoma cells, survival, neurite outgrowth, signalling pathway.*

Introduction

Neurotrophic factors such as the ciliary neurotrophic factor (CNTF) are essential proteins for the maintenance and survival of neurons in both developing and mature nervous systems [14,16,21]. In particular, CNTF is responsible for neurotransmitter synthesis and neurite outgrowth in certain neuronal populations [22,26]. CNTF is a 25-kDa polypeptide that was originally isolated as a target-derived survival factor of parasympathetic ciliary ganglion neurons [19]. It is believed that CNTF's physiological role only becomes apparent after tissue injury due to its lack of hydrophobic sequence. Known cell-surface receptors for CNTF include CNTF receptor α (CNTFRα), gp130, and LIF receptor (LIFR) [3,4]. Binding of CNTF to CNTFRα triggers heterodimerization of gp130 and LIFR, forming an active trimeric receptor complex and activates the downstream signalling pathway [25]. It has been established that JAK2/STAT3 pathway is mainly involved in survival of neurons in

Communicating author:
Ling Zhu, Save Sight Institute, University of Sydney, New South Wales, Australia, phone: +86 13814247452, e-mail: ling.zhu@sydney.edu.au

response to CNTF [11,12,26]. Phosphorylated STAT3 dimerizes and translocates to the nucleus to regulate target gene transcription [27]. In addition, CNTF can also trigger and activate PI3K/Akt or MEK/ERK pathways, either concomitantly or independently of JAK2/STAT3 signalling pathway [1,5,6,24].

In cell-culture experiments, CNTF has also been established to be an important neurocytokine for the survival of a variety of neuronal subpopulations, including dorsal root ganglia, sympathetic neurons, GABAergic septohippocampal neurons, and motor neurons [8,9]. A previous study conducted by Kazunori *et al.* has found that CNTF may promote the survival and neurite outgrowth of DRG neuron from an adult rat after it had been cultured for 7 days [24]. However, currently, there is little information available on the effects of CNTF on human neuroblastoma cells. Human neuroblastoma cells are currently used as an *in vitro* model of neuronal function and differentiation [20]. In particular, a human neuroblastoma dopaminergic neuronal cell line – SH-SY5Y is used as a model for neurodegenerative disorders as the cells can be converted to various types of functional neurons through the addition of specific compounds such as retinoic acid (RA), phorbol ester or staurosporine [2,17]. In many studies, SH-SY5Y neuroblastoma cells are often induced to differentiate by RA to obtain more neuron-like properties, including neurite outgrowth and morphological changes, this in turn allows the mimicking of responses of neurons [7]. A previous study has reported that SH-SY5Y neuroblastoma cells expressed functional CNTF receptors and the expression levels were found to increase several folds through continuous exposure to RA [10,18]. However, limited studies have been reported about the CNTF response of SH-SY5Y neuroblastoma cells following RA treatment.

In this study, we tried to elucidate the biological effects of CNTF on RA-predifferentiated SH-SY5Y neuroblastoma cells for the first time. Moreover, the underlying molecular mechanisms of such effects were also explored in regards to change of related signalling pathways in SH-SY5Y neuroblastoma cells.

Material and methods

Materials and chemicals

Recombinant human CNTF was produced in *Escherichia coli* by our laboratory. The purity of CNTF is higher than 95% by high-performance liquid chromatography (HPLC) and the molecular weight of which is 24 kDa by sodium dodecyl sulfate-polyacrylamide gel electrophoresis SDS-PAGE (data not shown). All cell culture reagents were purchased from Gibco (Grand Island, NY, USA). Retinoic acid, AG490, Curcumin, LY-294002 and PD98059 were purchased from Sigma-Aldrich (St Louis, Mo, USA). Trypan blue, Ribonuclease A (Rnase A), Polyvinylidene Fluoride (PVDF) membranes and enhanced chemiluminescence (ECL) detection kit were purchased from Beyotime (Nantong, China). Antibodies against CNTFRα, gp130, LIFR and β-actin were obtained from Santa Cruz Biotechnology (CA, USA). Antibodies against P-STAT3, STAT3, P-Akt, Akt, P-ERK1/2, ERK1/2 were obtained from Cell Signalling Technology (MA, USA). All other chemicals and reagents were of analytical grade.

Cell culture

The SH-SY5Y neuroblastoma cell line was obtained from the Shanghai Institute of Cell Biology, Chinese Academy of Sciences (Shanghai, China). Cells were grown in Dulbecco's modified Eagle's medium (DMEM) supplemented with 10% foetal bovine serum and 1% penicillin-streptomycin. Cells were maintained at 37°C in a saturated humidity atmosphere containing 95% of air and 5% of CO_2. The medium was changed every 3 days. For cell survival and neurite outgrowth, cells were plated in 35-mm-diameter (Corning, NY, USA) at an initial density of 5×10^4 cells per well.

Assay for cell survival and neurite outgrowth

The number of living cells was established by staining with trypan blue and counting in the hemocytometer (Bürker). Cells were treated with RA at 10 μM for 5 days, washed three times with DMEM and switched to serum-free DMEM medium containing various concentrations of CNTF (0, 5, 50, 500 ng/mL) for 48 h. Before switching to CNTF-containing medium, the living cells were counted and the resulting value was defined as 100% survival. Results were therefore expressed as a mean ± SEM percentage of this value. For evaluation of neurite outgrowth, cells treated with the indicated drugs were observed in a phase-contrast microscope (Olympus X51, Japan) and the cell bodies and neurites were counted. The ratio between neurites and cell bodies was calculated yielding the average of neurites per neuron.

Measurement of neuropoietic activities of CNTF in the presence of signalling pathway inhibitors

The effects of related signalling pathway inhibitors on the CNTF-induced survival and neurite outgrowth of RA-differentiated SH-SY5Y neuroblastoma cells were investigated. Cells were treated for 5 days with RA at 10 μM and then cultured with CNTF (50 ng/mL) in the absence or presence of JAK2 inhibitor AG490 (25 μM), STAT3 inhibitor Curcumin (50 μM), PI3K inhibitor LY-294002 (50 μM) and MEK inhibitor PD98059 (50 μM) for 48 h, respectively. The survival and neurite outgrowth of cells were evaluated.

Immunocytochemistry

Cells were collected and fixed with 4% paraformaldehyde for 10 min at 4°C, and then treated with 0.1% Triton-X-100 in phosphate buffer saline (PBS) for 5 min at room temperature or with 100% methanol for 10 min at -20°C. The fixed cells were incubated overnight at 4°C with CNTFR antibody, gp130 polyclonal antibody and LIFR antibody, respectively. All of which were diluted with 20 mM of PBS containing 0.4% Block Ace. After rinsing with PBS, the cells were incubated for 1 h at 37°C with peroxidase-conjugated secondary antibodies. The immunoreaction was visualized as described above.

Western blot analysis

Cell extracts were prepared from cultured cells using lysis buffer (10 mM of Tris [pH 7.4], 150 mM of NaCl, 5 mM of ethylenediaminetetraacetic acid [EDTA], 1% Triton-X-100, 1% Tergitol-type NP40, and the following protease inhibitors: aprotinin, benzamidine, leupeptin, pepstatin A, and phenylmethanesulfonyl fluoride [PMSF]). The protein concentration of samples was determined with Bradford method [25]. The samples (50 μg) were then applied to 10% SDS-PAGE and transblotted onto PVDF membranes. After blocking with 5% bovine serum albumin (BSA) in Tris-buffer saline (TBST) for 1 hour, membranes were incubated with the primary antibodies (all in 1 : 500 dilutions) overnight and followed by a secondary antibody (all in 1 : 200 dilutions) incubation for 1 hour at room temperature. Protein bands were visualized by ECL detection kit. The density of each band was normalized by β-actin.

Statistical analysis

All data are expressed as mean ± SEM. Point-to-point comparisons were made by Student's *t*-test. Groups were compared by two-way ANOVA using the unpaired Tukey-Kramer method as post-test. All experiments were done in triplicates and the results were indicative of three independent studies. Results were considered significantly different if $P < 0.05$.

Results

Effects of RA treatment on the expressions of CNTF receptors

The immunocytochemical analysis confirmed that SH-SY5Y neuroblastoma cells expressed the CNTF receptor complex (CNTFRα, gp130 and LIFR) at the cell surface, which is consistent with previous studies

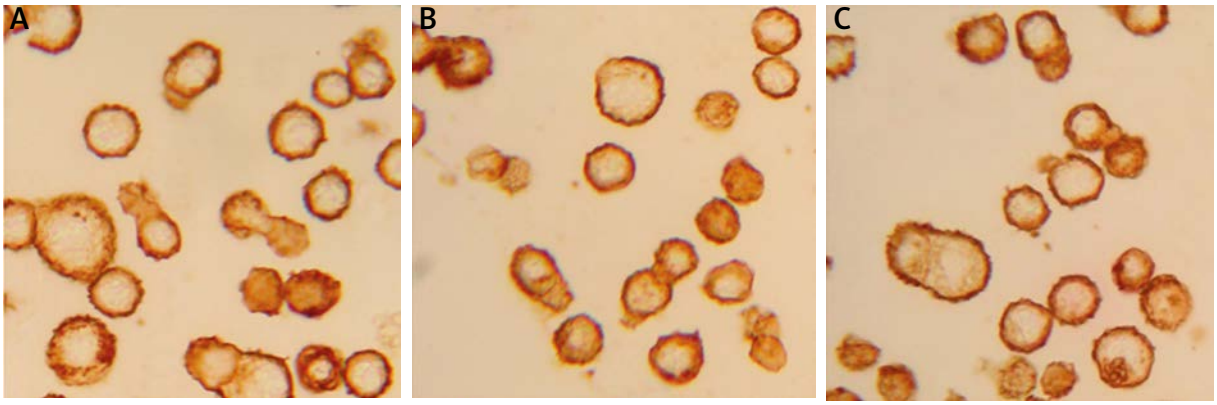

Fig. 1. Immunocytochemical localization of CNTFRα, gp130 and LIFR at the surface of cultured SH-SY5Y neuroblastoma cells. Cells were cultured for 24 h and the peroxidase reactions with antibodies to CNTFRα **(A)**, gp130 **(B)** and LIFR **(C)** were performed by immunocytochemical analysis.

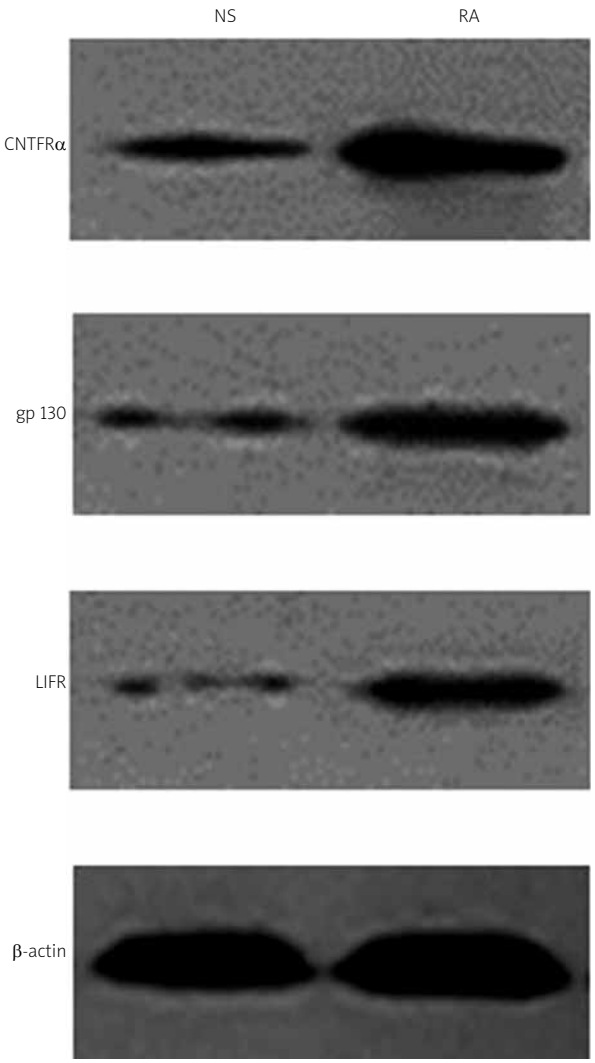

Fig. 2. Effects of RA treatment on the expressions of CNTF receptors (CNTFRα, gp130 and LIFR) on cultured SH-SY5Y neuroblastoma cells. Cells were treated for 5 days with 10 μM RA and the reactions with antibodies to CNTFRα, gp130 and LIFR (all in 1 : 500 dilutions) were performed by western blot analysis. NS: non-stimulated cells.

(Fig. 1) [12,18]. Effects of exposure of RA on the up-regulation of the expression level of CNTF receptors were also examined. As shown in Fig. 2, a 2.2-fold increase for CNTFRα, 2.7-fold increase for gp130 and 3.2-fold increase for LIFR in band intensity after 5 days of RA treatment (10 μM) as compared to those of non-stimulated controls were observed. The results suggested that RA might increase the responsiveness of CNTF via regulating the levels of CNTF receptors.

Effects of CNTF on survival and neurite growth of RA-pretreated cells

SH-SY5Y neuroblastoma cells were cultured for 5 days in the presence of 10 μM RA and then switched to serum-free medium supplemented with CNTF at various concentrations. After an additional 48 hours in culture, cell survival was evaluated by means of the trypan blue staining. The results showed that CNTF had a significant effect on the cell survival of RA-pretreated cells (Fig. 3A). In addition, effects of CNTF on neurite growth were further investigated. After cultured with CNTF for 48 hours, RA-pretreated cells acquired rounded, phase-bright bodies and displayed long neurites and the ratio between neurites and cell bodies was increased in a dose-dependent relationship (Fig. 3B).

Effects of CNTF on signalling pathways of RA-pretreated cells

The activation status of CNTF receptors-related signalling pathways was assessed to elucidate the molecular mechanism of the biological effects of CNTF. Western blot analysis showed that cells treated by RA for 5 days were acutely stimulated by CNTF where the expressions of phosphorylated signalling molecules including P-STAT3, P-Akt and P-ERK1/2 were undetectable initially but were rapidly induced by co-treatment with CNTF for 15 min and still detectable after 4 h of exposure to CNTF (Fig. 4). These findings suggested that CNTF could induce phosphorylation of STAT3, Akt and ERK1/2 in RA-pretreated SH-SY5Y cells.

Effects of signalling pathway inhibitors on CNTF-induced survival and neurite growth of RA-pretreated cells

Based on previous results, we further investigated which pathways are involved in CNTF-induced survival and neurite outgrowth, using the inhibitors of individual pathways: JAK2 inhibitor – AG490, STAT3 inhibitor – Curcumin, PI3K inhibitor – LY-294002 and MEK inhibitor – PD98059. The promoting activity of CNTF on survival and neurite growth of RA-pretreated cells was attenuated by co-treatment with AG490 (25 μM), Curcumin (50 μM), LY294002 (50 μM), but not by co-treatment with PD98059 (50 μM). These findings suggested that the JAK2/STAT3 pathway, as well as PI3K/Akt pathway, were the principal pathways in CNTF-induced survival and neurite growth of RA-pretreated cells.

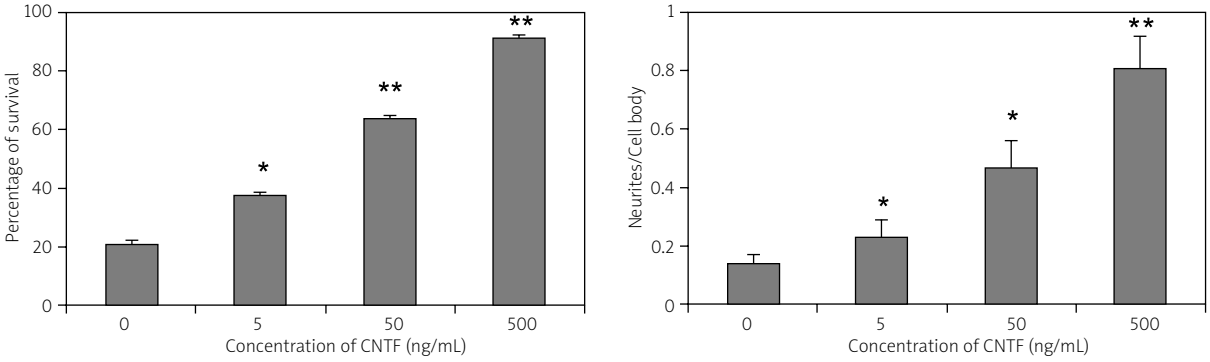

Fig. 3. Effects of CNTF on survival and neurite growth of RA-pretreated SH-SY5Y neuroblastoma cells. Cells were treated for 5 days with 10 μM RA and then cultured in a serum-free medium containing the indicated concentrations of CNTF (0, 5, 50, 500 ng/mL) for an additional period of 48 h. **A)** Cell survival was assessed by trypan blue staining. **B)** Neurite outgrowth of cells was scored as described in Materials and methods. Data are mean ± SEM values. **P* < 0.05 vs. control, ***P* < 0.01 vs. control.

Discussion

Until now, few studies have focused on the effects of CNTF on human neuroblastoma cells such as SH-SY5Y, which could be differentiated to neuronal-like cells using retinoic acid and used as a model for neurodegenerative disorders [15,22,23]. In this study, we examined the biological effects of CNTF on RA-predifferentiated SH-SY5Y neuroblastoma cells for the first time and further explored the molecular mechanisms of such effects.

Our data confirmed that SH-SY5Y cells express a functional CNTF receptor complex including CNTFRα, gp130 and LIFR at the cell surface and showed a stable increase in protein levels after treatment with RA for 5 days, which are consistent with those in previous studies [23]. We further investigated if RA pretreatment was able to enhance the cells sensitivity to CNTF via regulating the CNTF receptor levels. The results showed that CNTF exerted the most striking effects on cell survival and neurite growth of RA-pretreated cells compared with those lacking neurotrophic support, which indicated that high expressions of CNTF receptors induced by RA are biologically active.

The JAK2/STAT3 pathway is the main signalling cascade used by CNTF in many cell types, however, CNTF can also signal through PI3K/Akt and/or MEK/ERK pathways [13]. To clarify this, the signalling pathway of CNTF in RA-predifferentiated SH-SY5Y neuroblastoma cells was also investigated in this study. The results from our western blot analysis indicated that

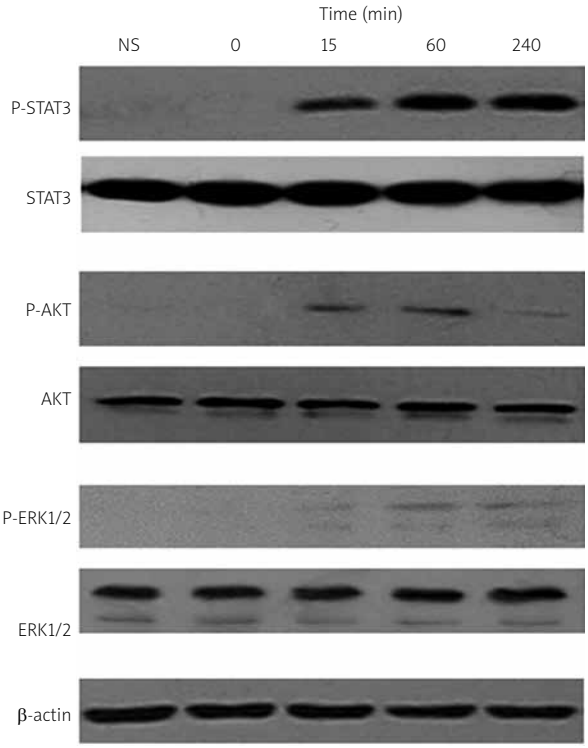

Fig. 4. Effects of CNTF on the expressions of signalling pathway molecules on RA-pretreated SH-SY5Y neuroblastoma cells. Cells were treated for 5 days with 10 μM RA and cultured in serum-free medium containing the 50 ng/mL CNTF for an additional time. Then, the reactions with antibodies to P-STAT3, STAT3, P-Akt, Akt, P-ERK1/2, ERK1/2 (all in 1 : 500 dilution) were performed by western blot analysis. The density of each band was normalized by β-actin. NS: non-stimulated cells.

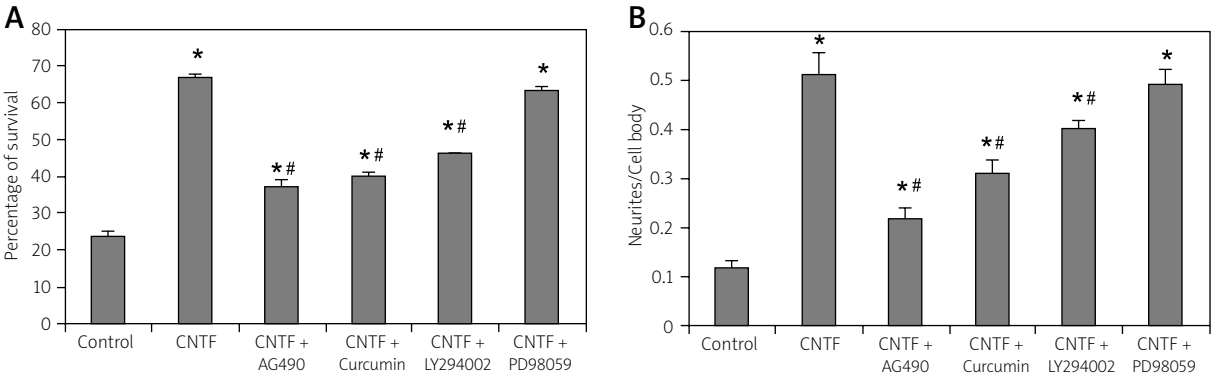

Fig. 5. Effects of signalling pathway inhibitors on CNTF-induced survival and neurite growth of RA-pretreated SH-SY5Y neuroblastoma cells. Cells were treated for 5 days with 10 μM RA and then cultured in serum-free medium containing the CNTF (50 ng/mL) and inhibitors [AG490 (25 μM), Curcumin (50 μM), LY-294002 (50 μM) and PD98059 (50 μM)] for an additional period of 48 h. **A)** Cell survival was assessed by trypan blue staining. **B)** Neurite outgrowth of cells was scored as described in Materials and methods. Data are mean ± SEM values. $^{*}P < 0.05$ vs. control, $^{\#}P < 0.05$ vs. CNTF.

CNTF could induce the expressions of phosphorylated signalling molecules including P-STAT3, P-Akt and P-ERK1/2 in cells pretreated by RA. Further survival and neurite outgrowth assays showed that promoting activity of CNTF was attenuated by co-treatment with JAK2 inhibitor AG490, STAT3 inhibitor Curcumin, PI3K inhibitor LY294002, but not by co-treatment with MEK inhibitor PD98059. These findings suggested that the MEK/ERK pathway is unlikely to be a crucial pathway for CNTF-induced survival and neurite outgrowth activity of RA-predifferentiated SH-SY5Y neuroblastoma cells, while the JAK2/STAT3 pathway, as well as PI3K/Akt pathway, played important roles in mediating the neuroprotective function of CNTF. Further research is required to elucidate how these signalling pathways exert their effect during CNTF-induced survival and neurite outgrowth in RA-predifferentiated SH-SY5Y neuroblastoma cells.

In conclusion, our study has enhanced our understanding towards the functional role of CNTF on RA-predifferentiated SH-SY5Y neuroblastoma cells in promoting cell survival and neurite growth. We also found that the JAK2/STAT3 and PI3K/Akt signalling pathways are mainly involved in the CNTF-induced survival and neurite outgrowth activity of RA-predifferentiated SH-SY5Y neuroblastoma cells. These results may supplement the current understanding of how CNTF functions in diverse tissues and organisms, which offers a convenient model to explore the therapeutic potential of CNTF in neurodegenerative diseases.

Acknowledgements

This work is supported by grants from the National Natural Science Foundation (81300787), the Natural Science Foundation of Jiangsu Province (BK2011168, BK2012105) and the Technology Infrastructure Plan of Jiangsu Province – Technology Public Service Platform (BM2012066).

Disclosure

Authors report no conflict of interest.

References

1. Alonzi T, Middleton G, Wyatt S, Buchman V, Betz UA, Müller W, Musiani P, Poli V, Davies AM. Role of STAT3 and PI 3-knase/Akt in mediating the survival actions of cytokines on sensory neurons. Mol Cell Neurosci 2001; 18: 270-282.
2. Cheung Y-T, Lau WK-W, Yu M-S, Lai CS-W, Yeung S-C, So K-F, Chang RC-C. Effects of all-trans-retinoic acid on human SH-SY5Y neuroblastoma as in vitro model in neurotoxicity research. Neurotoxicology 2009; 30: 127-135.
3. Davis S, Aldrich TH, Stahl N, Pan L, Taga T, Kishimoto T, Ip NY, Yancopoulos GD. LIFR beta and gp130 as heterodimerizing signal transducers of the tripartite CNTF receptor. Science 1993; 260: 1805-1808.
4. Davis S, Aldrich TH, Valenzuela DM, Wong V, Furth ME, Squinto SP, Yancopoulos GD. The receptor for ciliary neurotrophic factor. Science 1991; 253: 59-63.
5. Dolcet X, Soler RM, Gould TW, Egea J, Oppenheim RW, Comella JX. Cytokines promote motoneuron survival through the Janus kinase-dependent activation of the phosphatidylinositol 3-kinase pathway. Mol Cell Neurosci 2001; 18: 619-631.

6. Do Rhee K, Goureau O, Chen S, Yang X-J. Cytokine-induced activation of signal transducer and activator of transcription in photoreceptor precursors regulates rod differentiation in the developing mouse retina. J Neurosci 2004; 24: 9779-9788.
7. Encinas M, Iglesias M, Liu Y, Wang H, Muhaisen A, Cena V, Gallego C, Comella JX. Sequential Treatment of SH-SY5Y Cells with Retinoic Acid and Brain-Derived Neurotrophic Factor Gives Rise to Fully Differentiated, Neurotrophic Factor-Dependent, Human Neuron-Like Cells. J Neurochem 2000; 75: 991-1003.
8. Ernsberger U, Sendtner M, Rohrer H. Proliferation and differentiation of embryonic chick sympathetic neurons: effects of ciliary neurotrophic factor. Neuron 1989; 2: 1275-1284.
9. Ip N, Li Y, Van de Stadt I, Panayotatos N, Alderson R, Lindsay R. Ciliary neurotrophic factor enhances neuronal survival in embryonic rat hippocampal cultures. J Neurosci 1991; 11: 3124-3134.
10. Johnson RM, McNeeley PA, DeMoor K, Stewart GR, Glaeser BS, Pitchford S. Recombinant human ciliary neurotrophic factor stimulates the metabolic activity of SH-SY5Y cells as measured by a cytosensor microphysiometer. Brain Res 1994; 646: 327-331.
11. Kaur N, Kim IJ, Higgins D, Halvorsen SW. Induction of an interferon-γ Stat3 response in nerve cells by pre-treatment with gp130 cytokines. J Neurochem 2003; 87: 437-447.
12. Kaur N, Wohlhueter AL, Halvorsen SW. Activation and inactivation of signal transducers and activators of transcription by ciliary neurotrophic factor in neuroblastoma cells. Cell Signal 2002; 14: 419-429.
13. Kruger NJ. The Bradford method for protein quantitation. In: Basic Protein and Peptide Protocols. Walker JM (ed). Humana Press, New York 1994; pp. 9-15.
14. Linker R, Gold R, Luhder F. Function of neurotrophic factors beyond the nervous system: inflammation and autoimmune demyelination. Crit Rev Immunol 2009; 29: 43-68.
15. Li P, Wang Z, Yan J, Li Z, Jiang C, Ni X, Yang Y, Liu F, Lu C. Neuro-protective effects of CNTF on hippocampal neurons via an unknown signal transduction pathway. Chin Sci Bull 2006; 51: 48-53.
16. Maisonpierre PC, Belluscio L, Squinto S, Ip NY, Furth ME, Lindsay RM, Yancopoulos GD. Neurotrophin-3: a neurotrophic factor related to NGF and BDNF. Science 1990; 247: 1446-1451.
17. Malek RL, Halvorsen SW. ciliary neurotrophic factor and phorbol ester each decrease selected STAT3 pools in neuroblastoma cells by proteasome-dependent mechanisms. Cytokine 1999; 11: 192-199.
18. Malek RL, Halvorsen SW. Opposing regulation of ciliary neurotrophic factor receptors on neuroblastoma cells by distinct differentiating agents. J Neurobiol 1997; 32: 81-94.
19. Negro A, Corona G, Bigon E, Martini I, Grandi C, Skaper S, Callegaro L. Synthesis, purification, and characterization of human ciliary neuronotrophic factor from E. coli. J Neurosci Res 1991; 29: 251-260.
20. Påhlman S, Mamaeva S, Meyerson G, Mattsson ME, Bjelfman C, Ortoft E, Hammerling U. Human neuroblastoma cells in culture: a model for neuronal cell differentiation and function. Acta Physiol Scand Suppl 1990; 592: 25-37.
21. Recio-Pinto E, Rechler MM, Ishii D. Effects of insulin, insulin-like growth factor-II, and nerve growth factor on neurite formation and survival in cultured sympathetic and sensory neurons. J Neurosci 1986; 6: 1211-1219.
22. Rezende LF, Stoppiglia LF, Souza KL, Negro A, Langone F, Boschero AC. Ciliary neurotrophic factor promotes survival of neonatal rat islets via the BCL-2 anti-apoptotic pathway. J Endocrinol 2007; 195: 157-165.
23. Saleh A, Roy Chowdhury SK, Smith DR, Balakrishnan S, Tessler L, Martens C, Morrow D, Schartner E, Frizzi KE, Calcutt NA. Ciliary neurotrophic factor activates NF-κB to enhance mitochondrial bioenergetics and prevent neuropathy in sensory neurons of streptozotocin-induced diabetic rodents. Neuropharmacology 2012; 65: 65-73.
24. Sango K, Yanagisawa H, Komuta Y, Si Y, Kawano H. Neuroprotective properties of ciliary neurotrophic factor for cultured adult rat dorsal root ganglion neurons. Histochem Cell Biol 2008; 130: 669-679.
25. Stahl N, Yancopoulos GD. The tripartite CNTF receptor complex: activation and signaling involves components shared with other cytokines. J Neurosci 1994; 25: 1454-1466.
26. Wishingrad MA, Koshlukova S, Halvorsen SW. Ciliary neurotrophic factor stimulates the phosphorylation of two forms of STAT3 in chick ciliary ganglion neurons. J Biol Chem 1997; 272: 19752-19757.
27. Zhong Z, Wen Z, Darnell J. Stat3: a STAT family member activated by tyrosine phosphorylation in response to epidermal growth factor and interleukin-6. Science 1994; 264: 95-98.

Original article

Folia Neuropathologica

Anaplastic transformation of low-grade gliomas (WHO II) on magnetic resonance imaging

Barbara Bobek-Billewicz[1], Gabriela Stasik-Pres[1], Anna Hebda[1], Krzysztof Majchrzak[2], Wojciech Kaspera[2], Marek Jurkowski[3]

[1]Radiodiagnostic Department, Maria Sklodowska-Curie Memorial Cancer Center and Institute of Oncology, Gliwice Branch, [2]Department of Neurosurgery, Medical University of Silesia, Sosnowiec, [3]Nuclear Medicine and Endocrine Oncology Department, Maria Sklodowska-Curie Memorial Cancer Center and Institute of Oncology, Gliwice Branch, Poland

Folia Neuropathol 2014; 52 (2): 128-140 DOI: 10.5114/fn.2014.43784

Abstract

Introduction: *Malignant transformation among gliomas WHO II ranges between 35% and 89%. However, according to some reports, all gliomas WHO II undergo such transformation over time. The aim of the study was to analyse MRI parameters indicating anaplastic transformation of gliomas WHO II.*

Material and methods: *Forty-six consecutive patients were enrolled in the study (20 females and 26 males; range of age 36 ± 9 years) with supratentorial glioma WHO II. Multiparametric MR examination included morphological imaging, perfusion-weighted imaging, diffusion-weighted imaging and proton magnetic resonance spectroscopy. Group division depended on the course of disease (ST – stable group, AT – anaplastic transformation group).*

Results: *Subtotal tumour resection was achieved in the whole AT group, whereas in the ST group, total tumour resection was achieved in 10/29 (34%) patients. The size of the residual tumour after surgery was statistically significantly higher in the AT group compared to the ST group (AT: 51.5 cm^3 ± 37.7 vs. ST: 29.0 cm^3 ± 37.9; p = 0.011). Contrast enhancement in the AT group occurred in 5/11 (45%) of tumours and in none of the patients' areas of contrast enhancement were resected during surgery/biopsy. However, the initial MR showed contrast enhancement in 10/29 (34%) of patients in the ST group. The areas of contrast enhancement were totally resected in all patients. Compared to the ST group tumours that underwent anaplastic transformation had statistically significantly higher values of mean nrCBV and max nrCBV on the initial MR, the follow-up and final MR examinations. However, statistically significant differences between the groups in ADC values were observed on the follow-up and final MR whereas mean Cho/Cr and mean Cho/NAA were observed as late as on the final MR examination.*

Conclusions: *Multiparametric MR examination allows the detection of LGGs with high probability of rapid anaplastic transformation and the detection of transformation prior to the occurrence of contrast enhancement. The value of nrCBV is the most useful in the diagnosis of anaplastic transformation. The resection of contrast enhancement area of the tumour significantly increases time to anaplastic transformation of LGGs.*

Key words: *anaplastic transformation, low-grade glioma, MR imaging.*

Communicating author:
Gabriela Stasik-Pres, Radiodiagnostic Department, Maria Sklodowska-Curie Memorial Cancer Centre and Institute of Oncology, Gliwice Branch, Wybrzeze Armii Krajowej 15, 44-101 Gliwice, e-mail: gabastasik@poczta.onet.pl

Introduction

According to the National Cancer Registry, malignant tumours comprised about 156 000 new cases and 93 000 deaths in Poland in 2009. Primary brain tumours were the 11th most common cause of malignant tumour in males (2.1%; 1444 new cases in 2009) and the 15th most common in females (2.0%; 1362 new cases in 2009). Brain tumour mortality rate has remained stable since 1965 and according to the latest report, it was 2.8% (7.98/100 000) in males and 3.6% (7.48/100 000) in females [16]. Similar percentages of cases and deaths are reported in Europe and in the USA [11,26,35].

Gliomas comprising more than 40% of intracranial tumours constitute high-grade gliomas (HGGs) in 70-80% of cases [30]. Surgical excision with subsequent radio- and chemo-radiotherapy is the gold standard in treatment of HGGs. However, low-grade gliomas (LGGs) are mainly treated surgically and in some cases complimentary radiotherapy is administered. According to the 2011 diagnostic-therapeutic recommendations by the Polish Society of Clinical Oncology (PTOK), postoperative radiotherapy may be abandoned in the case of total surgical resection of oligodendroglioma, gemistocytic astrocytoma, if the tumour did not show contrast enhancement on preoperative (CT and MR) examination and if the patient was < 40 years of age. Postoperative chemotherapy may be considered in oligodendroglioma with 1p/19q loss of heterozygosity [3,21,36]. Gliomas WHO II which predominantly affect patients at the age of 30-40 are mostly characterised by diffuse infiltration of multiple cerebral structures [30]. Malignant transformation to a higher grade (WHO III and IV) in this group of tumours ranges between 35% and 89%. However, according to some reports, all gliomas WHO II undergo such transformation over time [37,48]. The median survival in patients with glioma WHO IV is < 2 years, whereas WHO II is 5-10 years. It is believed that the early detection of factors/parameters indicating anaplastic transformation may improve the prognosis [21,30,40].

Imaging studies are currently the standard method for early detection of changes in biology and malignancy of the tumour and precede the surgical procedure or stereotactic biopsy which is associated with an increased complication risk [21,27]. Malignancy is characterised by significant vascular proliferation within the tumour (neoangiogenesis) [6,22,30,39,47]. According to the "angiogenic switch" theory, LGG progression to HGG must be accompanied by vascular proliferation within the tumour [22,47]. Neoangiogenesis results in increased relative cerebral blood flow (rCBF) and relative cerebral blood volume (rCBV) and at a later stage contrast tumour enhancement on MR examination. Contrast enhancement as a marker of anaplastic transformation presents some disadvantages and poses some limitations. It appears late and its appearance proves that anaplastic transformation has already occurred. Additionally, it is a non-specific feature, resulting from the blood-brain barrier (BBB) breakdown due to e.g. inflammatory and ischaemic changes, radiotherapy as well as lack of the normal BBB in vasculature formed by neoangiogenesis. The extent of contrast enhancement also depends on the dose of glucocorticoids and even on the examination technique [5,17,35]. Although contrast enhancement is considered to be typical of HGGs, it should be remembered that about 40% of high-grade tumours do not show contrast enhancement whereas 10-39% of LGGs show contrast enhancement [21,28,30,35,37,45].

The aim of the study was to analyse MRI parameters indicating anaplastic transformation of gliomas WHO II.

Material and methods

Material

Forty-six consecutive patients were enrolled in the study (20 females and 26 males; range of age 36 ± 9 years) with supratentorial glioma WHO II. Patients were diagnosed in 2005-2011 at the Radiodiagnostic Department, Cancer Centre and Institute of Oncology in Gliwice, Poland. Surgical procedure/biopsy was performed at the Department of Neurosurgery, Medical University of Silesia, Sosnowiec, Poland. Multiparametric MR examination included morphological imaging, perfusion-weighted imaging (PWI), diffusion-weighted imaging (DWI) and proton magnetic resonance spectroscopy (^{1}H-MRS). Pathologic diagnosis was confirmed either by a surgical procedure or biopsy. In the majority of patients, i.e. (36/46) 78.3%, surgery was followed by excised area radiotherapy and/or radiotherapy for residual tumour 2 to 9 months after the diagnosis. The follow-up between the pathological diagnosis and the final follow-up MR examination was at least 18 months except for patients with earlier anaplastic transformation.

Methods

Magnetic resonance examinations were performed on a 1.5T (Magnetom Avanto, Siemens) or a 3.0T scanner (Achieva, Philips) with the standard head coil.

Conventional MR imaging

Conventional MR imaging consisted of morphological sequences of T1-weighted images before and after intravenous contrast agent application, T2-weighted images and fluid attenuated inversion recovery (FLAIR) images. Tumour volume was calculated based on T2-weighted images and FLAIR images, approximating to an ellipsoid.

Perfusion-weighted imaging

Perfusion-weighted imaging (PWI) was performed using dynamic susceptibility contrast perfusion magnetic resonance imaging (DSC MRI).

Scanner 1.5T: EPI SE (Echo Planar Imaging Spin Echo), TR/TE 1560/30 ms, Thk/gap 5.0/1.5 mm, matrix 128 × 128, FOV 250 × 250 mm, 50 data sets were acquired with a time resolution 1 per data set. TA was 1 min 26 s.

Scanner 3.0T: EPI GE (Echo Planar Imaging Gradient Echo), TR/TE 16(7°)/24(7°), Thk/gap 4.0/0.0 mm, matrix 64 × 128, FOV 230 × 230 mm. 50 data sets were acquired with a time resolution 1 per data set. TA was 1 min 29 s.

A gadolinium-based contrast agent was administered at the dose of 0.1 mmol/kg with the injection rate of 6 mL/s, followed by administration of 20 mL bolus of saline. Parametric maps of rCBV were calculated automatically by the software provided by the scanner producer. The region of interest (ROI) which was the basis for calculating rCBV drawn manually on each layer of the parametric map on which in the correlation with morphological images the tumour was detected. ROI was drawn in the solid tumour area ignoring cortical vessels, necrotic areas and treatment-induced changes. The value of rCBV in the tumour was normalised to normal appearing white matter in the contralateral hemisphere (normalised rCBV – nrCBV). The mean nrCBV was calculated and the max nrCBV was determined in the tumour.

Diffusion-weighted imaging

Diffusion-weighted imaging (DWI) was performed using Echo Planar Imaging Spin Echo (EPI SE).

Scanner 1.5T: TR/TE 3100/99 ms, b = 0, 500, 1000 mm^2/s, FOV 230 × 230 mm; matrix 192 × 192, Thk/gap 5.0/1.0 mm.

Scanner 3.0T: TR/TE 3080/70 ms, b = 0, 500, 1000 mm^2/s, FOV 230 × 230, matrix 112 × 256, Thk/gap 4.0/1.0 mm.

Apparent Diffusion Coefficient (ADC) maps were calculated automatically using the software provided by the scanner producer. ROI was drawn manually on each layer of the parametric map in the solid tumour area in the correlation with morphological images. The mean ADC was calculated and the min ADC was determined in the tumour.

Proton MR spectroscopy

Point resolved localised spectroscopy (PRESS) was used for single-voxel spectroscopy (SVS) and chemical shift imaging multi voxel (CSI).

Scanner 1.5T: 3D CSI – TR/TE 2000/135 ms, SVS – TR/TE 1500/135 ms.

Scanner 3.0T: 3D CSI – TR/TE 2000-1500/144-288 ms, SVS – 2000-1500/144-288 ms.

Spectroscopy data were evaluated using Linear Combination of Model Spectra software (LCModel, version 6.1-4.F). Cho/Cr, Cho/NAA and NAA/Cr ratios (Choline, Cr – creatine, NAA – *N*-Acetylaspartic acid) were calculated. The voxel in SVS was placed in the solid tumour area. Spectroscopy data from every voxel placed in the solid tumour area were analysed in 3D CSI and in the subsequent analysis, the mean Cho/Cr, Cho/NAA, NAA/Cr were used.

Statistical analysis

Continuous parameters with normal distribution were presented as mean ± standard deviation (SD). Median and interquartile ranges were used to describe quantitative variables whose distribution differed from the standard. Significance of mean differences was tested with a *t*-Student test and an ANOVA proceeded by evaluation of normality and Levine's test. When significant effects were found, post hoc testing (NIR Fisher tests) of all possible comparisons was applied. Friedman's repeated measures ANOVA was used to test changes in not continuous values. Wilcoxon's test was used for post hoc analysis. To assess the differences between the variables, the Mann-Whitney *U* test was used to compare two independent groups. Statistically significant *p*-levels were assumed as < 0.05 (two-sided).

Statistical calculations and analyses were performed with STATISTICA (StatSoft) software version 9.0.

Results

Patients were divided into three groups depending on the course of disease (Fig. 1).

ST – stable group – total/subtotal tumour resection with no relapse/progression in clinical observation and follow-up MR examinations.

AT – anaplastic transformation group – pathologically verified tumour transformation to a higher grade of malignancy (WHO grade III or IV). Time to anaplastic transformation varied between 2 and 38 months. Transformation occurred within 12 months of the follow-up in 6/11 patients, between the 12th and the 24th month in 3/11 patients and after 24 months in 2 patients.

RP – radiological progression group – radiological progression without pathologically confirmed transformation.

Radiological progression was detected based on the increase in tumour volume by over 40% (1 patient in the RP group) or the occurrence of contrast enhancement with the normalised max nrCBV > 1.75 (11 patients in the AT group and 5 patients in the RP group) [17,23-26].

Initial pathologic diagnosis is presented in Table I.

The comparative analysis included 40 patients (29 from the ST group and 11 from the AT group). The selected parameters of PWI, DWI and ^{1}H-MRS were analysed prior to surgery/biopsy (initial MR), after surgery/biopsy (follow-up MR) and in the AT group in the final MR examination (final MR) where anaplastic transformation was detected prior to the surgical procedure and in the ST group in the final MR follow-up in which the tumour was stable at least 18 months after pathological diagnosis (final MR). Mean time of the follow-up MR in the AT group was 3 (1-8) months and in the ST group was 3 (1-8) months. Mean time of the final MR in the AT group was 16 (3-38) months and in the ST group was 32 (18-66) months.

Subtotal tumour resection was achieved in the whole AT group, whereas in the ST group total tumour resection was achieved in 10/29 (34%) patients. The size of the residual tumour after surgery was statistically significantly higher in the AT group compared to the ST group (AT: 51.5 cm^3 ± 37.7 vs. ST: 29.0 cm^3 ± 37.9; p = 0.011).

Contrast enhancement on the initial MR was found in 15/40 (38%) tumours. Contrast enhancement in the AT group occurred in 5/11 (45%) tumours and in none of the patients, areas of contrast enhancement were resected during surgery/biopsy. However, the initial MR showed contrast enhancement in 10/29 (34%) patients in the ST group. The areas of contrast enhancement were totally resected in all patients, in 5/10 (50%) patients, total tumour resection was achieved and in 5/10 (50%), subtotal tumour resection was achieved in the area of contrast enhancement.

In the AT group on the initial MR in the area of contrast enhancement, mean nrCBV, mean Cho/Cr and mean Cho/NAA were significantly higher and the values of min ADC, mean ADC and NAA/Cr were

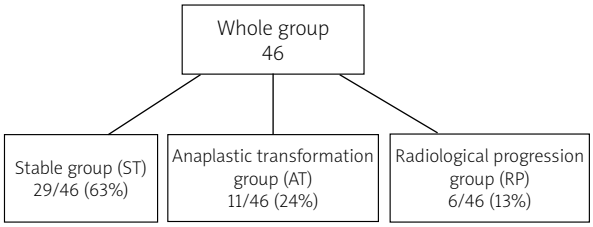

Fig. 1. Group division depending on the course of disease.

Table I. Initial pathologic diagnosis

Pathologic diagnosis	ST*	AT#	RP	Whole
Fibrillary astrocytoma WHO II	10/29 (34%)	6/11 (55%)	3/6 (50%)	19/46 (42%)
Gemistocytic astrocytoma WHO II	6/29 (21%)	4/11 (36%)	2/6 (33%)	12/46 (26%)
Oligodendroglioma WHO II	2/29 (7%)	0/11 (0%)	0/6 (0%)	2/46 (4%)
Oligoastrocytoma WHO II	11/29 (38%)	1/11 (9%)	1/6 (17%)	13/46 (28%)

ST – stable group, AT – anaplastic transformation group, RP – radiological progression group
** – 10/29 total surgical resection, # – 1/11 glioma transformed into glioblastoma and 10/11 gliomas transformed into anaplastic astrocytoma*

Table II. Parameters of PWI, DWI, ^{1}H-MRS obtained in the contrast enhancement area and non-contrast enhancement area of the tumour, on the initial MR, in the stable group and the anaplastic transformation group

Parameters	ST* (*n* = 10/29)			AT** (*n* = 5/11)		
	CE	Non-CE	*p*	CE	Non-CE	*p*
Max nrCBV	2.67 (1.60-4.24)	1.44 (0.71-3.16)	0.005	3.15 (2.29-4.64)	1.47 (1.03-2.85)	0.079
Mean nrCBV	1.92 (1.39-3.67)	1.14 (0.63-2.69)	0.050	2.00 (1.68-3.19)	1.10 (0.77-1.78)	0.043
Mean Cho/Cr	1.60 (1.34-2.60)	1.44 (1.16-1.80)	0.007	1.85 (1.45-2.60)	1.59 (1.19-2.20)	0.043
Mean Cho/NAA	1.09 (0.55-3.81)	0.87 (0.49-1.80)	0.007	1.73 (1.42-2.26)	1.01 (0.80-1.79)	0.043
Mean NAA/Cr	1.36 (0.69-2.84)	1.65 (1.00-2.73)	NS	1.10 (0.82-1.51)	1.41 (0.89-2.79)	0.043
Min ADC#	1.24 (1.04-1.78)	1.32 (0.99-1.71)	NS	0.98 (0.70-1.14)	1.29 (0.81-1.43)	0.043
Mean ADC#	1.31 (1.13-1.86)	1.46 (1.13-1.79)	NS	1.20 (0.88-1.27)	1.38 (1.04-1.48)	0.043

ST – stable group, AT – anaplastic transformation group, CE – contrast enhancement area of the tumour, Non-CE – non-contrast enhancement area of the tumour
*#ADC values *10^{-3} mm^2/s, *On the initial MR in the ST group 10/29 (34%) tumours had CE area, **On the initial MR in the AT group, 5/11 (45%) tumours had CE area. The increase in max nrCBV > 1.75 preceded contrast enhancement up to 5-8 months in those tumours which did not enhance on the initial MR*

Table III. Statistically significant differences between the stable group and the anaplastic transformation group on the initial MR, follow-up MR and final MR

	Initial MR					
	max nrCBV	mean nrCBV				
AT	4.21 ± 0.67	2.48 ± 0.69				
ST	2.37 ± 0.69	1.47 ± 0.49				
p	0.001	0.001				
	Follow-up MR					
	max nrCBV	mean nrCBV	min ADC	mean ADC		
AT	4.39 ± 1.09	2.56 ± 0.62	0.71 (0.59-1.02)	1.00 (0.70-1.21)		
ST	1.75 ± 0.81	1.13 ± 0.40	1.05 (0.79-1.59)	1.22 (1.1-1.71)		
p	0.001	0.001	0.001	0.006		
	Final MR					
	max nrCBV	mean nrCBV	min ADC	mean ADC	mean Cho/Cr	mean Cho/NAA
AT	4.42 ± 1.83	2.93 ± 1.31	0.88 (0.75-1.31)	1.08 (0.87-1.44)	1.78 (1.34-3.17)	1.49 (0.78-2.09)
ST	1.68 ± 0.81	1.01 ± 0.44	1.09 (0.93-1.35)	1.22 (1.09-1.73)	1.30 (1.00-2.15)	0.84 (0.60-1.94)
p	0.001	0.001	0.020	0.049	0.030	0.030

AT – anaplastic transformation group, ST – stable group. In the ST group, max nrCBV and mean nrCBV values on the follow-up MR and final MR were significantly statistically lower compared to the results of the initial MR. Max nrCBV (2.37 ± 0.69 vs. 1.75 ± 0.81 vs. 1.68 ± 0.81; p = 0.042, p = 0.023). Mean nrCBV (1.47 ± 0.49 vs. 1.13 ± 0.4 vs. 1.01 ± 0.44; p = 0.030, p = 0.004).
In the AT group, on the follow-up MR, a statistically significant decrease in min ADC and mean ADC values in the remaining tumour area was observed compared to the initial MR examination. Min ADC (1.05 [0.71-1.36] vs. 0.71 [0.59-1.02]; p = 0.030). Mean ADC (1.29 [0.98-1.50] vs. 1.00 [0.70-1.21]; p = 0.030). Additionally, in the AT group an increase was observed in the value of Cho on the final MR compared to the initial MR examination. Cho/Cr (1.68 [1.10-2.19] vs. 1.78 [1.34-3.17]), Cho/NAA (1.32 [0.59-3.17] vs. 1.49 [0.78-2.09])

significantly lower compared to the non-enhancing area of the tumour (Table II).

Also in the ST group on the initial MR examination in the area of contrast enhancement, max nrCBV, mean nrCBV, mean Cho/Cr and mean Cho/NAA were significantly higher compared to the non-enhancing area of the tumour (Table II).

Compared to the ST group, tumours that underwent anaplastic transformation had statistically significantly higher values of mean nrCBV and max nrCBV on the initial MR examination, the follow-up and final MR examinations (Figs. 2 and 3, Table III). However, statistically significant differences between the groups in ADC values were observed on the fol-

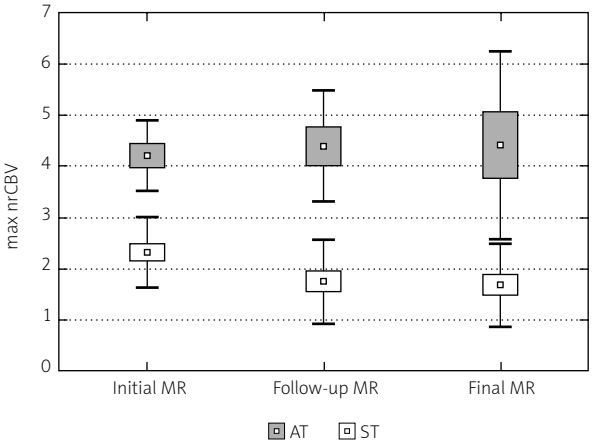

Fig. 2. Values of max nrCBV on the initial MR, follow-up MR and the final MR examinations in the stable group and the anaplastic transformation group.

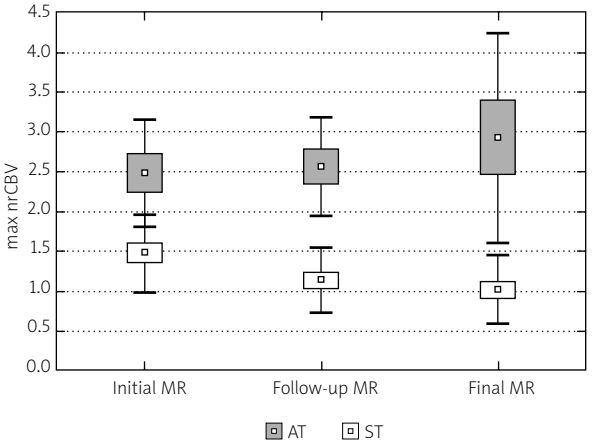

Fig. 3. Values of mean nrCBV on the initial MR, follow-up MR and the final MR examinations in the stable group and the anaplastic transformation group.

low-up and final MR whereas mean Cho/Cr and mean Cho/NAA were observed as late as on the final MR examination (Figs. 4A-H and 5A-J, Table III).

Discussion

Magnetic resonance imaging is a non-invasive method of evaluating certain features of the tumour assessed by pathological examination, for instance tissue microvascular density (MVD), cellularity, the presence of necrosis [4,5,12,15,32,34,38,50]. Malignancy is characterised by vascular proliferation within the tumour (neoangiogenesis) [6,22,30,39,47]. According to the "angiogenic switch" theory, the essence of LGG anaplastic transformation is vascular proliferation in a previously avascular tumour [22,47]. Vessels formed by neoangiogenesis differ in their structure from normal vasculature (tortuosity, lack of maturity and increased permeability). On standard MR imaging, neoangiogenesis manifests as the area of contrast enhancement. Contrast enhancement as a marker of anaplastic transformation appears late and its appearance proves that anaplastic transformation has already occurred. However, PWI gives access to information on the capillary microcirculation of tissues and reflects tissue MVD by measuring rCBV, prior to the occurrence of contrast enhancement [5,35]. Danchaivijitr *et al.* confirmed that in the group of gliomas which underwent anaplastic transformation, continuous rCBV growth (within 12-18 months) preceded the occurrence of an abnormal area of contrast enhancement in the tumour [13]. Law *et al.* suggested the cut-off value for the normalised to the normal appearing white matter rCBV > 1.75 on MR examination prior to surgery as the feature differentiating rapidly progressive LGGs (median 8 vs. 154 months) [24,26]. The similar correlation was confirmed by Caseiras *et al.* using the same cut-off value for rCBV – "the median time to progression among subjects with rCBV > 1.75 was 365 days, while there was 95% confidence that the median time to progression was at least 889 days among subjects with rCBV < 1.75" [7]. Referring to the findings of Law *et al.*, Al-Okaili *et al.* used the same cut-off value for rCBV characterising the area of the increased perfusion in the study on differential diagnosis of intra-axial brain masses. Gliomas with rCBV > 1.75 corresponded to HGGs with sensitivity of 88%, specificity of 100%, PPV of 100%, NPV of 67%, compared to LGGs [1]. Although the normalised rCBV = 1.75 is the most frequently accepted cut-off value differentiating LGGs from HGGs as well as LGGs with short and long transformation time, other clearly distinct values are also reported. In the study by Arvinda *et al.*, the cut-off point for nrCBV mostly differentiating LGGs from HGGs was 2.93, whereas Morita *et al.* obtained nrCBV = 0.94 [2,33]. In our material in the AT group, the increase in max nrCBV > 1.75 preceded contrast enhancement in the same tumour area within 5-8 months in 6/11 (45%) patients. In the remaining 5/11 (55%) patients, max nrCBV > 1.75 was found in the area of contrast enhancement from

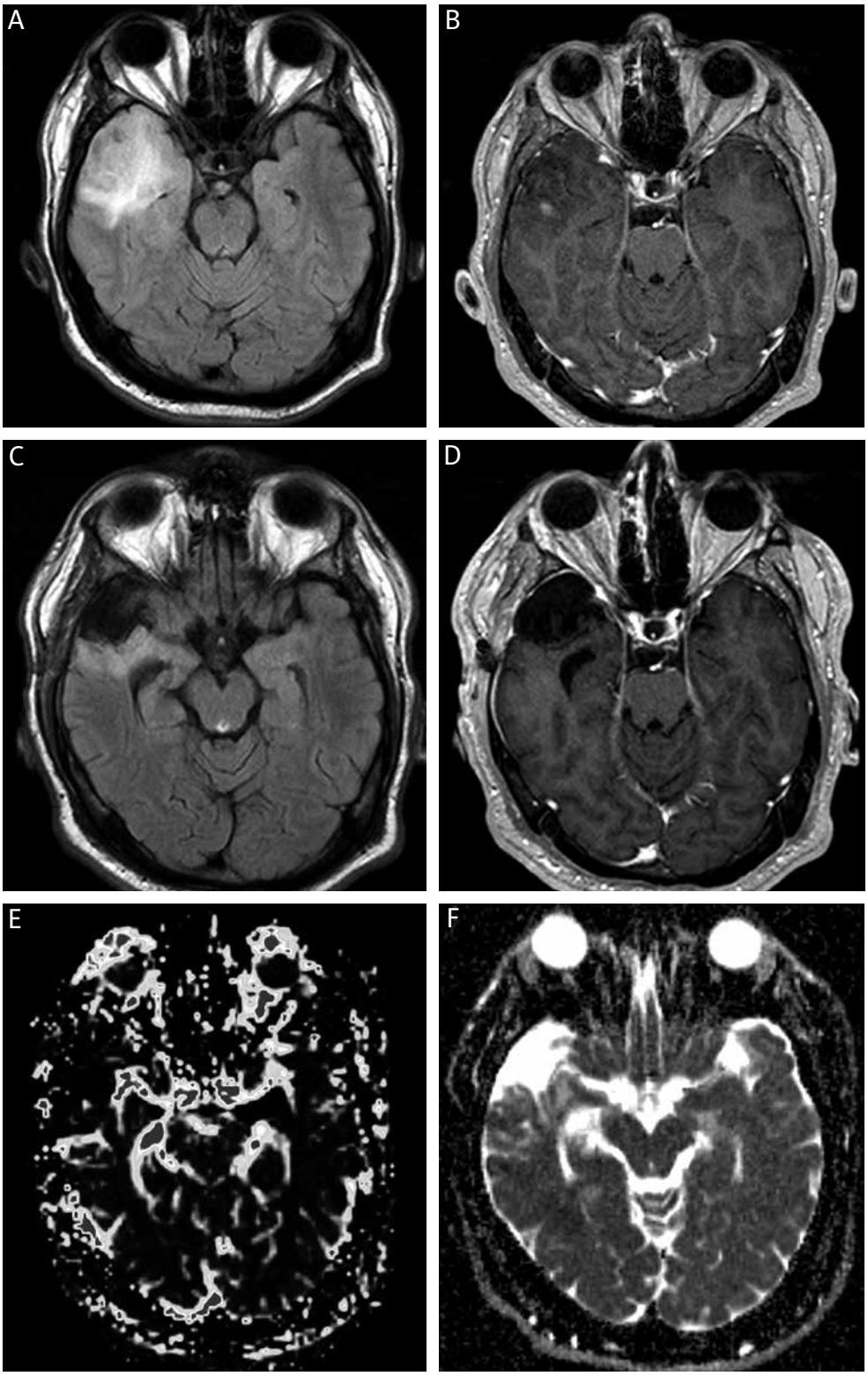

Fig. 4. A–F) Fibrillary astrocytoma WHO II out of the stable group, the initial MR: FLAIR **(A)** and T1-weighted image after intravenous contrast agent application **(B)**, the final MR: FLAIR **(C)** and T1-weighted image after intravenous contrast agent application **(D)**, PWI – rCBV map **(E)**, DWI – ADC map **(F)**.

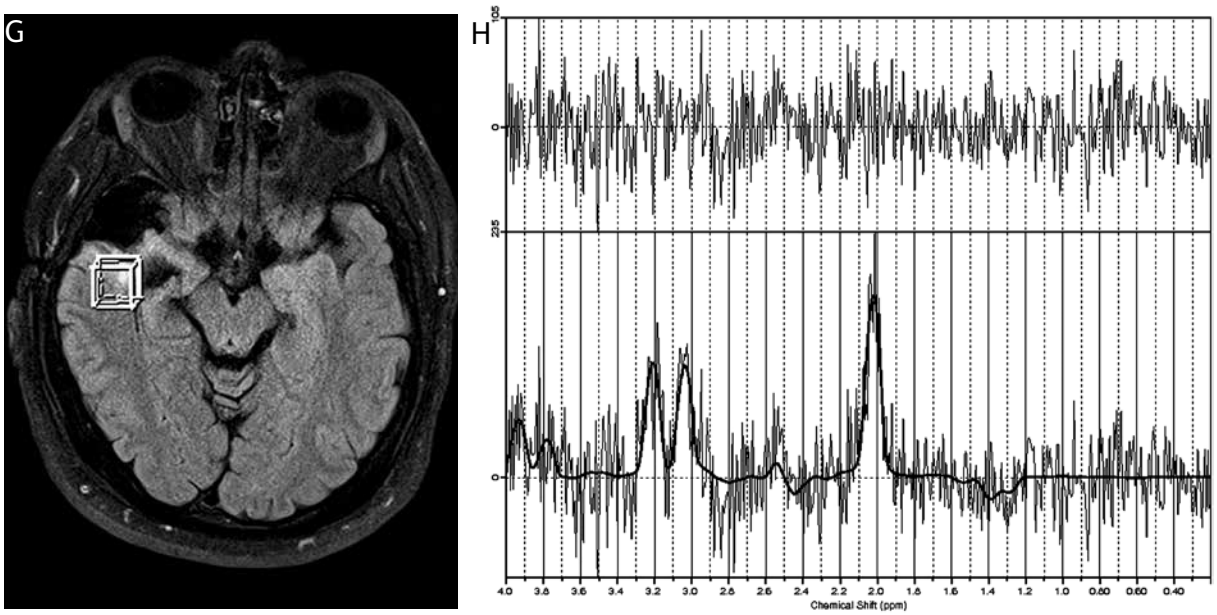

Fig. 4. G–H) Fibrillary astrocytoma WHO II out of the stable group, the initial MR: ^{1}H-MRS.

the very beginning. Moreover, max nrCBV and mean nrCBV in AT group were significantly higher on the initial MR, follow-up MR and the final MR examinations compared to the ST group. In the ST group max nrCBV and mean nrCBV were significantly lower on the follow-up MR and the final MR examinations compared to the initial MR examination, which may have been due to resection of contrast enhancement area characterised by significantly increased nrCBV in relation to the remaining tumour area.

In our material, the extent of tumour resection in the ST group was significantly higher compared to the AT group. The extent of tumour resection significantly influenced progression-free survival (PFS) and overall survival (OS) in LGG patients, which is consistent with the reports of other researchers [19,31,43]. Our observations confirm that next to the extent of resection, excision of contrast enhancement area is essential for further course of disease. In our material, none of the patients from the AT group had contrast enhancement area resected whereas in the ST group contrast enhancement area was resected in all patients. In both groups in the area of contrast enhancement nrCBV and Cho/Cr and Cho/NAA ratios were significantly higher compared to the non-enhanced tumour area, which indicates higher potential malignancy of this part of tumour. Additionally, in the AT group in the area of contrast enhancement ADC was significantly lower compared to the outside of this area. Chaichan *et al.* confirmed that in patients with LGGs enhanced after contrast agent administration, the 5-year OS, PFS and malignant transformation-free survival were shorter compared to patients with non-enhancing LGGs (70 *vs.* 85% [p = 0.002], 32 *vs*. 49% [p = 0.008] and 74 *vs*. 90% [p = 0.002], respectively). Moreover, the only factors that were consistently shown to be associated with tumour recurrence or malignant degeneration are preoperative contrast enhancement, tumour size, and subtotal resection. Additionally, in the multifactorial analysis, Chaichan *et al.* confirmed that LGG contrast enhancement is an independent factor determining decreased survival (p = 0.006), increased recurrence (p = 0.04) and the trend towards a higher incidence of malignant degeneration (p = 0.15). However, Chaichan *et al.* did not analyse parameters of PWI, DWI, proton MR spectroscopy (^{1}H-MRS) [9,10]. The criteria for Response Assessment in Neuro-Oncology (RANO) regarding the assessment of response to treatment of non-enhancing LGGs indicate that the area of contrast enhancement in the tumour corresponds to malignant transformation although it is a non-specific feature [45], and parameters of PWI, DWI, ^{1}H-MRS, PET though mentioned in the model protocol are not included in the treatment-response assessment. According to the authors of the RANO

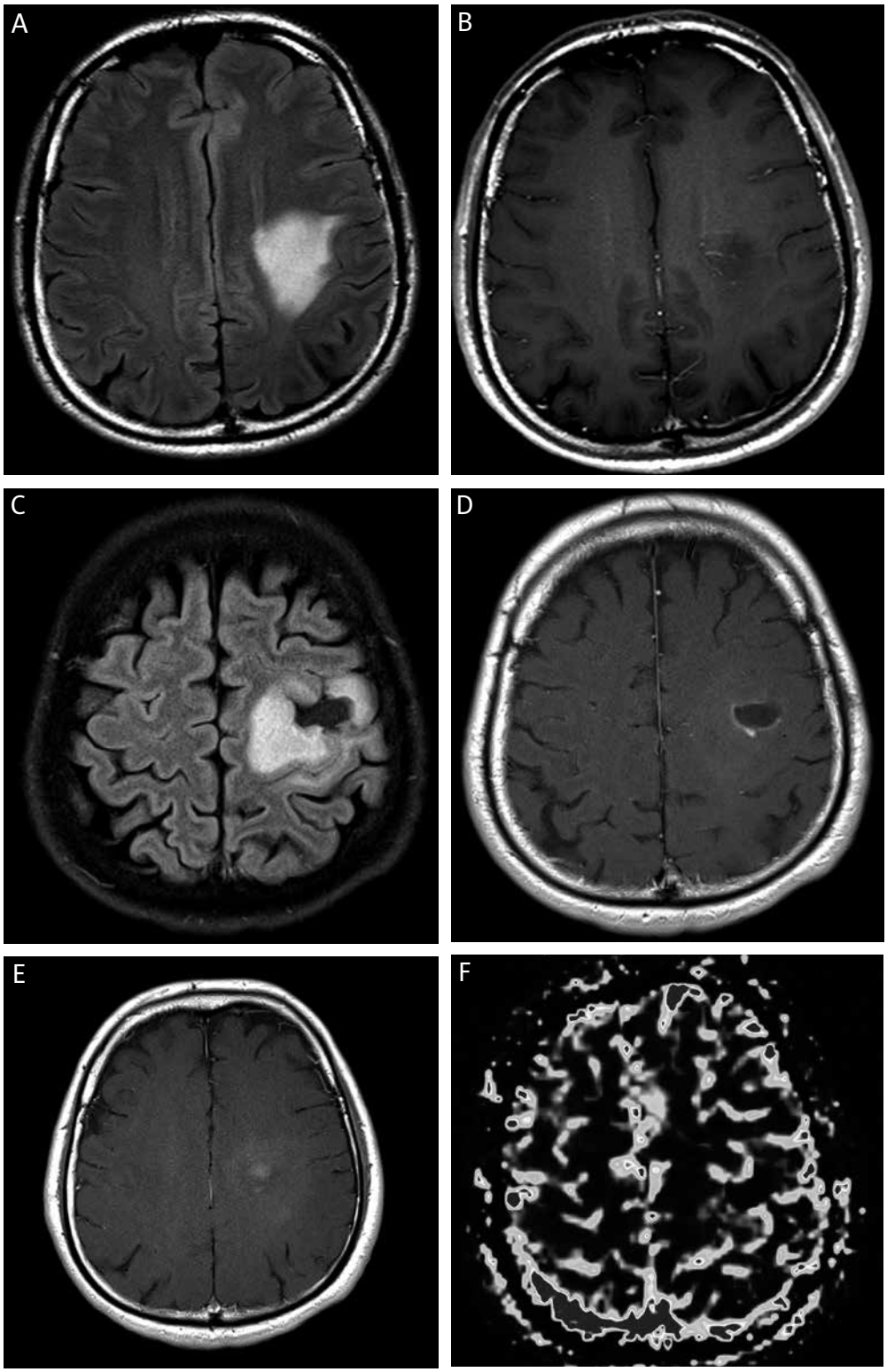

Fig. 5. A–F) Fibrillary astrocytoma WHO II out of the anaplastic transformation group, the initial MR: FLAIR **(A)** and T1-weighted image after intravenous contrast agent application **(B)**, the final MR: FLAIR **(C)** and T1-weighted image after intravenous contrast agent application **(D, E)**, PWI – rCBV map **(F, G)**.

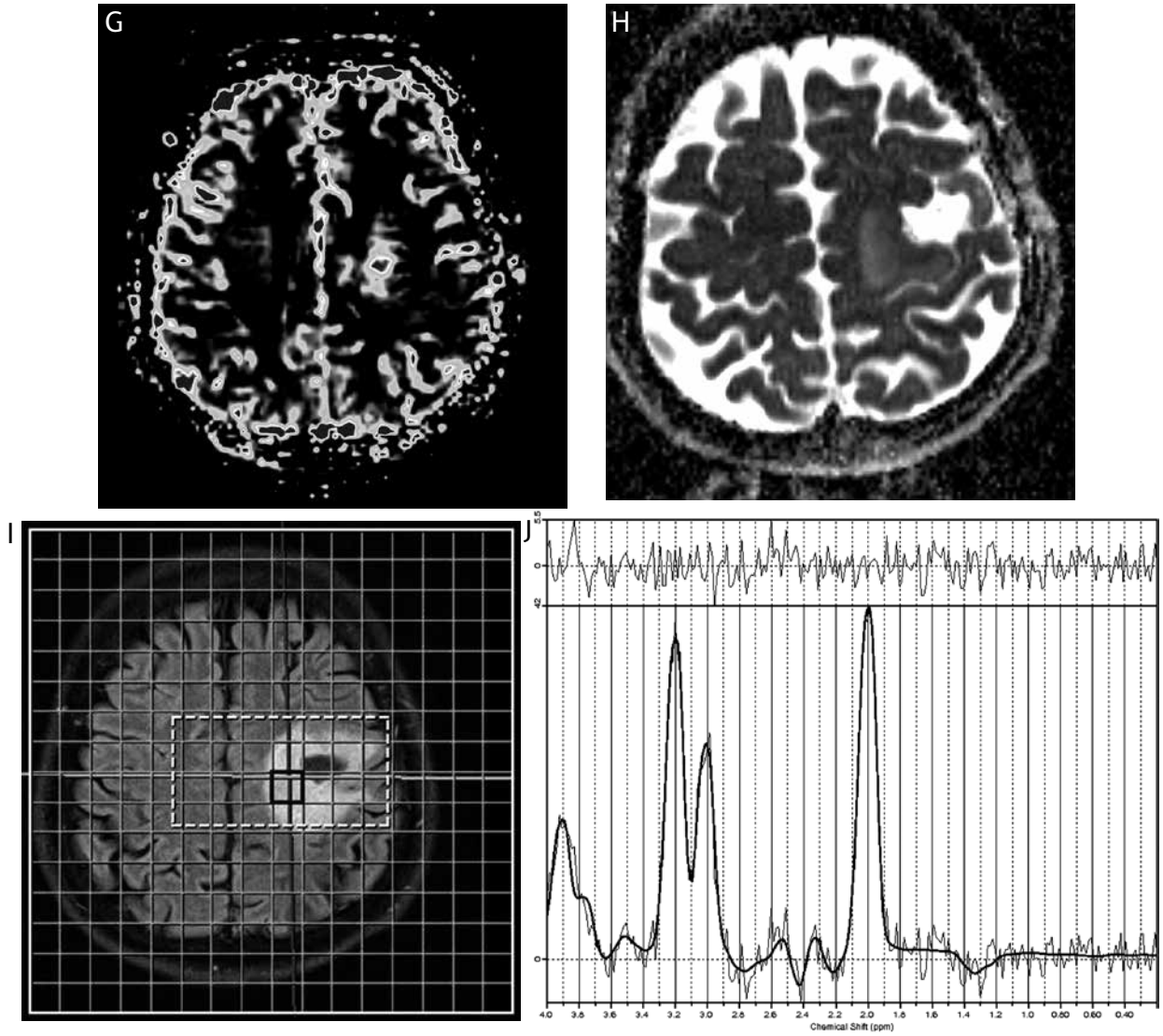

Fig. 5. G–J) Fibrillary astrocytoma WHO II out of the anaplastic transformation group, the initial MR: PWI – rCBV map **(F, G)**, DWI – ADC map **(H)**, ^{1}H-MRS **(I, J)**.

criteria, the percentage of gliomas WHO II enhancing after contrast agent administration is reported to be at the level of 10% and mainly in the oligodendroglioma subgroup. The post-treatment occurrence of a new area of contrast enhancement in gliomas WHO II is first interpreted as malignant transformation [45]. According to RANO, "for progression, two types of MRI progression have to be distinguished and reported separately: the development of or an increase in enhancement suggestive of malignant transformation, and linear progression of a still non-enhancing lesion".

In our study, astrocytomas and oligoastrocytomas occurred in both groups (ST and AT) whereas oligodendrogliomas exclusively in the ST group. A gemistocytic component was found more frequently in the AT group (36% of tumours) compared to the ST group (21% of tumours).

In the multifactorial analysis regarding early prognostic factors related to progression and malignant transformation of LGGs, Joung *et al.* confirmed that apart from total tumour resection, a gemistocytic component in LGGs was related to shorter PFS and independently influenced the occurrence of malignant transformation [19]. Additionally, in trials regarding LGG treatment with radiotherapy, the median survival of > 5 years was reported for patients with oligodendroglioma compared to other

gliomas WHO II for which the median survival was < 5 years [20,42,44].

There are no explicit reports on the ADC cut-off value differentiating gliomas depending on the tumour grade [2,8,41,46]. However, it is generally accepted that the higher the tumour grade, the lower ADC values [46]. Server *et al.* and Arvinda *et al.* suggested the minimum ADC = 1.07×10^{-3} mm^2/s and the mean ADC = 0.985×10^{-3} mm^2/s as the ADC cut-off values differentiating HGGs from LGGs [2,41]. However, Catalaa *et al.* noted that HGGs and LGGs did not differ in ADC values [8]. In our material, min ADC and mean ADC did not differ significantly between AT and ST groups on the initial MR examination. However, min ADC and mean ADC were significantly lower in the AT group on the follow-up MR and the final MR examinations compared to the ST group. In the AT group the follow-up MR revealed a statistically significant decrease in min ADC and mean ADC values in the remaining tumour area compared to the initial MR examination. It may be related to the increased component of post-treatment ischaemic changes or gliosis. It cannot be clearly determined which process or component mainly contributed to the decrease in the ADC value.

The cut-off value for Cho/Cr and Cho/NAA reported by various researchers differentiating LGGs from HGGs is wide (1.35 to 2.04 for Cho/Cr and 1.60 to 2.49 for Cho/NAA) [14,23,29,41,49]. Hlaihel *et al.* confirmed that in the group of oligodendrogliomas WHO II which underwent anaplastic transformation, mean Cho/Cr ratio above 2.4 was the earliest marker of the transformation with a mean delay of 15.4 months. Whereas normalised rCBV elevation > 2 occurred an average of 8 months before the malignant transformation. Authors suggested that "the increase in cell membrane production and cell density, as attested by the elevation of the choline/creatine ratio, may generate an ischaemic process that initiates vascular proliferation in the infiltrative tissue" [18]. In our study, in the AT group mean Cho/Cr and mean Cho/NAA were significantly higher as late as on the final MR examination compared to the ST group. The increase in Cho over time was observed in the AT group, i.e. mean Cho/Cr and mean Cho/NAA were higher on the final MR examination compared to the initial MR examination. Our analysis comprised of ^{1}H-MRS with a long TE: 135-288 ms, whereas Hlaihel *et al.* analysed mainly single-voxel short TE: 32 ms ^{1}H-MRS. Moreover, in our material there were different gliomas WHO II (fibrillary astrocytoma, gemistocytic astrocytoma, oligodendroglioma, oligoastrocytoma), whereas Hlaihel *et al.* analysed only oligodendrogliomas. We had longer follow-up and more gliomas which underwent anaplastic transformation.

Conclusions

Multiparametric MR examination allows the detection of LGGs with high probability of rapid anaplastic transformation and the detection of transformation prior to the occurrence of contrast enhancement. The value of nrCBV is the most useful in the diagnosis of anaplastic transformation. The resection of contrast enhancement area of the tumour significantly increases time to anaplastic transformation of LGGs.

Acknowledgements

The authors would like to thank Arkadiusz Badziński for translating the article.

Disclosure

This study was supported by the Ministry of Science and Higher Education grant no. NN 403278933 which was approved by the local research ethics committee.

Authors report no conflict of interest.

References

1. Al-Okaili RN, Krejza J, Woo JH, Wolf RL, O'Rourke DM, Judy KD, Poptani H, Melhem ER. Intraaxial brain masses: MR imaging-based diagnostic strategy – initial experience. Radiology 2007; 243: 539-550.
2. Arvinda HR, Kesavadas C, Sarma PS, Thomas B, Radhakrishnan VV, Gupta AK, Kapilamoorthy TR, Nair S. Glioma grading: sensitivity, specificity, positive and negative predictive values of diffusion and perfusion imaging. J Neurooncol 2009; 94: 87-96.
3. Brady LW, Heilmann HP, Molls M, Neider C. Radiation Oncology an evidence based approach. Springer-Verlag, Berlin, Heidelberg 2008, pp. 483-499.
4. Bobek-Billewicz B, Hebla A, Stasik-Pres G, Majchrzak K, Żmuda E, Trojanowska A. Measurement of glycine in a brain and brain tumors by means of 1H MRS. Folia Neuropathol 2010; 48: 190-199.
5. Bobek-Billewicz B, Stasik-Pres G, Majchrzak H, Zarudzki L. Differentiation between brain tumor recurrence and radiation injury using perfusion, diffusion-weighted imaging and MR spectroscopy. Folia Neuropathol 2010; 48: 81-92.
6. Carmeliet P, Jain RK. Angiogenesis in cancer and other diseases. Nature 2000; 407: 249-257.
7. Caseiras GB, Chheang S, Babb J, Rees JH, Pecerrelli N, Tozer DJ, Benton C, Zigzag D, Johnson G, Waldman AD, Jäger HR, Law M.

Relative cerebral blood volume measurements of low-grade gliomas predict patient outcome in a multi-institution setting. Eur J Radiol 2010; 73: 215-220.
8. Catalaa I, Henry R, Dillon WP, Graves EE, McKnight TR, Lu Y, Vigneron DB, Nelson SJ. Perfusion, diffusion and spectroscopy values in newly diagnosed cerebral gliomas. NMR Biomed 2006; 19: 463-475.
9. Chaichana KL, McGirt MJ, Niranjan A, Olivi A, Burger PC, Quinones-Hinojosa A. Prognostic significance of contrast-enhancing low-grade gliomas in adults and a review of the literature. Neurol Res 2009; 31: 931-939.
10. Chaichana KL, McGirt MJ, Laterra J, Olivi A, Quiñones-Hinojosa A. Recurrence and malignant degeneration after resection of adult hemispheric low-grade gliomas. J Neurosurg 2010; 112: 10-17.
11. Crocetti E, Trama A, Stiller C, Caldarella A, Soffietti R, Jaal J, Weber DC, Ricardi U, Slowinski J, Brandes A; RARECARE working group. Epidemiology of glial and non-glial brain tumours in Europe. Eur J Cancer 2012; 48: 1532-1542.
12. Czernicki T, Szeszkowski W, Marchel A, Gołebiowski M. Spectral changes in postoperative MRS in high-grade gliomas and their effect on patient prognosis. Folia Neuropathol 2009; 47: 43-49.
13. Danchaivijitr N, Waldman AD, Tozer DJ, Benton CE, Brasil Caseiras G, Tofts PS, Rees JH, Jäger HR. Low-grade gliomas: do changes in rCBV measurements at longitudinal perfusion-weighted MR imaging predict malignant transformation? Radiology 2008; 247: 170-178.
14. Delorme S, Weber MA. Applications of MRS in the evaluation of focal malignant brain lesions. Cancer Imaging 2006; 6: 95-99.
15. Dhermain FG, Hau P, Lanfermann H, Jacobs AH, van den Bent MJ. Advanced MRI and PET imaging for assessment of treatment response in patients with gliomas. Lancet Neurol 2010; 9: 906-920.
16. Didkowska J, Wojciechowska U, Zatonski W. Nowotwory złośliwe w Polsce w 2009 roku. Centrum Onkologii – Instytut, Warszawa 2011.
17. Henson JW, Ulmer S, Harris GJ. Brain tumor imaging in clinical trials. AJNR Am J Neuroradiol 2008; 29: 419-424.
18. Hlaihel C, Guilloton L, Guyotat J, Streichenberger N, Honnorat J, Otton F. Predictive value of multimodality MRI using conventional, perfusion, and spectroscopy MR in anaplastic transformation of low-grade oligodendrogliomas. J Neurooncol 2010; 97: 73-80.
19. Jung TY, Jung S, Moon JH, Kim IY, Moon KS, Jang WY. Early prognostic factors related to progression and malignant transformation of low-grade gliomas. Clin Neurol Neurosurg 2011; 113: 752-757.
20. Karim AB, Maat B, Hatlevoll R, Menten J, Rutten EH, Thomas DG, Mascarenhas F, Horiot JC, Parvinen LM, van Reijn M, Jager JJ, Fabrini MG, van Alphen AM, Hamers HP, Gaspar L, Noordman E, Pierart M, van Glabbeke M. A randomized trial on dose-response in radiation therapy of low-grade cerebral glioma: European Organization for Research and Treatment of Cancer (EORTC) Study 22844. Int J Radiat Oncol Biol Phys 1996; 36: 549-556.
21. Krzakowski M, Fijuth M, Herman K, Jarosz J, Jassem J, Kawecki A, Kornafel J, Krzemieniecki K, Litwiniuk M, Potemski P, Rubach M, Rutkowski P, Stelmach A. Onkologia w praktyce klinicznej. Zalecenia postępowania diagnostyczno-terapeutycznego w nowotworach złośliwych. Tom I. Via Medica, Gdańsk 2011, pp. 33-67.
22. Lacerda S, Law M. Magnetic resonance perfusion and permeability imaging in brain tumors. Neuroimaging Clin N Am 2009; 19: 527-557.
23. Law M, Yang S, Wang H, Babb JS, Johnson G, Cha S, Knopp EA, Zagzag D. Glioma grading: sensitivity, specificity, and predictive values of perfusion MR imaging and proton MR spectroscopic imaging compared with conventional MR imaging. AJNR Am J Neuroradiol 2003; 24: 1989-1998.
24. Law M, Oh S, Babb JS, Wang E, Inglese M, Zagzag D, Knopp EA, Johnson G. Low-grade gliomas: dynamic susceptibility-weighted contrast-enhanced perfusion MR imaging-prediction of patient clinical response. Radiology 2006; 238: 658-667.
25. Law M, Yang S, Babb JS, Knopp EA, Golfinos JG, Zagzag D, Johnson G. Comparison of cerebral blood volume and vascular permeability from dynamic susceptibility contrast-enhanced perfusion MR imaging with glioma grade. AJNR Am J Neuroradiol 2004; 25: 746-755.
26. Law M, Young RJ, Babb JS, Peccerelli N, Chheang S, Gruber ML, Miller DC, Golfinos JG, Zagzag D, Johnson G. Gliomas: predicting time to progression or survival with cerebral blood volume measurements at dynamic susceptibility-weighted contrast-enhanced perfusion MR imaging. Radiology 2008; 247: 490-498.
27. Lesniak MS, Klem JM, Weingart J, Carson BS. Surgical outcome following resection of contrast-enhanced pediatric brainstem gliomas. Pediatr Neurosurg 2003; 39: 314-322.
28. Liu X, Tian W, Kolar B, Yeaney GA, Qiu X, Johnson MD, Ekholm S. MR diffusion tensor and perfusionweighted imaging in preoperative grading of supratentorialnonenhancing gliomas. Neuro Oncol 2011; 13: 447-455.
29. Liu ZL, Zhou Q, Zeng QS, Li CF, Zhang K. Noninvasive evaluation of cerebral glioma grade by using diffusion-weighted imaging-guided single-voxel proton magnetic resonance spectroscopy. J Int Med Res 2012; 40: 76-84.
30. Louis DN, Ohgaki H, Wiestler OD, Cavenee WK. 4th Edition WHO Classification of Tumours of the Central Nervous System. International Agency for Research on Cancer, Lyon 2007.
31. Majchrzak K, Kaspera W, Bobek-Billewicz B, Hebda A, Stasik-Pres G, Majchrzak H, Ladziński P. The assessment of prognostic factors in surgical treatment of low-grade gliomas: A prospective study. Clin Neurol Neurosurg 2012; 114: 1135-1144.
32. Matulewicz L, Sokół M, Wydmański J, Hawrylewicz L. Could lipid CH2/CH3 analysis by in vivo 1H MRS help in differentiation of tumor recurrence and post-radiation effects? Folia Neuropathol 2006; 44: 116-124.
33. Morita N, Wang S, Chawla S, Poptani H, Melhem ER. Dynamic susceptibility contrast perfusion weighted imaging in grading of nonenhancing astrocytomas. J Magn Reson Imaging 2010; 32: 803-808.
34. Provenzale JM. Imaging of angiogenesis: clinical techniques and novel imaging methods. AJR Am J Roentgenol 2007; 188: 11-23.
35. Quant EC, Wen PY. Response assessment in neuro-oncology. Curr Oncol Rep 2011; 13: 50-56.
36. Ręcławowicz D, Stempniewicz M, Biernat W, Limon J, Słoniewski P. Loss of genetic material within 1p and 19q chromosom-

al arms in low grade gliomas of central nervous system. Folia Neuropathol 2013; 51: 26-32.
37. Romanowski CAJ, Hoggard N, Jellinek DA, Levy D, Wharton SB, Kotsarini C, Batty R, Wilkinson ID. Low grade gliomas. Can we predict tumour behaviour from imaging features? NRJ 2008; 21: 41-66.
38. Rowley HA, Grant P, Roberts T. Diffusion MR imaging. Theory and applications. Neuroimaging Clin N Am 1999; 9: 343-361.
39. Russell SM, Elliott R, Forshaw D, Golfinos JG, Nelson PK, Kelly PJ. Glioma vascularity correlates with reduced patient survival and increased malignancy. Surg Neurol 2009; 72: 242-247.
40. Schomas DA, Laack NN, Rao RD, Meyer FB, Shaw EG, O'Neill BP, Giannini C, Brown PD. Intracranial low-grade gliomas in adults: 30-year experience with long-term follow-up at Mayo Clinic. Neuro Oncol 2009; 11: 437-445.
41. Server A, Kulle B, Gadmar ØB, Josefsen R, Kumar T, Nakstad PH. Measurements of diagnostic examination performance using quantitative apparent diffusion coefficient and proton MR spectroscopic imaging in the preoperative evaluation of tumor grade in cerebral gliomas. Eur J Radiol 2011; 80: 462-470.
42. Shaw E, Arusell R, Scheithauer B, O'Fallon J, O'Neill B, Dinapoli R, Nelson D, Earle J, Jones C, Cascino T, Nichols D, Ivnik R, Hellman R, Curran W, Abrams R. Prospective randomized trial of low- versus high-dose radiation therapy in adults with supratentorial low-grade glioma: initial report of a North Central Cancer Treatment Group/Radiation Therapy Oncology Group/Eastern Cooperative Oncology Group study. J Clin Oncol 2002; 20: 2267-2276.
43. Smith JS, Chang EF, Lamborn KR, Chang SM, Prados MD, Cha S, Tihan T, Vandenberg S, McDermott MW, Berger MS. Role of extent of resection in the long-term outcome of low-grade hemispheric gliomas. J Clin Oncol 2008; 26: 1338-1145.
44. van den Bent MJ, Afra D, de Witte O, Ben Hassel M, Schraub S, Hoang-Xuan K, Malmström PO, Collette L, Piérart M, Mirimanoff R, Karim AB; EORTC Radiotherapy and Brain Tumor Groups and the UK Medical Research Council. Long-term efficacy of early versus delayed radiotherapy for low-grade astrocytoma and oligodendroglioma in adults: the EORTC 22845 randomised trial. Lancet 2005; 366: 985-990. Erratum in: Lancet 2006; 367: 1818.
45. van den Bent MJ, Wefel JS, Schiff D, Taphoorn MJ, Jaeckle K, Junck L, Armstrong T, Choucair A, Waldman AD, Gorlia T, Chamberlain M, Baumert BG,Vogelbaum MA, Macdonald DR, Reardon DA, Wen PY, Chang SM, Jacobs AH. Response assessment in neuro-oncology (a report of the RANO group): assessment of outcome in trials of diffuse low-grade gliomas. Lancet Oncol 2011; 12: 583-593.
46. Weber MA, Henze M, Tüttenberg J, Stieltjes B, Meissner M, Zimmer F, Burkholder I, Kroll A, Combs SE, Vogt-Schaden M, Giesel FL, Zoubaa S, Haberkorn U, Kauczor HU, Essig M. Biopsy targeting gliomas: do functional imaging techniques identify similar target areas? Invest Radiol 2010; 45: 755-768.
47. Verheul HM, Voest EE, Schlingemann RO. Are tumours angiogenesis-dependent? J Pathol 2004; 202: 5-13.
48. Wessels PH, Weber WE, Raven G, Ramaekers FC, Hopman AH, Twijnstra A. Supratentorial grade II astrocytoma: biological features and clinical course. Lancet Neurol 2003; 2: 395-403.
49. Zeng Q, Liu H, Zhang K, Li C, Zhou G. Noninvasive evaluation of cerebral glioma grade by using multivoxel 3D proton MR spectroscopy. Magn Reson Imaging 2011; 29: 25-31.
50. Zhang W, Zhao J, Guo D, Zhong W, Shu J, Luo Y. Application of susceptibility weighted imaging in revealing intratumoral blood products and grading gliomas. J Radiol 2010; 91: 485-490.

Original article

Folia Neuropathologica

Secretory meningiomas: immunohistochemical pattern of lectins and ultrastructure of pseudopsammoma bodies

Anna Taraszewska, Ewa Matyja

Department of Experimental and Clinical Neuropathology, Mossakowski Medical Research Centre, Polish Academy of Sciences, Warsaw, Poland

Folia Neuropathol 2014; 52 (2): 141-150 DOI: 10.5114/fn.2014.43785

Abstract

Secretory meningioma is an infrequent histological subtype of benign, WHO grade I meningioma, that is characterized by focal epithelial and secretory transformation of meningothelial cells. The leading histopathological feature of neoplastic tissue is the presence of eosinophilic hyaline inclusions, defined as "pseudopsammoma bodies". These inclusions are mostly intracytoplasmic, different in size and often multiple. They are stained with periodic acid-Schiff (PAS) and are immunopositive for epithelial and secretory markers.

The aim of this study was to determine the pattern of lectin bindings and ultrastructural features of secretory meningiomas. The examination was performed on 8 cases of secretory meningiomas that occurred in women and were mostly associated with prominent peritumoural oedema. Histologically, the tumours exhibited numerous eosinophilic, PAS positive pseudopsammoma bodies. Immunohistochemical studies revealed a strong, ring-like cytokeratin expression around the pseudopsammoma bodies. The inclusions were CEA and EMA positive but negative for vimentin. The immunolabeling with four lectins (PNA, SBA, Con A and DBA) was studied. The majority of pseudopsammoma bodies and surrounding tumour cells were strongly labelled with PNA and SBA. Immunolabelling with Con A showed irregular staining with high intensity in small inclusions. Immunostaining with DBA was seldom positive in inclusions and negative in the tumour cell cytoplasm. Ultrastructure of pseudopsammoma bodies exhibited advanced heterogeneity. The size of inclusions and the content of intracytoplasmic lumina varied greatly. Some pseudopsammoma bodies seemed to be located extracellularly and lacked the obvious lumina.

Our ultrastructural study and lectin binding pattern support the unique epithelial and secretory transformation of neoplastic cells connected with their altered glycosylation.

Key words: *secretory meningioma, pseudopsammoma bodies, lectins, ultrastructure, immunohistochemistry.*

Introduction

Secretory meningioma is an unusual histological subtype of meningiomas, characterized by focal epithelial and secretory transformation of meningothelial cells. It is a benign, slowly growing lesion, referred to as grade I tumour, according to the 2007 World Health Organization (WHO) classification of tumours of the central nervous system [24]. The incidence of this specific variant, reported in various studies, ranged from 1.1% to 4.4% of all meningiomas [7,12,

Communicating author:

Anna Taraszewska, MD, Department of Clinical and Experimental Neuropathology, Mossakowski Medical Research Centre, Polish Academy of Sciences, 5 Pawinskiego St., 02-106 Warsaw, Poland, e-mail: ataraszewska@imdik.pan.pl

22,25,34,38]. Only one study documented a high incidence, accounting for 9.3% [1].

Secretory meningiomas are characterized by the presence of eosinophilic inclusions [20], which were originally described as hyaline bodies by Cushing and Eisenhart in 1938 (2nd edition 1962) [8] and later defined as "pseudopsammoma bodies" by Kepes in 1961 [14]. These inclusions are strongly stained with periodic acid-Schiff (PAS) and were immunopositive for some epithelial antigens, including cytokeratins (CKs), epithelial membrane antigens (EMA) and carcinoembryonic antigen (CEA) [2,5,7,25]. Moreover, pseudopsammoma bodies exhibit positivity for various secretory components, as immunoglobulins [4], α-1-antitripsin (AT) and α-1-antichymotrypsin (ACT) [7]. Ultrastructural features of secretory properties of the neoplastic cells were primarily demonstrated by Kepes [13] and confirmed by other electron microscopic findings [3,9,15-17,22]. Subsequently, the tumour was defined as "secretory meningioma" in 1986 by Alguacil-Garcia *et al*. [1]. From a clinical point of view, secretory meningiomas appear predominantly in women, with the most frequent location at the sphenoid ridge and frontal region. In comparison with other ordinary meningiomas, they are often associated with significant peritumoral oedema [5,12,25,26,36,38,40]. It has been speculated that some products of pseudopsammoma bodies might be involved in the development of cerebral oedema [23,26,36].

The aim of this report was to evaluate the clinico-pathological and ultrastructural features in the series of secretory meningiomas, including the immunohistochemical pattern of the lectin binding sites in tumour cells and pseudopsammoma bodies.

Material and methods

The study was performed on the surgical archival material from eight patients with postoperative diagnosis of secretory meningioma. Clinico-pathological characteristics of the patients are summarized in Table I.

All tumour specimens were fixed in 10% buffered formalin and routinely embedded in paraffin blocks. Sections were stained with haematoxylin and eosin (H&E) and periodic acid-Schiff (PAS).

Immunohistochemistry was performed on paraffin-embedded specimens; labelling was carried out by the avidin-biotin complex (ABC) method, with 3,3'-diaminobenzidine (DAB) as a chromogen. The following primary antibodies were used: anti-epithelial membrane antigen (EMA), anti-cytokeratin AE1/AE3 (CK), anti-CD34, anti-vimentin (vim) and anti-carcinoembryonic antigen (CEA); all reagents were obtained from Dako. Immunohistochemical staining of the lectin glycoconjugates was performed with 4 biotinylated lectins, as summarized in Table II: Peanut agglutinin (PNA), Soybean agglutinin (SBA), Dolichos biflorus agglutinin (DBA), Concanavalin A (Con A) (obtained from Vector Laboratories, Burlingame, CA, USA). Briefly, the deparaffinized sections were incubated with lectins in concentration of 10 µg/ml for 1 h, and then with the avidin-biotin peroxidase complex (ABC Kit) and 3'3'diaminobenzidine (DAB, Dako) reagents and counterstained with haematoxylin; details of the used method are presented in our previous report [33].

For electron microscopy, the small fragments of paraffin embedded specimens were selected, then deparaffinized, rinsed in 0.1 phosphate buffer, post-

Table I. Clinico-pathologic data

No.	Gender/Age	Tumour localization	Diameter of tumour (cm)	Peritumoural oedema	Basic histopathological pattern of meningioma
1	Female/51	Frontal convexity	5.0	No data	Meningothelial
2	Female/58	No data	2.5	Yes	Transitional
3	Female/73	Sphenoid ridge	No data	No data	Meningothelial
4	Female/50	Petrous apex	2.0	Yes	Angiomatous
5	Female/67	Sphenoid ridge	3.5	Yes	Fibroblastic
6	Female/55	Sphenoid ridge	2.5	Yes	Angiomatous
7	Female/58	Temporal basis	3.3	Yes	Meningothelial
8	Female/55	Temporal basis	4.0	No data	Meningothelial

Table II. Characteristics of lectins used for the study

Lectin names	Abbreviations	Sugar specificities
Peanut agglutinin	PNA	β-D-galactose (1-3)N-acetylgalactosamine/Gal(β1-3)GalNAc/
Soybean agglutinin	SBA	N-acetylgalactosamine (α1-3)galactose/GalNAc (α1-3)Gal/
Dolichos biflorus agglutinin	DBA	α-N-acetylgalactosamine/α-GalNAc/
Concanavalin A	Con A	α-D-mannose and β-D-glucose

fixed in solutions of 2% glutaraldehyde and 1% osmium tetroxide in the same buffer, dehydrated in graded alcohols and embedded in Epon 812. Ultrathin sections stained with uranyl acetate and lead citrate were examined with a JEM-1010 electron microscope (JEOL, Japan).

Results

Histopathological findings

All meningiomas were characterized by the presence of eosinophilic and PAS-positive pseudopsammoma bodies (Fig. 1A, B) that occurred on the background of various basic histopathological growth patterns, assessed as meningothelial, transitional, fibroblastic or angiomatous type (Table I). Pseudopsammoma bodies exhibited a wide spectrum of morphology, regarding their size and shape. The number and distribution of inclusions greatly varied within the same tumour. The bodies were loosely scattered or collected in groups and exhibited diverse forms, ranging from minute homogenous and brightly eosinophilic spheres to huge heterogeneous, weakly eosinophilic deposits, surrounded by clear "halo" (Fig. 1A).

Immunohistochemistry

Immunohistochemical studies revealed a strong immunoreactivity for CK, limited to the part of the cytoplasm of tumour cell that bordered the pseudopsammoma bodies. This CK expression usually displayed the form of a strong ring-like pattern around pseudopsammoma bodies (Fig. 2A). Immunoreactivity for CEA, of varying intensity, was evidenced both in the pseudopsammoma bodies and in the surrounding cytoplasm of neoplastic cells (Fig. 2B). Pseudopsammoma bodies were also immunopositive for EMA (Fig. 2C) but they were negative for vimentin, what was in contrast to overall positivity of tumour cells (Fig. 2D).

Immunohistochemical staining with the lectins showed that the majority of pseudopsammoma bodies and surrounding neoplastic cell cytoplasm were strongly labelled with PNA (Fig. 3A) and SBA (Fig. 3B), although the individual bodies remained unstained or were only weakly stained with the both lectins. Immunolabelling with Con A showed irregular staining of pseudopsammoma bodies. It was intense mainly in small bodies and weak in larger ones, whereas several bodies and the cytoplasm of

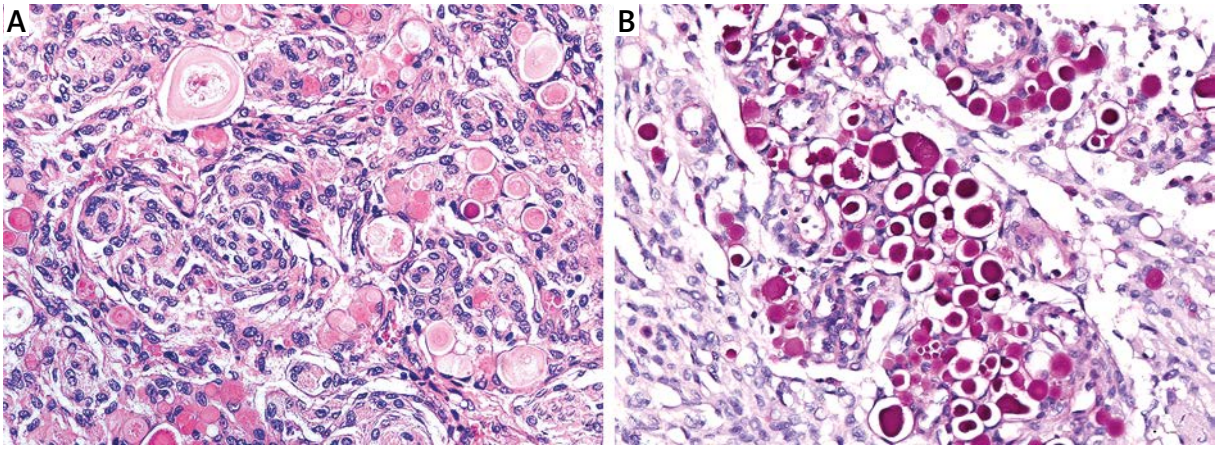

Fig. 1. A) Secretory meningioma with multiple, hyaline, eosinophilic cytoplasmic inclusion. **B)** PAS positive pseudopsammoma bodies. Original magnification **(A, B)** ×200.

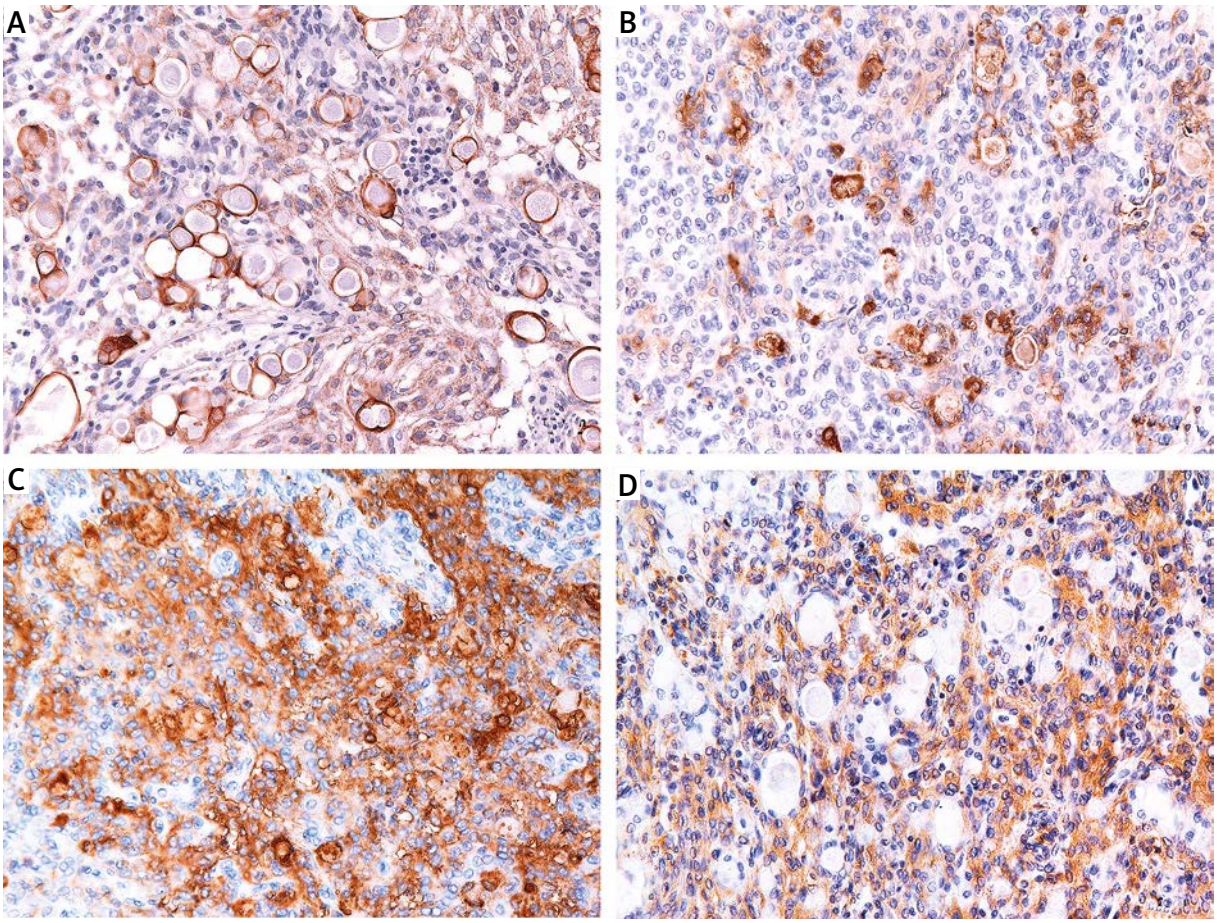

Fig. 2. Immunohistochemistry of secretory meningioma. **A)** CK expression with a distinct ring-like pattern around pseudopsammoma bodies. **B)** Immunoreactivity for CEA in the pseudopsammoma bodies and in the cytoplasm of surrounding tumour cells. **C)** Diffuse EMA immunoexpression in the pseudopsammoma bodies and in the tumour cells. **D)** Negative immunostaining for vimentin in the psammoma bodies and positive in the tumour cells. Original magnification **(A-D)** ×200.

neoplastic cells were unlabelled (Fig. 3C). Immunostaining with DBA was rarely positive in pseudopsammoma bodies and was negative in the tumour cells cytoplasm, however, the slight reactivity for DBA was seen in the nuclei of neoplastic cells (Fig. 3D).

Electron microscopy

Electron microscopic examination revealed the presence of numerous neoplastic cells, exhibiting intracytoplasmic lumina filled with microvilli and aggregations of homogenous or heterogeneous material, corresponding to pseudopsammoma bodies (Fig. 4A, B). The cytoplasm of these cells was characterized by increased electron-density, rich endoplasmic reticulum and Golgi complex vesicles and conspicuous bundles of tonofilaments, often in the close connection with intracytoplasmic lumina and microvilli (Fig. 4A, B). Furthermore, distinct interdigitations of cell processes with desmosomes and numerous microvilli, projecting from the plasmalemma to the extracellular space, were seen (Fig. 4C, D). The size of the pseudopsammoma bodies and content of intracytoplasmic lumina greatly varied. Small lumina usually contained moderately electron dense, fine filamentous and rather homogenous substance, similar to those covering the surface of microvilli (Fig. 4B). Enlarged lumina were filled with polymorphic, filamentous or granular electron dense material, either homogenous or exhibiting a mixture of heterogeneous vesicles, membranaceous structures and dense bodies (Fig. 5A, B). Numerous lumina of dif-

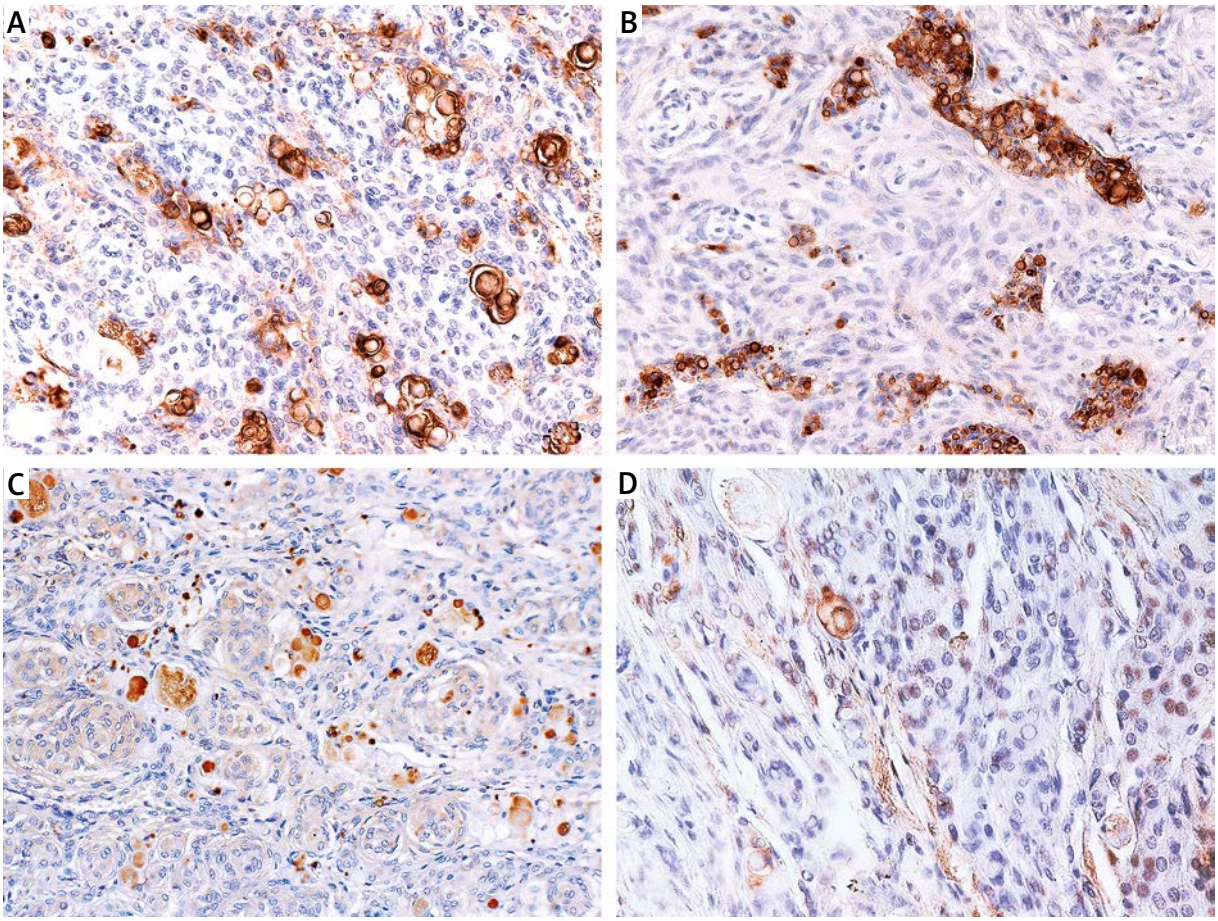

Fig. 3. Immunohistochemical staining with lectins. **A)** Strong PNA immunolabelling in the majority of pseudopsammoma bodies and the cytoplasm of surrounding tumour cells. **B)** Strong labelling with SBA of pseudopsammoma bodies and the cytoplasm of surrounding cells. **C)** Irregular staining of pseudopsammoma bodies with Con A with high intensity in small inclusions. **D)** Labelling with DBA in some pseudopsammoma bodies. Slight reactivity in the nuclei of tumour cells. Original magnification **(A-B)** ×200.

ferent size, filled with polymorphic pseudopsammoma bodies, were often seen in the cytoplasm of the same cell. Some pseudopsammoma bodies seemed to be located extracellularly and lacked the obvious lumina. They were associated with numerous microvilli, extending into intercellular space (Fig. 5C). Pseudopsammoma bodies were frequently surrounded by numerous fascicles of tonofilaments (Fig. 5D).

Discussion

All secretory meningiomas in our series showed focal epithelial and secretory transformation with accumulation of pseudopsammoma bodies. The same features have been previously demonstrated in other reports [13,22,29,35,38]. Pseudopsammoma bodies are most frequently associated with the meningothelial pattern of the tumour, however they might occur also in other histological subtypes of benign meningiomas, including lipomatous or vacuolated component [18,20,21,39]. The secretory meningiomas of the present study, comprised tumours with the basic growth pattern of the meningothelial type (4 cases), angiomatous type (2 cases), transitional type (1 case) and fibroblastic type (1 case). The mechanism, by which the individual neoplastic cells of any subtype of meningioma might be transformed into the secretory cells, is unknown. The most characteristic cellular abnormalities, corresponding to the epithelial and secretory features, consist of the presence of intracytoplasmic lumina with accumulation of secretory products [6,7,11,19]. Epithelial and

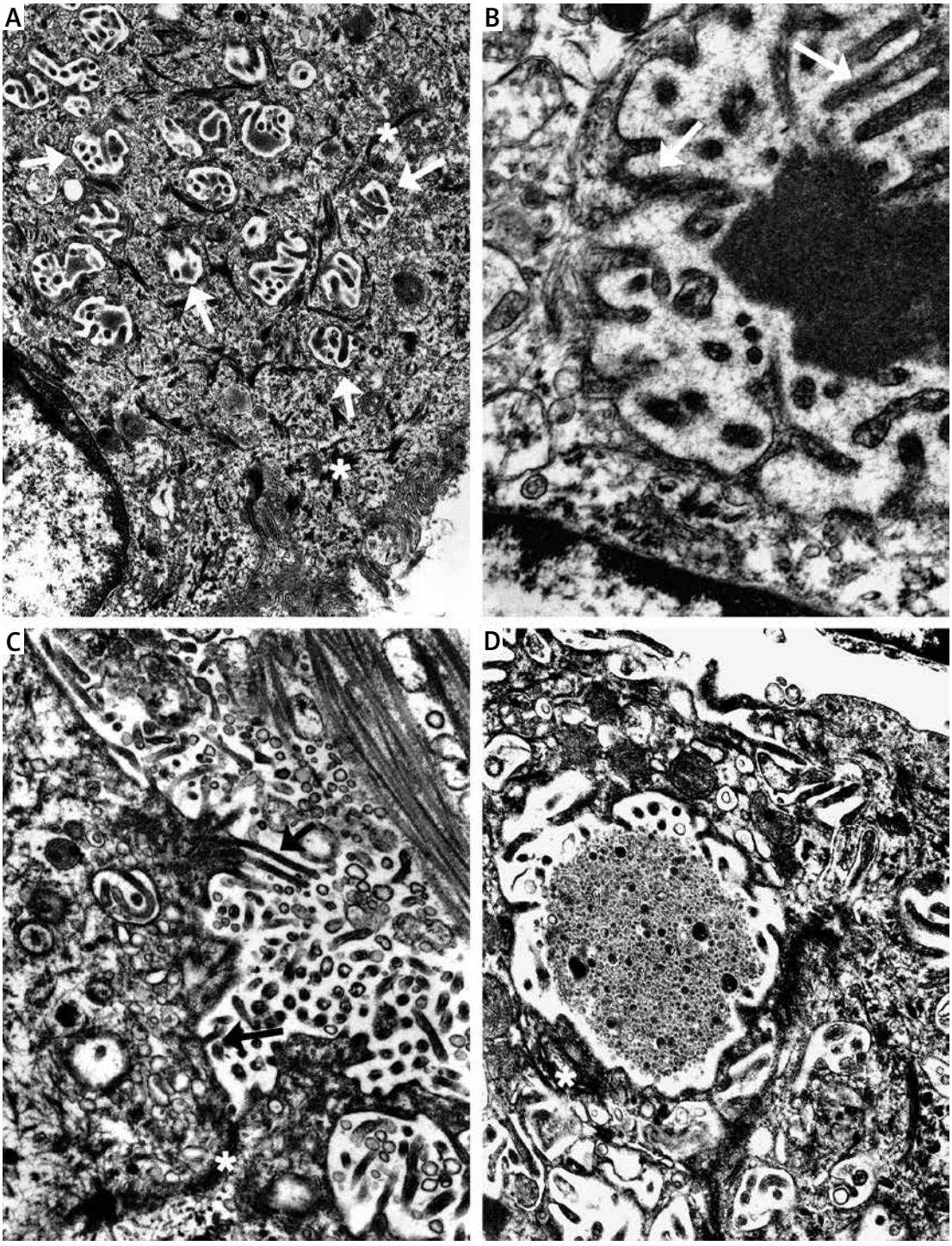

Fig. 4. Ultrastructural features. **A)** Tumour cell exhibiting numerous small intracytoplasmic cavities filled with microvilli (arrows). The cytoplasm of tumour displays increased electron-density, abundant vesicles and conspicuous bundles of tonofilaments (asterisk). **B)** Intracytoplasmic lumina containing microvilli (arrows) and homogenous or fine filamentous material. **C)** Distinct interdigitation of cell processes with desmosomes (asterisk) and numerous microvilli (arrows), projecting from the plasmalemma to the extracellular space. **D)** Multiple intercytoplasmic lumina of different size filled by microvilli and microvesicles and surrounded by tonofibrils (arrows). Original magnification: **A** ×7500; **B** ×15 000; **C–D** ×12 000.

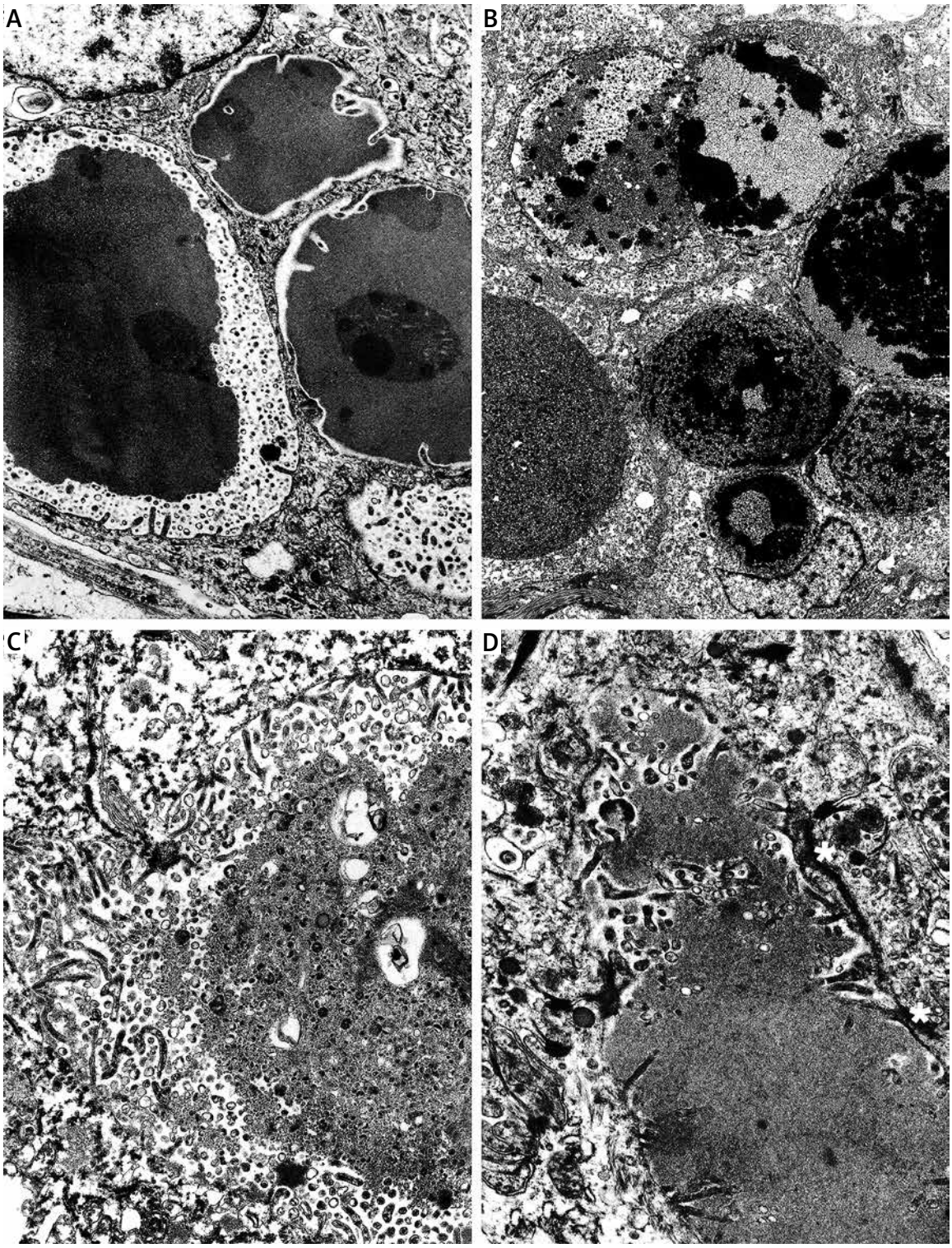

Fig. 5. Ultrastructural features. **A)** Enlarged lumina filled with homogenous, electron dense material and mixture of microvesicles. **B)** Multiple, enlarged pseudopsammoma bodies exhibiting high heterogeneity of their structure. **C)** Extracellularly located pseudopsammoma bodies associated with numerous microvilli and lacking the obvious lumen. **D)** Pseudopsammoma body surrounded by numerous fascicles of tonofilaments (asterisk). Original magnification: **A** ×6000; **B** ×2500; **C–D** ×75 000.

glandular-like differentiation of the cells has been also indicated with CK, EMA and CEA immunoreactivity in many studies [1,2,25,32,35]. Moreover, our present study demonstrated the abnormal glycosylation pattern of secretory meningioma cells.

Considering the morphology of pseudopsammoma bodies, it ought to be noted that histochemical and ultrastructural patterns of pseudopsammoma bodies exhibit the striking resemblance to the inclusions, observed within intracellular lumina in some epithelial neoplasms, especially in mammary and gastro-intestinal carcinoma or mesothelioma [4,13,16]. In epithelial cancer cells, the intracytoplasmic lumina appears as spherical cavities with microvilli and accumulation of secretion products, and they are usually surrounded by a filamentous network [27,28]. Various types of intracytoplasmic lumina have been demonstrated in electron microscopic study of breast carcinoma: type A with many microvilli on the luminal surface and abundant secretion within the lumen; type B with fewer microvilli and little or abundant secretion, and a third type of large intracytoplasmic lumina with abundant secretion and compression of the nucleus [30,31].

The present ultrastructural investigations of secretory meningiomas documented that the pseudopsammoma bodies were predominately located within large intracytoplasmic lumina, lined by microvilli. The same ultrastructural features of pseudopsammoma bodies were also demonstrated in other studies [3,9,13,16,37]. Less frequently the pseudopsammoma bodies were observed within extracellular space, filling by numerous projecting microvilli [13,15]. Both intracellular and extracellular secretory material might exhibit various forms of homogenous deposits of moderately electron-dense fine filamentous and granular substances or polymorphic large inclusions with a mixture of microvesicles, lamellar structures and electron dense clumps. These findings indicated that ultrastructural features of the secretory type of meningioma differ from the fine structure of other types of meningothelial tumours [10].

We found also some cells with predominance of small intracytoplasmic cavities, accompanied by intraluminal protrusions of microvilli and scanty secretory material. These features probably represent an initial stage of secretory activity. Sometimes, the small lumina coexisted with larger and polymorphic pseudopsammoma bodies. These observations indicate the dynamic secretory process and support the suggestion that formation of the large polymorphic bodies represent the final stage of accumulation and degradation of secretory products [3,15-17,22].

The previous histochemical reports showed that the products of secretion are composed mainly of conjugated glycoproteins [9,13,17] and are reminiscent to the glycoproteinaceous coating seen on the surface of intestinal and respiratory epithelia [16]. Immunohistochemical characteristics of pseudopsammoma bodies with one lectin were given by Kuratsu *et al*. [17]. The authors used only Concanavalin A staining and postulated that secretory bodies in meningiomas belong to mucosubstances of class II and III.

In the present study we demonstrated the reaction of the pseudopsammoma bodies and the tumour cells with four lectins, including glucose and mannose binding Con A and three lectins specific to galactose/N-acetylgalactosamine (GalNAc) glycoconjugates with differential binding sites, i.e. PNA, SBA and DBA. Our results showed that pseudopsammoma bodies and surrounding cells presented a large range of glycan structures. Pseudopsammoma bodies were stained more intensely with PNA and SBA, moderately with Con A and weakly with DBA, whereas the cytoplasm of the surrounding neoplastic cells was labelled mostly with PNA and SBA. Very small secretory granules, probably corresponding to small intracytoplasmic lumina, were also labelled with the lectins and visualized especially with Con A. These findings and our previous study of the lectin binding in various subtypes of meningioma indicated that the pattern of lectin glycoconjugates in secretory meningioma differs from other variants of meningothelial tumours [33]. Moreover, the variations in lectin bindings were demonstrated between the secretory cells and other neoplastic cells within the same tumour. Enhanced expression of the lectin glycoconjugates in the meningioma secretory cells probably reflects the selective changes in tumour cell glycosylation, that may be important for their phenotypic heterogeneity. Expression of CEA, which is a highly N-glycosylated glycoprotein, is also the characteristic finding in secretory meningiomas [1,5,22,36,37]. We demonstrated a similar pattern of the immunoreactivity for CEA and the binding sites for PNA in the pseudopsammoma bodies and the cells surrounding them.

Concluding, the present study documented the heterogenous ultrastructural and lectin binding pat-

tern of pseudopsammoma bodies and illustrated the status of altered glycosylation in the neoplastic cells of secretory meningiomas.

Disclosure

Authors report no conflict of interest.

References

1. Alguacil-Garcia A, Pettigrew NM, Sima AA. Secretory meningioma. A distinct subtype of meningioma. Am J Surg Pathol 1986; 10: 102-111.
2. Assi A, Declich P, Iacobellis M, Cozzi L, Tonnarelli G. Secretory meningioma, a rare meningioma subtype with characteristic glandular differentation: an histological and immunohistochemical study of 9 cases. Adv Clin Path 1999; 3: 47-53.
3. Berard M, Tripier MF, Choux R, Chrestian MA, Hassoun J, Toga M. Ultrastructural study of meningiothelial meningioma with 'hyaline inclusions' (author's transl). Acta Neuropathol 1978; 42:59-62 [in French].
4. Budka H. Hyaline inclusions (Pseudopsammoma bodies) in meningiomas: immunocytochemical demonstration of epithel-like secretion of secretory component and immunoglobulins A and M. Acta Neuropathol 1982; 56: 294-298.
5. Buhl R, Hugo HH, Mihajlovic Z, Mehdorn HM. Secretory meningiomas: clinical and immunohistochemical observations. Neurosurgery 2001; 48: 297-301; discussion 301-292.
6. Cenacchi G, Ferri GG, Salfi N, Tarantino L, Modugno GC, Ceroni AR, Martinelli GN. Secretory meningioma of the middle ear: a light microscopic, immunohistochemical and ultrastructural study of one case. Neuropathology 2008; 28: 69-73.
7. Colakoglu N, Demirtas E, Oktar N, Yuntem N, Islekel S, Ozdamar N. Secretory meningiomas. J Neurooncol 2003; 62: 233-241.
8. Cushing H, L E. The meningiomas: their classification, regional behavior, life history and surgical end results. Hafner Publishing Company, New York 1962; 175.
9. Font RL, Croxatto JO. Intracellular inclusions in meningothelial meningioma. A histochemical and ultrastructural study. J Neuropathol Exp Neurol 1980; 39: 575-583.
10. Jaskolski D, Papierz T, Liberski PP, Sikorska B. Ultrastructure of meningiomas: autophagy is involved in the pathogenesis of "intranuclear vacuoles". Folia Neuropathol 2012; 50: 187-193.
11. Jeong HS, Lee GK. Secretory meningioma – a case report with histopathological, immunohistochemical and ultrastructural analysis. J Korean Med Sci 1996; 11: 369-372.
12. Kamp MA, Beseoglu K, Eicker S, Steiger HJ, Hanggi D. Secretory meningiomas: systematic analysis of epidemiological, clinical, and radiological features. Acta Neurochir (Wien) 2011; 153: 457-465.
13. Kepes J. The fine structure of hyaline inclusions (pseudopsammoma bodies) in meningiomas. J Neuropathol Exp Neurol 1975; 34: 282-294.
14. Kepes J. Observations on the formation of psammoma bodies and pseudopsammoma bodies in meningiomas. J Neuropathol Exp Neurol 1961; 20: 255-262.
15. Kock KF, Teglbjaerg PS. Meningiomas with a non-meningotheliomatous component. A new type of tumour? Acta Neuropathol 1981; 55: 199-203.
16. Kubota T, Hirano A, Yamamoto S. The fine structure of hyaline inclusions in meningioma. J Neuropathol Exp Neurol 1982; 41: 81-86.
17. Kuratsu J, Matsukado Y, Sonoda H. Pseudopsammoma bodies in meningotheliomatous meningioma. A histochemical and ultrastructural study. Acta Neurochir (Wien) 1983; 68: 55-62.
18. Liebig T, Hoffmann T, Hosten N, Sander B, van Landeghem F, Stoltenburg-Didinger G, Lanksch WR. Lipomatous secretory meningioma: case report and review of the literature. Neuroradiology 1998; 40: 656-658.
19. Louis DN, Hamilton AJ, Sobel RA, Ojemann RG. Pseudopsammomatous meningioma with elevated serum carcinoembryonic antigen: a true secretory meningioma. Case report. J Neurosurg 1991; 74: 129-132.
20. Matyja E, Naganska E. History and nature of pseudopsammoma bodies. Clin Neuropathol 2006; 25: 204.
21. Nakamura N, Nojima T, Inoue K, Terasaka S, Aida T, Abe H. Vacuolated meningioma with secretory features: a case report. Noshuyo Byori 1993; 10: 99-101.
22. Nishio S, Morioka T, Suzuki S, Hirano K, Fukui M. Secretory meningioma: clinicopathologic features of eight cases. J Clin Neurosci 2001; 8: 335-339.
23. Osawa T, Tosaka M, Nagaishi M, Yoshimoto Y. Factors affecting peritumoral brain edema in meningioma: special histological subtypes with prominently extensive edema. J Neurooncol 2013; 111: 49-57.
24. Perry A, Louis DN, Scheithauer BW, Budka H, A. VD. Meningiomas. In: Louis DN, Oghaki H, Wiesttler D, Cavenee WK (eds.). WHO Classification of Tumors of the Central Nervous System, 4th edn. IARC Press, Lyon 2007, pp. 164-172.
25. Probst-Cousin S, Villagran-Lillo R, Lahl R, Bergmann M, Schmid KW, Gullotta F. Secretory meningioma: clinical, histologic, and immunohistochemical findings in 31 cases. Cancer 1997; 79: 2003-2015.
26. Regelsberger J, Hagel C, Emami P, Ries T, Heese O, Westphal M. Secretory meningiomas: a benign subgroup causing life-threatening complications. Neuro Oncol 2009; 11: 819-824.
27. Remy L. The intracellular lumen: origin, role and implications of a cytoplasmic neostructure. Biol Cell 1986; 56: 97-105.
28. Remy L, Marvaldi J. Origin of intracellular lumina in HT 29 colonic adenocarcinoma cell line. An ultrastructural study. Virchows Arch B Cell Pathol Incl Mol Pathol 1985; 48: 145-153.
29. Slowinski J, Kaluza J, Sabat D, Mrowka R, Lange D, Adamek D, Betlej M. Secretory meningioma of the brain. Report of two cases. Folia Neuropathol 1999; 37: 87-92.
30. Sun YK, Bi XL. Secretory carcinoma of the breast as a separate entity – histological, histochemical and ultrastructural study. Zhonghua Zhong Liu Za Zhi 1988; 10: 177-179.
31. Suzuki F, Saito A, Ishi K, Okazaki T, Kina K, Koyatsu J, Sugiyama K. Secretory carcinoma of the breast: an immunohistochemical and ultrastructural study. Med Electron Microsc 1999; 32: 50-56.
32. Tada T, Ishii K, Oshima S, Hara H, Kobayashi S. Secretory meningioma associated with numerous meningothelial rosettes. Acta Neuropathol 1992; 84: 342-345.

33. Taraszewska A, Matyja E. Lectin binding pattern in meningiomas of various histological subtypes. Folia Neuropathol 2007; 45: 9-18.
34. Tirakotai W, Mennel HD, Celik I, Hellwig D, Bertalanffy H, Riegel T. Secretory meningioma: immunohistochemical findings and evaluation of mast cell infiltration. Neurosurg Rev 2006; 29: 41-48.
35. Tsunoda S, Takeshima T, Sakaki T, Morimoto T, Hoshida T, Watabe Y, Goda K. Secretory meningioma with elevated serum carcinoembryonic antigen level. Surg Neurol 1992; 37: 415-418.
36. Tsuzuki N, Nakau H, Sugaya M, Hashizume K, Matsukuma S, Wada R, Kuwabara N. Secretory meningioma with severe perifocal edema - case report. Neurol Med Chir (Tokyo) 1997; 37: 620-623.
37. Vakili ST, Muller J. Intracytoplasmic lumina in meningioma: an ultrastructural and immunohistological study. Neurosurgery 1988; 23: 180-184.
38. Wang DJ, Xie Q, Gong Y, Wang Y, Cheng HX, Mao Y, Zhong P, Huang FP, Zheng K, Wang YF, Bao WM, Yang BJ, Chen H, Xie LQ, Zheng MZ, Tang HL, Zhu HD, Chen XC, Zhou LF. Secretory meningiomas: clinical, radiological and pathological findings in 70 consecutive cases at one institution. Int J Clin Exp Pathol 2013; 6: 358-374.
39. Yamada H, Hanada T, Okuda S, Yokota A, Haratake J. Secretory meningioma with lipomatous component: case report. Brain Tumor Pathol 1999; 16: 77-80.
40. Zielinski G, Grala B, Koziarski A, Kozlowski W. Skull base secretory meningioma. Value of histological and immunohistochemical findings for peritumoral brain edema formation. Neuro Endocrinol Lett 2013; 34: 111-117.

Original article

Folia Neuropathologica

Effects of hypothermia on *ex vivo* microglial production of pro- and anti-inflammatory cytokines and nitric oxide in hypoxic-ischemic brain-injured mice

Tomohiro Matsui[1], Hiroyuki Kida[2], Takuya Iha[1], Tabito Obara[1], Sadahiro Nomura[3], Tatsuya Fujimiya[4], Michiyasu Suzuki[3]

[1]Department of Laboratory Sciences, Yamaguchi University Graduate School of Medicine, [2]Department of Systems Neuroscience, Yamaguchi University Graduate School of Medicine, [3]Department of Neurosurgery, Yamaguchi University Graduate School of Medicine, [4]Department of Legal Medicine, Yamaguchi University Graduate School of Medicine, Yamaguchi, Japan

Folia Neuropathol 2014; 52 (2): 151-158 DOI: 10.5114/fn.2014.43786

Abstract

Introduction: *Activated microglia produce neurotoxic factors, including pro-inflammatory cytokines and nitric oxide (NO), in response to neuronal destruction. Therapeutic suppression of microglial release of these factors by various approaches including hypothermia is considered to be neuroprotective after severe brain damage. We examined the effects of hypothermic culture on the production of pro- and anti-inflammatory cytokines and NO in ex vivo microglia that were derived from mice with hypoxic-ischemic (HI) brain injury, through the stimulation of toll-like receptors (TLRs) that play significant roles in the pathological processes underlying a sterile central nervous system injury.*
Material and methods: *Two-day-old mice underwent the right common carotid artery ligation followed by 6% oxygen for 30 min, and thereafter were placed at 37°C for 24 h, after which microglia were isolated and then cultured with TLR2 and TLR4 agonists at 33°C and 37°C. Cytokine and NO levels in culture supernatants were measured.*
Results: *Compared with 37°C, hypothermia (33°C) reduced the production of tumour necrosis factor-alpha (TNF-α: a pro-inflammatory cytokine) at 6 h and interleukin-10 (IL-10: an anti-inflammatory cytokine) and NO at 48 h.*
Conclusions: *In TLR-activated microglia that were derived from mice with HI brain injury, hypothermia reduced the production of TNF-α, IL-10, and NO temporally, a clinically relevant finding suggesting that neuroprotection conferred by therapeutic hypothermia is related to attenuation of early-phase and late-phase inflammatory factors as well as that of late-phase anti-inflammatory factor(s) released from microglia.*

Key words: *hypothermia, hypoxic-ischemic brain injury, microglia, pro-inflammatory cytokine, anti-inflammatory cytokine, toll-like receptor, nitric oxide, ex vivo setting, temporal change.*

Introduction

Increased levels of several pro-inflammatory cytokines, such as interleukin-1 (IL-1) and interleukin-6 (IL-6), and nitric oxide (NO) in the cerebrospinal fluid (CSF) have been reported after severe head injuries in humans [6,13,32]. These potentially neurotoxic factors are produced by activated microglia when neurons are destroyed following ischaemia or trauma [38,48], and they are associated with secondary brain dam-

Communicating author:
Tomohiro Matsui, Department of Laboratory Sciences, Yamaguchi University Graduate School of Medicine, 1-1-1 Minami-kogushi, Ube, Yamaguchi 755-8505, Japan, phone/fax: +81-836-22-2865, e-mail: giants@yamaguchi-u.ac.jp

age [3,21,40]. Therapeutic suppression of microglial release of the above-mentioned factors by various approaches including hypothermia is considered to be neuroprotective after severe brain damage such as that occurring after traumatic brain injury (TBI) and cardiac arrest [1,7,23,32]. Previously, we and other groups have demonstrated a reduced production of tumour necrosis factor-alpha (TNF-α: another pro-inflammatory cytokine that is associated with neuronal injury [3,40]), IL-6, interferon-beta (IFN-β, which is known to be associated with neuronal cell death [15]), interleukin-10 (IL-10: an anti-inflammatory cytokine), and NO in hypothermic culture conditions [20,31,33-36,42]. In particular, we proposed that these effects were temporally related to the reduction of early-phase and late-phase inflammatory factors as well as that of late-phase anti-inflammatory factor(s) [33-36].

In the present study, to further explore the relationship between hypothermia and microglial responses in a more clinically relevant manner, we examined the effects of hypothermic culture on the temporal production of TNF-α, IL-10, and NO as representative pro- and anti-inflammatory factors in *ex vivo* microglia derived from mice with hypoxic-ischemic (HI) brain injury, through the stimulation of the toll-like receptor 2 (TLR2) and toll-like receptor 4 (TLR4). An *ex vivo* setting was chosen as it more closely reflects *in vivo* conditions compared with cell-culture systems *in vitro* [18,44], and the cultures of *ex vivo* microglia obtained directly from the central nervous system (CNS) show functional and temporal similarities in the responsiveness of these cells *in vivo* to a stimulus [12,51]. Moreover, while TLRs are major sensors of pathogen-associated molecular patterns that mediate innate immunity and are involved in the adaptive immune response [2], they can also be stimulated by the non-physiological appearance or unusual concentrations of certain endogenous molecules [24], which may be produced and released by damaged cells in CNS. Thus, TLRs play a significant role in the pathological processes underlying sterile CNS injury. For example, both TLR2- and TLR4-deficient mice exhibit reduced cerebral ischaemia-induced CNS injuries [10,27]. Both microglial TLR2 and TLR4 establish mechanisms by which innate immunity perpetuates CNS inflammation and neuronal damage by responding to endogenous compounds [5,22,28]. Therefore, an understanding of TLR-driven neuroinflammation in microglia derived from a brain injury model, along with their responses to hypothermia, was of particular significance in this study.

Material and methods

All protocols in this study were reviewed and approved by the Animal Care Committee of Yamaguchi University School of Medicine.

Animal model

HI brain injury was induced in the Institute of Cancer Research (ICR) mice on postnatal day 2 (P2). Pups of either sex were anesthetized with halothane (4% for induction, 2% for maintenance) in a 75 : 25 mixture of N_2O and O_2, after which the right common carotid artery was isolated and ligated. The procedure was completed within 5 min. After the procedure, the pups recovered for 1 h in a temperature-controlled incubator. They were then placed in a chamber perfused with a humidified gas mixture (6% oxygen in nitrogen) for 30 min. The temperature in the incubator and that of the water used to humidify the gas mixture were kept at 37°C. The operated pups were placed without the dam in a chamber submerged in a water bath at a stable temperature of 37°C for 24 h, where they entered the P3 stage. Control animals were anesthetized, but not subjected to HI.

To identify the extent of the brain injury induced by HI followed by 24 h at 37°C, hematoxylin staining was performed. In brief, at the end of the 24-h period after the HI, the animals were deeply anesthetized with an overdose (40 mg/kg) of pentobarbital and perfused transcardially with phosphate-buffered saline followed by 4% paraformaldehyde in phosphate buffer (PB). The brain was removed for post-fixation in 4% paraformaldehyde in PB for 4-12 h. It was then embedded in paraffin, cut into 4-µm coronal sections with a microtome, and attached to silane-coated glass slides. After slides were deparaffinized in xylene and hydrated to distilled water, hematoxylin staining was conducted. In the injured animals, mild laminar disruption was observed in the ipsilateral hemisphere to the injury, while cortical organization in the contralateral hemisphere was normal (Fig. 1). We used the brains from the injured animals in this study.

We are aware that P7 rats have become a widely used model for the study of HI brain injury [17,19,29, 46,49]. However, the overall increases in the severity

of cerebral lesions on the side of the common carotid artery ligation are similar between P2-P3 and P7 rats, while HI brain injury produces age-dependent and region-specific injuries [45]. In addition, we chose to examine mice and not rats in this study because the only commercially available kit separates mouse, but not rat, microglia (see below for the details of the method used to separate microglia).

In preliminary experiments, we first examined the possibility that microglia taken from injured brains may have become primed and accordingly responded more robustly to subsequent TLR2 and TLR4 challenges for 6 h at 37°C (see below for the culture method details). To do this, we compared microglial TNF-α production in mice with P3 HI brain injury with that from day-matched (P3) control animals; however, the TNF-α levels were very similar in injured and control animals. Next, we compared microglial TNF-α production from the ipsilateral hemisphere to the injury with that from the contralateral hemisphere in P3 HI brain-injured mice in the same culture system and, again, found a very little difference between the two groups. Based on these preliminary experiments, we decided to use both hemispheres of P3 HI brain-injured mice for the extraction of microglia. This was consistent not only with the same model used for determining the markers of apoptosis and necrosis [39] but also with another model of focal ischemic brain injury that has been used for determining the expression of several inflammatory factors [41]. In contrast, we are aware that *in vivo* pro-inflammatory cytokine levels and histological microglial activation in the ipsilateral hemisphere of HI brain-injured rats were higher than those in the contralateral hemisphere, albeit in a time-dependent manner [17,43].

Magnetic cell sorting of microglia using CD11b MicroBeads

Both cerebral hemispheres from P3 HI brain-injured pups (4-7 pups for each experiment) were removed and converted to a single-cell suspension by enzymatic degradation using a neural tissue dissociation kit and a gentleMACS dissociator (Miltenyi Biotec, Bergisch Gladbach, Germany), according to the manufacturer's protocol. In brief, brain tissues were weighed before mincing, enzyme mixes were added to the tissue pieces, and the mixture was dissociated both by mechanical trituration and by agitation at 37°C. The single-cell suspension was then

Fig. 1. Representative photomicrograph of hematoxylin staining of the brain after hypoxic-ischemic injury followed by 24 h at 37°C, demonstrating mild laminar disruption in the ipsilateral (right) hemisphere to the injury and normal cortical organization in the contralateral (left) hemisphere. White scale bar = 1 mm.

poured into a 70-µm cell strainer. The resulting cells were processed immediately using MACS MicroBead separation as follows. To separate the microglia, the CD11b-positive cells were magnetically labelled with CD11b (microglia) MicroBeads (Miltenyi Biotec). The cell suspension was loaded onto a MACS column (Miltenyi Biotec), which was placed in the magnetic field of a MACS separator (Miltenyi Biotec). The magnetically labelled CD11b-positive cells were retained within the column. After removing the column from the magnetic field, the magnetically retained CD11b-positive cells were eluted as the positively selected cell fraction. These procedures were completed within 3.5 h. The purity of the separated microglia was confirmed at > 91% by double staining with CD11b and CD45 antibodies (Miltenyi Biotec) using FACSCalibur (Becton Dickinson, Franklin Lakes, NJ, USA). The microglia in Dulbecco's Modified Eagle's Medium (DMEM) (Gibco, Grand Island, NY, USA) containing 10% foetal bovine serum (FBS) were allowed to stabilize for 1 day in a 5% CO_2 incubator at 37°C before the cells were stimulated in subsequent experiments.

Microglial cell culture

Microglia (4×10^4 cells/well in untreated 96-well plates (Becton Dickinson)) were cultured with or without 10 ng/ml Pam_3CSK_4 (*N*-palmitoyl-*S*-(2,3-bis (palmitoyloxy)-(2R,S)-propyl)-(*R*)-cysteinyl-seryl-(lysyl) 3-lysine: a TLR2 agonist) (Imgenex, San Diego, CA,

USA) or 1 μg/ml lipopolysaccharide (LPS: a TLR4 agonist) (Sigma-Aldrich, St Louis, OH, USA) to measure TNF-α, IL-10, and NO production. Culture was performed in DMEM containing 10% FBS in a 5% CO_2 incubator at temperatures of 33°C (hypothermia) and 37°C (normothermia) for 6 h for TNF-α assays and 48 h for IL-10 and NO assays. In our preliminary investigations, the doses of the TLR agonists (for Pam_3CSK_4; 10 and 100 ng/ml and for LPS; 0.001, 0.01, 0.1, and 1 μg/ml) for TNF-α production for 6 h were tested. Accordingly, the Pam_3CSK_4 dose of 10 ng/ml and LPS dose of 1 μg/ml were determined because there were very little differences in TNF-α production (pg/ml) between the two doses of Pam_3CSK_4 (10 ng/ml; 94 ± 6 and 100 ng/ml; 101 ± 8, n = 3) and dose-dependent increases in LPS (0.001 μg/ml; 87 ± 6, 0.01 μg/ml; 156 ± 19, 0.1 μg/ml; 190 ± 27, and 1 μg/ml; 258 ± 37, n = 3). These doses were in accordance with our previous *in vitro* studies including those of IL-10 and NO [33,36]. Because the present study was designed to exploit our previous *in vitro* findings in terms of the temporal change of TNF-α, IL-10, and NO production [33,35,36], we selected each culture period above for the cytokines/NO as representative time points.

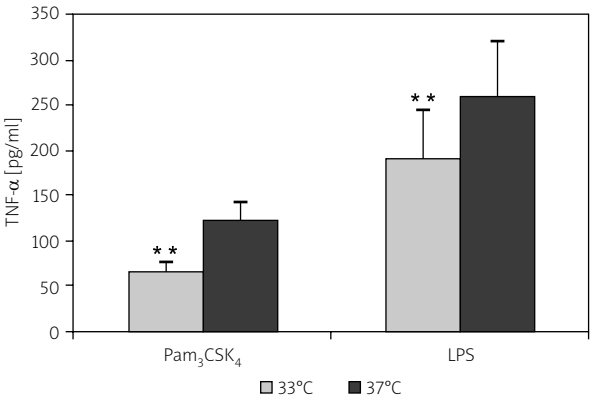

Fig. 2. Effects of hypothermic culture on TNF-α production by TLR2- and TLR4-stimulated *ex vivo* microglia derived from mice with hypoxic-ischemic brain injury. Microglia (4×10^4 cells/well) were cultured with 10 ng/ml Pam_3CSK_4 (a TLR2 agonist) or 1 μg/ml LPS (a TLR4 agonist) in hypothermic (33°C) and normothermic (37°C) conditions for 6 h. TNF-α levels in culture supernatants were measured by ELISA. Data are expressed as mean ± SEM (n = 5 for Pam_3CSK_4 stimulation and n = 6 for LPS stimulation). $^{**}p < 0.01$ compared with 37°C.

Cytokine assay

Concentrations of TNF-α and IL-10 in microglial culture supernatants were measured in duplicate using an enzyme-linked immunosorbent assay (ELISA) kit (Invitrogen, Camarillo, CA, USA), according to the manufacturer's instructions.

NO assay

NO production was quantified as nitrite (NO_2^-), a relatively stable metabolite of NO, accumulating in the culture medium. A colorimetric assay with Griess reagent (Sigma-Aldrich) was performed, as described in our previous reports [33-36].

Statistical analysis

Data are expressed as mean ± standard error of the mean (SEM). Although the number of samples (n) in this study is modest, each experiment required microglia pooled from 4-7 brains as mentioned above. Differences in values between two groups were analyzed using the paired t-test (StatFlex ver. 5.0, Arteck, Osaka, Japan). $P < 0.05$ was considered to indicate a significant difference.

Results

Effects of hypothermic culture on TNF-α production

TNF-α was virtually undetectable in microglia without TLR agonists after 6 h of culture (basal conditions). Application of TLR agonists to microglia elicited significant TNF-α production, and this effect was greater for TLR4 stimulation than for TLR2 stimulation (Fig. 2). For both types of TLR stimulation, microglial TNF-α production was significantly reduced at 33°C compared with 37°C (Fig. 2).

Effects of hypothermic culture on IL-10 production

IL-10 was virtually undetectable in microglia without TLR agonists after 48 h of culture (basal conditions). Application of TLR agonists to microglia increased IL-10 production, and this effect was greater for TLR4 stimulation than for TLR2 stimulation (Fig. 3). For both types of TLR stimulation, microglial IL-10 production was significantly reduced at 33°C compared with 37°C (Fig. 3).

Effects of hypothermic culture on NO production

NO_2^- was virtually undetectable in microglia without TLR agonists after 48 h of culture (basal conditions). Application of the TLR4 agonist to microglia increased NO_2^- production (Fig. 4), while application of the TLR2 agonist did not (*i.e.*, NO_2^- remained virtually undetectable). Compared with 37°C, this increase was significantly reduced at 33°C (Fig. 4).

Discussion

With the aim of elucidating the possible mechanisms underlying the neuroprotective effects of therapeutic hypothermia, we have previously shown that hypothermia reduces the production of early-phase and late-phase inflammatory factors as well as that of late-phase anti-inflammatory factor in primary microglia *in vitro* [33-36]. We considered that an approach using microglia removed directly from injured brains may yield more clinically relevant information. Hence, in this study, we utilized *ex vivo* microglia with high purity that were derived from mice with HI brain injury. With this approach, we demonstrated that hypothermia (33°C) reduced the production by these cells of TNF-α in the early phase (6 h) and that of IL-10 and NO in the late phase (48 h) after the stimulation of TLR2 and/or TLR4. To the best of our knowledge, this is the first report to describe the direct responses of microglia derived from injured animals to hypothermia.

The finding that hypothermia reduced the TLR2- and TLR4-activated microglial release of pro- and anti-inflammatory cytokines and NO in *ex vivo* conditions was consistent with the findings of reports of the same stimuli *in vitro* [33,36]. In *in vivo* studies, therapeutic hypothermia has also been shown to attenuate the increases in the CNS levels of pro-inflammatory cytokines and NO after brain injury [1,32,50], and this has been associated with a favourable outcome compared with normothermia [1,32]. Furthermore, hypothermia during severe perinatal asphyxia prevents increases in 3',5'-cyclic monophosphate, which is a marker of NO, in the rat brain. In this study, 100% of the hypothermic rats survived, whereas 70% mortality was observed in the normothermic group [30]. Therefore, the present findings strongly supported the idea that a reduction in the microglial production of pro-inflammatory cytokines and NO is an important neuroprotective effect of

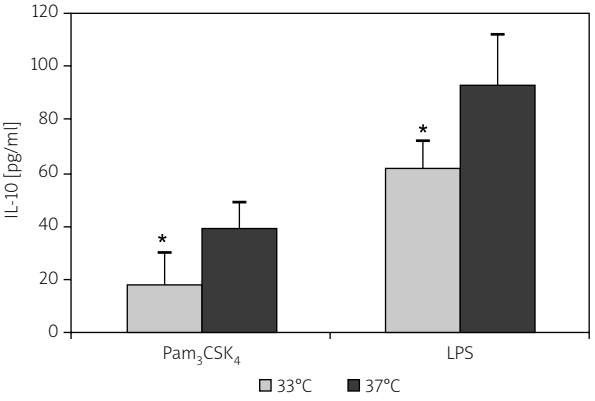

Fig. 3. Effects of hypothermic culture on IL-10 production by TLR2- and TLR4-stimulated *ex vivo* microglia derived from mice with hypoxic-ischemic brain injury. Microglia (4×10^4 cells/well) were cultured with 10 ng/ml Pam_3CSK_4 (a TLR2 agonist) or 1 µg/ml LPS (a TLR4 agonist) in hypothermic (33°C) and normothermic (37°C) conditions for 48 h. IL-10 levels in culture supernatants were measured by ELISA. Data are expressed as mean ± SEM (n = 4 for Pam_3CSK_4 stimulation and n = 5 for LPS stimulation). *$p < 0.05$ compared with 37°C.

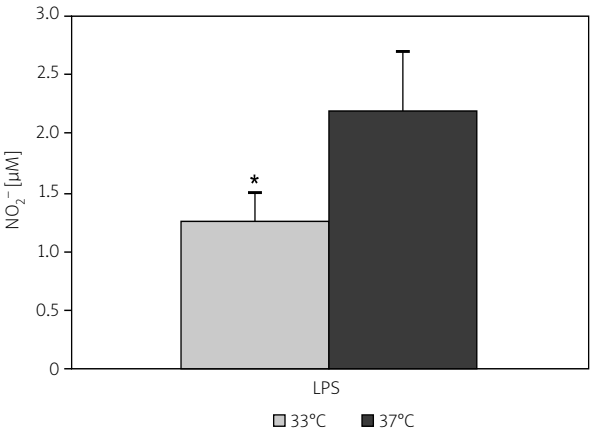

Fig. 4. Effects of hypothermic culture on NO production by TLR4-stimulated *ex vivo* microglia derived from mice with hypoxic-ischemic brain injury. Microglia (4×10^4 cells/well) were cultured with 1 µg/ml LPS (a TLR4 agonist) in hypothermic (33°C) and normothermic (37°C) conditions for 48 h. Nitrite (NO_2^-, a relatively stable metabolite of NO) levels in culture supernatants were measured by colorimetric assay with Griess reagent. Data are expressed as mean ± SEM (n = 5). *$p < 0.05$ compared with 37°C.

therapeutic hypothermia [33-36]. IL-10 has been considered to be neuroprotective because it reduces the production of pro-inflammatory cytokines [8,26]. In contrast, the CSF levels of IL-10 have been shown to increase after severe TBI and to be independently associated with increased mortality [6], indicating a detrimental *in vivo* effect of increased levels of IL-10 in CNS. Microglial activation by TLR2 and TLR4 has been found to lead initially to the synthesis of pro-inflammatory cytokines and later to the synthesis of IL-10 [33,36]. As noted, microglial IL-10 production was reduced by hypothermia in the late phase. Taken together, our findings further suggested that the neuroprotective effects of therapeutic hypothermia are related to the attenuation of the production of early-phase and late-phase inflammatory factors as well as that of late-phase anti-inflammatory factor(s) by microglia. This mechanism may also be applicable to treatment for HI brain injury because in the CSF of patients with neonatal HI encephalopathy (HIE), pro-inflammatory cytokines and NO levels have been shown to be increased, and their concentrations correlate with the degree of injury [4,16], although the involvement of IL-10 in this mechanism is unknown. Interestingly, the concept that we proposed here and in our previous study [36] of the temporal modulation of cytokine production and/or inflammation (neuroinflammatory response) by hypothermia is associated with its neuroprotective effect is supported by the findings of two recent studies: one in animals and one in humans. In an animal model of CNS injury that was induced by cerebral ischaemia, reducing the brain temperature attenuated the early-phase (8 h) production of interleukin-1 beta (IL-1β) in the brain, and this coincided with a reduced infarct size and improved functional outcome [11]. In patients with ischemic and hemorrhagic stroke, the beneficial effects of low temperature on functional outcomes occurred within the first 24 h after the stroke onset, whereas the harmful effects of high temperatures that are associated with inflammation occurred later (in the first 48 h) [9]. Such time- and inflammation-targeted therapeutic interventions may be worth considering in the future.

With the aim of determining a possible pathophysiological significance of the reduced production of TNF-α, IL-10, and NO by microglia for hypothermic neuronal protection, we have recently demonstrated that they individually induced the death of neuronal PC12 cells in a concentration-dependent manner [35,37]. Taking these findings and the facts that their elevated levels in the CNS after brain injury *in vivo* [6,13,47,50] together, these results further support the conclusion that a decrease in the levels of TNF-α, IL-10, and NO during hypothermia contributes toward the protection of neurons.

In animals with HI brain injury, hypothermia has been shown to reduce the mRNA expression of interleukin-18 (IL-18: another pro-inflammatory cytokine), TNF-α, and IL-6 in the brain [19,49]. However, in this model, the sources of these cytokines were unclear, and the effects of hypothermia on IL-10 expression were unknown. Moreover, an investigation of the responses of microglia derived from brain-injured animals to TLR stimulation, along with their responses to hypothermia, is of particular significance because both microglial TLR2 and TLR4 play an important role in triggering immediate responses and/or enhancing reactions to tissue injury and inflammation [5,22,28]. In addition, an *ex vivo* culture of microglia isolated from CNS preserves the *in vivo* phenotype of microglia [18,51]. Importantly, as mentioned above, in terms of the temporal changes of neuroinflammatory responses, our present *ex vivo* findings, as well as our previous *in vitro* findings [33-36], appear to be similar to the *in vivo* findings for brain injury [9,11], as well as to those regarding IL-10 *in vivo*, which indicate that the levels in the brain show a peak during the first days (24-48 h) after brain injury [6,14,25]. Temporal similarity between the *ex vivo* and *in vivo* expressions of a signalling molecule in microglia has also been reported [12,51]. Thus, our *ex vivo* experiments with TLR stimulation may also allow us to study microglial function in pathophysiological states and therefore be useful in examining the effects of hypothermia.

In conclusion, we demonstrated that it is possible to rapidly isolate and functionally culture active microglia from mice with HI brain injury and that hypothermia (33°C) reduced the temporal production of pro- and anti-inflammatory cytokines and NO from TLR-activated *ex vivo* microglia derived from these animals. We were able to further explore the relationships between hypothermia and microglial responses using a brain-injured model.

Acknowledgements

We would like to thank Dr. Jinyao Liu (Department of Legal Medicine, Yamaguchi University Grad-

uate School of Medicine) for his kind support in performance of microglial separation. This research was supported in part by a Grant-in-Aid for Young Scientists (B), No. 22791435, from the Ministry of Education, Culture, Sports, Science, and Technology of Japan to T.M., and a grant from Yamaguchi University Foundation to T.M.

Disclosure

Authors report no conflict of interest.

References

1. Aibiki M, Maekawa S, Ogura S, Kinoshita Y, Kawai N, Yokono S. Effect of moderate hypothermia on systemic and internal jugular plasma IL-6 levels after traumatic brain injury in humans. J Neurotrauma 1999; 16: 225-232.
2. Akira S, Uematsu S, Takeuchi O. Pathogen recognition and innate immunity. Cell 2006; 124: 783-801.
3. Allan SM, Tyrrell PJ, Rothwell NJ. Interleukin-1 and neuronal injury. Nat Rev Immunol 2005; 5: 629-640.
4. Aly H, Khashaba MT, El-Ayouty M, El-Sayed O, Hasanein BM. IL-1beta, IL-6 and TNF-alpha and outcomes of neonatal hypoxic ischemic encephalopathy. Brain Dev 2006; 28: 178-182.
5. Babcock AA, Wirenfeldt M, Holm T, Nielsen HH, Dissing-Olesen L, Toft-Hansen H, Millward JM, Landmann R, Rivest S, Finsen B, Owens T. Toll-like receptor 2 signaling in response to brain injury: an innate bridge to neuroinflammation. J Neurosci 2006; 26: 12826-12837.
6. Bell MJ, Kochanek PM, Doughty LA, Carcillo JA, Adelson PD, Clark RS, Wisniewski SR, Whalen MJ, DeKosky ST. Interleukin-6 and interleukin-10 in cerebrospinal fluid after severe traumatic brain injury in children. J Neurotrauma 1997; 14: 451-457.
7. Bernard SA, Gray TW, Buist MD, Jones BM, Silvester W, Gutteridge G, Smith K. Treatment of comatose survivors of out-of-hospital cardiac arrest with induced hypothermia. N Engl J Med 2002; 346: 557-563.
8. Bethea JR, Nagashima H, Acosta MC, Briceno C, Gomez F, Marcillo AE, Loor K, Green J, Dietrich WD. Systemically administered interleukin-10 reduces tumor necrosis factor-alpha production and significantly improves functional recovery following traumatic spinal cord injury in rats. J Neurotrauma 1999; 16: 851-863.
9. Blanco M, Campos F, Rodríguez-Yáñez M, Arias S, Fernández-Ferro J, Gómez-Sánchez JC, Castillo J. Neuroprotection or increased brain damage mediated by temperature in stroke is time dependent. PLoS One 2012; 7: e30700. doi: 10.1371/journal.pone.0030700.
10. Cao CX, Yang QW, Lv FL, Cui J, Fu HB, Wang JZ. Reduced cerebral ischemia-reperfusion injury in Toll-like receptor 4 deficient mice. Biochem Biophys Res Commun 2007; 353: 509-514.
11. Ceulemans AG, Zgavc T, Kooijman R, Hachimi-Idrissi S, Sarre S, Michotte Y. Mild hypothermia causes differential, time-dependent changes in cytokine expression and gliosis following endothelin-1-induced transient focal cerebral ischemia. J Neuroinflammation 2011; 8: 60.
12. Clark AK, D'Aquisto F, Gentry C, Marchand F, McMahon SB, Malcangio M. Rapid co-release of interleukin 1beta and caspase 1 in spinal cord inflammation. J Neurochem 2006; 99: 868-880.
13. Clark RS, Kochanek PM, Obrist WD, Wong HR, Billiar TR, Wisniewski SR, Marion DW. Cerebrospinal fluid and plasma nitrite and nitrate concentrations after head injury in humans. Crit Care Med 1996; 24: 1243-1251.
14. Csuka E, Morganti-Kossmann MC, Lenzlinger PM, Joller H, Trentz O, Kossmann T. IL-10 levels in cerebrospinal fluid and serum of patients with severe traumatic brain injury: relationship to IL-6, TNF-alpha, TGF-beta1 and blood-brain barrier function. J Neuroimmunol 1999; 101: 211-221.
15. Dedoni S, Olianas MC, Onali P. Interferon-β induces apoptosis in human SH-SY5Y neuroblastoma cells through activation of JAK-STAT signaling and down-regulation of PI3K/Akt pathway. J Neurochem 2010; 115: 1421-1433.
16. Ergenekon E, Gücüyener K, Erbaş D, Aral S, Koç E, Atalay Y. Cerebrospinal fluid and serum vascular endothelial growth factor and nitric oxide levels in newborns with hypoxic ischemic encephalopathy. Brain Dev 2004; 26: 283-286.
17. Feng Y, LeBlanc MH. Effect of agmatine on the time course of brain inflammatory cytokines after injury in rat pups. Ann N Y Acad Sci 2003; 1009: 152-156.
18. Frank MG, Wieseler-Frank JL, Watkins LR, Maier SF. Rapid isolation of highly enriched and quiescent microglia from adult rat hippocampus: immunophenotypic and functional characteristics. J Neurosci Methods 2006; 151: 121-130.
19. Fukui O, Kinugasa Y, Fukuda A, Fukuda H, Tskitishvili E, Hayashi S, Song M, Kanagawa T, Hosono T, Shimoya K, Murata Y. Post-ischemic hypothermia reduced IL-18 expression and suppressed microglial activation in the immature brain. Brain Res 2006; 1121: 35-45.
20. Gibbons H, Sato TA, Dragunow M. Hypothermia suppresses inducible nitric oxide synthase and stimulates cyclooxygenase-2 in lipopolysaccharide stimulated BV-2 cells. Brain Res Mol Brain Res 2003; 110: 63-75.
21. Guo MF, Yu JZ, Ma CG. Mechanisms related to neuron injury and death in cerebral hypoxic ischaemia. Folia Neuropathol 2011; 49: 79-87.
22. Hoffmann O, Braun JS, Becker D, Halle A, Freyer D, Dagand E, Lehnardt S, Weber JR. TLR2 mediates neuroinflammation and neuronal damage. J Immunol 2007; 178: 6476-6481.
23. Hypothermia after Cardiac Arrest Study Group. Mild therapeutic hypothermia to improve the neurologic outcome after cardiac arrest. N Engl J Med 2002; 346: 549-556.
24. Johnson GB, Brunn GJ, Platt JL. Activation of mammalian Toll-like receptors by endogenous agonists. Crit Rev Immunol 2003; 23: 15-44.
25. Kamm K, Vanderkolk W, Lawrence C, Jonker M, Davis AT. The effect of traumatic brain injury upon the concentration and expression of interleukin-1beta and interleukin-10 in the rat. J Trauma 2006; 60: 152-157.
26. Knoblach SM, Faden AI. Interleukin-10 improves outcome and alters proinflammatory cytokine expression after experimental traumatic brain injury. Exp Neurol 1998; 153: 143-151.
27. Lehnardt S, Lehmann S, Kaul D, Tschimmel K, Hoffmann O, Cho S, Krueger C, Nitsch R, Meisel A, Weber JR. Toll-like receptor 2

mediates CNS injury in focal cerebral ischemia. J Neuroimmunol 2007; 190: 28-33.
28. Lehnardt S, Schott E, Trimbuch T, Laubisch D, Krueger C, Wulczyn G, Nitsch R, Weber JR. A vicious cycle involving release of heat shock protein 60 from injured cells and activation of toll-like receptor 4 mediates neurodegeneration in the CNS. J Neurosci 2008; 28: 2320-2331.
29. Lin S, Rhodes PG, Cai Z. Whole body hypothermia broadens the therapeutic window of intranasally administered IGF-1 in a neonatal rat model of cerebral hypoxia-ischemia. Brain Res 2011; 1385: 246-256.
30. Loidl CF, De Vente J, van Ittersum MM, van Dijk EH, Vles JS, Steinbusch HW, Blanco CE. Hypothermia during or after severe perinatal asphyxia prevents increase in cyclic GMP-related nitric oxide levels in the newborn rat striatum. Brain Res 1998; 791: 303-307.
31. Maekawa S, Aibiki M, Si QS, Nakamura Y, Shirakawa Y, Kataoka K. Differential effects of lowering culture temperature on mediator release from lipopolysaccharide-stimulated neonatal rat microglia. Crit Care Med 2002; 30: 2700-2704.
32. Marion DW, Penrod LE, Kelsey SF, Obrist WD, Kochanek PM, Palmer AM, Wisniewski SR, DeKosky ST. Treatment of traumatic brain injury with moderate hypothermia. N Engl J Med 1997; 336: 540-546.
33. Matsui T, Kakeda T. IL-10 production is reduced by hypothermia but augmented by hyperthermia in rat microglia. J Neurotrauma 2008; 25: 709-715.
34. Matsui T, Motoki Y, Inomoto T, Miura D, Kato Y, Suenaga H, Hino K, Nojima J. Temperature-related effects of adenosine triphosphate-activated microglia on pro-inflammatory factors. Neurocrit Care 2012; 17: 293-300.
35. Matsui T, Motoki Y, Yoshida Y. Hypothermia reduces Toll-like receptor 3-activated microglial interferon-β and nitric oxide production. Mediators Inflamm 2013; 2013: 436263. doi: 10.1155/2013/436263.
36. Matsui T, Tasaki M, Yoshioka T, Motoki Y, Tsuneoka H, Nojima J. Temperature- and time-dependent changes in TLR2-activated microglial NF-κB activity and concentrations of inflammatory and anti-inflammatory factors. Intensive Care Med 2012; 38: 1392-1399.
37. Matsui T, Yoshida Y, Yanagihara M, Suenaga H. Hypothermia at 35°C reduces the time-dependent microglial production of pro-inflammatory and anti-inflammatory factors that mediate neuronal cell death. Neurocrit Care 2014; 20: 301-310.
38. Minghetti L, Levi G. Microglia as effector cells in brain damage and repair: focus on prostanoids and nitric oxide. Prog Neurobiol 1998; 54: 99-125.
39. Ohmura A, Nakajima W, Ishida A, Yasuoka N, Kawamura M, Miura S, Takada G. Prolonged hypothermia protects neonatal rat brain against hypoxic-ischemia by reducing both apoptosis and necrosis. Brain Dev 2005; 27: 517-526.
40. Ott L, McClain CJ, Gillespie M, Young B. Cytokines and metabolic dysfunction after severe head injury. J Neurotrauma 1994; 11: 447-472.
41. Shichita T, Sugiyama Y, Ooboshi H, Sugimori H, Nakagawa R, Takada I, Iwaki T, Okada Y, Iida M, Cua DJ, Iwakura Y, Yoshimura A. Pivotal role of cerebral interleukin-17-producing gammadelta T cells in the delayed phase of ischemic brain injury. Nat Med 2009; 15: 946-950.
42. Si QS, Nakamura Y, Kataoka K. Hypothermic suppression of microglial activation in culture: inhibition of cell proliferation and production of nitric oxide and superoxide. Neuroscience 1997; 81: 223-239.
43. Sizonenko SV, Kiss JZ, Inder T, Gluckman PD, Williams CE. Distinctive neuropathologic alterations in the deep layers of the parietal cortex after moderate ischemic-hypoxic injury in the P3 immature rat brain. Pediatr Res 2005; 57: 865-872.
44. Stein VM, Czub M, Hansen R, Leibold W, Moore PF, Zurbriggen A, Tipold A. Characterization of canine microglial cells isolated ex vivo. Vet Immunol Immunopathol 2004; 99: 73-85.
45. Towfighi J, Mauger D, Vannucci RC, Vannucci SJ. Influence of age on the cerebral lesions in an immature rat model of cerebral hypoxia–ischemia: a light microscopic study. Brain Res Dev Brain Res 1997; 100: 149-160.
46. Vannucci RC, Connor JR, Mauger DT, Palmer C, Smith MB, Towfighi J, Vannucci SJ. Rat model of perinatal hypoxic-ischemic brain damage. J Neurosci Res 1999; 55: 158-163.
47. Vitarbo EA, Chatzipanteli K, Kinoshita K, Truettner JS, Alonso OF, Dietrich WD. Tumor necrosis factor alpha expression and protein levels after fluid percussion injury in rats: the effect of injury severity and brain temperature. Neurosurgery 2004; 55: 416-424.
48. Woodroofe MN, Sarna GS, Wadhwa M, Hayes GM, Loughlin AJ, Tinker A, Cuzner ML. Detection of interleukin-1 and interleukin-6 in adult rat brain, following mechanical injury, by in vivo microdialysis: evidence of a role for microglia in cytokine production. J Neuroimmunol 1991; 33: 227-236.
49. Xiong M, Yang Y, Chen GQ, Zhou WH. Post-ischemic hypothermia for 24h in P7 rats rescues hippocampal neuron: association with decreased astrocyte activation and inflammatory cytokine expression. Brain Res Bull 2009; 79: 351-357.
50. Yamaguchi S, Nakahara K, Miyagi T, Tokutomi T, Shigemori M. Neurochemical monitoring in the management of severe head-injured patients with hypothermia. Neurol Res 2000; 22: 657-664.
51. Yip PK, Kaan TK, Fenesan D, Malcangio M. Rapid isolation and culture of primary microglia from adult mouse spinal cord. J Neurosci Methods 2009; 183: 223-237.

Original article

Folia Neuropathologica

Monitoring of very long-chain fatty acids levels in X-linked adrenoleukodystrophy, treated with haematopoietic stem cell transplantation and Lorenzo's Oil

Teresa J. Stradomska[1], Katarzyna Drabko[2], Elżbieta Moszczyńska[3], Anna Tylki-Szymańska[4]

[1]Department of Biochemistry, Radioimmunology and Experimental Medicine, Children's Memorial Health Institute, Warsaw, [2]Department of Paediatric Haematology, Oncology and Transplantology, Medical University of Lublin, [3]Department of Endocrinology and Diabetology, Children's Memorial Health Institute, Warsaw, [4]Department of Paediatrics, Nutrition and Metabolic Diseases, Children's Memorial Health Institute, Warsaw, Poland

Folia Neuropathol 2014; 52 (2): 159-163 DOI: 10.5114/fn.2014.43787

Abstract

X-linked adrenoleukodystrophy is a rare, neurodegenerative peroxisomal disorder connected with mutation in the ABCD1 gene, causing impairment of the peroxisomal β-oxidation process and in consequence, accumulation of very long-chain fatty acids (VLCFA) in blood and tissues. In this study we present serum very long-chain fatty acids levels during clinical course in an X-linked adrenoleukodystrophy patient after haematopoietic stem cell transplantation (HSCT) and on Lorenzo's Oil in a 11 years' period. The patient was diagnosed at the age of 8 months by family screening. The administration of LO was started at 2 years of age. HSCT from a family donor was performed twice. VLCFA serum levels were detected by the GC method. Chimaerism subsequent to HSCT was also analyzed.
Increasing very long-chain fatty acids levels correlate with a decreasing chimaerism level after haematopoietic stem cell transplantation. The sequential monitoring of very long-chain fatty acids serum levels is important and useful for assessment of engraftment, graft failure or rejection.

Key words: *adrenoleukodystrophy, haematopoietic stem cell transplantation, very long-chain fatty acids, VLCFA, chimaerism, Lorenzo's Oil.*

Introduction

X-linked adrenoleukodystrophy (X-ALD) is the most common peroxisomal neurodegenerative disorder affecting males. The clinical spectrum ranges from rapidly progressing cerebral demyelinization or slowly progressive myelopathy to isolated adrenal insufficiency. Biochemically it is characterized by the accumulation of very long-chain fatty acids (C24:0, C26:0) in plasma and tissues. X-linked adrenoleukodystrophy results from mutations in the *ABCD1* gene, which encodes an ABC half transporter, adrenoleukodystrophy protein (ALDP). ALD peroxisomal membrane protein imports very long-chain fatty acids (VLCFA) or very long-chain fatty acids-CoA into peroxisomes, where they are degraded by a peroxisomal β-oxidation pathway. ALDP deficiency leads to impaired VLCFA β-oxidation and the accumulation of very

Communicating author:
Teresa J. Stradomska, Department of Biochemistry, Radioimmunology and Experimental Medicine, The Children's Memorial Health Institute, Al. Dzieci Polskich 20, 04-730 Warsaw, Poland, fax: +48 22 815 13 13, e-mail: jstradomska@op.pl, j.de.stradomska@gmail.com

long-chain fatty acids-CoA esters in cells and body fluids. The diagnosis of X-linked adrenoleukodystrophy is based on the identification of an increased level of VLCFA in blood [1].

Lorenzo's Oil (LO) administration is an option in management of X-linked adrenoleukodystrophy patients. Lorenzo's Oil, a mixture of glyceryl trioleate and glyceryl trierucate, decreases very long-chain fatty acids levels in serum. The Oil administration has been proposed in asymptomatic patients [5].

Allogeneic haematopoietic stem cell transplantation (HSCT), if available, remains the recommended therapeutic intervention that can arrest the progress of cerebral demyelinization in X-linked adrenoleukodystrophy patients. The principle behind haematopoietic stem cell transplantation is that the donor-derived cells replace the bone marrow of the recipient. Physiological very long-chain fatty acids β-oxidation takes place in the donor's leucocytes [2,6-8].

The aim of this study is to evaluate the serum VLCFA levels measured in an X-linked adrenoleukodystrophy patient during his treatment. Firstly, the patient was treated with Lorenzo's Oil; secondly, he had haematopoietic stem cell transplantation twice.

Material and methods

A male child, currently 11 years and 7 months old, was diagnosed with X-linked adrenoleukodystrophy at the age of 8 months during family screening (his elder brother died from childhood cerebral X-linked adrenoleukodystrophy at the age of 10 years). Lorenzo's Oil was administered from the age of 2 years old. At 5 months before the haematopoietic stem cell transplantation, the Lorenzo's Oil treatment was interrupted. At the age of 4 years and 7 months at the presymptomatic stage of the disease, the first haematopoietic stem cell transplantation from a family donor was performed. The first graft was rejected after a year. The second haematopoietic stem cell transplantation from the same donor was performed at the age of 6 years when the patient was still asymptomatic. At the age of 7 years and 4 months, Lorenzo's Oil was re-administered.

Analytical investigations

Very long-chain fatty acids serum levels were monitored during the Lorenzo's Oil administration before and after haematopoietic stem cell transplantations. Serum very long-chain fatty acids, such as methyl ester derivatives were detected according to a previously described method [9].

Evaluation of chimaerism after allo-SCT by fluorescence in situ hybridization analysis (XY-FISH) was performed.

The adrenal function was evaluated by a Synacthen test; detection of cortisol and ACTH and DHEAS was also carried out.

Radiological investigation

Magnetic resonance imaging (MRI) was performed on average once a year.

Results

At the age of diagnosis (8 months), detected VLCFA parameters were C24:0/C22:0 = 1.564, C26:0/C22:0 = 0.047, C26:0 = 0.74 µg/ml (n < 0.95; < 0.2; < 0.29 µg/ml, respectively). The VLCFA of his mother were at heterozygote levels (C24:0/C22:0 = 1.076; C26:0/C22:0 = 0.024, C26:0 = 0.335 µg/ml).

After 2 months of the first oral administration of Lorenzo's Oil with a reduction of fat in the diet, i.e. at the age of 2 years and 2 months, very long-chain fatty acids serum levels decreased to the normal level (Fig. 1A-B).

The first haematopoietic stem cell transplantation at the age of 4 years and 7 months was performed 5 months after cessation of Lorenzo's Oil therapy. Eight months after the engraftments, serum VLCFA levels decreased to heterozygote levels, mainly C24:0/C22:0. However, they subsequently increased to the levels characteristic of X-linked adrenoleukodystrophy hemizygotes, parallel with decreased chimaerism (5% XX and 95% XY a year after HSCT). The first graft was rejected.

The second haematopoietic stem cell transplantation was performed when the patient was 5 years and 10 months old. Immediately after the second transplantation, a rapid increase in VLCFA was observed, mainly as C26:0 concentration and C26:0/C22:0 ratio. For 3.5 months after the transplantation, chimaerism was maintained above the 85% level and then C26:0 concentration slowly decreased to 50%. The lowest value of C26:0 and C24:0 was obtained at chimaerism of 55% XX and 45% XY and CD3 detected in lymphocytes T was 88% and 12%, respectively, 5 months after the engraftment. Since the 8.5 months after the transplantation, a repeated increase in C26:0 concentration was observed, approximately

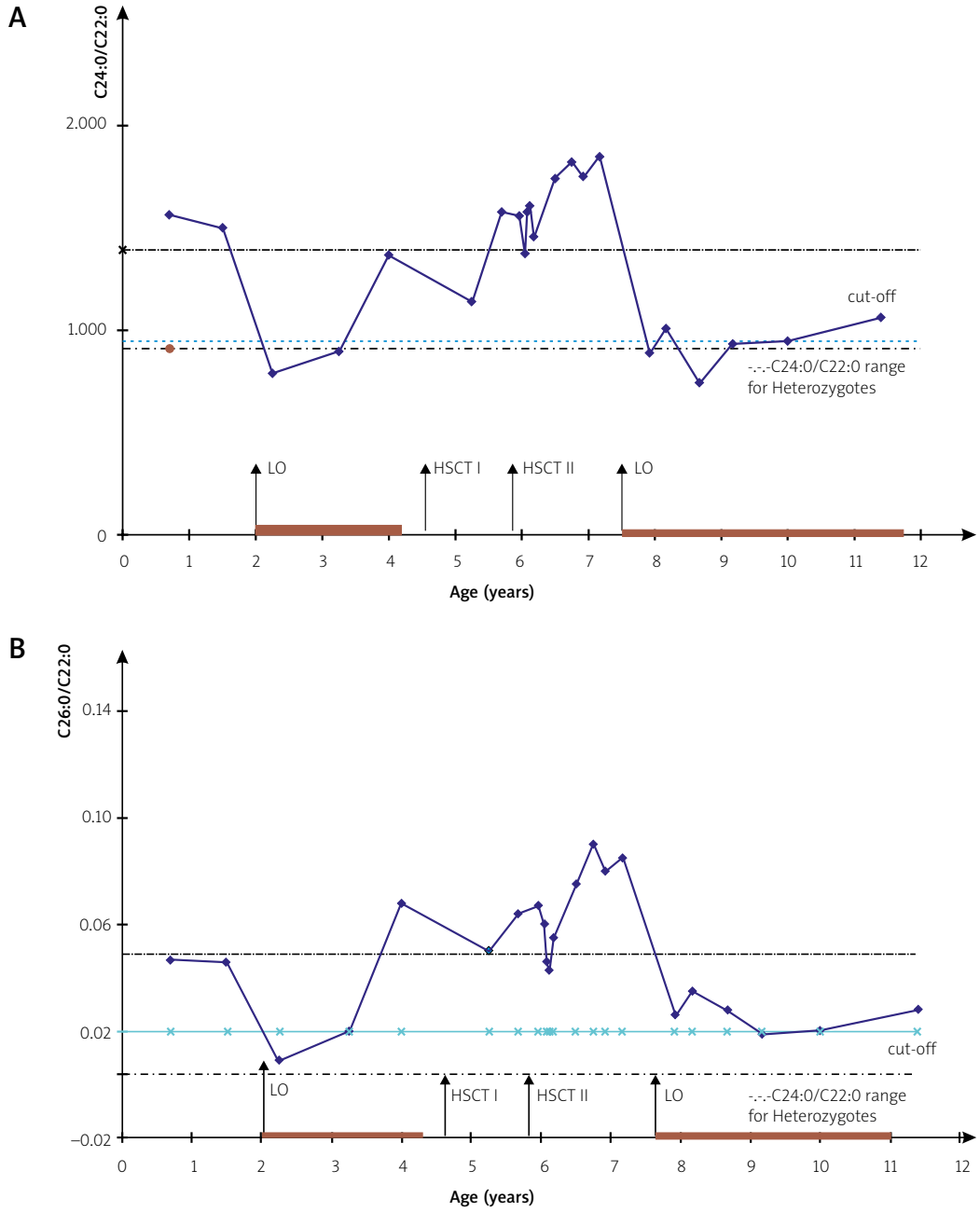

Fig. 1. The C24:0/C22:0 ratio and C26:0/C22:0 ratio in various approaches to the treatment of X-linked adrenoleukodystrophy in the presented patient (bold line – time of Lorenzo's Oil treatment).

80%, at chimaerism of 32% XX although detected CD3 levels were 63% XX and 37% XY. Twenty months after the engraftment, established C26:0 concentration was elevated to about 200% as compared to the first diagnosis result (Table I). In this case, the detected increasing VLCFA levels were accompanied by a decline in chimaerism.

Very long-chain fatty acids levels following the second haematopoietic stem cell transplantation decreased slightly but were maintained at the level characteristic of hemizygotes.

When the XX chimaerism was lower than 50%, all VLCFA parameters increased even over the diagnostic levels (Fig. 1; Table I). The VLCFA levels showed

Table I. Chimaerism and C26:0 [µg/ml] and C24:0/C22:0 ratio after the second haematopoietic stem cell transplantation in an X-linked adrenoleukodystrophy patient

After the second HSCT (months)	Chimaerism [%]		C24:0/ C22:0 (n < 0.950)	C26:0 [µg/ml]
	Donor XX	Recipient XY		
1	100	0	1.558	0.977
2	95	5	1.376	0.817
2.5	97	3	1.579	0.819
3.5	85	15	1.509	0.711
5	55	45	1.457	0.509
8	32	68	1.741	0.916
12	34	66	1.752	1.600
15	25	75	1.848	1.200

a negative correlation with chimaerism, the highest for C24:0/C22:0 (r = 0.991).

One and a half years after the second HSCT, because of the increase in serum VLCFA levels, Lorenzo's Oil was restarted in the patient, which in turn resulted in a repeated decline in very long-chain fatty acids levels (Fig. 1).

At the age of 7 years, the patient was clinically and radiologically asymptomatic, although signs of adrenal insufficiency were noted (test with Synacthen; ACTH – 441 pg/ml). The supplementation of adrenocortical insufficiency was started using hydrocortisone 2 × 5 mg/daily.

At the age of 11 years and 5 months, the patient showed the first signs of cerebral demyelinisation in MRI.

Discussion

Very long-chain fatty acids levels are the characteristic biochemical biomarkers of X-linked adrenoleukodystrophy but their role as a pathogenic factor is still unclear. Due to the continuing lack of markers that can predict the phenotype of the disease, it is difficult to reliably assess the application of treatment methods in asymptomatic patients. In this study we monitored VLCFA levels in X-linked adrenoleukodystrophy in an asymptomatic patient treated with Lorenzo's Oil or haematopoietic stem cell transplantations.

Our data showed that the most effective decrease in very long-chain fatty acids serum levels was observed during Lorenzo's Oil administration. The VLCFA levels in a patient decreased to the normal range, similar as in patients described earlier [10]. Although it is difficult to show a clinical effect in asymptomatic patients, Moser *et al*. found an association between a reduction in VLCFA plasma concentration and the development of the childhood cerebral form of X-linked adrenoleukodystrophy [5]. However, previous studies with Lorenzo's Oil have not shown relevant clinical effects [13,15].

Similarly, as has been observed earlier [7], in our study, immediately after the engraftments, a large increase in VLCFA levels was found. This could be a result of the application of the necessary transplantation procedure.

From 6 to 8 months after the transplantation, the VLCFA decreased to the heterozygote levels as demonstrated in Fig. 1. Previous reports revealed that in the case of successful haematopoietic stem cell transplantation, VLCFA serum is decreased but not normalized and maintained at the heterozygote level [7,9,11,14].

The analysis of very long-chain fatty acids parameters showed a correlation between the chimaerism after haematopoietic stem cell transplantation and a serum VLCFA level.

In our study we found, at 6-8 months after the HSCT, that chimaerism correlated negatively with very long-chain fatty acids serum levels and the increasing VLCFA level indicates rejection of the transplant. On the contrary, CD3 in lymphocytes T and very long-chain fatty acids shows no correlation.

Previously it was suggested that analysis of very long-chain fatty acids levels after haematopoietic stem cell transplantation is not indispensable [6]. Although it is true that we still do not know the exact pathological mechanisms in adrenoleukodystrophy, recent studies shed more light on the role of VLCFA. Hein *et al*. showed the very long-chain fatty acids cytotoxic effect on the nervous system. The increased VLCFA concentrations induce cell death in oligodendrocytes and astrocytes and also deregulation of intracellular calcium homeostasis. Other investigations revealed that VLCFA take part in reactive oxygen species formation [3,4,12]. This evidence, just as our results demonstrated above, tends to conclude that VLCFAs should be controlled after any therapeutic approach in X-linked adrenoleukodystrophy patients.

The presented data showed that the sequential monitoring of very long-chain fatty acids serum levels after haematopoietic stem cell transplantation is important for assessment of engraftment, graft failure or rejection, and could be useful in the treatment effectiveness.

Disclosure

Authors report no conflict of interest.

References

1. Berger J, Gartner J. X-linked adrenoleukodystrophy: clinical, biochemical and pathogenetic aspects. Biochim Biophys Acta 2006; 1763: 1721-1732.
2. Cartier N, Aubourg P. Hematopoietic stem cell transplantation and hematopoietic stem cell gene therapy in X-linked adrenoleukodystrophy. Brain Pathol 2010; 20: 857-862.
3. Fourcade S, Lopez-Erauskin J, Galino J et al. Early oxidative damage underlying neurodegeneration in X-adrenoleukodystrophy. Hum Mol Genet 2008; 17: 1762-1773.
4. Hein S, Schonfeld P, Kahlert S, Reiser G. Toxic effects of X-linked adrenoleukodystrophy associated, very long chain fatty acids on glial cells and neurons from rat hippocampus in culture. Hum Mol Genet 2008; 17: 1750-1761.
5. Moser HW, Raymond GV, Lu SE, Muenz LR, Moser AB, Xu J, Jones RO, Loes DJ, Melhem ER, Dubey P, Bezman L, Brereton NH, Odone A. A Follow-up of 89 asymptomatic patients with adrenoleukodystrophy treated with Lorenzo's oil. Arch Neurol 2005; 62: 1073-1080.
6. Peters C, Charnas LR, Tan Y et al. Cerebral X-linked adrenoleukodystrophy: the international hematopoietic cell transplantation experience from 1982 to 1999. Blood 2004; 104: 881-888.
7. Shapiro E, Krivit W, Lockman L, Jambaqué I, Peters C, Cowan M, Harris R, Blanche S, Bordigoni P, Loes D, Ziegler R, Crittenden M, Ris D, Berg B, Cox C, Moser H, Fischer A, Aubourg P et al. Long-term effect of bone-marrow transplantation for childhood-onset cerebral X-linked adrenoleukodystrophy. Lancet 2000; 356: 713-718.
8. Shimozawa N. Molecular and clinical findings and diagnostic flowchart of peroxisomal diseases. Brain Dev 2011; 33: 770-776.
9. Stradomska TJ, Tylki-Szymańska A. Serum very long-chain fatty acids levels determined by gas chromatography in the diagnosis of peroxisomal disorders. Folia Neuropathol 2009; 47: 306-313.
10. Stradomska TJ, Tylki-Szymańska A. Examination of very long chain fatty acids in diagnosis of X-linked adrenoleukodystrophy. Pediatr Pol 1996; 71: 197-201.
11. Stradomska TJ, Tylki-Szymańska A. Adrenoleukodystrophy (X-ALD) – changes in serum VLCFA profile and clinical course of patients following bone marrow transplantation and administration of Lorenzo oil. Eur J Paediatr Neurol 2008; 12: S73.
12. Stradomska TJ. Peroksysomy – funkcje i zaburzenia metaboliczne. Post Biochemii 2011; 57: 183-190.
13. Suzuki Y, Imamura A, Shimozawa N, Kondo N. The clinical course of childhood and adolescent adrenoleukodystrophy before and after Lorenzo's oil. Brain Dev 2001; 23: 30-33.
14. Suzuki Y, Isogai K, Teramoto T, Tashita H, Shimozawa N, Nishimura M, Asano T, Oda M, Kamei A, Ishiguro H, Kato S, Ohashi T, Kobayashi H, Eto Y, Kondo N. Bone marrow transplantation for the treatment of X-linked adrenoleukodystrophy. J Inherit Metab Dis 2000; 23: 453-458.
15. van Geel BM, Assies J, Haverkort EB, Koelman JH, Verbeeten B Jr, Wanders RJ, Barth PG. Progression of abnormalities in adrenomyeloneuropathy and neurologically asymptomatic in X-Linked adrenoleukodystrophy despite treatment with "Lorenzo's oil". J Neurol Neurosurg Psychiatry 1999; 67: 290-299.

Original article

Folia Neuropathologica

Involvement of D_1/D_2 dopamine antagonists upon open-arms exploratory behaviours induced by intra-nucleus accumbens shell administration of *N*-methyl-*D*-aspartate

Samira Razavi[1], Ali Haeri-Rohani[1], Akram Eidi[1], Mohammad R. Zarrindast[2,3,4,5]

[1]Department of Biology, Science and Research Branch, Islamic Azad University, Tehran, [2]Institute for Cognitive Science Studies (ICSS), Tehran, [3]Department of Neuroscience, School of Advanced Medical Technologies and Department of Pharmacology, School of Medicine, Tehran University of Medical Sciences, Tehran, [4]Iranian National Center for Addiction Studies, Tehran University of Medical Sciences, Tehran, [5]School of Cognitive Sciences, Institute for Research in Fundamental Sciences (IPM), Tehran, Iran

Folia Neuropathol 2014; 52 (2): 164-178 DOI: 10.5114/fn.2014.43788

Abstract

Glutamatergic system stimulation in some parts of the brain may affect anxiety-related behaviours, aversive learning and memory. This system retains many interactions with dopaminergic neurotransmission. We have studied the effect of nucleus accumbens (NAc) shell glutamatergic system activation on anxiety-related behaviours as well as aversive learning and memory in adult male Wistar rats using the N-methyl-D-aspartate (NMDA) receptor agonist, NMDA. Furthermore, the possible involvement of the NAc shell dopamine D_1 and D_2 receptors upon NMDA-induced effects was evaluated. The elevated plus-maze task was used to assess the drugs' concomitant effects on anxiety, learning and memory in rats. All drugs were delivered into the NAc shell via bilaterally implanted indwelling cannulae. The NMDA-induced anxiolytic-like behaviours upon retest could possibly be attributed to the further avoidance acquisition impairments. Moreover, the inhibition of dopaminergic system using SCH 23390 and sulpiride induced an anxiolytic-like response and impaired the aversive memory acquisition during retest. However, the concurrent intra-NAc shell microinjection of the subthreshold dose of SCH 23390 and sulpiride (0.125 µg/rat) reversed the anxiolytic-like effect and blocked the aversive memory impairment induced by intra-NAc shell NMDA. Our results suggest a modulatory role of the NAc shell dopaminergic system on NMDA-induced effects in the aversive memory.

Key words: *glutamate, dopamine, anxiety, aversive learning, elevated plus-maze, nucleus accumbens, rat.*

Introduction

Nucleus accumbens (NAc) is one of the main limbic system nuclei receiving rich dopaminergic inputs hence taking an important role in the regulation of many physiological cognitive and non-cognitive behaviours [39]. Anatomical studies have determined at least two main functionally important parts in NAc, i.e. the core and the shell [8,87]. With regard to the dopaminergic system, these two parts seem different. For instance, the dopamine plexus and concentration are richer and higher in the shell than in the core, respectively [20,80]. Evidence has indicated the pivotal role of NAc dopaminergic system

Communicating author:
Samira Razavi, Department of Biology, Science and Research Branch, Islamic Azad University, Tehran, Iran,
e-mail: s.razavimovahed@gmail.com

in the modulation of learning, memory [11,14,43], fear and/or anxiety-like behaviours [50]. Dopamine exerts its effect via two different dopamine subtypes receptors, called the D_1- and D_2-like families [55]. These two dopamine family receptors have a high expression in both parts of NAc while at different distribution patterns. For example, the D_1- and D_2-like dopamine receptor families are higher and lower in the NAc shell than in core, respectively [30]. This may partly explain the different physiological functions of the two parts of NAc [40,42]. Due to the abundant dopaminergic inputs which NAc shell receives from various brain parts and the consequent high contraction level of dopamine in the NAc shell, this part is believed to render a critical role in dopamine-mediated functions [30]. The NAc receives its dopaminergic afferents from the ventral tegmental area (VTA) and the substantia nigra (SN), and the glutamatergic inputs from several brain areas such as prefrontal cortex, amygdala and hippocampus [30].

On the other hand, glutamate is known as one of the most excitatory neurotransmitters modulating learning, memory and anxiety-like behaviours in different parts of the brain [33,94]. With respect to the preferential agonists, at least three subtypes have been identified for glutamate, including *N*-methyl-*D*-aspartate (NMDA), AMPA and kainate [57]. Investigations have revealed that the NMDA receptor plays a critical part in regulation of learning, memory formation (possibly through long-term potentiation and depression) [9,38] and anxiety-related behaviours [26,46,63,73,78]. A plethora of anatomical experiments have demonstrated that there are close relationships between NAc glutamatergic and dopaminergic systems [66,67]. For instance, it has been shown that NMDA receptors are localized on dopamine D_1 receptor-containing neurons in the NAc shell [27].

Emotional states (including, fear and aversion) can be modulated through amplification of impairment in memory formation [51]. Due to possible misinterpretations, the available animal models for learning and memory seem to have a limited ability to detect the effect of drugs on fear and anxiety. Therefore, the proposed test-retest paradigm in the elevated plus-maze (EPM) task is an attempt to concomitantly assess the effects of drugs on anxiety, learning and memory in rodents [6]. The use of EPM in testing anxiety is based on the natural tendency of animals to avoid dangerous situations when they face height and open spaces [91]. In general, animals acquire information with regard to safe and dangerous areas in the maze upon test. Animals retested in the EPM avoid exploring open spaces and displaying a clear enclosed arm preference with a low percentage of entries and time spent in the open arms [59], relative to their respective measures during the test [10,22,44,74,79]. The aversive and fear-inducing nature of the open arms represents a useful tool for the study of aversively motivated learning processes in the EPM [16]. Based on the above, learning and memory are usually studied in the EPM through avoidance to open-arms during the retest session. Given this, the purpose of the current study was to examine the possible involvement of the NAc shell D_1 and/or D_2 dopaminergic receptors on NMDA-induced effects in the aversive memory using the elevated-plus maze (EPM) task.

Material and methods

Animals

Male Wistar rats weighing approximately 250-280 g were provided by the Central Animal House of the Institute for Cognitive Science Studies (ICSS), Tehran, Iran. Prior to the experiments, animals underwent a period of seven days habituation in groups of five in polypropylene home cages (45 × 30 × 15 cm), having access to food and water *ad libitum*, under a light/dark cycle of 12 h (lights on at 06:00) and the temperature ranging between 20°C and 24°C. Animal handling was restricted to the time of home cage cleaning (each 48 h), weighing and drug administration. Each experimental group comprised eight animals. All experimental procedures were conducted in compliance with the recommendations set down by the Institute's Ethics Commission for the use of experimental animals.

Stereotaxic surgery and microinjections

Animals were anaesthetized intraperitoneally using ketamine hydrochloride (50 mg/kg) and xylazine (4 mg/kg) then placed in a Stoelting stereotaxic instrument (Wood Dale, IL, USA). Two stainless steel guide cannulae (22 gauge) were implanted in the right and left of the NAc shell regions according to the atlas of Paxinos and Watson [58]. The stereotaxic coordinates for the NAc regions were as follows: +1.4 mm posterior to bregma, ±0.8 mm lateral to the Midline and –5.5 mm ventral to the dorsal surface of

the skull. The cannulae were fixed to the skull using acrylic dental cement. Rats were allowed 5 days before the test to recover from surgery. The left and right of the NAc areas were infused by means of an internal cannula (27 gauge), terminating 2 mm below the tip of the guides and connected by polyethylene tubing to a 2 µL Hamilton syringe (Bonaduz, GR, Switzerland). A volume of 0.3 µL solution was injected over a 60-second period, in each side. The inner cannulae were left in place for an additional 60 seconds to allow diffusion of the solution and to reduce the possibility of reflux. Intra-NAc shell injections were made just five minutes before testing. Control groups and drug infused groups were surgeried and all of the animals were anaesthetized using a ketamine solution, therefore all of groups were under the same condition and under the same effect of ketamine anaesthesia.

Elevated plus-maze (EPM) apparatus

This plexiglas, plus-shaped apparatus, was set at 50 cm height from the floor. This apparatus was composed of two 50 × 10-cm open arms and two 50 × 10 × 40-cm enclosed arms, each with an open roof. The junction area of the four arms (central platform) measured 10 × 10 cm. The maze was placed at the centre of a quiet and dimly lit room [91,92].

Behavioural testing

Rats were placed in the experimental room at least 1 h before testing. All experiments were done during the light phase of the light/dark cycle between 11 a.m. and 2 p.m. Animals were randomly assigned to treatment conditions and tested in a counter-balanced order. Animals' behaviours were tracked and recorded by an observer who quietly sat 1 m behind one of the closed arms of the maze, using a chronometer. During the five-minute post-drug treatment, rats were individually placed at the centre of the plus maze facing one of the open arms and allowed for 5 min free exploration in EPM (test session) then were taken back to their home cages. In 24 hours, rats were returned to the test room and placed again in the EPM for a new exploration period of 5 min (retest session). The observer measured: 1) time spent in open arms, 2) time spent in closed arms, 3) number of entries into open arms and 4) number of entries into closed arms during the five-minute period both upon test and retest. An entry was defined as 'all four paws in the arm'. Between EPM sessions and after each rat the maze was cleaned with distilled water. The obtained data were used to calculate: a) % OAT (the ratio of time spent in open arms to the time spent in all arms ×100); b) % OAE (the ratio of entries into open arms to total entries ×100) [55,97,98], and c) the total closed and open arm entries were considered as a relatively pure index for the locomotor activity [93,95].

Drugs

The drugs used in the present study were ketamine and xylazine (Alfasan Chemical Co, Woerden, Holland) for animal anaesthesia, NMDA (*N*-methyl-*D*-aspartic acid as NMDA receptor agonist, Tocris Cookson, Bristol, UK), SCH 23390 (as dopamine D_1 receptor antagonist) and sulpiride (as dopamine D_2 receptor antagonist). NMDA and SCH 23390 were dissolved in sterile 0.9% saline while sulpiride was dissolved in vehicle (the vehicle was one drop of glacial acetic acid from Hamilton microsyringe, made up to a volume of 5 ml with sterile 0.9% saline, then diluted to the required volume) just before the experiment. Control animals received either saline or vehicle. NMDA and SCH were administered into the shell of the nucleus accumbens at a volume of 0.3 µL/rat.

Drug treatments

Experiment 1: Effects of NMDA administration on open arms exploratory-like behaviours in the presence or absence of SCH 23390

To substantiate whether the microinjection of drugs involved in anxiety, the drug infusion took place before EPM testing. In this experiment, 12 groups of animals were examined. These were as follows: 1) animals which received intra-NAc shell saline (0.3 µL/rat) or NMDA (0.125, 0.25, and 0.5 µg/rat), 5 min after saline (0.3 µL/rat); 2) animals which received intra-NAc shell saline (0.3 µL/rat) or SCH (0.125, 0.25 and 0.5 µg/rat), 5 min before saline (0.3 µL/rat) and 3) animals which received intra-NAc shell saline (0.3 µL/rat) or the subthreshold dose of SCH (0.0125 µg/rat), 5 min before different doses of NMDA (0.125, 0.25, and 0.5 µg/rat).

To investigate the possible drug carryover effects of aversive learning during test day to aversive memory upon retest, treated groups were retested undrugged in EPM 24 h later.

Experiment 2: Effects of NMDA administration on open-arms exploratory-like behaviours in the presence or absence of sulpiride

To substantiate whether the microinjection of drugs involved in anxiety, the drug infusions were done before EPM testing. In this experiment, 12 groups of animals were examined. These included: 1) animals which received intra-NAc shell saline (0.3 µL/rat) or NMDA (0.125, 0.25, and 0.5 µg/rat), 5 min after saline (0.3 µL/rat); 2) animals which received intra-NAc shell vehicle (0.3 µL/rat) or sulpiride (0.125, 0.25 and 0.5 µg/rat), 5 min before saline (0.3 µL/rat) into NAc shell, and 3) animals which received intra-NAc shell vehicle (0.3 µL/rat) or the subthreshold dose of sulpiride (0.0125 µg/rat), 5 min before different doses of NMDA (0.125, 0.25, and 0.5 µg/rat).

To investigate the possible drug carryover effects of aversive learning during test day to aversive memory upon retest, treated groups were retested undrugged in EPM 24 h later.

Histology

Following the completion of behavioural testing, animals were euthanized using an overdose of chloroform. Ink (0.3 µL of 1% aquatic methylene blue solution) was injected into the guide cannulae using 27-gauge injection cannulae. Brains were then removed and fixed in a 10% formalin solution for 48 hours before sectioning. The brains were sliced using the vibro-slice apparatus in transverse planes (40 µm). Cannula placements were verified based on the corresponding map of Paxinos and Watson atlas of rodents' brain [58]. Data from the animals in which injection sites were located outside the NAc shell were not included in the analyses.

Statistical analysis

Data were expressed as mean ± SEM and analyzed using the repeated measure protocol during test and retest days. In addition to the analysis made to compare test to test or retest to retest, the two-way analysis of variance (ANOVA) was also applied. Where *F*-value was significant, one-way ANOVA and post-hoc analysis (Tukey-test) were performed. Between-groups differences with $p < 0.05$ were considered statistically significant.

Results

Histology

Data from the animals in which injection sites were located outside the NAc shell were not included in the analyses and in the present study we used only data from animals that were cannulated clearly within-NAc-shell. Cannulae were implanted into the NAc shell of a total of 208 rats, however only the data from 192 animals with correct cannulae implants were included in statistical analyses.

Experiment 1 results

Effects of NMDA administration on open arms exploratory-like behaviours

Repeated measure and post hoc analyses demonstrated that NMDA increases the %OAT (at 0.25 and 0.5 µg/rat, as seen in Fig. 1; panel 1A and Fig. 2; panel 1A, respectively), %OAE (at 0.25 and 0.5 µg/rat as seen in Fig. 1; panel 1B and Fig. 2; panel 1B, respectively) and decreases the locomotor activity (non-significantly and significantly as seen in Fig. 1; panel 1C and Fig. 2; panel 1C, respectively), indicating an anxiolytic-like response to NMDA.

Adding to the above, data showed that NMDA increases the %OAT (at 0.25 and 0.5 µg/rat, as shown in Fig. 1; panel 2A and at 0.125 and 0.5 µg/rat in Fig. 2; panel 2A) and %OAE (at 0.25 and 0.5 µg/rat as shown in Fig. 1; panel 2B and at 0.125 and 0.5 µg/rat in Fig. 2; panel 2B). However, this did not alter the locomotor activity (Fig. 1, panel 2C and Fig. 2, panel 2C) upon retest as compared to the control group, indicating an NMDA-induced impairment of the aversive memory acquisition.

According to the above data, NMDA induced anxiolytic-like behaviours. Furthermore, the retest data suggested that the NMDA anxiolytic-like effect may also be linked to the impairment in further avoidance acquisition. The corresponding repeated measure results have been demonstrated in Table I and Table II.

Effects of intra-NAc shell microinjection of SCH 23390 on open arms exploratory-like behaviours

In this experiment two-way ANOVA analysis was done to assess the NMDA treated group dose-response as compared to controls as well as the interac-

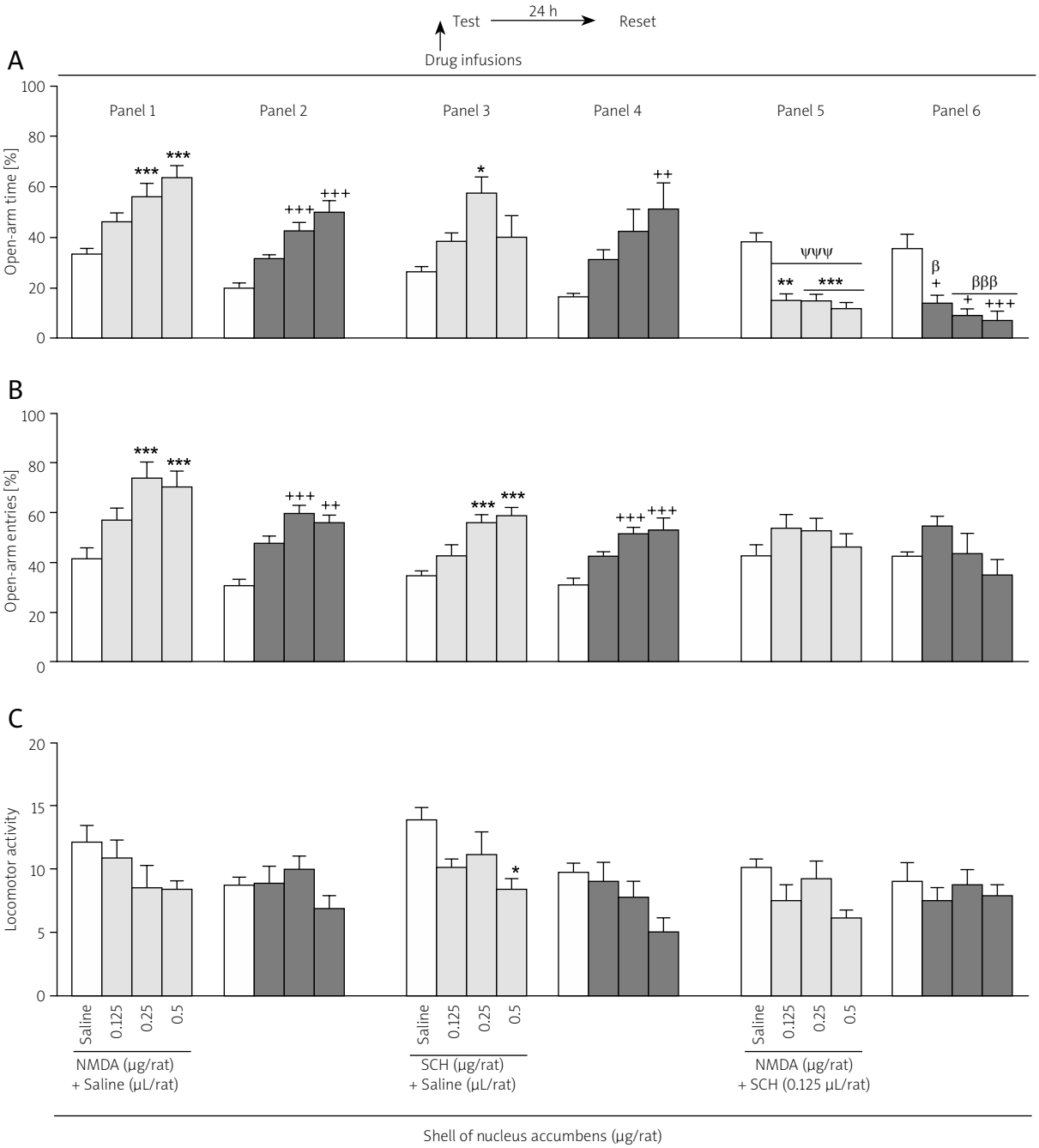

Fig. 1. The effects of NMDA administration on open-arms exploratory-like behaviours in the presence or absence of SCH 23390. Rats were tested in the EPM, 5 min after concurrent microinjection of saline (0.3 μL/rat) or NMDA (0.125, 0.25 and 0.5 μg/rat) or saline (0.3 μL/rat) or SCH 23390 (0.125, 0.25 and 0.5 μg/rat) and the subthreshold dose of SCH 23390 prior to intra-NAc shell NMDA. In 24 h, all groups were retested in the EPM, undrugged. $^{*}p < 0.05$, $^{**}p < 0.01$ and $^{***}p < 0.001$ different from the control group on the test day. $^{+}p < 0.05$, $^{++}p < 0.01$ and $^{+++}p < 0.001$ different from control groups on the retest day. $^{\alpha}p < 0.05$, $^{\alpha\alpha}p < 0.01$ and $^{\alpha\alpha\alpha}p < 0.001$ different from the test and retest groups. $^{\Psi}p < 0.05$, $^{\Psi\Psi}p < 0.01$ and $^{\Psi\Psi\Psi}p < 0.001$ different from the test groups. $^{\beta}p < 0.05$, $^{\beta\beta}p < 0.01$ and $^{\beta\beta\beta}p < 0.001$ different from the retest groups.

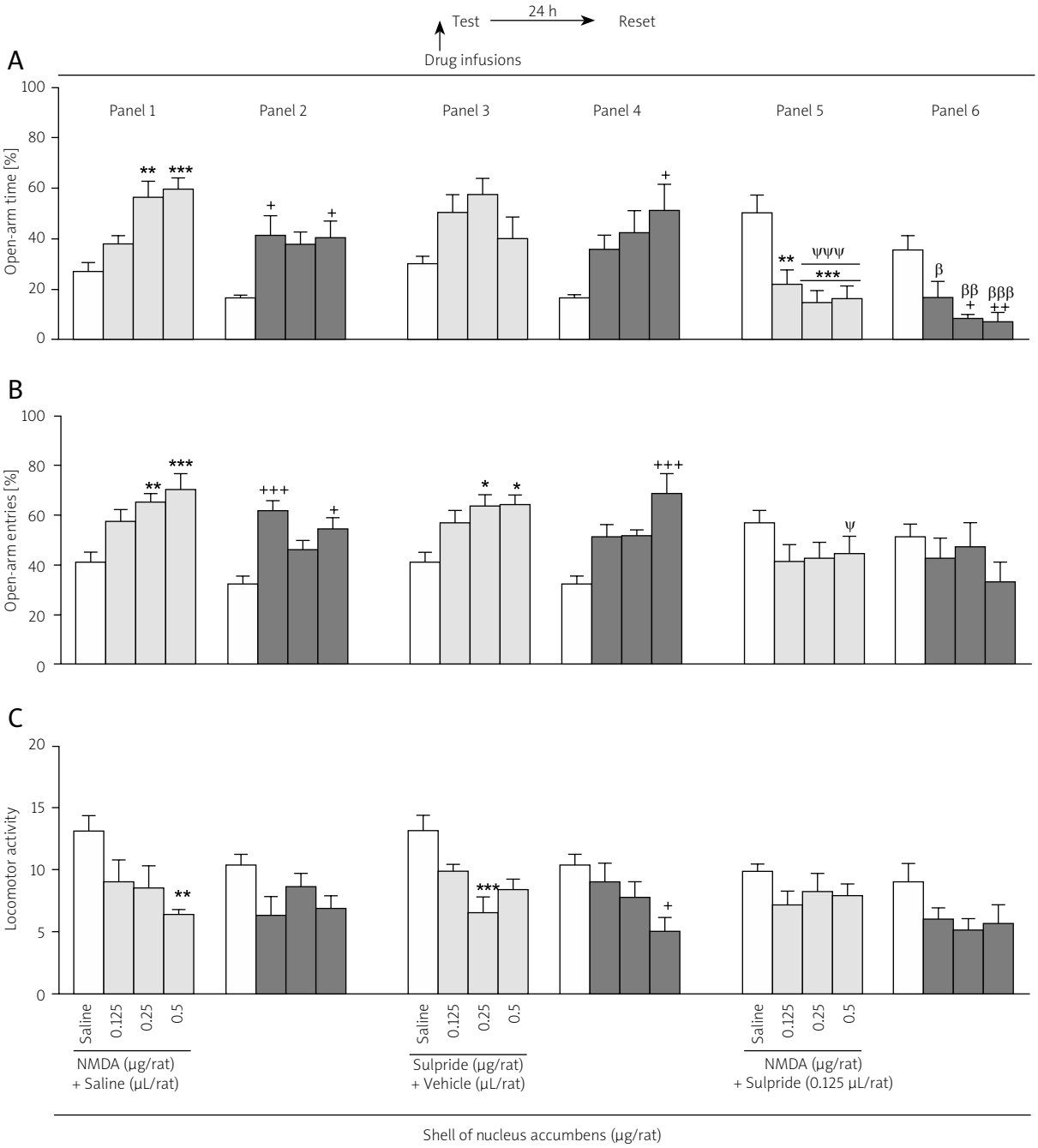

Fig. 2. The effects of NMDA administration on open-arms exploratory-like behaviours in the presence or absence of sulpiride. Rats were tested in the EPM, 5 min following the concurrent microinjection of saline (0.3 μL/rat) or NMDA (0.125, 0.25 and 0.5 μg/rat) or vehicle (0.3 μL/rat) or sulpiride (0.125, 0.25 and 0.5 μg/rat) and the subthreshold dose of sulpiride prior to the intra-NAc shell NMDA. In 24 h, all groups were retested in the EPM, undrugged. $^{*}p < 0.05$, $^{**}p < 0.01$ and $^{***}p < 0.001$ different from the control saline group on the test day. $^{+}p < 0.05$, $^{++}p < 0.01$ and $^{+++}p < 0.001$ different from control saline groups on the retest day. $^{\alpha}p < 0.05$, $^{\alpha\alpha}p < 0.01$ and $^{\alpha\alpha\alpha}p < 0.001$ different from the test and retest groups. $^{\Psi}p < 0.05$, $^{\Psi\Psi}p < 0.01$ and $^{\Psi\Psi\Psi}p < 0.001$ different from the test groups. $^{\beta}p < 0.05$, $^{\beta\beta}p < 0.01$ and $^{\beta\beta\beta}p < 0.001$ different from the retest groups.

Table I. Repeated measure and two ANOVA results with *p* values for experiment 1

Experiments	Behaviours	Day		Group		Day and group interaction		Final results/ conclusion of each experiment
Repeated measure results (panel 1 and 2 of Fig. 1)		$F_{(1, 28)}$	*p*	$F_{(3, 28)}$	*p*	$F_{(3, 28)}$	*p*	NMDA at doses of 0.25 and 0.5 µg/rat induced anxiolytic-like behaviour and impaired aversive memory acquisition
	% OAT	30.516	0.000	25.923	0.000	0.012	0.998	
	% OAE	21.514	0.000	14.052	0.000	0.424	0.737	
	Locomotion	3.661	0.066	1.591	0.214	2.141	0.118	
Repeated measure results (panel 3 and 4 of Fig. 1)		$F_{(1, 28)}$	*p*	$F_{(3, 28)}$	*p*	$F_{(3, 28)}$	*p*	SCH at doses of 0.25 and 0.5 µg/rat induced anxiolytic-like behaviour and impaired aversive memory acquisition
	% OAT	1.258	0.272	9.286	0.000	1.506	0.235	
	% OAE	2.954	0.097	18.856	0.000	0.330	0.804	
	Locomotion	17.398	0.000	5.332	0.005	0.816	0.496	
Two ANOVA results (panel 5 and 1 of Fig. 1)		$F_{(1, 56)}$	*p*	$F_{(3, 56)}$	*p*	$F_{(3, 56)}$	*p*	SCH at a dose of 0.125 µg/rat in the NAc decreases the anxiolytic-like behaviours induced by the intra-NAc shell injection of NMDA at doses of 0.125, 0.25 and 0.5 µg/rat and meanwhile improves the aversive memory impairment
	% OAT	149.065	0.000	1.581	0.220	25.770	0.000	
	% OAE	9.469	0.003	5.621	0.002	2.731	0.052	
	Locomotion	4.092	0.048	3.500	0.021	1.062	0.373	
Two ANOVA results (panel 6 and 2 of Fig. 1)		$F_{(1, 56)}$	*p*	$F_{(3, 56)}$	*p*	$F_{(3, 56)}$	*p*	
	% OAT	63.043	0.000	1.074	0.368	26.897	0.000	
	% OAE	1.342	0.252	5.307	0.003	6.047	0.001	
	Locomotion	0.198	0.658	1.265	0.295	0.566	0.640	

tion with SCH 23390 or sulpiride treatment. According to the repeated measure and Post hoc analyses, SCH 23390 increased the %OAT (at 0.25 µg/rat, Fig. 1; panel 3A), %OAE (at 0.25 and 0.5 µg/rat, Fig. 1, panel 3B) and decreased the locomotor activity (at 0.5 µg/rat, Fig. 1; panel 3C) upon test, indicating that SCH 23390 may induce an anxiolytic-like response.

Moreover, the data revealed that SCH 23390 increases the %OAT (at 0.5 µg/rat, Fig. 1; panel 4A), and %OAE (at 0.25 and 0.5 µg/rat, Fig. 1; panel 4B), while does not alter the locomotor activity (Fig. 1; panel 4C) on retest day as compared to the control group, indicating that SCH 23390 possibly impairs the aversive memory retrieval.

In conclusion, the data revealed that SCH 23390 induces an anxiolytic-like response. Besides, the increased %OAT upon retest indicates that SCH 23390-treated rats had their aversive memory to open-arm exploration negatively affected as compared to the control group. The corresponding repeated measure results have been summarized in Table I.

Effects of NAc shell microinjection of SCH 23390 prior to NMDA on open arms exploratory-like behaviours

Two-way ANOVA and post hoc analyses revealed that intra-NAc microinjection of SCH 23390 prior to NMDA causes a significant decrease in %OAT (at 0.125, 0.25 and 0.5 µg/rat, Fig. 1; panel 5A) while exerts no significant change in the %OAE and the locomotor activity (Fig. 1; panel 5B, 5C) on test day as compared to NMDA-treated groups (Fig. 1; panel 1A, 1B and 1C), indicating that SCH 23390 potentially reverses the anxiolytic-like response induced by the intra-NAc shell microinjection of NMDA.

On the other hand, this intervention resulted in a significant decrease in the %OAT (at 0.125, 0.25 and 0.5 µg/rat, Fig. 1; panel 6A) while leading to no significant change in %OAE and locomotor activity (Fig. 1; panel 6B, 6C) on retest day as compared to NMDA-treated groups (Fig. 1; panel 2A, 2B and 2C). The above indicates that SCH 23390 potentially restores the aversive memory impairment already induced by the intra-NAc shell microinjection of NMDA.

Table II. Repeated measure and two ANOVA results with *p* values for experiment 2

Experiments	Behaviours	Day		Group		Day and group interaction		Final results/ conclusion of each experiment
Repeated measure results (Panel 1 and 2 of Fig. 2)		$F_{(1, 28)}$	*p*	$F_{(3, 28)}$	*p*	$F_{(3, 28)}$	*p*	NMDA at doses of 0.25 and 0.5 µg/rat induced anxiolytic-like behaviour and at doses of 0.125 and 0.25 µg/rat impaired aversive memory acquisition
	% OAT	10.031	0.004	11.111	0.000	2.264	0.103	
	% OAE	11.446	0.002	12.033	0.000	3.188	0.039	
	Locomotion	3.740	0.063	4.047	0.016	1.983	0.139	
Repeated measure results (Panel 3 and 4 of Fig. 2)		$F_{(1, 28)}$	*p*	$F_{(3, 28)}$	*p*	$F_{(3, 28)}$	*p*	Sulpiride at doses of 0.25 and 0.5 µg/rat induced anxiolytic-like behaviour and at dose of 0.5 µg/rat impaired aversive memory acquisition
	% OAT	2.466	0.128	6.472	0.002	1.591	0.214	
	% OAE	2.414	0.131	14.298	0.000	1.058	0.383	
	Locomotion	5.324	0.029	6.447	0.002	2.795	0.059	
Two ANOVA results (Panel 5 and 1 of Fig. 2)		$F_{(1, 56)}$	*p*	$F_{(3, 56)}$	*p*	$F_{(3, 56)}$	*p*	Sulpiride at a dose of 0.125 µg/rat in the NAc decreases the anxiolytic-like behaviours induced by the intra-NAc shell injection of NMDA at doses of 0.25 and 0.5 µg/rat, and meanwhile improves the aversive memory impairment by the intra-NAc shell injection of NMDA
	% OAT	28.098	0.000	1.137	0.342	18.014	0.000	
	% OAE	8.996	0.004	0.984	0.407	5.668	0.002	
	Locomotion	1.242	0.270	4.772	0.005	1.394	0.254	
Two ANOVA results (Panel 6 and 2 of Fig. 2)		$F_{(1, 56)}$	*p*	$F_{(3, 56)}$	*p*	$F_{(3, 56)}$	*p*	
	% OAT	21.579	0.000	0.541	0.656	10.833	0.000	
	% OAE	1.517	0.223	1.070	0.369	4.634	0.006	
	Locomotion	3.574	0.064	3.574	0.064	0.657	0.582	

Having mentioned these, we may conclude that the intra-NAc shell injection of the subthreshold dose of SCH 23390 decreases the anxiolytic-like behaviours induced by the intra-NAc shell injection of NMDA, and meanwhile improves the aversive memory impairment. The two-way ANOVA results have been outlined in Table I.

Experiment 2 results

Effects of NAc shell microinjection of sulpiride on open arms exploratory-like behaviours

According to the repeated measure and post hoc analyses, the data showed that sulpiride does not alter the %OAT (Fig. 1; panel 3A) while increases the %OAE (at 0.25 and 0.5 µg/rat, Fig. 2, panel 3B) and decreases the locomotor activity (at 0.25 and 0.5 µg/rat, Fig. 2; panel 3C) upon test, indicating that sulpiride may induce an anxiolytic-like response.

Moreover, the data revealed that sulpiride increases the %OAT (at 0.5 µg/rat, Fig. 2; panel 4A), %OAE (at 0.5 µg/rat, Fig. 2; panel 4B) whereas decreases the locomotor activity (at 0.5 µg/rat, Fig. 2; panel 4C) on retest day as compared to the control group, indicating that sulpiride possibly impairs the aversive memory retrieval.

In conclusion, the data revealed that sulpiride induces an anxiolytic-like response. Besides, the increased %OAT upon retest indicates that sulpiride-treated rats had their aversive memory to open-arm exploration negatively affected as compared to the control group. The corresponding repeated measure results have been summarized in Table II.

The effects of intra-NAc shell microinjection of sulpiride prior to NMDA on open arms exploratory-like behaviours

Two-way ANOVA and post hoc analyses demonstrated that the intra-NAc microinjection of sulpiride prior to NMDA causes a significant decrease in %OAT (at 0.25 and 0.5 µg/rat, Fig. 2; panel 5A) and %OAE

(at 0.5 µg/rat, Fig. 2; panel 5B) while exerts no significant change in locomotor activity (Fig. 2; panel 5C) on test day as compared to NMDA-treated groups (Fig. 2; panel 1A, 1B and 1C). This indicates that sulpiride potentially reverses the anxiolytic-like response induced by intra-NAc shell microinjection of NMDA.

On the other hand, this intervention resulted in a significant decrease in %OAT (at 0.125, 0.25 and 0.5 µg/rat, Fig. 2; panel 6A) while leading to no significant change in %OAE and locomotor activity (Fig. 2; panel 6B, 6C) on retest day as compared to NMDA-treated groups (Fig. 2; panel 2A, 2B and 2C). The above indicates that sulpiride potentially restores the aversive memory impairment already induced by the intra-NAc shell microinjection of NMDA.

Based on these, we may conclude that the intra-NAc shell microinjection of the subthreshold dose sulpiride decreases the anxiolytic-like behaviours induced by the intra-NAc shell injection of NMDA, and meanwhile improves the aversive memory impairment. The corresponding two-way ANOVA results are outlined in Table II.

Discussion

In our study, animals were given pretest intracerebral drugs injection followed by no injection upon retest 24 h later. Based on this, drug effects on anxiety-like behaviours and aversive learning with subsequent long-term effects on memory in 24 h were tested. It has been reported that the prior experience of an undrugged EPM testing session may alter the behavioural responses in an undrugged retest session [13,74]. The injury caused by the injection might change the expression of messenger RNAs and proteins. But there is a study that investigated changes in the expression of messenger RNAs for trkA, trkB and trkC in the brain following an injury caused by insertion of a 30-gauge needle into adult rat hippocampus or neocortex. The increased levels of mRNA after the injury returned to control levels a few hours after the injury. Pretreatment of the animals with the ketamine completely prevented the changes of trkB and trkC messenger RNAs, suggesting that the brain injury caused a release of glutamate with subsequent activation of NMDA receptor [54]. In the present study, rats were allowed 5 days before the test to recover from surgery so the changes of mRNA levels after the injury may be returned to control levels after the recovery days.

Effects of intra-NAc shell NMDA administration on anxiolytic-like behaviours and aversive memory formation

Our results indicated that the intra-NAc shell infusion of NMDA receptor agonist at applied doses induces an anxiolytic-like response in EPM. This NMDA-induced anxiolytic-like effect emerges into the retest day. Current findings suggest that NMDA treatment induces impairment in the aversive memory acquisition upon test. There is a body of evidence supporting that NAc shell is an essential brain site regulating emotion, motor activity [17], motivation-related learning, memory [12,29], and anxiety-like behaviours [48,49,61]. On the other hand, the NMDA receptor (as an ionotropic glutamate receptor) plays a critical role in the regulation of glutamate-induced behaviours such as learning and memory formation (possibly through long-term potentiation and depression) [9,38], and anxiety-related behaviours [26,63].

Our results are in agreement with the previous investigation showing that NMDA agonist releases behavioural and anxiolytic-like behaviours indicating the role of NMDA receptors in modulation of anxiety-related behaviours [26,73]. Moreover, there is also an investigation showing that the activation of NMDA receptor induces anxiogenic-like effects in EPM and social interaction tasks [21].

Evidence has suggested the critical role of NAc in regulation of several learning functions which require a flexible use of sensory information [47,64, 65]. It has been postulated that NAc manipulations induce spatial memory deficit in the Morris water maze [64,68] and radial maze [24,70]. In agreement with our results, evidence has demonstrated that the systemic administration of NMDA leads to an impaired dark-avoidance learning in rats [89]. On the other hand, some investigations have postulated that the deactivation of the NAc glutamatergic ionotropic receptors disrupt the working memory [7,35, 41] and spatial responses [71] while other contradictory studies have shown that the NMDA receptor blockade in NAc shell does not alter the spatial learning [47,71]. Furthermore, it appears that the NAc shell is more involved in the regulation of spatial learning and memory as compared to the NAc core since the NAc shell (but not the core) lesions disrupt the spatial learning [35]. The NAc sends a dense GABA pro-

jection to the ventral pallidum (VP), and stimulation of either the NAc or its glutamatergic afferents can inhibit VP neuronal firing [23]. The VP can influence DA neural activity via a direct projection to the ventral tegmental area (VTA) [23]. Dopaminergic neurons projection of the VTA sends back to the NAc. Dopaminergic terminals arising from this area make synaptic contacts with NAc GABAergic neurons. According to the present results, stimulation of the NAc by injection of NMDA in this area would have increased firing of GABAergic projection neurons of the NAc causing a decrease in VP the GABAergic neural activity. The decrease in VP activity would then be expected to cause a reduction of the GABAergic inhibition over the VTA and this could alter an increased release of dopamine in NAc. The present data suggested that maybe glutamate exerts its function by affecting the release of dopamine. Several studies have indicated that dopaminergic system modulates the neuronal activities involved in fear or anxiety-like behaviours [25,60]. Several investigations have substantiated that the mesocortical DA system produces a robust and specific response to stressors [28]. Some investigations have suggested that these high levels of DA released under stress are above the optimal range for working memory and therefore impair this cognitive function [5,88].

Effect of intra-NAc shell dopamine D_1 and D_2 receptors antagonists injection on anxiolytic-like behaviours and aversive memory formation

It has been made clear that the NAc shell plays a critical part in modulation of dopamine-mediated functions as it contains the largest amount of dopaminergic terminals and thus the highest concentration of dopamine [20,27,80]. Therefore, the NAc dopaminergic system has a pivotal role in modulation of learning and memory [11,14,43], fear and/or anxiety [50]. The idea of investigating the role of NAc shell dopamine D_1 and D_2 receptors in NMDA-induced effects using the elevated plus-maze test, appealed to our interest.

Present results indicated that the intra-NAc shell microinjection of SCH 23390 (a dopamine D_1 receptor antagonist) increases both %OAT and %OAE whereas decreases the locomotor activity. On the other hand, inhibition of the dopamine D_2 receptor in NAc shell by sulpiride (a dopamine D_2 receptor antagonist) did not affect the %OAT, however; increased %OAE and decreased the locomotor activity. Several investigations have substantiated that the extensive D1- and D2-like receptors are on the presynaptic varicosities of medium-spiny neurons of nucleus accumbens [84]. Similar to the response seen with SCH 23390 and sulpiride on anxiolytic-like behaviours there is a study showing that dopamine D_1 and D_2 receptors blockade in the basolateral amygdala exerts anxiolytic-like behaviours [96]. Intra-NAc injection of SCH 23390 or sulpiride induced anxiolytic- and did not alter anxiety-like behaviours, respectively [90]. Furthermore, our present data indicated that beside the increased %OAT on the test day, the increased %OAT upon retest in both SCH 23390 and sulpiride show that these drug-induced anxiolytic-like effects emerge on the retest day. Current findings suggest that SCH 23390 and sulpiride treatments impair the aversive memory function upon retest. Moreover, evidence has reemphasized the crucial role of dopaminergic system in the regulation of several neural activities which are involved in learning and memory (see [34], for a review). For instance, it has been shown that the activation or deactivation of dopamine receptors provides a capability to learn and store information [1]. Other studies have demonstrated that the immediate post-training blockade of D_1 and D_2 receptors located within the NAc impairs the performance of spatial learning tasks [52]. Based on some other reports, the intra-dorsal hippocampal [62] and peripheral [2,15] administration of the antagonists impair the one-trial passive avoidance and spatial or non-spatial memories in mice, respectively. However, other investigations indicate that pre-test single administration of SCH 23390 or sulpiride causes no significant change in the step-down latency [56]. One study demonstrated that inhibition of the dopamine exocytosis from pre-synaptic neuron via Ca^{2+}-channel blockade by SKF96365 decreases anxiolytic-like behaviours induced by sulpiride in the NAc shell region indicating the involvement of the pre-synaptic dopamine D_2 receptors in sulpiride induced anxiolytic-like behaviours [3]. However, blockade of pre-synaptic dopamine D_2 receptors increases the presynaptic release of dopamine, which in turn induced anxiolytic-like behaviours and aversive memory acquisition impairment. The anxiolytic-like behaviours and aversive memory acquisition impairment that induced by SCH may be related to its effects on pre-synaptic

dopamine D_1 receptors in shell on NAc which will cause the increase in dopamine release.

Effect of intra-NAc shell microinjection of D_1 and D_2 receptors antagonists on anxiolytic-like behaviours and aversive memory deficits induced by the intra-NAc shell NMDA

Data indicated that the intra-NAc shell administration of the subthreshold dose (0.125 µg/rat) of SCH 23390 or sulpiride together with different doses of NMDA, reduce the anxiolytic-like response and improve the aversive memory impairment already induced by the intra-NAc shell infusion of NMDA. These results may suggest the involvement of the dopamine transmission through D_1 and D_2 receptors of the NAc. Several investigations have suggested the possible dopaminergic and glutamatergic systems interaction in the NAc [66,67] based on which the NAc glutamate transmission is modulated by the dopamine system [37,53,82]. With respect to the interaction of these systems, there is a study showing that the NMDA receptors are localized on the NAc shell neurons which abundantly contain dopamine D_1 receptors [81]. Some evidence has also indicated the modulation of dopamine function through NMDA and AMPA receptors [30]. In an interesting report, Kalivas *et al*. declared that SCH 23390 and sulpiride restore the amphetamine-induced glutamate level decrease in NAc suggesting the involvement of presynaptic dopamine receptors in this phenomenon [36]. Furthermore, Dalia *et al*. indicated that dopamine increases the extracellular glutamate levels in the NAc [18]. Meanwhile, activation of glutamate receptor increases the dopamine release in the NAc [31]. We also know from the literature that NAc dopamine and glutamate signalling interactions are crucially required in behavioural reinforcement and habit formation and dopamine can modulate excitatory glutamatergic projection from the PFC [82]. The elevation of extracellular dopamine and glutamate levels in the striatum might disrupt Ca^{2+} homeostasis leading to the endoplasmic reticulum (ER) stress response [4,72]. The stimulation of dopamine D_1 receptors in the mouse neostriatum activates the cAMP/protein kinase A (PKA) pathway [76]. PKA activated increases in the levels of nitric oxide (NO) in the dorsal striatum [45]. NO in turn produces peroxynitrite which can regulate poly (ADPribose) polymerase-1 (PARP-1) activation [86]. Activation of three subtypes of glutamatergic ionotropic receptors leads to calcium influx, nitric oxide (NO) and reactive oxygen species (ROS) generation. Superoxide can combine with NO forming peroxynitrite ($ONOO^-$). Excessive production of peroxynitrite and other free radicals induces chromosomal DNA nicks and breaks resulting in PARP-1 activation [19,83]. This enzyme is the nuclear target for different types of stress and signalling pathways. PARP-1 plays a crucial role in regulation of many transcription factors and nuclear proteins. Under physiological conditions, this enzyme is involved in memory formation and it should not be inhibited [32]. However, under massive stress and other pathological conditions it could be over-activated and involved in cell death by different mechanisms including activation of pro-inflammatory gene expression or modulation of NMDA and cholinergic receptor signalling [75,77]. Thus, there are three possible mechanisms for PARP-1 activation: first, dopamine D_1 receptor-dependent cAMP/PKA pathway is able to activate PARP-1; second, group I mGluRs and NMDA receptors interact with each other to increase PAPR-1 activation; and third, crosstalk between dopamine and glutamate receptors may provide another means of interaction [85]. Another study demonstrated that systemic inflammation evoked by an intraperitoneal injection of lipopolysaccharide induces morphological and biochemical changes in the brain including alterations of PARP-1 activity and expression of several genes [32]. PARP-1 inhibitor protects against LPS-evoked recognition impairment and significantly improves spatial memory in LPS-treated mice. PARP-1 inhibitor in control mice decreased memory function because under physiological conditions this enzyme is involved in memory formation and it should not be inhibited [32].

In conclusion, the stimulation of NMDA receptors in the shell of NAc and the effects of dopamine antagonists on presynaptic receptors might cause the increase in dopamine levels in the striatum and disrupt Ca^{2+} homeostasis leading to the endoplasmic reticulum (ER) stress response [4,72]. In addition, stimulating dopamine and glutamate receptors increases nitric oxide efflux which activates PARP-1 in the central nervous system [69,86]. Under physiological conditions, this enzyme is involved in memory formation and it should not be inhibited [32]. Activation of PARP-1 by elevation of extracellular dopamine and glutamate levels in the striatum might disrupt memory function and induce anxiolyt-

ic-like behaviours. Finally, our results suggest a modulatory role of the NAc shell dopaminergic system on NMDA-induced effects in the aversive memory.

Disclosure

Authors report no conflict of interest.

References

1. Adriani W, Felici A, Sargolini F, Roullet P, Usiello A, Oliverio A, Mele A. N-methyl-D-aspartate and dopamine receptor involvement in the modulation of locomotor activity and memory processes. Exp Brain Res 1998; 123: 52-59.
2. Adriani W, Sargolini F, Coccurello R, Oliverio A, Mele A. Role of dopaminergic system in reactivity to spatial and non-spatial changes in mice. Psychopharmacology (Berl) 2000; 150: 67-76.
3. Ahmadi H, Nasehi M, Rostami P, Zarrindast MR. Involvement of the nucleus accumbens shell dopaminergic system in prelimbic NMDA-induced anxiolytic-like behaviors. Neuropharmacology 2013; 71: 112-123.
4. Ahn SM, Kim SW, Choe ES. Cocaine increases immunoglobulin heavy chain binding protein and caspase-12 expression in the rat dorsal striatum. Psychopharmacology (Berl) 2007; 195: 407-414.
5. Arnsten AF. Catecholamine modulation of prefrontal cortical cognitive function. Trends Cogn Sci 1998; 2: 436-447.
6. Asth L, Lobao-Soares B, Andre E, Soares Vde P, Gavioli EC. The elevated T-maze task as an animal model to simultaneously investigate the effects of drugs on long-term memory and anxiety in mice. Brain Res Bull 2012; 87: 526-533.
7. Baiardi G, Ruiz AM, Beling A, Borgonovo J, Martinez G, Landa AI, Sosa MA, Gargiulo PA. Glutamatergic ionotropic blockade within accumbens disrupts working memory and might alter the endocytic machinery in rat accumbens and prefrontal cortex. J Neural Transm 2007; 114: 1519-1528.
8. Bardo MT, Hammer RP, Jr. Autoradiographic localization of dopamine D_1 and D_2 receptors in rat nucleus accumbens: resistance to differential rearing conditions. Neuroscience 1991; 45: 281-290.
9. Barkus C, McHugh SB, Sprengel R, Seeburg PH, Rawlins JN, Bannerman DM. Hippocampal NMDA receptors and anxiety: at the interface between cognition and emotion. Eur J Pharmacol 2010; 626: 49-56.
10. Bertoglio LJ, Carobrez AP. Previous maze experience required to increase open arms avoidance in rats submitted to the elevated plus-maze model of anxiety. Behav Brain Res 2000; 108: 197-203.
11. Bossert JM, Poles GC, Wihbey KA, Koya E, Shaham Y. Differential effects of blockade of dopamine D1-family receptors in nucleus accumbens core or shell on reinstatement of heroin seeking induced by contextual and discrete cues. J Neurosci 2007; 27: 12655-12663.
12. Cardinal RN, Everitt BJ. Neural and psychological mechanisms underlying appetitive learning: links to drug addiction. Curr Opin Neurobiol 2004; 14: 156-162.
13. Carvalho MC, Albrechet-Souza L, Masson S, Brandao ML. Changes in the biogenic amine content of the prefrontal cortex, amygdala, dorsal hippocampus, and nucleus accumbens of rats submitted to single and repeated sessions of the elevated plus-maze test. Braz J Med Biol Res 2005; 38: 1857-1866.
14. Cheer JF, Wassum KM, Sombers LA, Heien ML, Ariansen JL, Aragona BJ, Phillips PE, Wightman RM. Phasic dopamine release evoked by abused substances requires cannabinoid receptor activation. J Neurosci 2007; 27: 791-795.
15. Coccurello R, Adriani W, Oliverio A, Mele A. Effect of intra-accumbens dopamine receptor agents on reactivity to spatial and non-spatial changes in mice. Psychopharmacology (Berl) 2000; 152: 189-199.
16. Da Cunha IC, Jose RF, Orlandi Pereira L, Pimenta JA, Oliveira de Souza IA, Reiser R, Moreno H, Jr., Marino Neto J, Paschoalini MA, Faria MS. The role of nitric oxide in the emotional learning of rats in the plus-maze. Physiol Behav 2005; 84: 351-358.
17. da Cunha IC, Lopes AP, Steffens SM, Ferraz A, Vargas JC, de Lima TC, Marino Neto J, Paschoalini MA, Faria MS. The microinjection of AMPA receptor antagonist into the accumbens shell, but not into the accumbens core, induces anxiolysis in an animal model of anxiety. Behav Brain Res 2008; 188: 91-99.
18. Dalia A, Uretsky NJ, Wallace LJ. Dopaminergic agonists administered into the nucleus accumbens: effects on extracellular glutamate and on locomotor activity. Brain Res 1998; 788: 111-117.
19. Dawson VL, Dawson TM. Deadly conversations: nuclear-mitochondrial cross-talk. J Bioenerg Biomembr 2004; 36: 287-294.
20. Deutch AY, Cameron DS. Pharmacological characterization of dopamine systems in the nucleus accumbens core and shell. Neuroscience 1992; 46: 49-56.
21. Dunn RW, Corbett R, Fielding S. Effects of 5-HT1A receptor agonists and NMDA receptor antagonists in the social interaction test and the elevated plus maze. Eur J Pharmacol 1989; 169: 1-10.
22. Fernandes C, File SE. The influence of open arm ledges and maze experience in the elevated plus-maze. Pharmacol Biochem Behav 1996; 54: 31-40.
23. Floresco SB, Todd CL, Grace AA. Glutamatergic afferents from the hippocampus to the nucleus accumbens regulate activity of ventral tegmental area dopamine neurons. J Neurosci 2001; 21: 4915-4922.
24. Gal G, Joel D, Gusak O, Feldon J, Weiner I. The effects of electrolytic lesion to the shell subterritory of the nucleus accumbens on delayed non-matching-to-sample and four-arm baited eight-arm radial-maze tasks. Behav Neurosci 1997; 111: 92-103.
25. Garpenstrand H, Annas P, Ekblom J, Oreland L, Fredrikson M. Human fear conditioning is related to dopaminergic and serotonergic biological markers. Behav Neurosci 2001; 115: 358-364.
26. Guimaraes FS, Carobrez AP, De Aguiar JC, Graeff FG. Anxiolytic effect in the elevated plus-maze of the NMDA receptor antagonist AP7 microinjected into the dorsal periaqueductal grey. Psychopharmacology (Berl) 1991; 103: 91-94.
27. Hara Y, Pickel VM. Overlapping intracellular and differential synaptic distributions of dopamine D1 and glutamate N-methyl-D-aspartate receptors in rat nucleus accumbens. J Comp Neurol 2005; 492: 442-455.

28. Horger BA, Roth RH. The role of mesoprefrontal dopamine neurons in stress. Crit Rev Neurobiol 1996; 10: 395-418.
29. Huang YH, Ishikawa M, Lee BR, Nakanishi N, Schluter OM, Dong Y. Searching for presynaptic NMDA receptors in the nucleus accumbens. J Neurosci 2011; 31: 18453-18463.
30. Ikeda H, Kamei J, Koshikawa N, Cools AR. Nucleus accumbens and dopamine-mediated turning behavior of the rat: role of accumbal non-dopaminergic receptors. J Pharmacol Sci 2012; 120: 152-164.
31. Imperato A, Honore T, Jensen LH. Dopamine release in the nucleus caudatus and in the nucleus accumbens is under glutamatergic control through non-NMDA receptors: a study in freely-moving rats. Brain Res 1990; 530: 223-228.
32. Jacewicz M, Czapski GA, Katkowska I, Strosznajder RP. Systemic administration of lipopolysaccharide impairs glutathione redox state and object recognition in male mice. The effect of PARP-1 inhibitor. Folia Neuropathol 2009; 47: 321-328.
33. Jamali-Raeufy N, Nasehi M, Zarrindast MR. Influence of N-methyl D-aspartate receptor mechanism on WIN55,212-2-induced amnesia in rat dorsal hippocampus. Behav Pharmacol 2011; 22: 645-654.
34. Jay TM. Dopamine: a potential substrate for synaptic plasticity and memory mechanisms. Prog Neurobiol 2003; 69: 375-390.
35. Jongen-Relo AL, Kaufmann S, Feldon J. A differential involvement of the shell and core subterritories of the nucleus accumbens of rats in memory processes. Behav Neurosci 2003; 117: 150-168.
36. Kalivas PW, Duffy P. Dopamine regulation of extracellular glutamate in the nucleus accumbens. Brain Res 1997; 761: 173-177.
37. Kalivas PW, Duffy P, Barrow J. Regulation of the mesocorticolimbic dopamine system by glutamic acid receptor subtypes. J Pharmacol Exp Ther 1989; 251: 378-387.
38. Kew JN, Kemp JA. Ionotropic and metabotropic glutamate receptor structure and pharmacology. Psychopharmacology (Berl) 2005; 179: 4-29.
39. Kienast T, Heinz A. Dopamine and the diseased brain. CNS Neurol Disord Drug Targets 2006; 5: 109-131.
40. Kitamura M, Koshikawa N, Yoneshige N, Cools AR. Behavioural and neurochemical effects of cholinergic and dopaminergic agonists administered into the accumbal core and shell in rats. Neuropharmacology 1999; 38: 1397-1407.
41. Klein S, Hadamitzky M, Koch M, Schwabe K. Role of glutamate receptors in nucleus accumbens core and shell in spatial behaviour of rats. Neuroscience 2004; 128: 229-238.
42. Koshikawa N, Kitamura M, Kobayashi M, Cools AR. Contralateral turning elicited by unilateral stimulation of dopamine D2 and D1 receptors in the nucleus accumbens of rats is due to stimulation of these receptors in the shell, but not the core, of this nucleus. Psychopharmacology (Berl) 1996; 126: 185-190.
43. Kuo YM, Liang KC, Chen HH, Cherng CG, Lee HT, Lin Y, Huang AM, Liao RM, Yu L. Cocaine-but not methamphetamine-associated memory requires de novo protein synthesis. Neurobiol Learn Mem 2007; 87: 93-100.
44. Lee C, Rodgers RJ. Antinociceptive effects of elevated plus-maze exposure: influence of opiate receptor manipulations. Psychopharmacology (Berl) 1990; 102: 507-513.
45. Lee DK, Koh WC, Shim YB, Shim I, Choe ES. Repeated cocaine administration increases nitric oxide efflux in the rat dorsal striatum. Psychopharmacology (Berl) 2010; 208: 245-256.
46. Liu JL, Li M, Dang XR, Wang ZH, Rao ZR, Wu SX, Li YQ, Wang W. A NMDA receptor antagonist, MK-801 impairs consolidating extinction of auditory conditioned fear responses in a Pavlovian model. PLoS One 2009; 4: e7548.
47. Maldonado-Irizarry CS, Kelley AE. Excitatory amino acid receptors within nucleus accumbens subregions differentially mediate spatial learning in the rat. Behav Pharmacol 1995; 6: 527-539.
48. Martinez G, Ropero C, Funes A, Flores E, Blotta C, Landa AI, Gargiulo PA. Effects of selective NMDA and non-NMDA blockade in the nucleus accumbens on the plus-maze test. Physiol Behav 2002; 76: 219-224.
49. Martinez G, Ropero C, Funes A, Flores E, Landa AI, Gargiulo PA. AP-7 into the nucleus accumbens disrupts acquisition but does not affect consolidation in a passive avoidance task. Physiol Behav 2002; 76: 205-212.
50. Martinez RC, Oliveira AR, Macedo CE, Molina VA, Brandao ML. Involvement of dopaminergic mechanisms in the nucleus accumbens core and shell subregions in the expression of fear conditioning. Neurosci Lett 2008; 446: 112-116.
51. McGaugh JL. The amygdala modulates the consolidation of memories of emotionally arousing experiences. Annu Rev Neurosci 2004; 27: 1-28.
52. Mele A, Avena M, Roullet P, De Leonibus E, Mandillo S, Sargolini F, Coccurello R, Oliverio A. Nucleus accumbens dopamine receptors in the consolidation of spatial memory. Behav Pharmacol 2004; 15: 423-431.
53. Morari M, Marti M, Sbrenna S, Fuxe K, Bianchi C, Beani L. Reciprocal dopamine-glutamate modulation of release in the basal ganglia. Neurochem Int 1998; 33: 383-397.
54. Mudo G, Persson H, Timmusk T, Funakoshi H, Bindoni M, Belluardo N. Increased expression of trkB and trkC messenger RNAs in the rat forebrain after focal mechanical injury. Neuroscience 1993; 57: 901-912.
55. Nasehi M, Mafi F, Oryan S, Nasri S, Zarrindast MR. The effects of dopaminergic drugs in the dorsal hippocampus of mice in the nicotine-induced anxiogenic-like response. Pharmacol Biochem Behav 2011; 98: 468-473.
56. Nasehi M, Piri M, Nouri M, Farzin D, Nayer-Nouri T, Zarrindast MR. Involvement of dopamine D1/D2 receptors on harmane-induced amnesia in the step-down passive avoidance test. Eur J Pharmacol 2010; 634: 77-83.
57. Ozawa S, Kamiya H, Tsuzuki K. Glutamate receptors in the mammalian central nervous system. Prog Neurobiol 1998; 54: 581-618.
58. Paxinos G, Watson C. The Rat Brain in Stereotaxic Coordinates. 6rd ed. Academic Press, London 2007.
59. Pellow S, Chopin P, File SE, Briley M. Validation of open:closed arm entries in an elevated plus-maze as a measure of anxiety in the rat. J Neurosci Methods 1985; 14: 149-167.
60. Pezze MA, Feldon J. Mesolimbic dopaminergic pathways in fear conditioning. Prog Neurobiol 2004; 74: 301-320.
61. Plaznik A, Palejko W, Nazar M, Jessa M. Effects of antagonists at the NMDA receptor complex in two models of anxiety. Eur Neuropsychopharmacol 1994; 4: 503-512.

62. Rezayof A, Motevasseli T, Rassouli Y, Zarrindast MR. Dorsal hippocampal dopamine receptors are involved in mediating ethanol state-dependent memory. Life Sci 2007; 80: 285-292.
63. Riaza Bermudo-Soriano C, Perez-Rodriguez MM, Vaquero-Lorenzo C, Baca-Garcia E. New perspectives in glutamate and anxiety. Pharmacol Biochem Behav 2012; 100: 752-774.
64. Sargolini F, Florian C, Oliverio A, Mele A, Roullet P. Differential involvement of NMDA and AMPA receptors within the nucleus accumbens in consolidation of information necessary for place navigation and guidance strategy of mice. Learn Mem 2003; 10: 285-292.
65. Schacter GB, Yang CR, Innis NK, Mogenson GJ. The role of the hippocampal-nucleus accumbens pathway in radial-arm maze performance. Brain Res 1989; 494: 339-349.
66. Sesack SR, Pickel VM. In the rat medial nucleus accumbens, hippocampal and catecholaminergic terminals converge on spiny neurons and are in apposition to each other. Brain Res 1990; 527: 266-279.
67. Sesack SR, Pickel VM. Prefrontal cortical efferents in the rat synapse on unlabeled neuronal targets of catecholamine terminals in the nucleus accumbens septi and on dopamine neurons in the ventral tegmental area. J Comp Neurol 1992; 320: 145-160.
68. Setlow B, McGaugh JL. Sulpiride infused into the nucleus accumbens posttraining impairs memory of spatial water maze training. Behav Neurosci 1998; 112: 603-610.
69. Shin EH, Bian S, Shim YB, Rahman MA, Chung KT, Kim JY, Wang JQ, Choe ES. Cocaine increases endoplasmic reticulum stress protein expression in striatal neurons. Neuroscience 2007; 145: 621-630.
70. Smith-Roe SL, Kelley AE. Coincident activation of NMDA and dopamine D1 receptors within the nucleus accumbens core is required for appetitive instrumental learning. J Neurosci 2000; 20: 7737-7742.
71. Smith-Roe SL, Sadeghian K, Kelley AE. Spatial learning and performance in the radial arm maze is impaired after N-methyl-D-aspartate (NMDA) receptor blockade in striatal subregions. Behav Neurosci 1999; 113: 703-717.
72. Smith JA, Mo Q, Guo H, Kunko PM, Robinson SE. Cocaine increases extraneuronal levels of aspartate and glutamate in the nucleus accumbens. Brain Res 1995; 683: 264-269.
73. Solati J. Dorsal hippocampal N-methyl-D-aspartate glutamatergic and delta-opioidergic systems modulate anxiety behaviors in rats in a noninteractive manner. Kaohsiung J Med Sci 2011; 27: 485-493.
74. Stern CA, Do Monte FH, Gazarini L, Carobrez AP, Bertoglio LJ. Activity in prelimbic cortex is required for adjusting the anxiety response level during the elevated plus-maze retest. Neuroscience 2010; 170: 214-222.
75. Strosznajder JB, Jesko H, Strosznajder RP. Age-related alteration of poly(ADP-ribose) polymerase activity in different parts of the brain. Acta Biochim Pol 2000; 47: 331-337.
76. Strosznajder RP, Jesko H, Adamczyk A. Effect of aging and oxidative/genotoxic stress on poly(ADP-ribose) polymerase-1 activity in rat brain. Acta Biochim Pol 2005; 52: 909-914.
77. Strosznajder RP, Jesko H, Zambrzycka A. Poly(ADP-ribose) polymerase: the nuclear target in signal transduction and its role in brain ischemia-reperfusion injury. Mol Neurobiol 2005; 31: 149-167.
78. Tonetto LL, Terzian AL, Del Bel EA, Guimaraes FS, Resstel LB. Inhibition of the NMDA receptor/Nitric Oxide pathway in the dorsolateral periaqueductal gray causes anxiolytic-like effects in rats submitted to the Vogel conflict test. Behav Brain Funct 2009; 5: 40.
79. Treit D, Menard J, Royan C. Anxiogenic stimuli in the elevated plus-maze. Pharmacol Biochem Behav 1993; 44: 463-469.
80. Voorn P, Jorritsma-Byham B, Van Dijk C, Buijs RM. The dopaminergic innervation of the ventral striatum in the rat: a light- and electron-microscopical study with antibodies against dopamine. J Comp Neurol 1986; 251: 84-99.
81. Walaas I. Biochemical evidence for overlapping neocortical and allocortical glutamate projections to the nucleus accumbens and rostral caudatoputamen in the rat brain. Neuroscience 1981; 6: 399-405.
82. Wang W, Dever D, Lowe J, Storey GP, Bhansali A, Eck EK, Nitulescu I, Weimer J, Bamford NS. Regulation of prefrontal excitatory neurotransmission by dopamine in the nucleus accumbens core. J Physiol 2012; 590: 3743-3769.
83. Wang Y, Dawson VL, Dawson TM. Poly(ADP-ribose) signals to mitochondrial AIF: a key event in parthanatos. Exp Neurol 2009; 218: 193-202.
84. Wong AC, Shetreat ME, Clarke JO, Rayport S. D1- and D2-like dopamine receptors are co-localized on the presynaptic varicosities of striatal and nucleus accumbens neurons in vitro. Neuroscience 1999; 89: 221-233.
85. Yang JH, Choe ES. Repeated cocaine administration increases cleaved poly(ADP-ribose) polymerase-1 expression in the rat dorsal striatum. Neurosci Lett 2010; 471: 58-61.
86. Yu SW, Wang H, Dawson TM, Dawson VL. Poly(ADP-ribose) polymerase-1 and apoptosis inducing factor in neurotoxicity. Neurobiol Dis 2003; 14: 303-317.
87. Zahm DS, Heimer L. Specificity in the efferent projections of the nucleus accumbens in the rat: comparison of the rostral pole projection patterns with those of the core and shell. J Comp Neurol 1993; 327: 220-232.
88. Zahrt J, Taylor JR, Mathew RG, Arnsten AF. Supranormal stimulation of D1 dopamine receptors in the rodent prefrontal cortex impairs spatial working memory performance. J Neurosci 1997; 17: 8528-8535.
89. Zajaczkowski W, Frankiewicz T, Parsons CG, Danysz W. Uncompetitive NMDA receptor antagonists attenuate NMDA-induced impairment of passive avoidance learning and LTP. Neuropharmacology 1997; 36: 961-971.
90. Zarrindast MR, Khalifeh S, Rezayof A, Rostami P, Aghamohammadi Sereshki A, Zahmatkesh M. Involvement of rat dopaminergic system of nucleus accumbens in nicotine-induced anxiogenic-like behaviors. Brain Res 2012; 1460: 25-32.
91. Zarrindast MR, Naghdi-Sedeh N, Nasehi M, Sahraei H, Bahrami F, Asadi F. The effects of dopaminergic drugs in the ventral hippocampus of rats in the nicotine-induced anxiogenic-like response. Neurosci Lett 2010; 475: 156-160.
92. Zarrindast MR, Nasehi M, Khansari M, Bananej M. Influence of nitric oxide agents in the rat amygdala on anxiogenic-like effect induced by histamine. Neurosci Lett 2010; 489: 38-42.
93. Zarrindast MR, Nasehi M, Khansari M, Bananej M. Influence of nitric oxide agents in the rat amygdala on anxiogenic-like effect induced by histamine. Neurosci Lett 2011; 489: 38-42.

94. Zarrindast MR, Nasehi M, Pournaghshband M, Ghorbani Yekta B. Dopaminergic system in CA1 modulates MK-801 induced anxiolytic-like responses. Pharmacol Biochem Behav 2012; 103: 102-110.
95. Zarrindast MR, Solati J, Oryan S, Parivar K. Effect of intra-amygdala injection of nicotine and GABA receptor agents on anxiety-like behaviour in rats. Pharmacology 2008; 82: 276-284.
96. Zarrindast MR, Sroushi A, Bananej M, Vousooghi N, Hamidkhaniha S. Involvement of the dopaminergic receptors of the rat basolateral amygdala in anxiolytic-like effects of the cholinergic system. Eur J Pharmacol 2011; 672: 106-112.
97. Zarrindast MR, Torabi M, Rostami P, Fazli-Tabaei S. The effects of histaminergic agents in the dorsal hippocampus of rats in the elevated plus-maze test of anxiety. Pharmacol Biochem Behav 2006; 85: 500-506.
98. Zarrindast MR, Valizadegan F, Rostami P, Rezayof A. Histaminergic system of the lateral septum in the modulation of anxiety-like behaviour in rats. Eur J Pharmacol 2008; 583: 108-114.

Original article

Folia Neuropathologica

Neuroprotective effect of rotigotine against complex I inhibitors, MPP^+ and rotenone, in primary mesencephalic cell culture

Khaled Radad[1], Dieter Scheller[2], Wolf-Dieter Rausch[3], Heinz Reichmann[4], Gabrielle Gille[4]

[1]Department of Pathology, Faculty of Veterinary Medicine, Assiut University, Assiut, Egypt, [2]UCB Pharma SA, Department of Parkinson's Disease and Movement Disorders, CNS Research, Chemin de Foriest, Braine-l'Alleud, Belgium, [3]Institute for Medical Chemistry, University of Veterinary Medicine, Vienna, Austria, [4]Department of Neurology, Technical University of Dresden, Dresden, Germany

Folia Neuropathol 2014; 52 (2): 179-186 DOI: 10.5114/fn.2014.43789

Abstract

Introduction: *Dopamine agonists are suggested to be more efficacious in treating Parkinson's disease (PD) as they have neuroprotective properties in addition to their receptor-related actions.*

Aim of the study: *The present study was designed to investigate the neuroprotective effects of rotigotine, a $D_3/D_2/D_1$ dopamine receptor agonist, against the two powerful complex I inhibitors, 1-methyl-4-phenylpyridinium (MPP^+) and rotenone, in primary mesencephalic cell culture relevant to PD.*

Material and methods: *Primary mesencephalic cell cultures were prepared from embryonic mouse mesencephala at gestation day 14. Three sets of cultures were treated with rotigotine alone, rotigotine and MPP^+, and rotigotine and rotenone to investigate the effect of rotigotine on the survival of dopaminergic neurons against age-, MPP^+- and rotenone-induced cell death. At the end of each treatment, cultures were fixed and stained immunohistochemically against tyrosine hydroxylase (TH). The effect of rotigotine against rotenone-induced reactive oxygen species (ROS) production was measured using CH-H_2DCFDA fluorescence dye.*

Results: *Rotigotine alone did not influence the survival of tyrosine hydroxylase immunoreactive (THir) neurons except at 10 μM, it significantly decreased the number of THir neurons by 40% compared to untreated controls. Treatment of cultures with 0.01 μM rotigotine rescued 10% of THir neurons against MPP^+-induced cell death. Rotigotine was also found to significantly rescue 20% of THir neurons at 0.01 μM of rotenone-treated cultures. Using of CH-H_2DCFDA fluorescence dye, it was found that rotigotine significantly attenuated ROS production compared to rotenone-treated cultures.*

Conclusions: *Rotigotine provides minor protection against MPP^+ and rescues a significant number of THir neurons against rotenone in primary mesencephalic cell cultures relevant to PD.*

Key words: *dopamine agonists, dopaminergic neurons, MPP^+, neuroprotection, Parkinson's disease, rotenone, rotigotine.*

Introduction

Dopamine replacement therapy using levodopa continues to be the gold standard in the treatment of Parkinson's disease (PD). It has remained the most effective drug for the symptomatic treatment of PD since its introduction by Birkmayer and Horny-

Communicating author:
Dr. Khaled Radad, PhD, Department of Pathology, Faculty of Veterinary Medicine, Assiut University, Assiut 71526, Egypt, tel.: +2-882-333938, fax: +2-882-366503, e-mail: khaledradad@hotmail.com

kiewicz in 1961 [3]. Interestingly, Hurny *et al*. [13] have shown recently that levodopa decreased the CD_{25}/CD_3 ratio, the antigen marker characteristic of apoptotic death within the $T/CD_3(+)$ lymphocyte population in the peripheral blood of PD patients. However, long-term levodopa treatment therapy is accompanied by abnormal involuntary movements known as levodopa-induced dyskinesia [1]. Moreover, there is an enduring belief from pre-clinical studies that levodopa or its metabolite dopamine might be toxic to the remaining substantia nigra (SN) dopaminergic neurons [17]. Accordingly, *de novo* and younger patients might be at high risk for the development of levodopa-induced complications as they require dopaminergic therapy for a longer period of time [8].

Dopamine receptor agonists are the next most effective antiparkinsonian drugs after carbidopa/levodopa medication. They are considered useful alternatives to levodopa in mild or early PD and as an additional drug in moderate to severe late disease [8]. They improve motor outcomes and decrease the risk of levodopa-induced motor complications [32]. In addition to their symptomatic effectiveness, dopamine agonists may have a neuroprotective effect. For instance, recipients of pramipexole and ropinirole showed slower neuronal deterioration compared with levodopa recipients by means of dopamine transporter imaging using single-photon emission computed tomography (SPECT) [21,34].

The non-ergoline dopamine agonist rotigotine is currently approved as monotherapy in early idiopathic PD, in moderate to severe idiopathic restless leg syndrome and as adjunct therapy to levodopa in advanced idiopathic PD. In PD it is supposed to reduce motor fluctuations by constant dopaminergic stimulation using a 24-h transdermal delivery system (patch). Rotigotine exhibits the highest affinity for the D_3 receptor (Ki = 0.71 nM) and acts as a full agonist at dopamine receptors (rank order: $D_3 > D_{2L} > D_1 = D_5 > D_{4.4}$) with potencies 2,600 and 53 times higher than dopamine at dopamine D_3 and D_{2L} receptors [31].

In contrast to other dopamine agonists, there is only limited knowledge of potential neuroprotective properties of rotigotine. In the acute 1-methyl-4-phenyl-1,2,3,6 tetrahydropyridine (MPTP) mouse or progressive MPTP macaque model, the agonist was shown to exert partial protective effects on dopaminergic nerve endings [29,30]. To date there have been no investigations exploring the direct neuroprotective effects of rotigotine towards dopaminergic neurons under conditions of inhibition of the mitochondrial respiratory chain reactions. Accordingly, the present study was carried out in primary dopaminergic cell cultures from embryonic mouse mesencephala stressed with mitochondrial complex I blockers, MPP^+ and rotenone. Such studies are of interest, since the pesticide rotenone was found to be associated with an increased risk of developing PD [5,33] and a subgroup of PD patients were demonstrated to exhibit a defect of complex I activity and structure [15,18,28].

Material and methods

Preparation of primary dopaminergic cell culture

Pregnant mice (OF1/SPF, Himberg, Austria) were cared and handled in accordance with the guidelines of the European Union Council (86/609/EU) for the use of laboratory animals. At gestation day 14, uterine horns were dissected and embryos were collected in Petri dishes containing sterile Dulbecco's phosphate buffered saline (DPBS, Invitrogen, Germany). Under a stereoscope (Nikon SMZ-1B, 10 × magnification), brains were dissected, ventral mesencephala excised and primary cultures were prepared according to Radad *et al*. [23]. Briefly, after careful removal of the meninges, tissues were mechanically cut into small pieces in DPBS and transferred into a sterile test tube containing 2 ml of 0.1% trypsin (Invitrogen, Germany) and 2 ml of 0.02% DNase I (Roche, Germany) in DPBS. The tube was incubated in a water bath at 37°C for 7 min. Then, 2 ml of trypsin inhibitor (0.125 mg/ml in DPBS) (Invitrogen, Germany) were added, the tissue was centrifuged (Hettich, ROTIXA/AP) at 100 g for 4 min. The tissue pellet was triturated with a fire-polished Pasteur pipette in Dulbecco's modified Eagle's medium (DMEM, Sigma, Germany) containing 0.02% DNase I. Dissociated cells were collected in DMEM supplemented with Hepes buffer (25 mM), glucose (30 mM), glutamine (2 mM), penicillin-streptomycin (10 U/ml and 0.1 mg/ml, respectively) and heat inactivated foetal calf serum (FCS, 10%) (all from Sigma, Germany). The cell suspension was plated into four-well multidishes (Nunclon, Germany) pre-coated with poly-D-lysine (50 µg/ml) (Sigma, Germany). Cultures were grown at 37°C in an atmosphere of 5% CO_2/95% air and 100% relative

humidity. The medium was exchanged on the 1st day *in vitro* (DIV) and on the 3rd DIV. On the 5th DIV half of the medium was replaced with serum-free DMEM containing 0.02 ml of B-27/ml (Invitrogen, Germany). Serum-free supplemented DMEM was used for feeding from the 6th DIV and subsequently replaced every 2nd day.

Treatment of cultures with rotigotine, MPP+ and rotenone

To investigate the effect of rotigotine (UCB, Belgium) on the survival of THir neurons, primary mesencephalic cell cultures were treated with different concentrations of rotigotine (0.01, 0.1, 1 and 10 μM) from the 6th DIV for 8 consecutive days. Rotigotine was added with each change of the culture medium every second day from a fresh stock solution (10 mM) prepared in DMSO (0.1% final concentration). To investigate the effect of rotigotine against MPP^+ or rotenone-induced cell death, rotigotine was added from the 6th DIV until the 14th DIV as described above and MPP^+ (10 μM) or rotenone (20 nM) were co-administered on the 12th DIV for 48 h.

Identification of THir neurons

Dopaminergic neurons were identified immunocytochemically by staining tyrosine hydroxylase. Cultures were rinsed carefully with phosphate buffered saline (PBS, pH 7.2) at the end of each treatment and fixed in 4% paraformaldehyde for 45 min at 4°C. After washing with PBS, cells were permeabilized with 0.4% Triton X-100 for 30 min at room temperature. Cultures were washed 3 times with PBS and incubated with 5% horse serum (Vectastain ABC Elite kit) for 90 min to block nonspecific binding sites. To determine the number of THir in cultures, cells were sequentially incubated with anti-TH primary antibody overnight at 4°C, biotinylated secondary antibody (Vectastain) and avidin-biotin-horseradish peroxidase complex (Vectastain) for 90 min at room temperature and washed with PBS between stages. The reaction product was developed in a solution of diaminobenzidine (1.4 mM) in PBS containing 3.3 mM of hydrogen peroxide (H_2O_2) and stained cells were counted with a Nikon inverted microscope in 10 randomly selected fields (1.13 mm^2 = field) in each well at 10× magnification. On the 14th DIV, the average number of THir cells in the various experiments was between 1000 and 1500 cells/well.

Measurement of ROS with CH-H_2DCFDA

When the production of ROS was measured, cultures were treated with rotigotine (0.01 μM, the protective concentration against rotenone) from the 6th DIV until the 12th DIV. Rotenone (20 nM) was co-administered on the 12th DIV for 48 h. On the 14th DIV cultures were washed and incubated with 5 μM of the fluorescence indicator, 5-(and 6)-chloromethyl-2',7'-dichlorodihydrofluorescein diacetate (CH-H_2DCFDA), for 30 min and ROS was measured according to Radad *et al*. [24]. In short, cultures were rinsed twice with colourless medium and photographed on a Nikon inverted microscope equipped with epifluorescence attachment using a rhodamine filter set (510 DM/520 BA, B-2A) and a Coolpix 990 digital camera (Nikon, Japan). In each experiment, four wells were cultivated for each treatment condition. Five micrographs were taken from each well. Ten cell bodies were randomly selected by a blinded researcher from each micrograph (meaning that 200 cells were evaluated for each treatment condition in each of three independent experiments) and the average density for 100 pixels in individual cell bodies was determined using Adobe Photoshop software®.

Statistical analysis

Data were expressed as mean ± standard error of mean (SEM). Statistical significance was calculated using the Kruskal-Wallis (H)-test followed by χ^2. Differences with $p < 0.05$ were regarded as statistically significant.

Results

Effect of rotigotine on the survival of dopaminergic neurons

Addition of rotigotine (0.01, 0.1, 1 μM) for 8 consecutive days produced no effect on the number of THir neurons in primary mesencephalic cell culture compared to untreated controls. However, rotigotine decreased the number of THir neurons by 40% when added at an unphysiological high concentration of 10 μM (Fig. 1).

Rotigotine slightly protected dopaminergic neurons against MPP+ toxicity

MPP^+ (10 μM) decreased the number of THir neurons by 43% compared to untreated control cultures

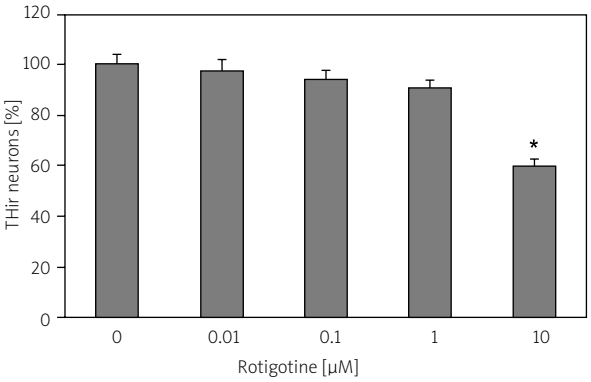

Fig. 1. Effect of incubation with various concentrations of rotigotine on the survival of THir neurons. Treatment was begun on the 6th DIV for 8 consecutive days with a change of medium together with rotigotine every 2nd day. 100% corresponds to the total number of dopaminergic neurons after a cultivation period of 14 days without rotigotine treatment. Values represent the mean ± SEM of three independent experiments in quadruplicate. *$p < 0.0001$ compared to untreated control.

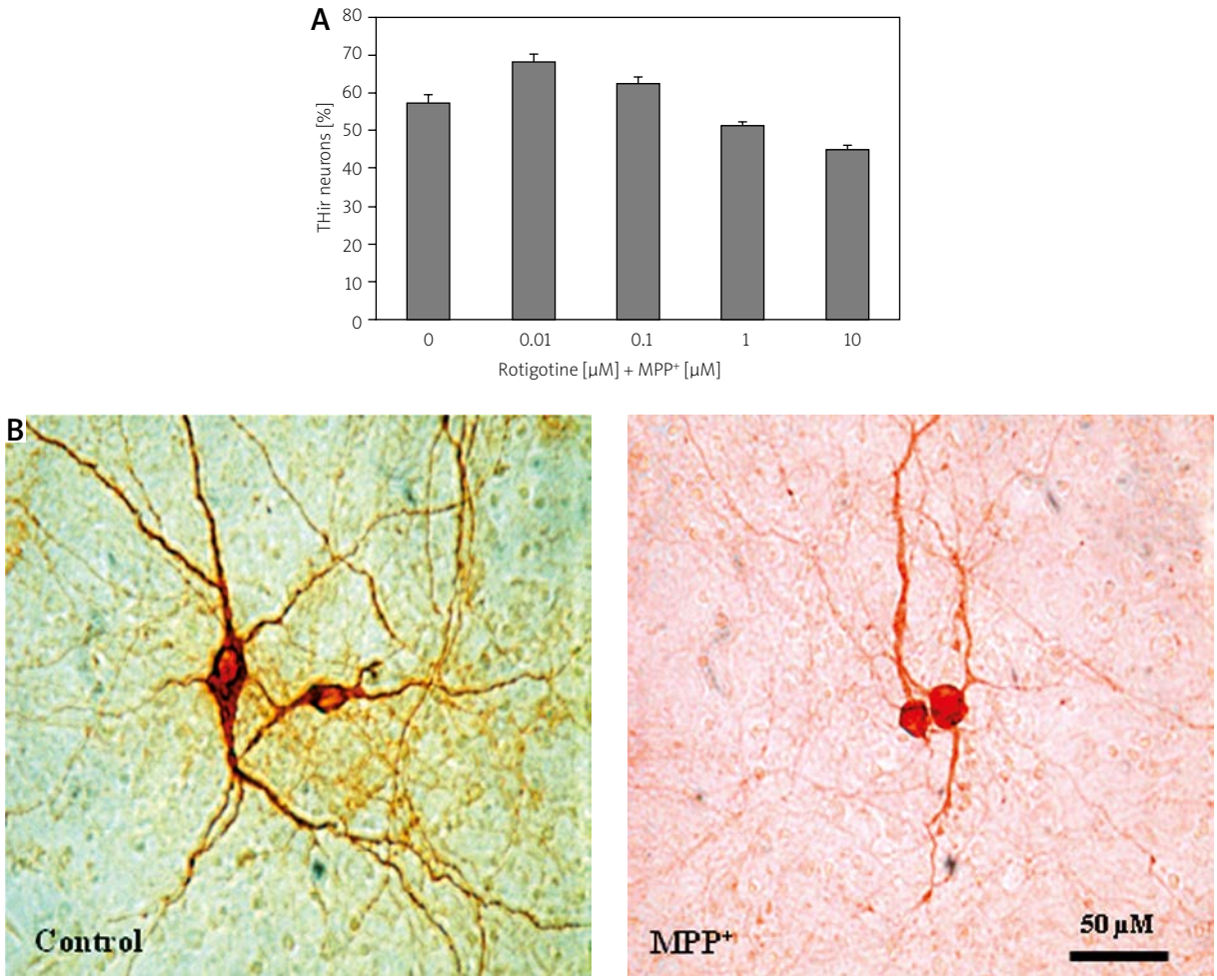

Fig. 2. A) Effect of rotigotine on the survival of MPP+-treated dopaminergic neurons. Treatment with rotigotine was begun on the 6th DIV for 8 consecutive days with a change of medium together with rotigotine every 2nd day. MPP+ (10 µM) was additionally added for 48 h from 12-14th DIV. 100% corresponds to the total number of dopaminergic neurons after a cultivation period of 14 days without any treatment. Values represent the mean ± SEM of three independent experiments in quadruplicate. **B)** Representative micrographs of THir neurons after 14 DIV. Control cultures were cultivated without any treatment while for MPP+ treatment, cultures were incubated with MPP+ for 48 h from 12-14th DIV.

(Fig. 2A). After MPP^+ treatment, surviving neurons had shortened and thickened neurites as well as atrophied cell bodies (Fig. 2B). The treatment of cultures with 0.01 µM rotigotine attenuated MPP^+-induced toxicity by increasing the number of dopaminergic neurons by 10%, although this effect did not reach significance (Fig. 2A).

Rotigotine significantly protected dopaminergic neurons against rotenone-induced cell death

The treatment of cultures with 20 nM rotenone decreased the number of THir neurons by 55% compared to untreated control cultures (Fig. 3A). After rotenone treatment, surviving neurons exhibited less and shortened neurites (Fig. 3B). On the other hand, 0.01 µM rotigotine was able to counteract rotenone-induced toxicity by significantly increasing the number of dopaminergic neurons by 20% (Fig. 3A).

Rotigotine significantly inhibited ROS production by rotenone

The formation of ROS in cultures was measured using CM-H_2DCFDA fluorescence staining. The treatment of cultures with 20 nM rotenone on the 10th DIV for 48 h significantly elevated overall

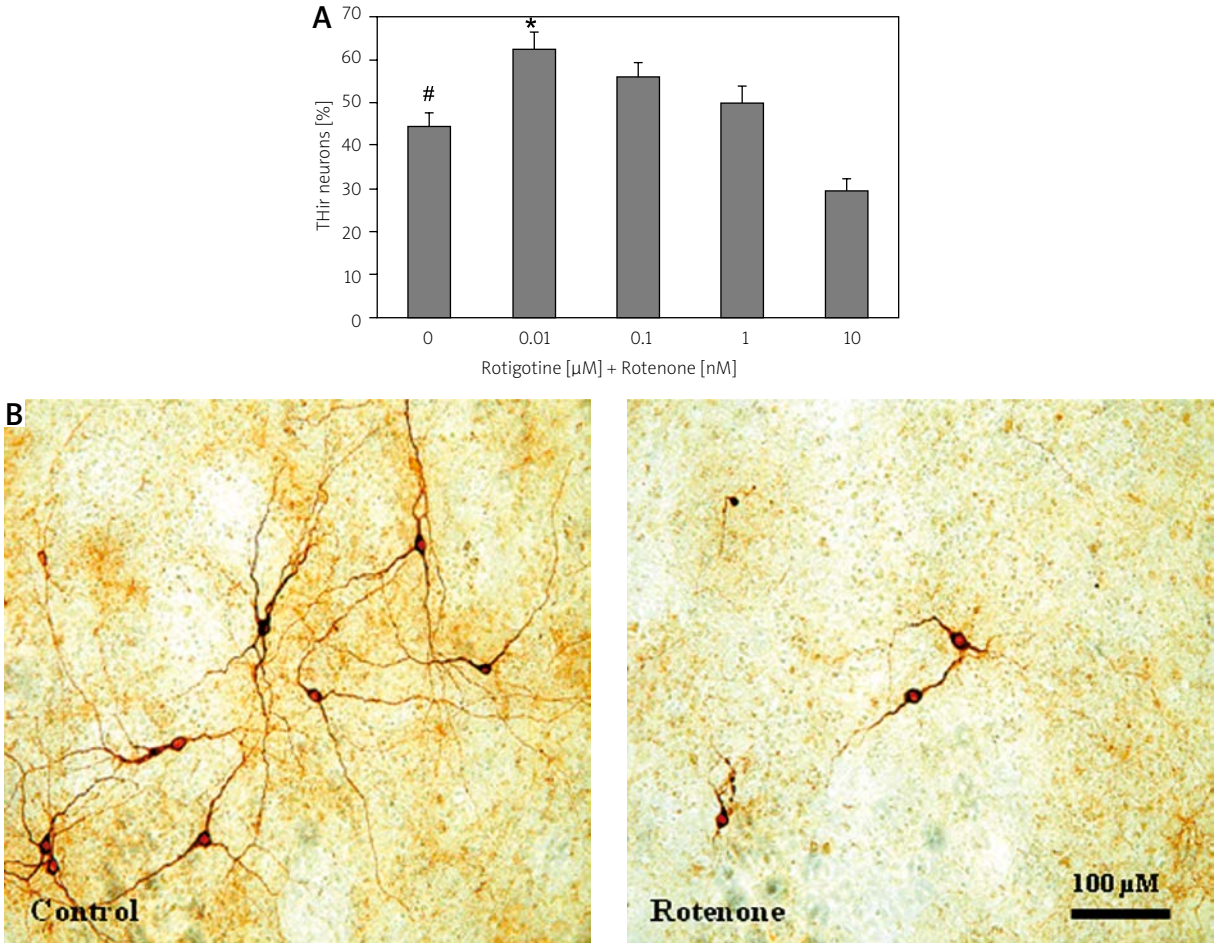

Fig. 3. A) Effect of rotigotine on the number of dopaminergic neurons after treatment with rotenone. Treatment with rotigotine was begun on the 6th DIV for 8 consecutive days with a change of medium together with rotigotine every 2nd day. Rotenone (20 nM) was additionally added for 48 h from 12-14th DIV. 100% corresponds to the total number of dopaminergic neurons after a cultivation period of 14 days without any treatment. Values represent the mean ± SEM of three independent experiments in quadruplicate. ($^{\#}p < 0.0001$ compared to untreated controls, $^{*}p < 0.0001$ compared to rotenone-treated cultures). **B)** Representative micrographs of THir neurons after 14 DIV. Control cultures were cultivated without any treatment while for rotenone treatment, cultures were incubated with rotenone for 48 h from 12-14th DIV.

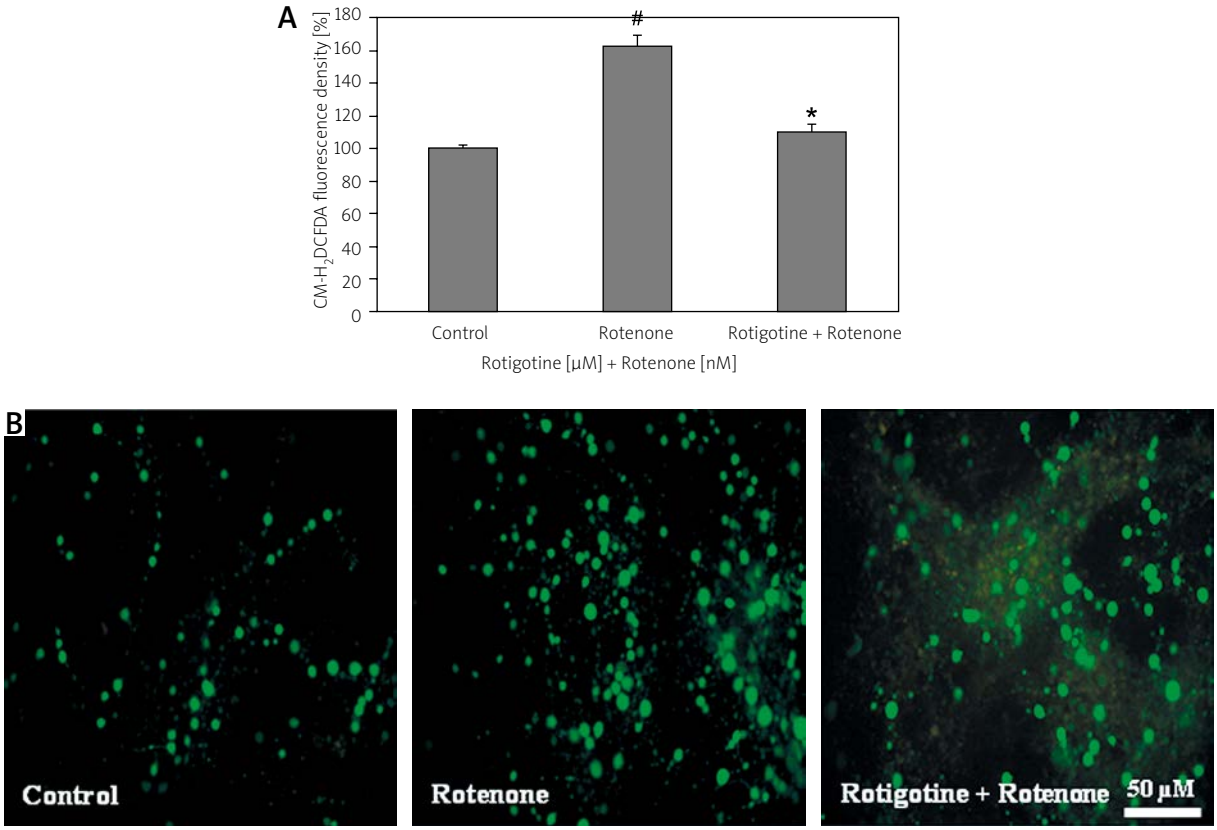

Fig. 4. A) Effect of rotigotine on ROS production by rotenone. Treatment with rotigotine (0.01 μM) was begun on the 6th DIV for 8 consecutive days with a change of medium together with rotigotine every 2nd day. Rotenone (20 nM) was added for 48 h from 12-14th DIV. 100% corresponds to the fluorescence density of the dye in untreated control cultures. Values represent the mean ± SEM of three independent experiments in quadruplicate. ($^{\#}p < 0.0001$ compared to untreated control cultures, $^{*}p < 0.0001$ compared to rotenone-treated cultures). **B)** Representative micrographs of fluorescence density of CM-H_2DCFDA in control, rotenone-treated and rotigotine plus rotenone-treated cultures. Higher fluorescence density indicates higher ROS production.

ROS production by 63% (Fig. 4A) as reflected in higher fluorescence density compared to untreated control culture (Fig. 4B). Rotigotine (0.01 μM, on the 6th DIV for six days) significantly decreased the intracellular production of ROS by 17% compared to rotenone-treated cultures (Fig. 4A). Figure 4B showed that treatment of cultures with rotigotine (0.01 μM) decreased the fluorescence density of CM-H_2DCFDA compared to rotenone-treated cultures.

Discussion

Protection of dopaminergic neurons by dopamine agonists has been a topic of interest for the past 20 years. While the lack of placebo groups in clinical studies did not allow a definite conclusion with respect to the neuroprotective effect of the dopamine agonists ropinirole and pramipexole [21,34], numerous preclinical studies were able to demonstrate distinct neuroprotective effects in animal or cell culture models [22,26,27]. In the present study, primary mesencephalic cell cultures were used to investigate the neuroprotective potential of the non-ergot dopamine agonist rotigotine against MPP^+ and rotenone toxicity. Both components are known inhibitors of complex I of the mitochondrial respiratory chain [20,25] and the detection of a defect in complex I in the SN of idiopathic PD cases provided a direct link to the MPTP (respectively MPP^+) and rotenone toxicity models.

In preliminary experiments, the effect of rotigotine on the survival rate of THir neurons was investigated. In a concentration range up to 1 μM, rotigo-

tine, when given for eight consecutive days, did not affect the survival of THir neurons. These results are similar to those achieved with the D_2 receptor agonist α-dihydroergocryptine that showed no stimulation of THir neurons, but differ from the D_2 receptor agonist lisuride which significantly enhanced the number of THir neurons under the same treatment conditions [9,11]. Treatment with 10 µM rotigotine decreased the number of THir neurons, which is similar to the behaviour of the D_2 agonist pergolide and α-dihydroergocryptine [9,10]. However, the high unphysiological concentration of 10 µM exceeds by far the therapeutic doses of 1-16 mg/day and the achieved plasma concentrations of unconjugated rotigotine which amount up to 1 ng/ml [7].

Some dopamine agonists have exhibited neuroprotection for dopaminergic neurons against MPTP in mice, for example bromocriptine [19] and pramipexole [16]. Neuroprotection against MPP^+ in primary dopaminergic culture from embryonic mouse or rat mesencephalon was demonstrated for lisuride [11], and pramipexole and ropinirole, respectively [6]. In contrast to these findings, rotigotine was not able to significantly counteract MPP^+-induced toxicity for dopaminergic neurons.

Since Betarbet *et al*. used the highly selective complex I inhibitor rotenone to reproduce PD's features in rats [2], rotenone has been considered a model neurotoxin for PD both *in vitro* and *in vivo*. Similar to our previous work [24], treatment of primary mesencephalic cell culture with 20 nM rotenone killed about 50% of dopaminergic neurons. Rotenone-induced cell death was shown to be attributed to overproduction of ROS and a decreased mitochondrial membrane potential [24]. Here we show that rotigotine was able to protect dopaminergic neurons from rotenone toxicity which might at least be partially attributed to a significant suppression of ROS production induced by rotenone treatment. Other dopamine agonists like pramipexole and ropinirole protected against rotenone-induced cell death in the dopaminergic neuroblastoma cell line SHSY-5Y [4,12] and pramipexole protected also against nigrostriatal dopaminergic degeneration and motor deficits in rotenone-treated mice [14].

In conclusion, rotigotine significantly protects dopaminergic neurons against rotenone toxicity in primary mesencephalic cell culture. The mechanism of protection involves counteracting of mitochondrial dysfunction as rotenone-induced radical production can be prevented by rotigotine.

Disclosure

Authors report no conflict of interest.

References

1. Ahlskog JE, Muenter MD. Frequency of levodopa-related dyskinesias and motor fluctuations as estimated from the cumulative literature. Mov Disord 2001; 16: 448-458.
2. Betarbet R, Sherer TB, MacKenzie G, Garcia-Osuna M, Panov AV, Greenamyre JT. Chronic systemic pesticide exposure reproduces features of Parkinson's disease. Nat Neurosci 2000; 3: 1301-1306.
3. Birkmayer W, Hornykiewicz O. The effect of l-3,4-dihydroxyphenylalanine (= DOPA) on akinesia in parkinsonism. 1961. Wien Klin Wochenschr 2001; 113: 851-854.
4. Chen S, Zhang X, Yang D, Du Y, Li L, Li X, Ming M, Le W. D2/D3 receptor agonist ropinirole protects dopaminergic cell line against rotenone-induced apoptosis through inhibition of caspase- and JNK-dependent pathways. FEBS Lett 2008; 582: 603-610.
5. Dhillon AS, Tarbutton GL, Levin JL, Plotkin GM, Lowry LK, Nalbone JT, Shepherd S. Pesticide/environmental exposures and Parkinson's disease in East Texas. J Agromedicine 2008; 13: 37-48.
6. Du F, Li R, Huang Y, Li X, Le W. Dopamine D3 receptor-preferring agonists induce neurotrophic effects on mesencephalic dopamine neurons. Eur J Neurosci 2005; 22: 2422-2430.
7. Elshoff JP, Braun M, Andreas JO, Middle M, Cawello W. Steady-state plasma concentration profile of transdermal rotigotine: an integrated analysis of three, open-label, randomized, phase I multiple dose studies. Clin Ther 2012; 34: 966-978.
8. Fernandez HH. Updates in the medical management of Parkinson disease. Cleve Clin J Med 2012; 79: 28-35.
9. Gille G, Radad K, Reichmann H, Rausch WD. Synergistic effect of alpha-dihydroergocryptine and L-dopa or dopamine on dopaminergic neurons in primary culture. J Neural Transm 2006; 113: 1107-1118.
10. Gille G, Rausch WD, Hung ST, Moldzio R, Janetzky B, Hundemer HP, Kolter T, Reichmann H. Pergolide protects dopaminergic neurons in primary culture under stress conditions. J Neural Transm 2002; 109: 633-643.
11. Gille G, Rausch WD, Hung ST, Moldzio R, Ngyuen A, Janetzky B, Engfer A, Reichmann H. Protection of dopaminergic neurons in primary culture by lisuride. J Neural Transm 2002; 109: 157-169.
12. Gu M, Irvani M, Cooper JM, King D, Jenner P, Schapira AH. Pramipexole protects against apoptotic cell death by non-dopaminergic mechanisms. J Neurochem 2004; 91: 1075-1081.
13. Hurny A, Michałowska-Wender G, Wender M. Impact of L-DOPA treatment of patients with Parkinson's disease on mononuclear subsets and phagocytosis in the peripheral blood. Folia Neuropathol 2013; 51: 127-131.
14. Inden M, Kitamura Y, Tamaki A, Yanagida T, Shibaike T, Yamamoto A, Takata K, Yasui H, Taira T, Ariga H, Taniguchi T. Neuroprotective effect of the antiparkinsonian drug pramipexole against nigrostriatal dopaminergic degeneration in rotenone-treated mice. Neurochem Int 2009; 55: 760-767.
15. Keeney PM, Xie J, Capaldi RA, Bennett JP, Jr. Parkinson's disease brain mitochondrial complex I has oxidatively damaged sub-

units and is functionally impaired and misassembled. J Neurosci 2006; 26: 5256-5264.
16. Kitamura Y, Kohno Y, Nakazawa M, Nomura Y. Inhibitory effects of talipexole and pramipexole on MPTP-induced dopamine reduction in the striatum of C57BL/6N mice. Jpn J Pharmacol 1997; 74: 51-57.
17. Lipski J, Nistico R, Berretta N, Guatteo E, Bernardi G, Mercuri NB. L-DOPA: a scapegoat for accelerated neurodegeneration in Parkinson's disease? Prog Neurobiol 2011; 94: 389-407.
18. Mizuno Y, Ohta S, Tanaka M, Takamiya S, Suzuki K, Sato T, Oya H, Ozawa T, Kagawa Y. Deficiencies in complex I subunits of the respiratory chain in Parkinson's disease. Biochem Biophys Res Commun 1989; 163: 1450-1455.
19. Muralikrishnan D, Mohanakumar KP. Neuroprotection by bromocriptine against 1-methyl-4-phenyl-1,2,3,6-tetrahydropyridine-induced neurotoxicity in mice. FASEB J 1998; 12: 905-912.
20. Nicklas WJ, Vyas I, Heikkila RE. Inhibition of NADH-linked oxidation in brain mitochondria by 1-methyl-4-phenyl-pyridine, a metabolite of the neurotoxin, 1-methyl-4-phenyl-1,2,5,6-tetrahydropyridine. Life Sci 1985; 36: 2503-2508.
21. Parkinson Study Group. Pramipexole vs levodopa as initial treatment for Parkinson disease: A randomized controlled trial. Parkinson Study Group. JAMA 2000; 284: 1931-1938.
22. Pirtosek Z, Flisar D. Neuroprotection and dopamine agonists. Adv Exp Med Biol 2004; 541: 55-74.
23. Radad K, Moldzio R, Rausch WD. Minocycline protects dopaminergic neurons against long-term rotenone toxicity. Can J Neurol Sci 2010; 37: 81-85.
24. Radad K, Rausch WD, Gille G. Rotenone induces cell death in primary dopaminergic culture by increasing ROS production and inhibiting mitochondrial respiration. Neurochem Int 2006; 49: 379-386.
25. Richardson JR, Quan Y, Sherer TB, Greenamyre JT, Miller GW. Paraquat neurotoxicity is distinct from that of MPTP and rotenone. Toxicol Sci 2005; 88: 193-201.
26. Schapira AH. Dopamine agonists and neuroprotection in Parkinson's disease. Eur J Neurol 2002; 9 Suppl 3: 7-14.
27. Schapira AH. Molecular and clinical pathways to neuroprotection of dopaminergic drugs in Parkinson disease. Neurology 2009; 72: S44-S50.
28. Schapira AH, Cooper JM, Dexter D, Jenner P, Clark JB, Marsden CD. Mitochondrial complex I deficiency in Parkinson's disease. Lancet 1989; 333: 1269.
29. Scheller D, Chan P, Li Q, Wu T, Zhang R, Guan L, Ravenscroft P, Guigoni C, Crossman AR, Hill M, Bezard E. Rotigotine treatment partially protects from MPTP toxicity in a progressive macaque model of Parkinson's disease. Exp Neurol 2007; 203: 415-422.
30. Scheller D, Stichel-Gunkel C, Lubbert H, Porras G, Ravenscroft P, Hill M, Bezard E. Neuroprotective effects of rotigotine in the acute MPTP-lesioned mouse model of Parkinson's disease. Neurosci Lett 2008; 432: 30-34.
31. Scheller D, Ullmer C, Berkels R, Gwarek M, Lubbert H. The in vitro receptor profile of rotigotine: a new agent for the treatment of Parkinson's disease. Naunyn Schmiedebergs Arch Pharmacol 2009; 379: 73-86.
32. Sprenger F, Poewe W. Management of motor and non-motor symptoms in Parkinson's disease. CNS Drugs 2013; 27: 259-272.
33. Tanner CM, Kamel F, Ross GW, Hoppin JA, Goldman SM, Korell M, Marras C, Bhudhikanok GS, Kasten M, Chade AR, Comyns K, Richards MB, Meng C, Priestley B, Fernandez HH, Cambi F, Umbach DM, Blair A, Sandler DP, Langston JW. Rotenone, paraquat, and Parkinson's disease. Environ Health Perspect 2011; 119: 866-872.
34. Whone AL, Watts RL, Stoessl AJ, Davis M, Reske S, Nahmias C, Lang AE, Rascol O, Ribeiro MJ, Remy P, Poewe WH, Hauser RA, Brooks DJ. Slower progression of Parkinson's disease with ropinirole versus levodopa: The REAL-PET study. Ann Neurol 2003; 54: 93-101.

Original article

Folia Neuropathologica

Primary angiitis of the central nervous system: a study of histopathological patterns and review of the literature

Vaishali Suri[1], Aanchal Kakkar[1], Mehar C. Sharma[1], Madakasira V. Padma[2], Ajay Garg[3], Chitra Sarkar[1]

[1]Department of Pathology, [2]Department of Neurology, and [3]Department of Neuroradiology, All India Institute of Medical Sciences (AIIMS), New Delhi, India

Folia Neuropathol 2014; 52 (2): 187-196 DOI: 10.5114/fn.2014.43790

Abstract

Primary angiitis of the central nervous system (PACNS) is a rare form of vasculitis of unknown aetiology. Multifaceted clinical manifestations, non-specific MRI findings, a broad range of differential diagnoses and diverse pathological appearances prove to be a diagnostic challenge. However, a prompt diagnosis and aggressive treatment are crucial to avoid permanent damage. Hence, we present the clinico-pathological spectrum of this entity and highlight the limitations of currently available diagnostic modalities. We describe in detail the histopathological findings of eight cases of PACNS diagnosed at the Department of Pathology, AIIMS, over a period of eight years. Eight cases of PACNS were identified during this period. Five cases (62.5%) showed features of granulomatous vasculitis, two (25%) showed lymphocytic vasculitis and one case (12.5%) showed a predominantly necrotizing pattern of vasculitis. Diagnosis of PACNS is a challenge and requires a high index of clinical suspicion. Appropriate work-up to exclude other conditions is mandatory. Brain biopsy is useful in making the diagnosis and ruling out mimicking conditions.

Key words: *central nervous system, primary angiitis, vasculitis, granulomatous inflammation.*

Introduction

Primary angiitis of central nervous system (PACNS) is a rare and diagnostically challenging form of vasculitis, which primarily affects small and medium-sized vessels supplying the brain parenchyma, spinal cord and leptomeninges [1]. Synonyms for this entity include "isolated angiitis of CNS" and "primary CNS vasculitis" (PCNSV). An annual incidence of 2.4 cases per million population has been reported in North America [33]. Majority of patients present in the fourth to sixth decade, with male preponderance [24]. There are no useful animal models to aid our understanding of this disease. It was first described as 'an unknown form of angiitis' by Harbitz in 1922 [15] and was considered a distinct clinical entity in 1959 by Cravioto and Feigin who coined the term "noninfectious granulomatous angiitis" with a predilection for the nervous system [10]. Primary angiitis of central nervous system remained rare with only 46 cases reported in the literature by 1986. In 1988, Calabrese and Mallek proposed the definite diagnostic criteria, which were later modified by Birnbaum *et al*. in 2009 [5,7].

The clinical presentations are diverse and non-specific [12]. Differential diagnoses include secondary vasculitides, collagen vascular disorders, certain viral and bacterial infections, and substance abuse [29,40]. Laboratory investigations indicative of systemic vas-

Communicating author:
Dr. Mehar C. Sharma, Professor, Department of Pathology, All India Institute of Medical Sciences, New Delhi-110029, phone: 91-11-26593371, fax: 91-11-26588663, e-mail: sharmamehar@yahoo.co.in

culitis are usually normal. CSF shows modest lymphocytic pleocytosis and raised protein levels [7].

MRI is abnormal in almost all patients, and abnormalities may be seen in the subcortical white matter, deep gray matter, deep white matter, and the cerebral cortex [9,13,17]. Angiogram shows characteristic alternating stenosis and dilatation, but is less specific and has been observed to be as low as 30% [11,16,33]. A definite diagnosis can be made only on the basis of biopsy findings [22]. Due to the segmental nature of the lesions, even biopsy may be negative in up to 35% of biopsies [8,12]. Based on distinct clinical, radiological and histopathological profiles, several clinical subsets of this entity have been described which vary in their treatment options and outcome [35]. We herein report eight cases of PACNS diagnosed by CNS biopsy over a period of eight years at the Department of Pathology, AIIMS, and discuss the advancements in clinical, radiological and histopathological patterns.

Material and methods

The records of all patients presenting in 2005-2012 with a clinical diagnosis of PACNS were retrieved. There were thirteen cases with a provisional diagnosis of PACNS. The routine hematoxylin and eosin stained histopathology slides were evaluated independently by three neuropathologists (CS, MCS, VS). In addition, special stains viz. Masson's trichrome, Verhoeff's Van Gieson (VVG), reticulin stain, Congo red, and immunohistochemical staining with antibodies for CD3, CD20, CD4, CD8, CD68, neurofilament protein (NF), myelin basic protein (MBP), glial fibrillary acidic protein (GFAP) and beta-amyloid were performed where required. The cases were classified on the basis of the classification proposed by Miller *et al*. in 2009 [22]. A final diagnosis of PACNS was rendered in eight cases.

Clinical and radiological features

All eight patients were males. The age range was 19 to 48 years, with mean age of 33.5 years. Majority of patients presented with a history of seizures (7/8; 87.5%), headache (5/8; 62.5%) and sudden onset weakness (5/8; 62.5%). Remaining symptoms varied with the site of intraparenchymal haemorrhage, and included visual disturbances, difficulty in walking, slurring of speech, impaired memory, and altered behaviour (Table I). On radiology, 6 patients (75%) had bilateral supratentorial patchy to confluent white matter lesions, with multiple micro- and macrohaemorrhages. Similar lesions were seen in the infratentorial compartment in one patient, involving the brainstem and cerebellar hemispheres (case 8). One patient (case 2) showed confluent white matter signal changes in the right and left temporal lobes, left frontoparietal lobe, bilateral cerebral peduncles and pons. However, microhaemorrhages were not seen. Seven patients underwent intra-arterial digital subtraction angiography (IADSA), which was normal in all but one patient (14%). IADSA in this patient (case 3) showed irregularity and tortuosity of venous channels, suggesting vasculitis (Fig. 1). One patient (case 6) underwent MR angiography, which showed multiple focal stenoses in left A1 segment of anterior cerebral artery, as well as right pericallosal and callosomarginal arteries, suggesting vasculitis. Radiological features of case 6 are seen in Figure 2.

Microscopic findings

On histopathological examination, five of the eight cases (62.5%) showed features of granulomatous vasculitis, which was typified by transmural destruction of the vessel wall by epithelioid cell granulomas, accompanied by lymphocytes with or without giant cells (Fig. 3). This pattern was seen involving the leptomeningeal as well as parenchymal vessels in all but one case (Table I). One of the cases also showed the presence of necrotizing vasculitis involving parenchymal arterioles. Apart from this case, necrotizing vasculitis with transmural fibrinoid necrosis and acute inflammatory cell infiltrate was seen in one other case. The remaining two cases showed features of lymphocytic vasculitis (Fig. 4), with infiltration of the vessel wall by lymphocytes and occasional plasma cells, without significant spill over into the adjacent parenchyma. On immunohistochemistry, the inflammatory cells comprised predominantly of CD3 positive T lymphocytes.

The surrounding brain parenchyma showed evidence of haemorrhage, ischaemia, and reactive gliosis in most of the cases. Verhoeff's Van Gieson stain showed focal to complete disruption of the internal elastic lamina in all the cases. Congo red stain and immunohistochemistry for beta-amyloid did not demonstrate amyloid deposits in any of the cases. Of the cases showing abnormalities on angiography, both showed granulomatous vasculitis (cases

Table I. Clinical and histological features in cases diagnosed as PACNSs

Case no.	Age	Sex	Clinical features	Histological patterns	Site of involvement	Other features
1.	38 years	Male	Recurrent headache, seizures – 4 yrs Left homonymous hemianopia – 9 mths	Granulomatous vasculitis	Meningeal blood vessels	Subpial gliosis, reactive gliosis in cortex
2.	43 years	Male	Recurrent seizures – 4 mths Altered behaviour, slurring of speech, right hemiparesis – 1 episode	Acute necrotizing vasculitis	Parenchymal blood vessels	Hemorrhagic necrosis of white matter
3.	28 years	Male	Headache – 6 mths Seizures – 4 mths Sudden onset weakness in the upper limb – 1 episode	Granulomatous vasculitis	Meningeal and parenchymal blood vessels	Ischemic changes in neurons
4.	19 years	Male	Seizures – 1 year Sudden onset weakness – 2 episodes	Lymphocytic vasculitis	Parenchymal blood vessels	–
5.	48 years	Male	Intermittent headache – 2 years Seizures – 3 months	Granulomatous vasculitis	Meningeal and parenchymal blood vessels	Subpial gliosis
6.	27 years	Male	Recurrent seizures – 5 yrs Difficulty in speaking – 2 yrs	Granulomatous vasculitis with necrotizing vasculitis	Meningeal and parenchymal blood vessels	Ischemic changes in neurons
7.	26 years	Male	Recurrent headache – 5 yrs Seizures – 4 months Difficulty in walking – 4 months Sudden onset weakness – 2 episodes	Granulomatous vasculitis	Meningeal and parenchymal blood vessels	Fresh thrombi in occasional blood vessels
8.	39 years	Male	Intermittent headache – 2 yrs Sudden onset weakness – 2 episodes Impaired memory, altered behaviour – 6 months	Lymphocytic vasculitis	Parenchymal blood vessels	–

3 and 6), with the latter also showing foci of necrotizing vasculitis.

Discussion

The term "Vasculitides" encompasses a heterogeneous group of disorders characterized by inflammatory disease of arteries, veins, or both that results in histologically demonstrable structural injuries to the vessel wall, often accompanied by thrombosis and evidence of ischemic damage to the tissues served by the affected blood vessels [38]. Vasculitis of the central nervous system (CNS) may occur in any of the systemic vasculitides or may be secondary to connective tissue disorders, infections, neoplasms, or due to substance abuse [8].

'Isolated angiitis' affecting either the central nervous system or the spinal cord is a rare form of vasculitis, where there is neither any clinically overt systemic vasculitis, nor any underlying causal disease [38]. It usually involves leptomeningeal, cortical and subcortical medium-sized arteries and, less frequently, vein and venules [8].

The incidence of PACNS from Olmsted County, Minnesota (USA) has been estimated at 2.4 cases per 1,000,000 person-years [33]. Amongst patients attending the regional vasculitis clinic at Manchester Royal Infirmary between 1988 and 2003 ($n = 105$), the frequency of PACNS was 10.5% [21]. The frequency of PACNS amongst vasculitides and connective tissue diseases associated with a diagnosis of CNS

Fig. 1. Venous phase of left internal carotid artery digital subtraction angiogram shows irregularities and indistinct pattern of deep veins suggestive of vasculitis.

vasculitis or angiitis at the Mayo Clinic over a 17-year period was 64%. Thus, it represents the most frequent vasculitis involving the CNS.

Pathogenesis

Data on the pathogenesis and immunological mechanisms involved in PACNS are sparse, as there are no useful animal models to aid our understanding of the disease. It is possible that viral infections initiate the inflammatory process that somehow becomes self-sustaining, or there may be a genetic predisposition in certain individuals, leading to an enhanced risk of a vasculitic process when there is an exposure to a particular antigen that "sets off" the immune system [18,20,27].

Diagnostic criteria

Clinical, laboratory, neuroimaging and histopathological analysis are important both for making a correct diagnosis and for excluding a wide variety of other conditions which may have a similar presentation. Definite criteria for diagnosis were proposed by Calabrese and Mallek in 1988 [5] and they include: (1) history of an unexplained neurologic deficit that remains after a vigorous diagnostic workup, including lumbar puncture and neuroimaging studies; (2) either classic angiographic evidence of vasculitis or histopathologic evidence of vasculitis within the CNS; (3) no evidence of systemic vasculitis or any other condition to which the angiographic or pathologic evidence can be attributed. A diagnosis of PACNS is made if all the above criteria are satisfied. To prevent misdiagnosis of reversible vasoconstriction syndrome (RCVS) as PACNS, Birnbaum *et al.* in 2009 suggested the following modification: definite diagnosis is given if analysis of a tissue biopsy specimen confirms the presence of vasculitis. Probable diagnosis is rendered in the absence of tissue confirmation, if there are high probability findings on an

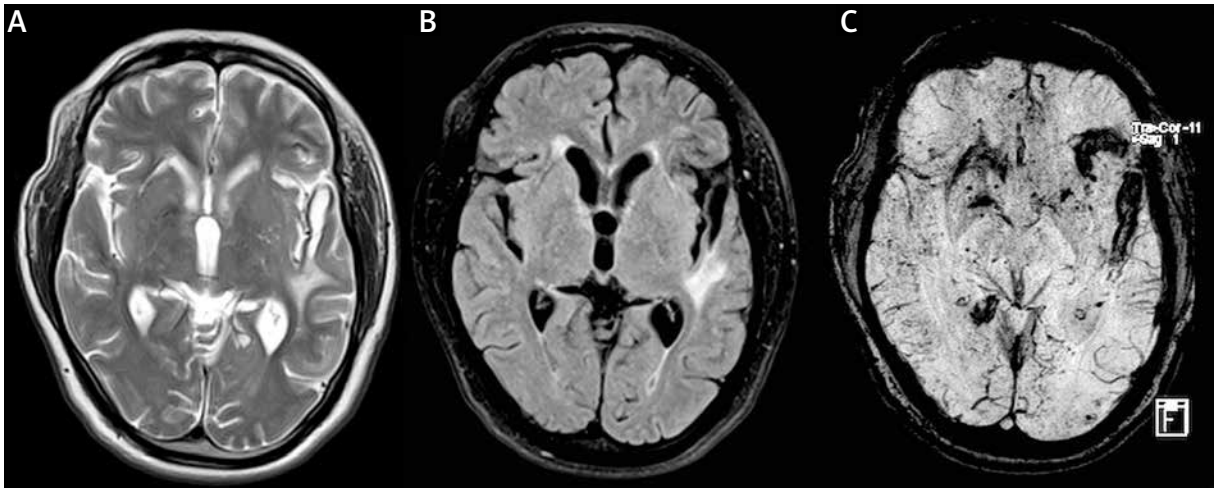

Fig. 2. T2 weighted MR **(A)**, FLAIR **(B)** and susceptibility weighted images **(C)** showing bilateral supratentorial white matter lesions, along with micro- and macro-haemorrhages.

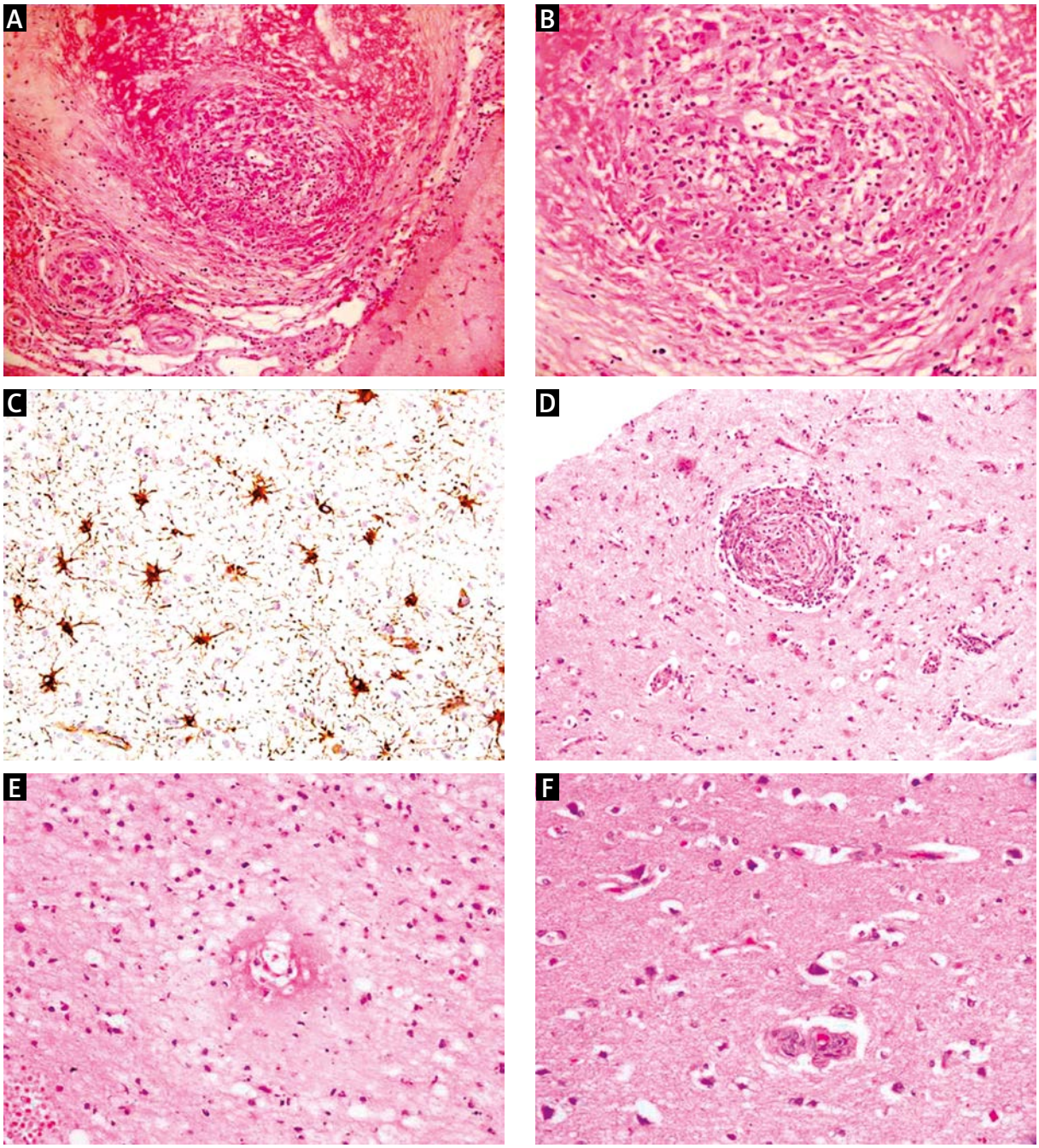

Fig. 3. Photomicrographs of case 1 showing **(A)** transmural granulomatous inflammation involving small and medium-sized leptomeningeal arteries (H&E, ×200). High magnification view **(B)** shows lymphocytes, epithelioid histiocytes and giant cells (H&E, ×400). GFAP stain **(C)** highlights reactive astrocytosis (IHC, ×400). Similar granulomatous vasculitis seen in a small cortical artery (**D**; H&E, ×200) in case 6, along with transmural fibrinoid necrosis **(E)** in an adjacent cortical arteriole (H&E, ×400). Surrounding cortex **(F)** shows ischemic neurons (H&E, ×400).

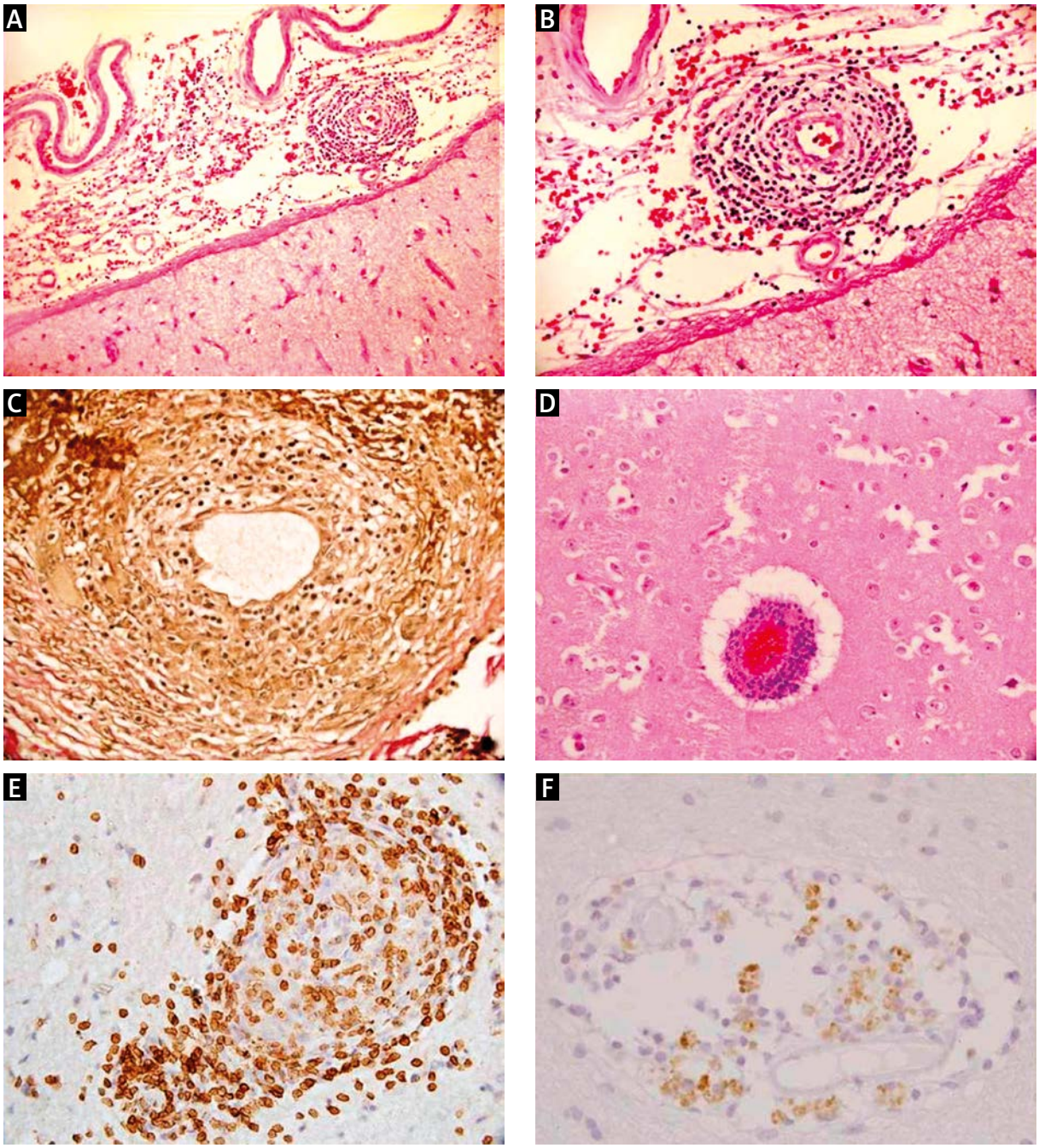

Fig. 4. Photomicrographs of case 4 showing **(A)** lymphocytic infiltrates within the wall of a leptomeningeal artery; there is no significant inflammatory infiltrate in the adjacent cortex (H&E, ×100). High power view **(B)** showing complete destruction of the vessel wall (H&E, ×200). VVG stain **(C)** demonstrates loss of internal elastic lamina (VVG, ×400). Cortical blood vessels **(D)** showed similar features (H&E, ×200). The inflammatory cells are predominantly CD3+ T cells **(E)** with only few CD20+ B cells **(F)** (IHC, ×400).

angiogram with abnormal findings on MRI and a CSF profile consistent with PACNS [5].

Clinical profile

The clinical manifestations of PACNS are diverse and non-specific. Giannini *et al.* summarized clinical findings in a 25-year follow up of 131 consecutive patients seen at the Mayo Clinic over a period of 25 years [12]. Headache, altered cognition, and persistent neurologic deficit or stroke were the most common manifestations, observed in 62%, 53% and 39% of cases, respectively. As part of a recent study of 101 consecutive patients with PCNSV seen at the Mayo Clinic over a 21-year period, and further from the updated cohort of 131 patients, Salvarani *et al.* identified several subsets of PCNSV which have distinct clinical, radiological and histopathological patterns, and also differ in terms of prognosis and optimal management [30,35,36]. Four subsets were identified from the cohort of 101 patients, which included a) PACNS with cerebral amyloid angiopathy (CAA); b) PACNS with spinal cord involvement; c) PACNS with prominent leptomeningeal enhancement; and d) angiography negative PACNS. Eight (26%) out of 31 cases with CNS biopsy specimens positive for PCNSV also showed findings of vascular amyloid deposits (CAA). All had a granulomatous vascular inflammatory pattern. Compared with patients with PCNSV only, these patients were older at diagnosis, predominantly male, had a more acute onset, a higher frequency of cognitive dysfunction and showed prominent gadolinium-enhanced leptomeningeal lesions on MRI [37]. Five cases had documented evidence of spinal cord involvement. Most patients had concurrent or subsequent brain involvement during the disease course. The thoracic cord was predominantly affected. The authors suggested that careful medical evaluation must be performed to exclude other conditions associated with acute or subacute transverse myelitis [36]. None of the cases in the present series showed either spinal cord involvement or histopathological evidence of amyloid deposition.

MRI showed prominent leptomeningeal enhancement in 8 of 101 patients with PCNSV. In six of those, cerebral angiography or magnetic resonance angiography results were normal, but biopsy from the brain or spinal cord showed vasculitis in all eight. Granulomatous vascular inflammation was found in six specimens. All eight patients showed a prompt response to therapy. The authors suggested that prominent gadolinium leptomeningeal enhancement on MRI may point to a distinct subtype of PCNSV with small leptomeningeal artery vasculitis and rapid response to therapy [31].

In 2005, Benseler and co-workers described a new disease entity, viz. angiography-negative primary CNS vasculitis of childhood. The authors studied four children with primary CNS vasculitis in whom results of magnetic resonance imaging studies were abnormal but results of conventional angiography were normal [4]. Further, on retrospective analysis of the series of 101 patients, Salvarani *et al.* also identified eight patients with angiography negative PCNSV.

On using the updated cohort of 131 consecutive patients at the Mayo Clinic, 11 cases with rapidly progressive PCNSV were documented [12]. This subset represents the worst end of the clinical spectrum of this vasculitis, characterized by bilateral, multiple, large cerebral vessel lesions, multiple CNS infarctions and poor response to traditional immunosuppressive therapy. In this cohort of 131 patients, sixteen patients (12.2%) had evidence of intracranial haemorrhage at or near the time of diagnosis. A necrotizing histopathologic pattern of vasculitis was observed in 3 of the 4 patients with positive biopsy findings (75%) [12].

In 2008, Molloy *et al.* examined the case records of the Cleveland Clinic (CC), Massachusetts General Hospital (MGH), and the English language medical literature, for biopsy-proven PACNS cases presenting as a solitary mass lesion (ML). They identified a total of 38 ML: eight of 202 (4.0%) patients from CC/MGH and 30 of 535 (5.6%) patients identified from the medical literature. Excision of the lesion may be curative; however, in some patients aggressive immunosuppressive therapy has led to a favourable outcome obviating the need of surgery [23].

Primary angiitis of central nervous system in children

Primary angiitis of central nervous system in the paediatric age group is poorly characterized. There are only few case reports and case series. Although the disease was earlier thought to be rare, recent studies have shown that childhood PACNS could be an important cause of vascular stroke in children [3]. Diagnostic features are based on rare autopsy find-

ings and, more recently, on angiographic findings [4,14,32]. Distinct phenotypes in children include progressive, angiography-positive, medium-to-large vessel CNS vasculitis; non-progressive, angiography-positive, medium to-large vessel CNS vasculitis; angiography-negative, small-vessel CNS vasculitis, confirmed by brain biopsy [4,32].

Neuroimaging

Magnetic resonance imaging is abnormal in almost all cases, with a sensitivity of 90-100%, and is the main neuroradiological modality for workup of these patients [5,26]. Abnormalities may be seen in the subcortical white matter, deep gray matter, the deep white matter, and the cerebral cortex [28]. Infarcts may be seen in approximately 50% of cases [32]. Other common patterns include diffuse small vessel changes of ischaemic demyelination. Both subarachnoid and intraparenchymal haemorrhages have been observed in 10% of cases. Leptomeningeal enhancement may be seen in 10% of cases [31]. Mass lesions may be seen in 5% of cases, and generally mimic a tumour or abscess [23]. Rarely, confluent white-matter lesions may be seen [5,33,41].

Angiographic features considered diagnostic of PACNS include multiple "beading" or segmental narrowing, in large, intermediate, or small arteries with interposed regions of ectasia or normal luminal architecture [9,13,17]. Angiography however has limited sensitivity (20-90%) and specificity (20-60%). Angiographic changes typical of vasculitis may be seen in non-vasculitic conditions such as vasospasm, atherosclerosis, CNS infections, lymphomas, cerebral arterial emboli, and radiation vasculopathy [2,11,19,25]. Angiography may be normal in vasculitis limited to small vessels below the resolution of conventional angiography [30]. Hence, angiography results should always be interpreted in conjunction with clinical, laboratory, and MRI findings.

Histopathological spectrum

Brain biopsy remains the gold standard for the diagnosis of PACNS. Histopathological evaluation is crucial not only for making the diagnosis of PACNS but also to rule out mimics, especially infections and malignancy. In a recent study by Giannini *et al*., biopsies were non diagnostic in 35% of cases [12]. This is attributed to the inherent patchiness of vasculitic inflammation, or to the fact that the affected vessels may be of a large diameter and hence do not extend to the superficial parenchyma and leptomeninges [12,14]. To enhance the diagnostic yield, targeted biopsies should be performed with inclusion of leptomeninges [6,22].

The most common histological pattern is of granulomatous vasculitis, characterized by vasculocentric mononuclear inflammation associated with well-formed granulomas and multinucleated giant cells and at least focal vessel wall destruction. Giannini *et al.* observed this pattern in 58% of cases [12]. Lymphocytic vasculitis is the second most predominant pattern. There is marked perivascular lymphocytic inflammation with occasional plasma cells, extending through the vascular wall with vascular distortion and destruction. There is absence of significant parenchymal inflammation [12,14]. The least frequent pattern is that of acute necrotizing vasculitis, characterized by acute inflammation and transmural fibrinoid necrosis. It involves predominantly small muscular arteries [12]. The histological patterns, as observed in patients who have undergone repeat biopsies, remain stable over time, suggesting that they are truly distinct patterns rather than different stages of disease [35]. In the recently updated series of 131 patients from the Mayo Clinic, the granulomatous pattern was seen in 56%, pure lymphocytic in 20% and acute necrotizing pattern in 22% of cases [12]. Concurrent parenchymal ischaemia/infarct was found in 51% of cases. Eleven cases (27%) with CNS biopsy specimens positive for PCNSV also showed findings of CAA. All the cases with CAA showed granulomatous inflammation [12]. In the present series, 62.5% showed granulomatous vasculitis, 25% lymphocytic vasculitis and 12.5% acute necrotizing vasculitis.

Treatment

There are no randomized clinical trials on drug therapy in PCNSV. Treatment recommendations have been extrapolated from therapeutic strategies used in other vasculitides. In general, a combination of steroids and pulsed cyclophosphamide is recommended. TNF-alpha blockers and mycophenolate mofetil have successfully been used to treat patients with PCNSV resistant to glucocorticoids and immunosuppressants [34,39].

To conclude, in view of non-specific clinical presentations and lack of highly efficient non-invasive

modalities, diagnosis of PACNS is a challenge and requires a high index of clinical suspicion, with appropriate work-up to exclude other conditions. Increased recognition and better understanding of the molecular pathogenesis of this entity will provide a key to prognostication and therapeutic decision making.

Disclosure

Authors report no conflict of interest.

References

1. Alba MA, Espígol-Frigolé G, Prieto-González S, Tavera-Bahillo I, García-Martínez A, Butjosa M, Hernández-Rodríguez J, Cid MC. Central nervous system vasculitis: still more questions than answers. Curr Neuropharmacol 2011; 9: 437-448.
2. Alhalabi M, Moore PM. Serial angiography in isolated angiitis of the central nervous system. Neurology 1994; 44: 1221-1226.
3. Amlie-Lefond C, Bernard TJ, Sebire G, Friedman NR, Heyer GL, Lerner NB, deVeber G, Fullerton HJ. Predictors of cerebral arteriopathy in children with ischemic stroke: results of the International Pediatric Stroke study. Circulation 2009; 119: 1417-1423.
4. Benseler SM, deVeber G, Hawkins C, Schneider R, Tyrrell PN, Aviv RI, Armstrong D, Laxer RM, Silverman ED. Angiography-negative primary central nervous system vasculitis in children: a newly recognized inflammatory central nervous system disease. Arthritis Rheum 2005; 52: 2159-2167.
5. Birnbaum J, Hellmann DB. Primary angiitis of the central nervous system. Arch Neurol 2009; 66: 704-709.
6. Calabrese LH, Furlan AJ, Gragg LA, Ropos TJ. Primary angiitis of the central nervous system: diagnostic criteria and clinical approach. Cleve Clin J Med 1992; 59: 293-306.
7. Calabrese LH, Mallek JA. Primary angiitis of the central nervous system. Report of 8 new cases, review of the literature, and proposal for diagnostic criteria. Medicine 1988; 67: 20-39.
8. Carolei A, Sacco S. Central nervous system vasculitis. Neurol Sci 2003; 24: S8-S10.
9. Cloft HJ, Phillips CD, Dix JE, McNulty BC, Zagardo MT, Kallmes DF. Correlation of angiography and MR imaging in cerebral vasculitis. Acta Radiol 1999; 40: 83-87.
10. Cravioto H, Feigin I. Noninfectious granulomatous angiitis with a predilection for the nervous system. Neurology 1959; 9: 599-609.
11. Duna GF, Calabrese LH. Limitations of invasive modalities in the diagnosis of primary angiitis of the central nervous system. J Rheumatol 1995; 22: 662-667.
12. Giannini C, Salvarani C, Hunder G, Brown RD. Primary central nervous system vasculitis: pathology and mechanisms. Acta Neuropathol 2012; 123: 759-772.
13. Greenan TJ, Grossman RI, Goldberg HI. Cerebral vasculitis, MR imaging and angiographic correlation. Radiology 1992; 182: 65-72.
14. Hajj-Ali RA, Singhal AB, Benseler S, Molloy E, Calabrese LH. Primary angiitis of the CNS. Lancet Neurol 2011; 10: 561-572.
15. Harbitz F. Unknown forms of arteritis with special reference to their relation to syphilitic arteritis and periarteritis nodosa. Am J Med Sci 1922; 163: 250-272.
16. Harris KG, Tran DD, Sickels WJ, Cornell SH, Yuh WT. Diagnosing intracranial vasculitis: the roles of MR and angiography. Am J Neuroradiol 1994; 15: 317-330.
17. Hellmann DB, Roubenoff R, Healy RA, Wang H. Central nervous system angiography, Safety and predictors of a positive result in 125 consecutive patients evaluated for possible vasculitis. J Rheumatol 1992; 19: 568-572.
18. Iwase T, Ojika K, Mitake S, Katada E, Katano H, Mase M, Yoshida S, Ueda R. Involvement of CD45RO+ T lymphocyte infiltration in a patient with primary angiitis of the central nervous system restricted to small vessels. Eur Neurol 2001; 45: 184-185.
19. Kadkhodayan Y, Alreshaid A, Moran CJ, Cross DT 3rd, Powers WJ, Derdeyn CP. Primary angiitis of the central nervous system at conventional angiography. Radiology 2004; 233: 878-882.
20. Kelley RE. CNS vasculitis. Front Biosci 2004; 9: 946-955.
21. MacLaren K, Gillespie J, Shrestha S, Neary D, Ballardie FW. Primary angiitis of the central nervous system: emerging variants. Q J Med 2005; 98: 643-654.
22. Miller DV, Salvarani C, Hunder GG, Brown RD, Parisi JE, Christianson TJ, Giannini C. Biopsy findings in primary angiitis of the central nervous system. Am J Surg Pathol 2009; 33: 35-43.
23. Molloy ES, Singhal AB, Calabrese LH. Tumour-like mass lesion: an under-recognized presentation of primary angiitis of the central nervous system. Ann Rheum Dis 2008; 67: 1732-1735.
24. Moore PM, Richardson B. Neurology of the vasculitides and connective tissue diseases. J Neurol Neurosurg Psychiatry 1998; 65: 10-22.
25. Moore PM. Diagnosis and management of isolated angiitis of the central nervous system. Neurology 1989; 39: 167-173.
26. Néel A, Pagnoux C. Primary angiitis of the central nervous system. Clin Exp Rheumatol 2009; 27: S95-S107.
27. Pagni F, Isimbaldi G, Vergani F, Casiraghi P, Marzorati L, Migliorino G, Cattoretti G. Primary angiitis of the central nervous system: 2 atypical cases. Folia Neuropathol 2012; 50: 293-299.
28. Pomper MG, Miller TJ, Stone JH, Tidmore WC, Hellmann DB. CNS vasculitis in autoimmune disease: MR imaging findings and correlation with angiography. Am J Neuroradiol 1999; 20: 75-85.
29. Rollnik JD, Brandis A, Dehghani K, Bufler J, Lorenz M, Heidenreich F, Donnerstag F. Primary angiitis of CNS (PACNS). Nervenarzt 2001; 72: 798-801.
30. Salvarani C, Brown RD Jr, Calamia KT, Christianson TJ, Huston J 3rd, Meschia JF, Giannini C, Miller DV, Hunder GG. Angiography-negative primary central nervous system vasculitis: a syndrome involving small cerebral vessels. Medicine 2008; 87: 264-271.
31. Salvarani C, Brown RD Jr, Calamia KT, Christianson TJ, Huston J 3rd, Meschia JF, Giannini C, Miller DV, Hunder GG. Primary central nervous system vasculitis with prominent leptomeningeal enhancement: a subset with a benign outcome. Arthritis Rheum 2008; 58: 595-603.
32. Salvarani C, Brown RD Jr, Calamia KT, Christianson TJ, Huston J 3rd, Meschia JF, Giannini C, Miller DV, Hunder GG. Primary cen-

tral nervous system vasculitis presenting with intracranial hemorrhage. Arthritis Rheum 2011; 63: 3598-3606.
33. Salvarani C, Brown RD Jr, Calamia KT, Christianson TJ, Weigand SD, Miller DV, Giannini C, Meschia JF, Huston J 3rd, Hunder GG. Primary central nervous system vasculitis, analysis of 101 patients. Ann Neurol 2007; 62: 442-451.
34. Salvarani C, Brown RD Jr, Calamia KT, Huston J 3rd, Meschia JF, Giannini C, Miller DV, Hunder GG. Efficacy of tumor necrosis factor alpha blockade in primary central nervous system vasculitis resistant to immunosuppressive treatment. Arthritis Rheum 2008; 59: 291-296.
35. Salvarani C, Brown RD Jr, Hunder GG. Adult primary central nervous system vasculitis: an update. Curr Opin Rheumatol 2012; 24: 46-52.
36. Salvarani C, Brown RD Jr., Calamia KT, Christianson TJ, Huston J 3rd, Meschia JF, Giannini C, Miller DV, Hunder GG. Primary CNS vasculitis with spinal cord involvement. Neurology 2008; 70: 2394-2400.
37. Salvarani C, Brown RD Jr., Calamia KT, Christianson TJ, Huston J 3rd, Meschia JF, Giannini C, Miller DV, Hunder GG. Primary central nervous system vasculitis: comparison of patients with and without cerebral amyloid angiopathy. Rheumatology 2008; 47: 1671-1677.
38. Scolding NJ. Central nervous system vasculitis. Semin Immunopathol 2009; 31: 527-536.
39. Sen ES, Leone V, Abinun M, Forsyth R, Ramesh V, Friswell M, O'Callaghan F, Ramanan AV. Treatment of primary angiitis of the central nervous system in childhood with mycophenolate mofetil. Rheumatology 2010; 49: 806-811.
40. Siva A. Vasculitis of the nervous system. J Neurol 2001; 248: 451-468.
41. Zuccoli G, Pipitone N, Haldipur A, Brown RD Jr, Hunder G, Salvarani C. Imaging findings in primary central nervous system vasculitis. Clin Exp Rheumatol 2011; 29: S104-S109.

Original article

Folia Neuropathologica

Dendritic and spinal alterations of neurons from Edinger-Westphal nucleus in Alzheimer's disease

Ioannis Asterios Mavroudis[1], Marina George Manani[1], Foivos Petrides[1], Constantina Petsoglou[2], Samuel N. Njau[2], Vasiliki G. Costa[1,3], Stavros J. Baloyannis[1,3]

[1]Laboratory of Neuropathology and Electron Microscopy, 1st Department of Neurology, Aristotelian University of Thessaloniki, [2]Laboratory of Forensic Medicine and Toxicology, Aristotelian University of Thessaloniki, [3]Institute for Alzheimer's disease research, Heraklion Langada, Greece

Folia Neuropathol 2014; 52 (2): 197-204 DOI: 10.5114/fn.2014.43791

Abstract

Alzheimer's disease (AD) is a heterogeneous neurodegenerative disorder, causing a progressive decline of intellectual faculties, impairment of behavior and social performance, and impairment of speech eloquence, associated with various neurological manifestations based on a variable neuropathological background. Edinger-Westphal nucleus is a selective target of Alzheimer pathology early in the course of the disease. We attempted to determine the morphological alterations of the dendrites and the dendritic spines in Edinger-Westphal nucleus of 7 cases that fulfilled the diagnostic criteria for Alzheimer's disease. For the histological study, we applied (a) routine neuropathological techniques and (b) rapid Golgi method. We proceeded to 3D neuronal reconstruction for the estimation of dendritic and spinal changes in Alzheimer's disease. The morphological and morphometric analysis revealed a substantial neuronal loss and synaptic alterations in Edinger-Westphal nucleus in all the cases of Alzheimer's disease. Distal dendritic branches are prominently affected. The neuronal loss and alteration of the spines in Edinger-Westphal nucleus in Alzheimer's disease may be related to the exaggerated pupillary reaction to cholinergic antagonists. Furthermore, the vulnerability of distal branches to Alzheimer's disease might be related to neuroplasticity impairment.

Key words: *Alzheimer's disease, Golgi method, 3D neuronal reconstruction, Edinger-Westphal nucleus.*

Introduction

Alzheimer's disease (AD) is the primary cause of dementia affecting, according to recent studies, as much as 6-8% of people over the age of 65 years and nearly 30% of people older than 85 years [6,31]. It is physically characterized by a progressive decline of intellectual faculties, loss of professional skills, and variable deficits in perceptual, visual and auditory functions [27,32]. Macroscopically, cerebral atrophy is easily recognized in the majority of cases of Alzheimer's disease, being the most obvious in the temporal and parietal lobes [1,14]. Light microscopy reveals senile plaques and neurofibrillary tangles in the entorhinal cortex and hippocampus before spreading in other brain areas such as the acoustic and visual cortex, frontal cortex, and cerebellum [5,18,19,30,35].

Communicating author:
Ioannis Mavroudis, Laboratory of Neuropathology and Electron Microscopy, Aristotle University of Thessaloniki, Greece, phone: 00302310993301, e-mail: iamav79@hotmail.com

Alzheimer's disease is found to be associated with reduced levels of acetylcholine, noradrenaline, serotonin, somatostatin, and corticotrophin-releasing factors, whereas the levels of glutamate increase [7]. The cognitive deficits are attributable to the degeneration of cholinergic neurons in the basal-forebrain-cholinergic system that projects to the neocortex, hippocampus, and other brain areas [7,11].

The nucleus of Edinger-Westphal is the most rostral of the parasympathetic nuclei in the brainstem and supplies parasympathetic fibers to the eye [21].

The nucleus is located posteriorly to the main CNIII motor nucleus (oculomotor nucleus) and anterolaterally to the cerebral aqueduct in the rostral midbrain at the level of the superior colliculus [3].

Edinger-Westphal (EW) nucleus is a selective target of Alzheimer pathology early in the course of the disease [29]. Scinto *et al*. showed severe focal pathology of the EW nucleus in AD. The same authors noticed that patients who suffer from AD show an exaggerated pupillary reaction to the cholinergic antagonist tropicamide and in 2001, noticed a significant selective neuronal loss in the EW nucleus, whereas the number of neurons in the somatic portion of the nucleus of the third cranial nerve remained intact [28,29]. They showed that although the somatic portion of the third cranial nerve nuclei did not show any signs of pathology, the EW nucleus contained plaques and tangles in AD patients.

In previous studies of ours using the Golgi method and 3D neuronal reconstruction techniques, severe dendritic and spinal alterations were seen in Alzheimer's disease and normal aged brains [18-20].

In the present study, we intend to describe the morphometric and morphological changes of the neurons of the Edinger-Westphal nucleus in Alzheimer's disease in comparison to normal ageing and to investigate if except for the neuronal loss, senile plaques deposition and neurofibrillary degeneration, the EW nucleus is characterized by dendritic and spinal alterations in Alzheimer's disease.

Material and methods

Subjects

Tissue samples were obtained from 8 neurologically normal individuals post-mortem, and 7 with Alzheimer's disease, all of them aged between 67 and 86 years (mean 77.4 ± 5.1). The average autolysis time for all subjects was 12 ± 4 hours.

All brains, after their excision from the skull were immersed in 10% neutral buffered formalin for at least 25 days.

All possible information on each subject, concerning their previous physical and illness history, was obtained from autopsy reports as well as medical records. All the brains were examined by an independent neuropathologist for gross and microscopic signs of pathology. The brains did not exhibit trauma, edema or chronic illness. No neurofibrillary tangles or senile plaques were observed in normal controls, whereas AD brains were classified as stage V/VI according to Braak and Braak classification and CERAD score indicative of the disease. Histological criteria for the diagnosis of AD were those outlined by the National Institutes of Health/American Association of Retired Persons (NIH/AARP) Research Workshop on the Diagnosis of Alzheimer's Disease. All cases fulfilled the histological criteria for AD [18].

Tissue selection and processing

A tissue block from the Edinger-Westphal nucleus was excised. The EW nucleus was identified according to Scinto *et al*.'s studies [28,29]. The tissue blocks were coded in order to prevent experimental bias and were used for silver techniques [18-20], Congo red method [2], Bielschowsky staining [16], Gallyas technique [33] and Nissl staining [24].

Cell selection criteria

Neurons examined for quantitative alterations met the criteria set forth by Jacobs *et al*. [15] that request uniform staining of neuronal processes, absence of precipitated debris, good contrast between cells and background and relatively uniform tissue thickness.

Golgi method

For silver impregnation, the specimens were immediately immersed in a dilution of potassium dichromate (7 g of potassium dichromate and 20 mL of formaldehyde solution 37% in 300 mL of tap water) at room temperature. They remained in that solution for one week, and then they were immersed in an aqueous solution of 1% silver nitrate where they remained for one more week at a temperature of 15°C in a photoprotected environment.

After fixation, the specimens were embedded in low-melting-point paraffin and cut with a slicing microtome in thick sections at a range of 120 µm

and after rapid differentiation they were covered with entellan.

Nissl staining and Congo red technique

Adjacent sections were cut in a range of 20 µm and used for Bielschowsky staining [16], Gallyas technique [33], Nissl staining [24] and Congo red method [2] in order to evaluate the neuronal population, the neurofibrillary degeneration and the deposition of senile and amyloid plaques.

Neuronal tracing and dendritic quantification

For each one of the 15 brains, 10 neuronal cells from each area were selected. For every cell, we took a 10-second video at a magnification of 400× while the microscope table was moving at the standard velocity of 20 µm/sec. Afterwards, the videos were analyzed in digital image sequences of 200 serial pictures, which were ultimately imported in Neuromantic application to trace the cells, quantifying them along x-, y- and z-coordinates.

Each one of the selected cells was traced using the Neuromantic application. The neuronal tracing started with the cell soma and moved onto the basilar dendrites and the apical shaft.

Dendritic trees were quantitatively evaluated in a centrifugal manner for apical dendrites and basal dendrites according to Uylings *et al.* [34]. Dendrites arising from the cell soma are considered first-order segments, up to their first symmetrical bifurcation. Dendritic branches arising from first-order segments are considered second-order segments, in turn, up to their symmetrical bifurcation into third-order segments, and so on. When asymmetric branching is met during the neuronal tracing, the offspring dendritic branch, recognized by a qualitatively thinner diameter, is classified as a next-order branch, whereas the parent dendrite would retain its order level past the branching point [11].

Dendritic measures and Sholl analysis

The parameters measured were soma size, total dendritic length, cell contraction, dendritic field asymmetry, total number of dendritic segments and bifurcations, as well as the length and number of dendritic segments per order. Furthermore, the tracing was quantitatively analyzed with Image J program based on Sholl's [28] method of concentric circles. Concentric circles were drawn, at intervals of 15 µm centered on the cell bodies, and dendritic intersections within each circle were counted.

Spine counts

Spine counts were carried out at 360 pictures, which were taken with an AxioCam HR, at the standard magnification of 1000×, on an Axiostar Plus photomicroscope. Visible spines were counted on three segments of the dendritic field. The first segment, 20-30 µm in length, was located on the first-order dendrite, the second segment, 20-30 µm in length, on second-order dendrite and the third one, 40-50 µm, along the tertiary dendrite.

Neuronal density

For the estimation of neuronal density in each area, we used a modified semi-automatic optical dissector method provided by the Image J software. For each one of the brains, after defining the region of interest at a size of 150 × 150 µm, we recorded a 3-second video at a magnification of 400× while the microscope table was moving at the standard velocity of 20 µm/sec. Afterwards, the videos were analyzed in digital image sequences of 50 serial pictures, which were converted to binary ones. Then, using the "cell counter" function in Image J, the neurons in each given ROI were counted.

Statistical analysis

Statistical analysis was based on the Student's test on the basis of 360 cells in SPSS v.17.0. Significance was taken as $p < 0.05$. To ensure that autolysis time did not affect dendritic measurements, two-tailed Pearson product correlations were performed between all dependent measures and autolysis time.

Results

Golgi impregnation technique revealed a significant loss of distal dendritic branches and an overall restriction of the dendritic field in the AD brains. Tortuous branches and varicosities were also observed.

Dendritic changes

The total length of the dendritic field was significantly decreased in AD specimens. A severe loss of distal dendritic branches (quaternary), decrease in

the total number of branches and bifurcations were also noticed. The branching ratio was also grossly affected.

Sholl analysis revealed a restriction of the dendritic field due to the loss of distal branches, although the proximal ones remained relatively intact (Fig. 1).

Neurons from the somatic portion of the third cranial nerve nuclei retained high spinal density and did not show statistically significant alterations in any of the morphometric parameters.

Dendritic spines

Spinal density was also significantly decreased in AD. Except for spinal loss, several branched, mushroom and claw ending spines were seen in the aged brains.

Neuronal density

Neuronal density in the Edinger-Westphal nuclei of AD brains was severely decreased, whereas in the

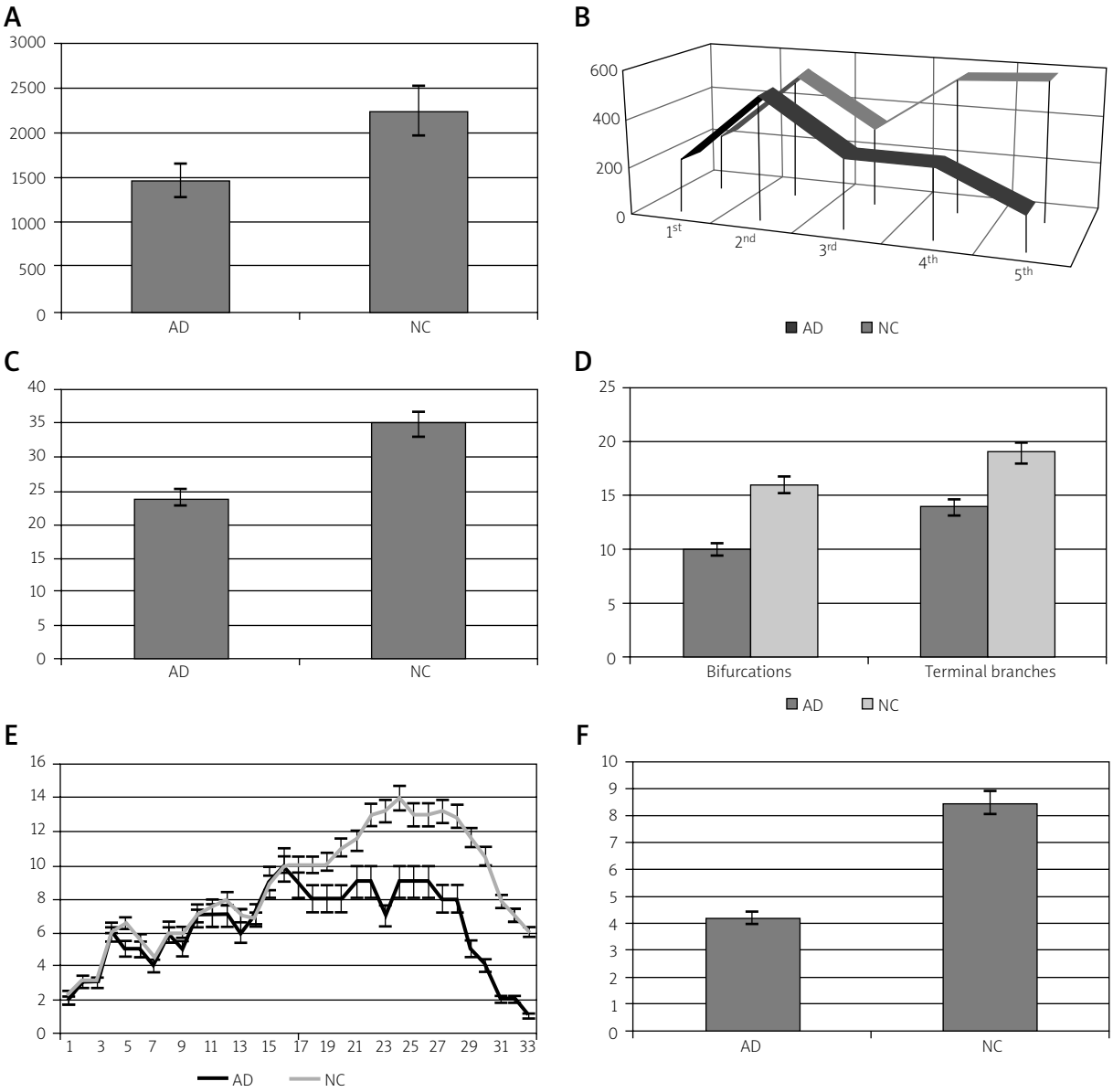

Fig. 1. A) Total dendritic length per neuron, **B)** dendritic length per branching order, **C)** total dendritic branches per neuron, **D)** number of bifurcations and terminal branches, **E)** Sholl analysis, and **F)** spine density in Edinger-Westphal neurons in Alzheimer's disease (AD) and in normal controls (NC).

somatic portion of the oculomotor nuclei, no significant difference in the neuronal density was seen (Fig. 2).

Senile plaques and neurofibrillary degeneration

Gallyas technique revealed neurofibrillary degeneration in the majority of the EW neurons.

Two types of plaque-like deposits were mainly encountered in AD EW nuclei. Typical and compact amyloid cored plaques, were mainly observed, while diffuse plaques were seen outside the EW nuclei.

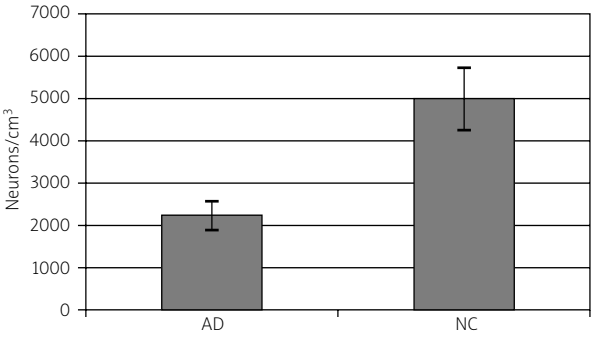

Fig. 2. Neuronal density (neurons/cm^3) in the Edinger-Westphal nucleus in Alzheimer's disease and normal controls.

Discussion

Early studies made in the mid-1970s were the first one to describe substantial neocortical deficits in the enzyme responsible for the synthesis of acetylcholine, choline acetyltransferase [4,8,26], while subsequent discoveries of reduced choline uptake, [28] acetylcholine release [23] and loss of cholinergic perikarya from the nucleus basalis of Meynert [35] confirmed the cholinergic deficit, leading to the cholinergic hypothesis of Alzheimer's disease.

On the other hand, biochemical studies showed a significant reduction of presynaptic markers of the cholinergic system early in the course of the disease [12].

From the neuropathologic point of view, Alzheimer's disease is characterized by neuronal loss, as well as dendritic and synaptic pathology in hippocampus and circumscribed regions of the neocortex [9,17,19]. Neurotransmitter-specific subcortical nuclei that project to the cortex are also affected by the implicated neurodegenerative processes, including the cholinergic nucleus basalis of Meynert and medial septum, the serotonergic raphe nuclei, and the noradrenergic locus coeruleus.

The nucleus of Edinger-Westphal is a selective target of Alzheimer pathology even in the early stages of the disease [28,29].

Scinto *et al*. (1999) showed that the EW nucleus alone contained plaques and tangles in AD patients as well as a severe and selective neuronal loss, thus sparing the somatic portion of the third cranial nerve nucleus [29]. They addressed these findings congruent to the exaggerated pupillary reaction to

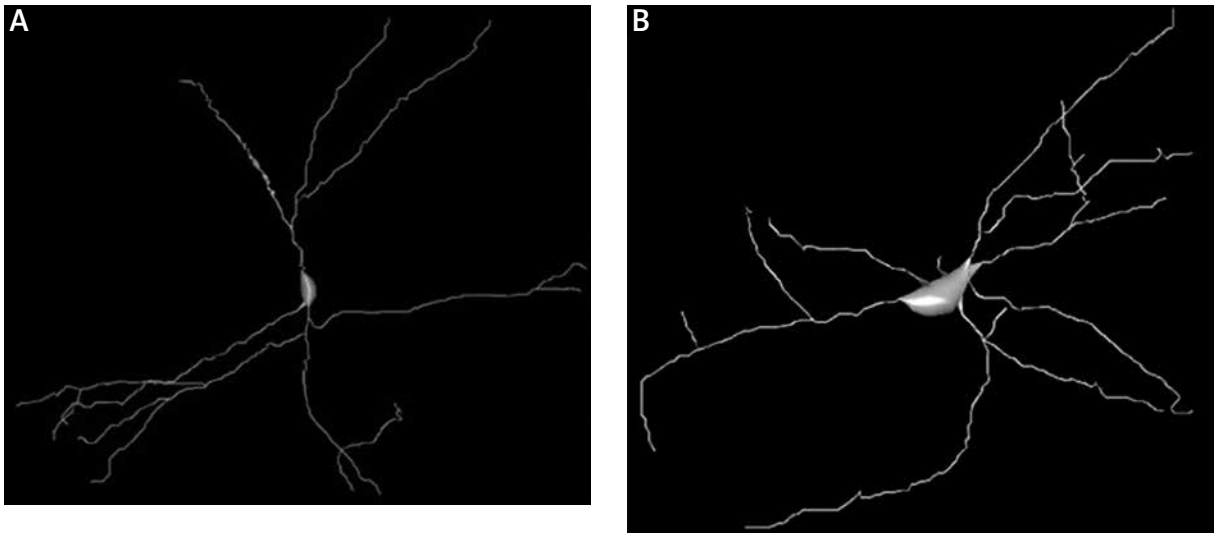

Fig. 3. Three dimensional reconstructions from a fusiform small soma sized neuron **(A)** and a multipolar large soma sized **(B)** neuron of the Edinger-Westphal nucleus.

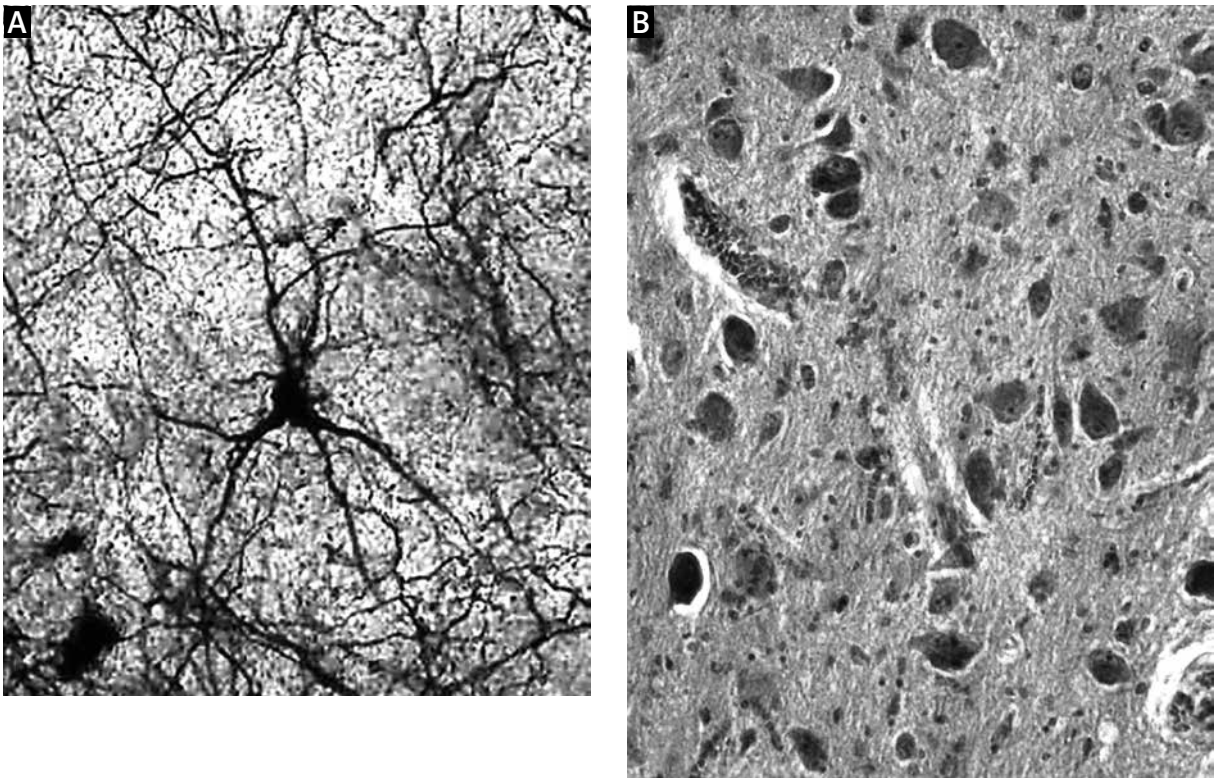

Fig. 4. A) Golgi stained neuron from the Edinger-Westphal nucleus from an AD brain, exhibiting a marked loss of dendrites, magnification 100×, **B)** Nissl stained neurons, astrocytes and microglial cells in the Edinger-Westphal nucleus from an AD brain, magnification 400×.

the cholinergic antagonist tropicamide seen in the disease.

Morawski *et al*. (2010) showed a high expression of Glutaminyl cyclase in the cholinergic nuclei of Meynert and Edinger-Westphal, related to high vulnerability of well-defined subcortical neuronal populations and their cortical projections in AD [22].

In the present study we encountered severe dendritic and spinal pathology in the EW nucleus, in early AD cases using silver impregnation methods. A substantial loss of distal dendritic branches, significant reduction of the total dendritic length per neuron, and severe decrease in dendritic spines were seen. Neurons from the somatic portion of the oculomotor nerve nuclei remained relatively intact in comparison to the control brains. Furthermore Bielschowsky and Gallyas methods revealed a high concentration of senile plaques and neurofibrillary tangles, and Nissl method showed a severe neuronal loss confirming the findings by Scinto *et al*. [28,29].

The present study is innovative in terms of depiction of dendritic changes of the neurons of EW nucleus, in relation to neurofibrillary degeneration and senile plaques deposition. Dendritic and spinal loss leads to a severe decrease in synaptic contacts. As a result, that should be related to the exaggerated pupillary reaction to cholinergic antagonists in AD. Furthermore, the present findings corroborate the hypothesis of cholinergic subcortical areas' vulnerability in AD.

An intriguing result of the present study is the prominent degeneration of the more distal branches of EW nucleus' neurons. From previous assays on similar topics, it is now acknowledged that distal branches are linked in the majority with neuronal plasticity and vice versa, therefore playing an important role in the process of learning and neuronal adaptation. On the other hand, neuronal plasticity is grossly affected by the accumulation of NFTs and is related to cholesterol metabolism, and therefore, at least ultimately, APP metabolism [13,19].

NFTs seem to clog dendritic branches leading to amputation of their more distal parts. As a result, they lead to both the severe loss of synapses and

interruption of neuronal plasticity [18,19]. The fact that NFTs, a prominent feature of the AD brain, are seen in the same portions of the CNIII and EW nucleus provides a possible explanation of this result [19].

Moreover, ApoE is a major factor in the pathogenesis of AD, by means of cholesterol transfer and APP metabolism, leading also to the neuroplasticity dysfunction [13]. Therefore, it could mean that the neuroplasticity dysfunction causes the distal and synaptic loss found, or the other way around.

Additionally, in the present study, there was a significant change in the morphology of the spines, besides the loss in their number. Whereas in normal controls, the majority of spines were of the long-neck type, in AD patients, about 80% of them were short-stubby ones, added the fact that giant dystrophic spines were also noticed. The morphology and structural plasticity of spines is related in a great amount to F-actin polymerization, which in turn, is thought to be a standard stage in NFT-linked degeneration. In conclusion, giant spines are usually a feature of increased oxidative stress, another alleged contributor of AD pathogenesis.

Summarizing the results, the present study, showing a loss of distal branches and alterations in spinal morphology and number that is coherent to the loss of synaptic contacts, comes in agreement with the disturbance of the neuronal function, thus providing an additional possible explanation for the pupillary reaction's particularities in AD.

Disclosure

Authors report no conflict of interest.

References

1. Baloyannis SJ (ed.). Neuropathology of Dementia. Thessaloniki, 1993.
2. Beauquis J, Pavía P, Pomilio C, Vinuesa A, Podlutskaya N, Galvan V, Saravia F. Environmental enrichment prevents astroglial pathological changes in the hippocampus of APP transgenic mice, model of Alzheimer's disease. Exp Neurol 2013; 239: 28-37.
3. Blokland A. Acetylcholine: a neurotransmitter for learning and memory? Brain Res Brain Res Rev 1995; 21: 285-300.
4. Bowen DM, Smith CB, White P, Davison AN. Neurotransmitter related enzymes and indices of hypoxia in senile dementia and other abiotrophies. Brain 1976; 99: 459-496.
5. Braak H, Braak E. Neuropathological staging of Alzheimer-related changes. Acta Neuropathol 1991; 82: 239-259.
6. Byrne GJ. Treatment of cognitive impairment in Alzheimer's disease. Aust J Hosp Pharm 1998; 28: 261-266.
7. Cutler NR, Sramek JJ. The role of bridging studies in the development of cholinesterase inhibitors for Alzheimer's disease. CNS Drugs 1998; 10: 355-364.
8. Davies P, Maloney AJF. Selective loss of central cholinergic neurons in Alzheimer's disease. Lancet 1976; 2: 1403.
9. De Kosky ST, Sche VSW, Styren SD. Structural correlates of cognition in dementia: quantification and assessment of synapse change. Neurodegeneration 1996; 5: 417-421.
10. Duan H, Wearne SL, Rocher AB, Macedo A, Morrison JH, Hof PR. Age-related dendritic and spine changes in corticocortically projecting neurons in macaque monkeys. Cereb Cortex 2003; 13: 950-961.
11. Francis PT, Palmer MA, Snape M, Wilcock GK. The cholinergic hypothesis of Alzheimer's disease: a review of progress. J Neurol Neurosurg Psychiatry 1999; 66: 137-147.
12. Francis PT, Sims NR, Procter AW, et al. Cortical pyramidal neuron loss may cause glutamatergic hypoactivity and cognitive impairment in Alzheimer's disease: investigative and therapeutic perspectives. J Neurochem 1993; 60: 1589-1604.
13. Hatzifilippou E, Banaki T, Traka M, Koutsouraki E, Costa V, Baloyannis SJ. Apolipoprotein E phenotype in demented patients in Greek population. Int J Neurosci 2008; 118: 163-172.
14. Hubbard BM, Anderson JM. A quantitative study of cerebral atrophy in old age and senile dementia. J Neurol Sci 1981; 50: 135-145.
15. Jacobs B, Driscoll L, Schall M. Life-span dendritic and spine changes in areas 10 and 18 of human cortex: A quantitative Golgi study. J Comp Neurol 1997; 386: 661-680.
16. Litchfield S, Nagy Z. New temperature modification makes the Bielschowsky silver stain reproducible. Acta Neuropathol 2001; 101: 17-21.
17. Mann DMA. Pyramidal nerve cell loss in Alzheimer's disease. Neurodegeneration 1996; 5: 423-429.
18. Mavroudis IA, Fotiou DF, Adipepe LF, Manani MG, Njau SD, Psaroulis D, Costa VG, Baloyannis SJ. Morphological changes of the human purkinje cells and deposition of neuritic plaques and neurofibrillary tangles on the cerebellar cortex of Alzheimer's disease. Am J Alzheimers Dis Other Demen 2010; 25: 585-591.
19. Mavroudis IA, Fotiou DF, Manani MG, Njaou SN, Frangou D, Costa VG, Baloyannis SJ. Dendritic and spinal pathology in Alzheimer's disease: A Golgi study in pathology. Int J Neurosci 2011; 121: 347-354.
20. Mavroudis I, Petrides F, Manani M, Theocharides C, Ciobica A, Padurariu M, Kiourexidou M, Njau S, Costa V, Baloyannis S. Dendritic and spinal alterations of the spiny stellate cells of the human visual cortex during normal aging. Folia Neuropathol 2012; 50: 261-269.
21. May PJ, Reiner AJ, Ryabinin AE. Comparison of the distributions of urocortin containing and cholinergic neurons in the perioculomotor midbrain of the cat and macaque. J Comp Neurol 2008; 507: 1300-1316.
22. Morawski M, Hartlage-Rübsamen M, Jäger C, Waniek A, Schilling S, Schwab C, McGeer PL, Arendt T, Demuth HU, Rossner S. Distinct glutaminyl cyclase expression in Edinger-Westphal nucleus, locus coeruleus and nucleus basalis Meynert contributes to pGlu-Abeta pathology in Alzheimer's disease. Acta Neuropathol 2010; 120: 195-207.

23. Nilsson L, Nordberg A, Hardy JA, Wester P, Winblad B. Physostigmine restores 3H-acetylcholine efflux from Alzheimer brain slices to normal level. J Neural Transm 1986; 67: 275-285.
24. Padurariu M, Ciobica A, Mavroudis I, Fotiou D, Baloyannis S. Hippocampal neuronal loss in the CA1 and CA3 areas of Alzheimer's disease patients. Psychiatr Danub 2012; 24: 152-158.
25. Perry E, Walker M, Grace J, Perry R. Acetylcholine in mind: a neurotransmitter correlate of consciousness? Trends Neurosci 1999; 22: 273-280.
26. Perry EK, Gibson PH, Blessed G, et al. Neurotransmitter enzyme abnormalities in senile dementia. Choline acetyltransferase and glutamic acid decarboxlyase activities in necropsy brain tissue. J Neurol Sci 1977; 34: 247-265.
27. Perry RJ, Watson P, Hodges JR. The nature and staging of attention dysfunction in early (minimal and mild) Alzheimer's disease: Relationship to episodic and semantic memory impairment. Neuropsychologica 2000; 38: 252-271.
28. Scinto LF, Frosch M, Wu CK, Daffner KR, Gedi N, Geula C. Selective cell loss in Edinger-Westphal in asymptomatic elders and Alzheimer's patients. Neurobiol Aging 2001; 22: 729-736.
29. Scinto LF, Wu CK, Firla KM, Daffner KR, Saroff D, Geula C. Focal pathology in the Edinger-Westphal nucleus explains pupillary hypersensitivity in Alzheimer's disease. Acta Neuropathol 1999; 97: 557-564.
30. Sholl DA. Dendritic organization in the neurons of the visual and motor cortices of the cat. J Anat 1953; 87: 387-406.
31. Small GW, Rabins PV, Barry PP, et al. Diagnosis and treatment of Alzheimer disease and related disorders. Consensus statement of the American Association for Geriatric Psychiatry, the Alzheimer's Association, and the American Geriatrics Society. JAMA 1997; 278: 1363-1371.
32. Terry RD, Katzman R. Senile dementia of Alzheimer's type. Ann Neurol 1983; 14: 497-506.
33. Tsamis K, Mytilinaios D, Njau SN, Psaroulis D, Mavroudis J, Costa V, Baloyannis SJ. The combination of silver techniques for studying the pathology of Alzheimer's disease. Int J Neurosci 2008; 118: 257-266.
34. Uylings HBM, Van Eden CG, Parnavelas JG, Kalsbeek A. The prenatal and postnatal development of rat cerebral cortex. In: Kolb E, Tees RC (eds). The cerebral cortex of the rat. MIT Press, Cambridge 1990; pp. 35-76.
35. Whitehouse PJ, Price DL, Struble RG, Clark AW, Coyle JT, Delon MR. Alzheimer's disease and senile dementia: loss of neurons in basal forebrain. Science 1982; 215: 1237-1239.
36. Xu Y, Jack CR Jr, O'Brien PC, Kokmen E, Smith EG, Ivnik RJ, Boeve BF, Tangalos JR, Petersen RC. Usefulness of MRI measures of entorhinal cortex versus hippocampus in AD. Neurology 2000; 54: 1760-1767.

Folia Neuropathologica

Iron-induced fibrin formation may explain vascular pathology in Alzheimer's disease

Boguslaw Lipinski[1], Etheresia Pretorius[2]

[1]Joslin Diabetes Center, Harvard Medical School, Boston, USA, [2]Faculty of Health Sciences, University of Pretoria, South Africa

Folia Neuropathol 2014; 52 (2): 205 DOI: 10.5114/fn.2014.43792

To the Editor

In their review article Serý *et al.* [6] have presented compelling arguments in favour of the role of vascular mechanisms in the development of Alzheimer's disease (AD). These arguments are in line with a recent series of publications questioning the prevailing concept of amyloid beta-induced neurodegeneration. Already in 2009 Pimplicar published a paper reassessing the amyloid hypothesis in AD [4]. More recently another important paper was published, in which the author has indicated that therapeutic targeting Abeta brain deposits had no significant effect in AD patients [5]. In the last decade of this century, a number of papers appeared that offered alternative explanations of the molecular mechanisms of AD that are related to cardiovascular diseases (CVD). It is well known that the hallmark of CVD is the intravascular formation of persistent fibrin deposits, or thrombi. Under the conditions of normal hemostasis, fibrin is gradually albeit completely removed by a powerful blood fibrinolytic enzyme system. It is known, however, that in the pathologic situations, such as coronary and/or cerebral thrombosis, fibrin clots are refractory to the thrombolytic dissolution [2].

We have recently shown that, when compared to thrombin-generated clots, the iron-induced fibrin has a radically different structure and morphological appearance as documented by scanning electron microscopy [1]. A characteristic feature of this novel form of fibrin (*parafibrin*) is its complete resistance to the proteolytic degradation. Thus, it may be argued that the formation of parafibrin in the cerebral circulation may be an important factor contributing to AD pathology. Apparently, unfolding of fibrinogen polypeptide chains and its scrambled refolding induced by iron potentiates and/or mimics amyloid deposits in the brain, and in this way contributes to AD pathology. This concept is supported by the findings of Strickland and his group, who have shown that persistent fibrin deposits contribute to neuro-inflammation [3]. In conclusion, we believe that the information presented above supports arguments presented by Serý *et al.* [6] that deserve further attention.

References

1. Lipinski B, Pretorius E. Novel pathway of iron-induced blood coagulation: implications for diabetes mellitus and its complications. Pol Arch Med Wewn 2012; 122: 115-122.
2. Lipinski B. Modification of fibrin structure as a possible cause of thrombolytic resistance. J Thromb Thrombolysis 2010; 29: 296-298.
3. Paul J, Strickland S, Melchor JP. Fibrin deposition accelerates neurovascular damage and neuroinflammation in mouse models of Alzheimer's disease. J Exp Med 2007; 204: 1999-2008.
4. Pimplicar SW. Reassessing the amyloid cascade hypothesis of Alzheimer's disease. Int J Biochem Cell Biol 2009; 41: 1261-1268.
5. Reitz C. Alzheimer's disease and the amyloid cascade hypothesis: a critical review. Int J Alzheimers Dis 2012; 2012: 3669808.
6. Serý O, Povová J, Míšek I, Pešák L, Janout V. Molecular mechanism of neuropathological changes in Alzheimer's disease: a review. Folia Neuropathol 2013; 51: 1-9.

Communicating author:
Etheresia Pretorius, Department of Physiology, Faculty of Health Sciences, University of Pretoria, Private Bag x323, Arcadia, 0007, South Africa, phone: +27 12 319 2907, e-mail: resia.pretorius@up.ac.za

Instructions to Authors

This instruction is based upon *Uniform Requirements for Manuscripts Submitted to Biomedical Reviews* (the complete document appears in N Engl J Med 1997; 336, 309-315).

Aims and scope

Folia Neuropathologica is an official journal of the Mossakowski Medical Research Centre Polish Academy of Sciences and the Polish Association of Neuropathologists. The journal publishes original articles and reviews that deal with all aspects of clinical and experimental neuropathology and related fields of neuroscience research. The scope of journal includes surgical and experimental pathomorphology, ultrastructure, immunohistochemistry, biochemistry and molecular biology of the nervous tissue. Papers on surgical neuropathology and neuroimaging are also welcome. The reports in other fields relevant to the understanding of human neuropathology might be considered.

Ethical consideration

Papers describing animal experiments can be accepted for publication only if the experiment conforms to the legal requirements in Poland as well as with the European Communities Council Directive of November 24, 1986 or the National Institute of Health Guide (National Institute of Health Publications No. 80-23, Revised 1978) for the care and use of Laboratory Animals for experimental procedure. Authors must provide a full description of their anesthetics and surgical procedures. Papers describing experiments on human subjects must include a statement that experiments were performed with the understanding and consent of each subject, with the approval of the appropriate local ethics committee.

Submission of manuscripts

Articles should be written in English. **All new manuscripts should be submitted through the online submission at http://panel2.termedia.pl/fn**
For authors unable to submit their manuscript online, please contact with Prof. E. Matyja, Editor-in-Chief of *Folia Neuropathologica*, ematyja@imdik.pan.pl
The Editorial Board reserves the right to reject a paper without reviewers' opinion if the content or the form of the paper does not meet minimum acceptance criteria or if the subject of the paper is beyond the aims and scope of the journal.

Legal aspects

In sending the manuscript the author(s) confirm(s) that (s)he has (they have) not previously submitted it to another journal (except for abstracts of no more than 400 words) or published it elsewhere. The author(s) also agree(s), if and when the manuscript is accepted for publication, to automatic and free transfer of copyright to the Publisher allowing for the publication and distribution of the material submitted in all available forms and fields of exploitation. The author(s) accept(s) that the manuscript will not be published elsewhere in any language without the written consent of the copyright holder, i.e. the Publisher.
All manuscripts submitted should be accompanied by an authors' statement including signed confirmation of the above and confirming that this publication has been approved by all co-authors (if any), as well as by the responsible authorities at the institution where the work has been carried out. The authors' statement should be signed by ALL co-authors. Additionally, the author(s) confirm(s) that (s)he is (they are) familiar with and will observe the "Instruction to Authors" included in *Folia Neuropathologica* and also that all sources of financial support have been fully disclosed. Materials previously published should be accompanied by written consent for reprinting from the relevant Publishers. In the case of photographs of identifiable persons, their written consent should also be provided. Any potential conflict of interest will be dealt with by the local court specific to the Publisher. Legal relations between the Publisher and the author(s) are in accordance with Polish law and with international conventions binding on Poland.
Authors agree to waive their royalties.

Anonymous review

All manuscripts will be subject to a process of anonymous editorial review.

Preparation of manuscripts

Articles must be written in English, with British spelling used consistently throughout. Authors not entirely familiar with English are advised to correct the style by professional language editors or native English speakers.

- The length of original article should not exceed 20 printed pages including text, illustrations, tables, and references.
- Manuscripts should be typed using 12pts.font, double-spaced, and fully corrected. Allow a margin at least 2.5 cm at the top, bottom and left side of the page. Text should not be justified.

- The title page should contain: the author's full names, title of the paper, all authors' affiliations, full name and address of the communicating author (including e-mail address and fax number), running title (not exceed 40 characters including spaces).
- The abstract should not exceed 350 words. A list of 3–10 key words is recommended below the abstract.
- The manuscript body should be organized in a standard form with separate sections: Introduction, Material and Methods, Results, Discussion, and References. Review articles should be divided into sections and subsections as appropriate without numbering.
- Do not underline in the text. Avoid footnotes.
- All dimensions and measurements must be specified in the metric system.
- The source of any drug and special reagent should be identified.
- Particular attention needs to be paid to the selection of appropriate analysis of data and the results of statistical test should be incorporated in the results section.
- The nomenclature used should conform to the current edition of the Nomina Anatomica or Nomina Anatomica Veterinaria.
- Acknowledgements should be made in a separate sheet following Discussion and before References. These should contain a list of dedications, acknowledgements, and funding sources.
- Legends of figures and tables should be typed on separate pages.
- The editor reserves the right to make corrections.

Tables

- Tables numbered in Roman numerals require a brief but descriptive heading.
- The major divisions of the table should be indicated by horizontal rules.
- Explanatory matter should be included in footnotes, indicated in the body of the table in order of their appearance.
- Tables must not duplicate material in the text or in illustration.

Illustrations

All figures should be supplied electronically at resolution 300dpi in all standard formats (tiff, jpg, Adobe Photoshop, Corel Draw, and EPS). Name your figure files with "Fig" and the figure number, e.g., Fig1.tif

- The maximum figure size is 84 mm or 174 mm for use in a single or double column width, respectively.
- When possible, group several illustrations on one block for reproduction. Like all other figures, block should be prepared within a rectangular frame to fit within a single or double column width of 84 and 174 mm, respectively, and a maximum page height of 226 mm.
- Each figure should include scale magnification bar; do not use magnification factors in the figure legends.
- All figures, whether photographs, graphs or diagrams, should be numbered using Arabic numerals and cited in the text in consecutive numerical order
- **Immunohistochemical study requires color illustrations of very good quality. The papers with white and black immunohistochemistry will not be accepted.**
- **The expense of color illustrations must be borne by the authors.** The cost of color print for every successive 8 pages is 200 euro irrespective of the number of color pages, i.e., the price remains the same whether there is one or eight pages.

The Publisher makes out the bill to the communicating Author.

References

The list of references (written on a separate page) should include only those publications that are cited in the text. Avoid citation of academic books, manuals and atlases. References may be arranged alphabetically and numbered consecutively. References should be given in square brackets with no space between the comma and the consecutive number, e.g. [3,4,6-12].

References should be written as follows:

Journal papers: initials and names of all authors, full title of paper, journal abbreviation (according to Index Medicus), year of publication, volume (in Arabic numerals), first and last page (example below):

1. Valverde F. The organization of area 18 in the monkey. Anat Embryol 1978; 154: 305-334.
2. Uray NJ, Gona AG. Calbindin immunoreactivity in the auricular lobe and interauricular granular band of the cerebellum in bullfrogs. Brain Behav Evol 1999; 53: 10-19.

Book and monographs: initials and names of all authors, full title, edition, publisher, place, year (examples below):

1. Pollack RS. Tumor surgery of the head and neck. Karger, Basel 1975.
2. Amaral DG, Price JL, Pitkanen A, Carmichael ST. Anatomical organization of the primate amygdaloid complex. In: Aggleton JP (ed.). The amygdala. Wiley-Liss, New York 1992; pp. 1-66.

Reference to articles that are accepted for publication may be cited as „in press" or Epub.

Proofs

Corrections to the proofs should be restricted to printer's errors only; other alterations will be charged to the authors. In order to maintain rapid publication, proofs should be returned within 48 hours, preferably by e-mail, fax or courier mail. If the Publisher receives no response from the authors after 10 days, it will be assumed that there are no errors to correct and the article will be published.

Subscription information

The journal is published in one volume per year consisting of four numbers. The annual subscription price is 160 PLN for Institutions from Poland and 80 PLN for individual subscribers from Poland and 140 Euro for foreign Institutions and 70 Euro for foreign individual subscribers.
Payment should be made to:
Termedia sp. z o.o., ul. Kleeberga 8, 61-615 Poznan
BZ WBK III O/Poznan PL 61 1090 1359 0000 0000 3505 2645
SWIFT: WBKPPLPP

The publisher must be notified of a cancellation of a subscription not later than two months before the end of the calendar year. After that date the subscription is automatically prolonged for another year.
Publishing, Subscription and Advertising Office:
TERMEDIA Publishing House
ul. Kleeberga 2
61-615 Poznan, Poland
phone/fax +48 61 822 77 81
e-mail: termedia@termedia.pl
http://www.folianeuro.termedia.pl

Folia Neuropathologica

AUTHOR'S STATEMENT

Title of the article

.....

.....

.....

The author(s) hereby confirm(s) that:

☐ The above-mentioned work has not previously been published and that it has not been submitted to the Publishers of any other journal (with the exception of abstracts not exceeding 400 words).

☐ All co-authors named and the relevant authorities of the scientific institutions at which the work has been carried out are familiar with the contents of this work and have agreed to its publication.

☐ In sending the manuscript together with illustrations and tables agree(s) to automatic and free transfer of copyright to the Publisher allowing for the publication and distribution of the material submitted in all available forms and fields of exploitation, without limits of territory or language, provided that the material is accepted for publication. At the same time the author(s) accept(s) that the submitted work will not be published elsewhere and in whatever language without the earlier written permission of the copyright holder, i.e. the Publisher.

☐ (S)he (they) agree to waive his(her)(their) royalties (fees).

☐ (S)he (they) empower(s) the Publisher to make any necessary editorial changes to the submitted manuscript.

☐ All sources of funding of the work have been fully disclosed.

☐ The manuscript has been prepared in accordance with the Publisher's requirements.

☐ (S)he (they) is (are) familiar with the regulations governing the acceptance of works as published in *Folia Neuropathologica* and agree(s) to follow them.

☐ (S)he (they) agree to accept appropriate invoice from the Publisher in case colour illustrations are implemented.

Date *Signatures of **all authors***

The covering letter formula can be found at: www.folianeuro.termedia.pl
-The covering letter should be sent to Associate Editor:

Milena Laure-Kamionowska
-Editorial Office of Folia Neuropathologica
Mossakowski Medical Research Centre, Polish Academy of Sciences
Poland Medical Research Centre
ul. Pawinskiego 5
02-106 Warszawa, Poland

CONTENTS